Vision at the Origin of Vertebrate Life

George Kafetzis

Submitted for the degree of Doctor of Philosophy

University of Sussex

September 2025

Declaration

The dissertation entitled "**Vision at the Origin of Vertebrate Life**", submitted for the degree of Doctor of Philosophy is a report of my own work. General and collaborative contributions are explicitly mentioned in the acknowledgements, methods, and herein.

Contributions by others:

Dr. Maxime Zimmermann assisted with building the shark facility.

Dr. Marvin Seifert previously assembled the recording setup and established the data processing backbone.

Prof. Takeshi Yoshimatsu, Dr. Michael Forsthofer performed the immunostaining protocols and subsequent imaging.

The perspective about the evolution of vertebrate lateral eyes, as documented in Chapter 3, represents my early version. A refined, extended and enriched, publicly available version now exists as a preprint with the title: A median eye origin of the vertebrate retina explains its unique circuitry together with Dr. Mike Bok, Prof. Tom Baden and Prof. Dan-Eric Nilsson. Ideas about disambiguating contributions of different environmental factors are by Prof. Dan-Eric Nilsson and illustrations contributed by Dr. Mike Bok and Prof. Tom Baden.

I hereby declare that this dissertation has not been and will not be, submitted in whole or in part to another University for the award of any other degree.

Brighton, September 2025

Summary

The basic blueprint of retinal organisation is highly conserved across all vertebrates. And yet, our detailed understanding of its functional properties has primarily come from only a handful of species that can not reflect the diversity of neither the lifestyle and behavioural repertoire of vertebrates nor the environments they inhabit. In search of universal principles of vertebrate visual processing, I explore the surprisingly understudied elasmobranch tree, the first branch of jawed vertebrates diverging over 400 million years ago, with species known to possess elaborate optics but historically assumed of having poor vision.

Primarily, I characterise the retinal output of the catshark *Scyliorhinus canicula* in structure and function. For examining light-driven responses of retina neurons, I presented a broad arsenal of visual stimuli and recorded with multi-electrode arrays simultaneously from hundreds of retinal ganglion cells. In line with the general concept, I confirm the early segregation of visual information in opposite elementary channels: ON and OFF, transient and sustained. Furthermore, I demonstrate that the -well described in mammals- retinal circuits for operating at dim light levels or computing direction of motion for stimuli of interest are also present in sharks and thus likely ancestral features of the vertebrate retina. Relying on pharmacological manipulations, I describe functional aspects of circuits wiring in the elasmobranch retina, and uncover unexpected crosstalk between different response polarity channels.

Apart from the structural and functional characterisation of the shark retina, in this dissertation I put forward a novel scenario for the origin of the vertebrate lateral eyes. In stark contrast to the classical view where complexity is regarded as a late, retina-specific property, I suggest we have got the sequence wrong; complexity predates and likely facilitates the emergence of the vertebrate retina.

Acknowledgements

This has been a long, challenging, but deeply rewarding journey. Straight on, one by no means worth undertaking (or safe to do so) alone.

I would like to thank my PhD supervisor, Prof. Tom Baden, not just for his mentorship, but for granting me the freedom to experiment, fail, and succeed (hopefully). For the inspiration and trust when I struggle(d) to trust myself.

My gratitude extends to all mentors that fuel my interest to neuroscience and the retinal circuits, Christos Makris, Prof. Domna Karagogeos, Dr. Maria Savvaki, Prof. Philipp Berens, Dr. Timm Schubert, Prof Thomas Euler and Prof. Dan-Eric Nilsson. Special thanks to my PhD committee – Dr. Sylvia Schroeder, Prof. Ivor Simpson and Prof. Bill Hughes –, as well to my future examiners, for their invaluable advice, comments and time invested to my shark findings.

Immensely grateful to all Baden lab members for helpful discussions and technical support, but importantly for all their great company in coffee breaks, drinks and Sunday roasts– you all know who you are! Deserving of a special mention are Dr. Maxime Zimmerman, Dr. Andre Maia Chagas, and Dr. Marvin Seifert; the road certainly far more challenging were it not for their contributions both in and outside the lab! Deeply thankful to my office roomie, Dr. Carola Yovanovich, who is always generous with her time for supportive conversations, as well as everyone who helped over the years with the shark facility maintenance when I needed to be away.

Thanks to all my friends- made along the way or from earlier days, still in touch or long lost. Impossible to name all, but equally impossible to have managed this without you: Thomas Papas, Nick Gravanis, Giannis Berberoglou, Dr. Maxime Zimmermann, Dr. Mikkel Roald- Arbøl, Dr. Sina Dominiak and Dr. Tessa Herzog.

Finally, deeply grateful to Katerina and my family, Aggela, Dimitris, Konstantia, Aggeliki and Jason, for their boundless patience, loving support, compassion and cheerful encouragement even when afar – my interests or accomplishments are worth nothing without all of you.

Table of Contents

Table of Figures

List of Abbreviations

AC	Amacrine cell
AME	Ancestral median eye
BC	Bipolar cell
ChAT	Choline acetyltransferase
CSF	Cerebrospinal fluid
ctr	control
DS	Direction selectivity
DSI	Direction-selectivity index
EM	Electron microscopy
FFF	Full field flashes
G	Gabazine
GABA	Gamma-aminobutyric acid
GC	Ganglion cell
Go	G protein o
GPCR	G-protein coupled receptor
Gt	G protein transducin
HC	Horizontal cell
hr	hour

Hz	Hertz
INL	Inner nuclear layer
IPL	Inner plexiform layer
IQR	Interquartile range
L-AP4	L-(+)-2-Amino-4-phosphonobutyric acid
LED	Light emitting diode
MAD	Median absolute deviation
MB	Moving bar
MEA	Multi-electrode array
mGluR6	Metabotropic glutamate receptor 6
ms	Millisecond
MS222	Ethyl3-aminobenzoate methanesulfonate salt
ND	Null direction
NT	Neurotransmitter
ONdOFF	ON-delayed-OFF
ONL	Outer Nuclear Layer
OPL	Outer plexiform layer
PBS	Phosphate buffered saline
PD	Preferred direction

ppm	Parts per million
PR	Photoreceptor
RBC	Rod bipolar cell
RGC	Retinal ganglion cell
rlBC	Retina-like bipolar cell
RPE	Retinal pigmented epithelium
s	second
S	strychnine
s.e.m	Standard error of the mean
SAC	Starburst amacrine cell
SBEM	Serial block-face scanning electron microscopy
T	TPMPA
TPMPA	(1,2,5,6-Tetrahydropyridin-4-yl)methylphosphinic acid hydrate
TSG	T – TPMPA,
VDF	Variable duration flashes

Chapter 1 – Introduction

For their survival and evolutionary success, most animals possess hierarchically organized nervous systems capable of sensorimotor transformations of varying complexity. To anatomically protect this highly modular, control-and-decision processing center, different strategies are employed across the animal kingdom, with vertebrates enclosing their brain within the cranium. Doing so nevertheless comes with sampling constraints and temporal delays, as the brain cannot directly interface with the external world but instead needs to rely on sensory systems and their own properties. In turn, these systems do not function in vacuum and cannot afford to be optimized for every task. Instead, they carry evolutionary history and subserve the organism's behavioral repertoire within specific ecological and environmental contexts. All species possess a battery of sensory modalities, each with different, and often species-specific contribution to the overall fitness. From an evolutionary perspective however, the emergence of eyes and visual systems was pivotal, likely sparking an arms race and the subsequent explosive radiation of life forms in the Cambrian[1–3].

Vision Underwater – And adaptations to it

Irrespective of the environment, all animals need to solve fundamental tasks like locating prey and conspecifics and avoiding predators. Vertebrate life started underwater, in particularly challenging conditions for vision compared to land because of the more pronounced, and often depth-dependent, contribution of light phenomena[4,5]. At shallow inshore environments, light absorption varies with content in chlorophyll (more green) and organic decay (more yellow) relatively to low concentration of either (more blue)[6]. With increasing depth, downwelling daylight intensity decreases exponentially and its spectral composition narrows so that only blue-green wavelengths can reliably penetrate the twilight zone (200-1000m)[7–9], whereas below that any available light is produced by bioluminescence[10–12]. And radically different to the 'low ambient noise' of terrestrial environments, water suspended particles scatter light and thus substantially veil objects of interest from the observer[4].

The effects of absorption (reducing image brightness) and scattering (reducing image contrast) would be detrimental on visual system performance were it not for compensating mechanisms and adaptations. In terms of increasing brightness, a bigger eye or pupil allows more light to reach the retina, while multibank photoreceptor layers or longer photoreceptor (PR) outer segments can pack more cells or more pigments, respectively, and thus capture a higher fraction of incoming photons[5,13,14], at the cost of temporal resolution[15,15]. In organisms inhabiting deeper and thus spectrally narrower environments, the sensitivity tuning of opsins often shifts to match the penetrating wavelength of the downwelling light[4,5] (but see[16,17]) and the representation of 'useful' photoreceptors is indirectly increased by the equivalent reduction of PR types whose alternative wavelength sensitivity no longer confers an advantage[18,19].

At depths or at times when photons are scarce, mechanisms both optical and neuronal can additionally amplify the incoming signals. Reaching this solution convergently, many vertebrates possess at the back of their eyes a tapetum[20], a highly reflective layer of cells or fibers that can optically redirect back to the retina photons that were not absorbed at the initial passage. Contrasting teleosts but like mammals, sharks additionally possess occlussible pupils, capable of adjusting retinal exposure in a light intensity-dependent manner. Given that specifically in underwater environments the downwelling light is of higher intensity relative to other paths, certain shark species reflect this light space asymmetry by permanently concealing the tapetum only at the retina region looking up whilst having it exposed elsewhere[21]. At the neuronal level, at some point the ancestral retina split the workload of handling the vast range of encountered light intensities into two types of photoreceptors: cones and rods. Among them, it is the rod that drives vision at dim light levels, often to the extreme capability of detecting single photons[22,22–24]. Such an operational adaptation is not limited to the input channels but rather spread to the network level too. At low light levels, retinal interneurons can increase their signal-to-noise ratio by lengthening their integration time or pooling together a higher number of PRs responses[20,25–29], at the expense of temporal and spatial resolution respectively[26,30–33]. Although primarily encountered in nocturnal animals, the above mechanisms are often dynamic, regulated in a circadian manner and selectively employed when light conditions

necessitate it. During daytime, photoreceptor outer segments are shortened[34,35], neuronal coupling decreases[36–43] or switches from lateral summation to inhibition[44–46], and pigment migrates in front of and thus conceals the tapetum[47–50].

Dealing with the low contrast of aquatic environments is not equally straightforward, because the spectral profile of background differs not only with depth but also with viewing angle. More specifically, a viewer encounters a spectrally broad background looking up, but a more monochromatic world in horizontal or nadir viewing and with increasing depth[4]. Considering that the spectral profile of the background contributes veiling noise to the image, the visual system needs to reduce its sampling of it. At the expense of optimal photosensitivity, visual contrast can be enhanced by adjusting the PR spectral absorbance to peak where the radiances of background and objects differ most[4,51]. Notwithstanding the photosensitivity tradeoff, this spectral offsetting of a photoreceptor is still not a panacea because its singular direction of displacement fails to simultaneously enhance contrast for light (reflective) and dark (nonreflective) objects.

As such, strong pressure for achieving versatile, background profile-independent, contrast sensitivity is considered the likely drive for the evolution of cone photoreceptor multiplicity[17,51–53] (but see[54–56]). The simultaneous presence of multiple, spectrally distinct, photoreceptors allows some to be matching and others be offset from the background spectral profile at all conditions[4,51], facilitating contrast detection. Moreover, a different and metabolically efficient strategy[57] for encoding both light increments and decrements is found in dividing the task for each polarity in two separate but parallel-running information pathways. As will be developed later, this ON and OFF pathway splitting is present in all vertebrate retinas to date and thus more conserved compared to the plastic, adaptively radiating[58,59] relative to the ancestral state, complement of photoreceptor types.

Irrespective of the driving force, photoreceptors are first-order sensory neurons and thus represent the interfacing node between the external world and the nervous system. As information cannot be generated de novo, the number of

photoreceptors (input channels) and their sampling properties determines the information available for downstream processing. At least four spectrally distinct cone photoreceptors were already present in the eyes of the common ancestor of all vertebrates [60–65]. Notwithstanding subsequent, adaptive and clade-specific tunings, expansions or shrinking, this ancestral multiplicity endowed early vertebrates with a rich visual information palette to inform behavior[55].

Structure and function of the vertebrate retina

What does then the vertebrate eye, and more specifically its neural component, the retina, tell the brain? Stemming from a camera-like appearance that is exemplified by optical components like a focusing lens and a contractile iris, it was historically assumed that the vertebrate eye is a camera itself, merely capturing intensity values and communicating to the brain a pixelated, unprocessed report of the external visual world. Early experiments in cats[66,67] and frogs[68,69] conclusively proved otherwise[70]. The presentation of visual stimuli varying not only in intensity but in their spatiotemporal properties, unveiled diverse neuron responses, each distinctly encoding and transmitting certain but not all features of a stimulus. Although differing in what is encoded, these neurons are nevertheless uniformly distributed within the retina, sampling the visual field in a spatially overlapping, retinotopically registered manner. As such, at the back of the camera-like vertebrate eye lies a neatly organized but complex photosensitive tissue consisting of distinct information processing channels running in parallel to the brain. And as I soon develop, it is both structural features and a high diversity in cellular composition that intertwine and contribute to this parallel-computing capacity.

At gross anatomical scale, the retina comprises of five neuronal cell classes organized in a cortex-like layered motif, with three cellular layers intervened by two synaptic (Fig. 1.1). Minor exceptions notwithstanding[71–73], each cell class occupies distinctive positions that together with the layered organization largely dictate its synaptic partners. More specifically, photoreceptors (PRs) occupy the outer nuclear layer (ONL) and synapse on bipolar (BCs) and horizontal cells (HCs) situated at the proximal part of the inner nuclear layer (INL), while amacrine (AC) and retina ganglion cells (RGCs), which receive bipolar cell output, are

located at the distal INL and the ganglion cell layer respectively. Vision at the retina begins with PRs converting photon energy to neuronal language, namely electrical signals, and ends with GCs conveying the already processed and compressed information to higher visual brain areas via their fasciculated axons, the optic nerve. Within the retina, the visual signal is transmitted along two perpendicular routes. The main, glutamatergic pathway is vertical and involves PRs, BCs and RGCs, while HCs and ACs, together constituting the lateral, use a variety of mostly inhibitory neurotransmitters to independently modulate the vertical route at the outer (OPL) and inner plexiform layer (IPL) respectively.

A fundamental task for any sensory system is distinguishing objects from background. Other than the already outlined benefit of possessing multiple, not spectrally overlapping, photosensitive systems, a neuronal, pathway-splitting strategy can contribute to further enhancing visual contrast. In vertebrates this implementation begins already at the first visual synapse. Although retina PRs hyperpolarize in response to light, they are continuously active at dark and synaptically release glutamate[74], an excitatory neurotransmitter. The response polarity of downstream-sitting BCs depends on their glutamate receptors; roughly half express ionotropic receptors[75,76] and depolarize at light offset (OFF-responding)[74,77], whilst in others the expression of metabotropic receptors[78–81] or glutamate transporters[82–87] leads to a cell depolarization when glutamate levels fall, namely at light onset (ON-responding)[88,89]. ON and OFF BCs then connect to ganglion cell dendrites in the IPL in a response type-specific, spatially segregated pattern[90–92]. Namely, ON BCs project proximally within the IPL and synapse with dendritic arbors of ON RGCs, while OFF BCs distally and with OFF RGCs[93]. Finally, a subset of RGCs (ON-OFF) ramify on both proximal and distal IPL, thus collecting both ON and OFF BC signals. Of note, this extensive “mono-stratification” pattern of input segregation, namely a distinct layer arborization for the different bipolar cell response polarities, is more abundant in mammals[94,95] (but see Ref[96]) salamanders[97,98] and sharks[99], while further relaxed in other vertebrates where bipolar cells are typically multi-stratifying[100–102]. In general however, the above demonstrates how the incoming visual image is first split into two parallel and opposite polarity channels (for brightness increments and decrements) via distinct molecular mechanisms in the OPL and retained as such

by lamina-specific wiring at the IPL, emphasizing the close interplay of different levels of organization in the vertebrate retina.

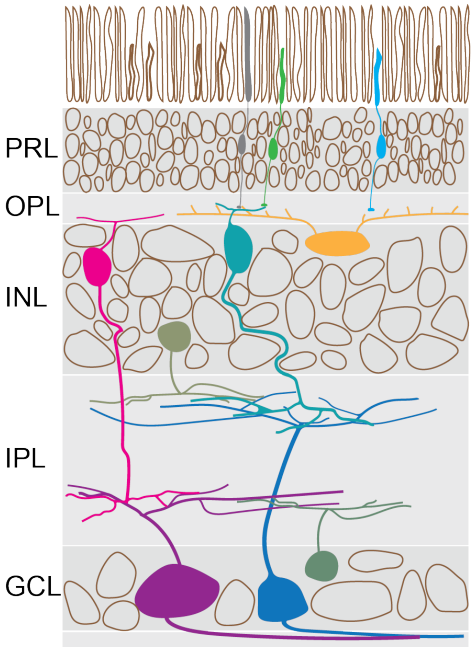

Figure 1.1 – The structure and composition of the vertebrate retina. The retina is organized in three nuclear layers (PRL, INL, GCL), intervened by two synaptic (OPL, IPL). It comprises of five neuronal classes, from top to bottom: Photoreceptors come in two flavors, rods (gray) and cones (green, cyan) of which there are different types. Photoreceptors synapse on horizontal (yellow) and bipolar cells (fuchsia, turquoise). Bipolar cells of different response polarity terminate at distinct depths in the IPL, and synapse onto amacrine cells (olive green, normally in INL but also displaced in GCL) and ganglion cells (purple, blue). PRL; photoreceptor layer, OPL; outer plexiform layer, INL; inner nuclear layer, IPL: inner plexiform layer, GCL; ganglion cell layer.

Now, the neat and dedicated IPL wiring described above primarily pertains to how cone signals are communicated from the outer to the inner retina. Instead, rod-driven signals appear to piggyback the cone circuits at different network locations (Fig. 1.2). For the primary pathway, also termed *canonical* given its prevalence in mammalian vision, rods synapse onto a rod bipolar cell (RBC) that does not contact RGCs directly despite terminating -and with characteristically large, bulbous terminals[103]- in the innermost IPL above the RGC somata. Instead, it synapses onto the Aii amacrine cell that forms electrical and chemical synapses with ON and OFF cone bipolar cells respectively[104–107]. In the secondary pathway,

rod signals again reach ON and OFF cone bipolar cells, but in this route independently of the RBC. Instead, rods and cones are connected via gap junctions that allow their electrical communication[108,109]. Finally, the third pathway is asymmetric, with rod synapsing on certain subtypes of OFF, but not ON, cone BCs[110,111]. Overall, the reliance on circuits routinely employed by cones together with the emergence of the rod opsin from a cone opsin[62,112–114] are presented as evidence for cones predating rods[64,115–117]. Compared to duplicating the number of BCs, the seemingly peculiar wiring of RBC, namely the utilization of the pre-existing circuits at lights where their direct cone input is virtually absent, would allow for economizing resources when extending the operational range to include dim light levels.

It would nevertheless be paradoxical if the complex processing occurring in the retina could be solely attributed to five neuronal classes and a couple of parallel information channels[70]. Indeed, starting over a century ago with Ramon y Cajal characterizing diversity on morphological grounds, and since further refined with every technical advance in molecular and physiological tools, we now know of an astounding diversity of subtypes, slightly short of 130 in the mouse retina[118]. Intriguingly, the degree of subtype diversity is not uniform across cell classes, but rather correlates with their position within circuits. Sitting at the origin of retinal computations, PRs and HCs come in single-digit variants[119], while ACs and RGCs together comprise over a hundred subtypes[120,121], yet indicative of an image progressively split into parallel running and differentially tuned processing units, with over 40 channels eventually feeding into the mouse brain[121–125].

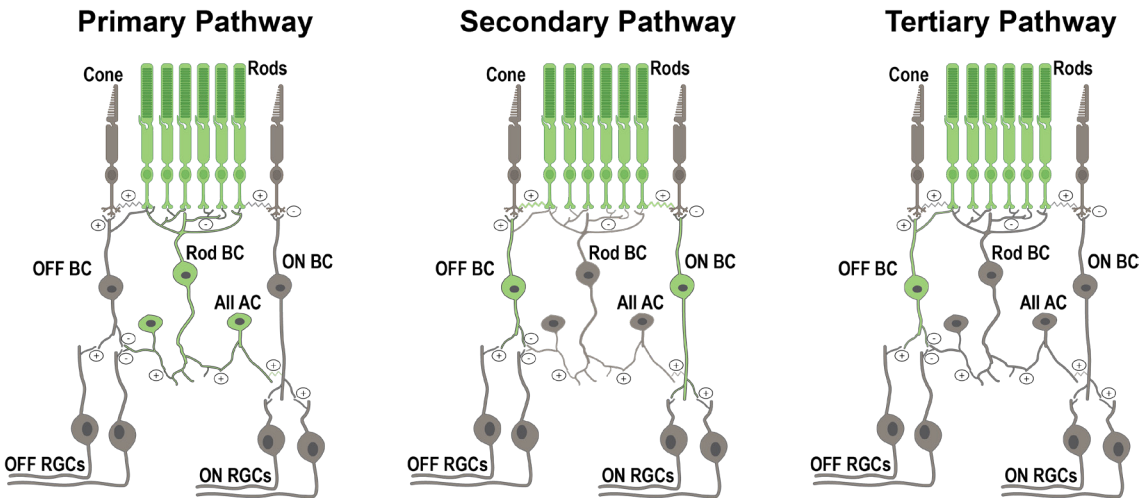

Figure 1.2 – Rod Pathways of the Mammalian Retina. To communicate their signals to RGCs, rods utilize three distinct routes. In the primary pathway (*left*), rods synapse onto rod bipolar cells, which in turn connect to Aii amacrine cells. They make sign-conserving, electrical synapses with ON cone-bipolar cells, and sign-inverting, glycinergic chemical synapses with OFF cone-bipolar cells. In the secondary pathway (*middle*), rod signals travel electrically via the gap junctions between rods and cones. In the tertiary pathway (*right*), rods synapse onto OFF, but not ON, cone bipolar cells. Thus, they only reach OFF RGCs. Highlighted in each panel is the respective rod route to RGCs. Plus and minus signs indicate sign-conserving and sign-inverting relationships. BC; bipolar cell, AC; amacrine cell, RGC; retinal ganglion cell. Adapted from Ref[126]. Photoreceptors are created in BioRender.

Retina conservation across vertebrates

Despite the mass species diversification during the Cambrian explosion and the occurrent wide range of eye shapes and sizes thereafter, the basis of retinal vision of all vertebrates is strikingly universal, based on the same, and thus likely ancestral, blueprint. Were you to randomly pick a vertebrate, from highly visual eagles and primates to “swimming noses”, as sharks are historically thought of because of their exquisitely sensitive olfaction, the retina would invariably present a layered organization and all five neuronal classes. And the homologies in fact run deeper, even within subtypes of classes. At the side of inputs for example, two types of visual photoreceptors are encountered in vertebrates, namely cones and -thought of later appearing[62,113]- rods, differing in membrane ramifications, kinetics and roles subserved[55,56,60,115,127,128]. As discussed earlier, cones additionally come in different flavours, with their spectral sensitivity determined by the opsin expressed, and mediate vision at higher light intensities than rods. Spanning the whole vertebrate lineage, each of these subtypes, when present, is homologous, with their transcriptomic signatures virtually indistinguishable from lampreys to mammals[129,130]. However, this degree of conservation of subtypes weakens substantially closer to the retinal output, likely indicative of species-specific divergence at the messages communicated to the brain.

Despite the structural conservation and owing to the ever-narrowing focus on model species, we currently have a detailed understanding of the retinal circuits’ function in only a handful of organisms, exemplified in mice, primates and to a

lesser extent also in zebrafish. If mice possess more than 40, functionally distinct, output channels from the retina to the brain[122,124], how many and which are rodent- or mammal-specific, reflect the specific organism's visual space statistics or behavioral repertoire, or are evolutionary conserved? How much can we learn from model species (alone), and how relevant will it turn out to be for understanding vision in a more general sense? Contrary to artificial neural networks, their biological counterparts are not engineered *de novo* but instead carry energetic and evolutionary constraints in their design. And although the past is no longer tangible, a lot can be learned by comparing extant organisms and inferring from common signatures the likely ancestral state.

The universal vertebrate retina template

In attempts to shed light on the evolution of vertebrate visual circuits, the so far extensively studied organisms are arguably not ideal representatives of ancestral states. Vertebrate life began underwater, in particularly challenging light conditions compared to terrestrial environments[4]. As such, early vertebrates populating the land encountered a radically different visual world, with their visual strategies adapting accordingly and diverging from the ancestral state[131]. Within aquatic premises, mammals are late returns and teleosts, the clade to which zebrafish belong, have undergone an ancient[132] clade-specific, extra round of whole genome duplication[133–135] that in principle endowed them with a richer, more amenable, but also further distant from the ancestral state, genetic template relative to all other vertebrates[136–138]. Undoubtedly, numerous crucial insights about visual circuits structure and function have been gained from established model organisms and these findings can be valuable anchors for comparative approaches, but these animals were nevertheless not studied based on the relevance of their phylogenetic position.

Which vertebrates would therefore be appropriate as a window to the past? Agnatha, meaning jawless in Greek, are the earliest diverging and still extant vertebrate lineage, represented only by few species of hagfish and lampreys. However, hagfish possess a relatively simple retina[139,140] (but see[141,142]), within a rudimentary eye that lacks fundamental optical components[116]. And although the lamprey retinas respect the fundamental vertebrate blueprint, they nevertheless

are of characteristically slow development[143] and come with certain peculiarities of still debated (basal or derived) status[144,145].

Next in line in terms of historical endurance are chondrichthyan fish. A slowly evolving[146–149], monophyletic group that comprises of Elasmobranchii (sharks, skates and rays) and Holocephali (chimaeras), Chondrichthyes have survived over 400 million years and occupy a key phylogenetic position in representing the early stages of gnathostome (i.e. possessing jaws) vertebrates. Despite inherent difficulties in studying them, they have already proven invaluable in deciphering the origin and diversification patterns of vertebrate body plan in several cases, from the emergence of paired appendages[150,151] to the development of the telencephalon and the cerebellum[152,153]. Interestingly for the characters above, due to teleosts and tetrapods displaying different states it was often hypothesised that the latter were the ones innovating. The inclusion of elasmobranch flipped the relation on its head, with sharks and tetrapods likely reflecting the ancestral state and with zebrafish diverging. So, what can we learn from the visual system of sharks?

The Visual System of Sharks

Despite their elaborate optics[154,155], sharks are historically considered to possess poor vision[156]. This view is partially rooted in early work identifying high sensitivity in other elasmobranch sensory modalities, and olfaction in particular[157], and further supported by the first examinations of elasmobranch eyes describing either a sole presence or heavy dominance of a single photoreceptor type, namely the rods[158,159]. At odds with all other vertebrates possessing a duplex[160] (rods and cones) retina, this suggested that the rod-dominated elasmobranch visual system could only cope within dimly lit environments, whilst saturating and rendering the animal virtually blind at higher light intensities.

As it turned out, this was due to two sampling issues. Although the incidentally first to be studied, benthic, bottom-dwelling sharks come with high rod to cone ratios, the representation of the cone is substantially increased in their epipelagic, actively swimming relatives[99,158], thus correlating with the organisms' lifestyle or penetrating light at the depth inhabited[13,161,162]. And second, even in the pure-rod retina of the skate, the photoreceptor terminals and connectivity demonstrate

certain conelike characteristics[163] and can nevertheless progressively escape saturation, functioning at intensities previously thought exclusively operational (i.e. non-saturating) for cones[164–166].

Notwithstanding this reduction in the number of input channels, the shark retina adheres to the vertebrate bauplan in its structure and cellular composition. All cell classes are present and occupy characteristic positions, except for a relatively increased, compared to other jawed vertebrates, ratio of displaced RGCs[71] in the IPL and INL[138,167–169], a feature nevertheless typical of early diverging vertebrates[72,143,144]. Moreover, within classes and for several different elasmobranch species, a vertebrate-conventional morphological diversity of subtypes has been described in properties like soma size, dendritic branching, and sublayer localization of the cell soma (for HCs) and synaptic terminals (for HCs, BCs and RGCs)[99,155,168,170,171].

Thesis Aims

With the structure, molecular and wiring complexity vastly conserved, what about the functional processing in these anciently diverging vertebrate retinas, and what can it tell us subsequently about visual circuits at the origin of vertebrate life?

The work presented here primarily provides a nearly complete description of the basic functional output of the elasmobranch retina. Due to the tools available, the few early attempts on elasmobranch retina physiology may have suffered from methodological limitations (low sampling or low resolution)[164,172–175]. Here I exploit state-of-the-art, high-throughput recording techniques and broadly characterize, for the first time, the functional output of a shark retina using the small-spotted catshark *Scyliorhinus canicula* as a model.

Chapter 4 is primarily centered on the structure and elementary response properties of the shark retina. Specifically, I examine how they encode fundamental parameters of the visual image, like brightness increments/decrements and spatial/temporal frequencies. Furthermore, I touch upon retinal computations. Of possible candidates, direction selectivity is the most meticulously investigated and, in its implementation, arguably among the best understood neural computations of the vertebrate central nervous system.

In vertebrates and invertebrates alike, visual systems compute direction of motion but algorithmically do so in fundamentally different ways[176–178]. In Chapter 5, I employ pharmacological perturbations to illuminate the wiring diagrams and neurotransmitter logic upstream of RGCs. Specifically, I evaluate how the ON pathway is implemented and what role inhibition plays in the organization of early visual circuits and their computations.

As already outlined, within vertebrates the retinal structure and molecular composition is fundamentally and strikingly conserved. But what about outside the vertebrate lineage? Across extant organisms, vertebrate retina-like complexity is virtually unheard of. Over the past century, several hypotheses have been put forward in attempts to identify homologous organs and account for the origin and evolution of the vertebrate retina. Currently, the frontal eye of amphioxus is regarded as the likely homologous tissue candidate[179–181], and a gradation of events for ever-increasing structural and molecular complexity is proposed for the evolution of the vertebrate eye[116,117]. Specifically, the classical view argues for a gradual transition from a state of close apposition of two ancestrally distinct photosensitive systems (represented in its modern-day retinal descendants by photoreceptors and ganglion cells, respectively) to their eventual wiring, and from there to the emergence of retina-specific interneurons, like the bipolar cells. In light of recent findings and a critical re-evaluation of the old, in Chapter 3 I argue that we most likely got the sequence of events wrong. Instead, I propose a novel theory for the origin and evolution of this enigmatic and computationally complex tissue, where retina-like complexity in fact predates the eye. Importantly, I posit that a third, previously undisclosed and ‘molecularly promiscuous’, photoreceptive type played a pivotal role in the early emergence in vertebrates of various chimeric cell types via co-option, and in such likely facilitated the subsequent wiring of the vertebrate retina into existence.

Chapter 2 – Methods

Animal Provision and Housing

Access to fresh ocular tissue is of paramount importance for recording physiologically meaningful responses. My initial attempts at sourcing shark eyes from bycatch of fishmongers, though successful, were not fruitful. By using off-the-shelf, commercially available components, I instead set up my own shark facility at the University of Sussex. Together with establishing a more standardized provision of animals, this allowed for controlled conditions and a concomitant increase in the reproducibility of experiments.

Embryos of different stages were obtained from North Wales Biologicals and kept both pre- and post-hatching in tanks of the custom-built water circulation system. Frozen blocks of krill (*Euphasia pacifica* and *Euphasia superba*) purchased from BCUK were provided ad libitum, and water parameters and partial changes were measured and performed on a regular basis. Water salinity and temperature were maintained within 32-35 ppm and 13-16 degrees Celsius respectively. Tanks were enriched with gravel and hollow caves, and animals were not kept in isolation at any point. The night-day cycle was fixed to 12 - 12hr, from 7pm to 7am.

Animal Handling

All procedures performed were in accordance with the UK Animals Scientific Procedures act 1968, and additionally locally approved at University of Sussex by the animal welfare committee. For the *ex vivo* retina recordings, shark hatchlings between the ages of 2 and 8 months old were dark-adapted overnight or minimum for 3 hours, and euthanized with tricane methanesulfonate (MS222 Sigma-aldrich) under dim red light.

Preparation of the *ex vivo* retina

Ringer Solution

The enucleated eye and under-dissection retina were retained in physiological conditions *ex vivo* by perfusion with oxygenated (95% O2 + 5% CO2) Ringer solution. Contrary to warm-blooded vertebrates, oxygen provision was not of vital importance for the shark retina both during dissection and during recordings, in agreement with previous reports of the elasmobranch retina being devoid of vasculature[154,182]. As the Ringer solution is meant to recapitulate the *in vivo* circulation of relevant nutrients and salts, getting the relevant concentrations right

is of high importance. Compared to more established model organisms, different Ringer solution variations had been used in earlier work on elasmobranch fish[175,183–190] and there is yet no established protocol for physiology recordings in these species (John Dowling, Nathan Hart, personal communications). Standardizing a reliable elasmobranch Ringer solution required over 7 months, and the one employed is an adapted version[191]. Namely, the following concentrations of salts were used (in mM): NaCl 260, KCl 2.95, Urea 350, $CaCl_2$ 3.97, $MgSO_4$ 0.24, $NaHCO_3$ 20, D-Glucose 10.

Tissue Preparation

Isolation of the eye was promptly achieved by carefully cutting the skin around the cornea followed by a single cut near the optic nerve head to avoid strain and mechanical damage of the RGC axons.

To allow for physiological-like replenishment of nutrients, the cornea was immediately after punctured, permitting perfusion of oxygenated Ringer solution. The following steps were performed for the isolation of the retina:

1) A shallow cut vertically, facilitating cutting away the cornea and removing the lens
2) Cutting away the ventral side of the retina (including the optic nerve head) to allow for easier flattening of the remaining tissue
3) To the extent possible, removing the vitreous fibers with forceps and carefully unwarping the inner limiting membrane in threads with needles
4) Transferring the tissue on an Ano Disk (Cytiva Whatman Anodisc Filter Membranes, FischerScientific) with the retina pigmented epithelium (RPE) side facing the disk
5) Swiftly and transiently drying out the disk+retina onto absorptive paper, facilitating tissue flattening on the Ano Disk
6) Transfer of the disk+retina back into the chamber for rehydration with Ringer
7) Covering the exposed side of the retina (RGC layer together with remnants of vitreous fibers and inner-limiting membrane) with a filter paper, and repeating step 5 and 6
8) Detaching the Ano Disk, with the retina (and often the RPE) staying attached on the filter paper
9) Cutting a retina+filter paper piece ca 5mm^2, corresponding to ventral or temporal region

10) Detaching the small retina piece from the underlying filter paper, and
11) Further trimming was performed as appropriate (resulting in pieces of 2.5-3mm^2) to avoid the tissue folding at any region, because that negatively and substantially affects the ability and quality of the RGC recordings with the multi-electrode array (MEA).

Placing the tissue on the MEA

1) The tissue was transferred to the MEA chamber using wide glass pipettes to ensure minimal injury during the process
2) The tissue was positioned on the array of the electrodes (recording area)
3) To ensure tissue flatness on the recording area, the recording chamber was gradually dried out, at a gross scale with a pipette and the remnants with absorptive paper
4) The chamber got swiftly rehydrated with a slow and steady flow of fresh Ringer to ensure the retina remained on the recording area
5) An appropriately light, custom designed and 3-D printed weight was gently placed on top of the retina to achieve maximum flatness and contact with the recording array of electrodes. This weight had an Anodisk-fitted window to allow for light stimulation of the tissue during recordings
6) The tissue was allowed to recover and achieve its final spatial coordinates on the array for 30 minutes before any recording attempt

Pharmacological Manipulation

In a subset of experiments, the functional organization of the shark retina was perturbed by pharmacological agents. The concentrations of all the applied pharmacological agents were well within ranges described in literature. Specifically, the AC-mediated inhibitory pathways of the retina were perturbed by application in extracellular space concentrations of: 10μM gabazine (Sigma-aldrich #S106-10MG) and 75μM TMPA (Sigma-aldrich #T200-10MG), as antagonists of $GABA_A$ and $GABA_C$ receptors respectively, and 20μM strychnine (Sigma-aldrich #S8753-25G) as antagonist of glycine receptors.

The ON-pathway of the retina was perturbed at the synapse between photoreceptor and ON BC by application in extracellular space of L-AP4 in concentration of 50 μM (Sigma-aldrich A7929-.5MG) as agonist of the mGluR6 receptor.

To ensure consistency, no stimuli were played for the first five minutes of administering the agents. The time lapse for effects to be observed was experimentally determined in pilot experiments by using a brief (1s, 3 repeats) 'white' light flash.

Light stimulation

Given that the recording array, which is direct contact with the RGCs, is not transparent, light stimulation is provided in the somewhat unnatural way (photoreceptors-first) of not travelling first through the non-photosensitive inner layers of the retina. However, this is a typical limitation of retina electrophysiology recordings with multi-electrode arrays.

Light stimulation during the MEA recordings was technically achieved by means previously described[192,193]. Briefly, for the presentation of custom-designed visual stimuli a beam splitter was used to combine light patterns generated by six spectrally distinct LEDs (with their emission peaks centered at 360, 420, 480, 505, 560, 630 nm). Split in two groups of 3, the LEDs were under the control of fibre-coupled LightCrafters (DLP 4500 MKII, Texas Instruments, EKB) communicating as display screens with the stimulation computer. By using the QDSpy syntax (developed by Dr. Thomas Euler, http://qdspy.eulerlab.de/), the relevant, custom-written in Python, stimuli were encoded on the LightCrafters. The images were finally focused on the tissue by appropriate lenses and mirrors.

The resistance of all LEDs except the 360 nm was adjusted accordingly for the stimulus power to be wavelength-independent, meaning that each LED at its full intensity illuminates the retina with the same power. Situated at its maximum power, the 360 nm LED was half the value of the others.

The stimuli routinely used in this work are as follows:

1) Full Field Flashes (FFF) – Alternating, 2s "steps" of light ON and OFF for each LED, in sequence of decreasing wavelength
2) Chirp – Interspaced by steps of light, a stimulus alternating in exponentially increasing frequency (up to 8 Hz, 100% contrast) or contrast (fixed at 0.2 Hz)
3) Moving Bar (MB) – A white light ON bar that sequentially moved in 8 directions (0, 180, 90, 270, 45, 225, 135, 315 degrees) entering from full dark and allowing for sufficient return to full dark before the next direction was sampled. To avoid

spatial location artefacts, the bar was stretched into a field. Therefore, a more accurate name for the stimulus would be ‘Moving Field’, but as no ‘stretching’ deviations are expected in the response, in line with literature I still refer to it as such.

The above comprise the template also used in the experiments where drug application was performed.

In some experiments, additional stimuli were employed:

1) Variable Duration Flashes (VDF) – Alternating, full field steps of white light ON and OFF, in sequence of increasing duration (50/100/200/500/1000/2000 ms)

MEA Recordings

Hardware

Both the platform (BioCam X) and the MEA chips (Arena HD-MEA, 3ml well) used are produced by 3Brain AG. The recording area (2.67 mm^2) of the chip consists of 4096 (64x64) electrodes (each 21 μm^2 and 42μm pitch).

Software

Live-monitoring and data acquisition was performed in Brainwave 4 (3Brain AG). The sampling frequency of recordings was 17852 Hz, determined by setting the integration time to ‘medium’.

Spike Sorting and Unit Clustering

Herding Spikes 2 (HS2) was used, with underlying algorithms taking into consideration (and weighting differently) both spike waveform and location information[194]. For the shark RGC recordings, the following values were assigned to the relevant parameters:

'clustering_bandwidth': 8.0,

'clustering_alpha': 5.5,

'clustering_n_jobs': -1,

'clustering_bin_seeding': True,

'clustering_min_bin_freq': 16,

'clustering_subset': None,

'left_cutout_time': 0.3,

'right_cutout_time': 1.8,

'detection_threshold': 5,

'probe_masked_channels': [],

'probe_inner_radius': 70,

'probe_neighbor_radius': 90,

'probe_event_length': 0.26,

'probe_peak_jitter': 0.2,

'num_com_centers': 1,

'maa': 12,

'ahpthr': 11,

'out_file_name': 'HS2_detected',

'out_file_cluster': 'HS2_sorted.hdf5',

'decay_filtering': False,

'save_all': False,

'amp_evaluation_time': 0.4,

'spk_evaluation_time': 1.0,

'pca_ncomponents': 2,

'pca_whiten': True,

'freq_min': 300.0,

'freq_max': 6000.0,

'filter': True,

'pre_scale': True,

'pre_scale_value': 20.0,

'filter_duplicates': True,

Data Analysis

Following Spike Detection and Unit Clustering, the data was subsequently analysed in Python using custom-written scripts.

Basic Processing and Evaluation

The elementary template with which data can be readily assessed, reshaped and evaluated relative to stimulus checkpoints was previously developed and employed by Dr. Marvin Seifert (see Ref[192]). As such, pre-existing scripts were modified and novel ones were developed on top on a case-by-case basis ensuring compatibility.

PSTH

Visualising the responses of single-cell (across trials) or population (across cells) by means of peri stimulus time histograms (PSTH) is the gold standard of neural recordings. Unless otherwise noted, such quantifications were calculated with a bin size of 0.05 s, separately for the three response polarity groups (ON, ONOFF, OFF). Unless otherwise noted, rows of individual neurons in the population plots were sorted by polarity, and then ordered by number of events (spikes). In the single-neuron plots, rows represent individual repeats of the same stimulus. For the responses to FFF and chirp, rows were sorted by presentation wavelength and ordered within their temporal sequence – bottom row of each group was the response to the first and top row to the last presentation of the stimulus.

Quality index (QI): The QI for the stimulus-specific response was computed as the division of the variance of the mean response by the mean variance of it[122], with the trial-specific kernel estimated by fitting a gaussian kernel for each spike.

$$\mathrm{QI} = \frac{\mathrm{var}[\mathrm{mean}(\mathrm{X})]}{\mathrm{mean}[\mathrm{var}(\mathrm{X})]}$$

The response matrix X is dependent on both the stimulus length and number of repeats and thus a different, stimulus-specific cutoff threshold was set for determining the quality of the response. The threshold was 0.146 and 0.497 for FFF and Chirp respectively, while the quality control for MB was performed statistically with a different method (see below). Upon pharmacological perturbations, an RGC was considered responsive if the quality index response was above 0.118 (manually assessed from the distribution of data and visual inspection).

Opsin templates and log transformations

The rod visual pigment of the catshark retina has λ_{max} of 502[13,182] and its absorbance is described by the Govardovskii template[195] (Python implementation

used here is by Dr. Marvin Seifert). Log-transformed opsin templates were acquired as described previously[196]. Briefly, a linear transformation was used, with its parameters optimised to minimise the mean squared error (MSE) between the function and the data (population responses to FFF).

$$f_{a,b,c}(\mathrm{x}) = \mathrm{a} * \log(x + b) + c,$$

$$a, b, c = \mathrm{argmin}_{\mathrm{a,b},c}, \mathrm{MSE}(f(\mathrm{a,b,c})(\mathrm{opsin}), y_{data})$$

Polarity index: The polarity index was computed as

$$\mathrm{PI} = \frac{\mathrm{A_{On}} - \mathrm{A_{Off}}}{\mathrm{A_{On}} + \mathrm{A_{Off}}}$$

where A_{On} and A_{Off} represent the number of spikes for luminance increments and decrements respectively. The index ranges from -1 to +1 (pure OFF and ON RGC respectively), and RGCs whose polarity value falls within -0.33 and +0.33 are considered ONOFF.

Transience index: The transience index was computed by calculating the interval [-MAD, +MAD], with MAD representing the median absolute deviation. For ONOFF cells, the mean value of the ON and OFF transience is reported.

Tuning Curves

The mean response amplitudes of single RGC cells or populations were computed within stimulus properties-dependent, relevant temporal windows.

Direction-selectivity index (DSI): The DSI was computed as

$$\mathrm{DSI} = \frac{\mathrm{A_{dom}} - \mathrm{A_{null}}}{\mathrm{A_{dom}} + \mathrm{A_{null}}}$$

where A_{dom} and A_{null} represent the number of spikes in the dominant (preferred) and in the reverse (null) direction, respectively.

Statistical significance for direction-selectivity: The statistical evaluation of how 'real' the observed DSI is based on bootstrapping. Specifically, for each neuron of interest, a population of n=1000 simulated neurons with the same total number of spikes as the real neuron is created (using the PySpike package[197], https://github.com/mariomulansky/PySpike), but with each having the spikes randomly assigned in time relative to the stimulus direction or repeat. The DSI for

each simulated neuron is then computed, and whether our neuron's DSI is above 95% of the simulated is evaluated.

Analysis of RGC responses to the Chirp stimulus

To establish the extent to which a responsive neuron is tuned in line with stimulus fluctuations in temporal frequency or spatial contrast, the vector strength of the phase-lock is computed as previously[198–200]. Briefly, the vector strength is a quantification of how well aligned the impulses are to features of the stimulus, and it ranges from 0 (random, stimulus-invariant response) to 1 (each impulse synchronised to the stimulus feature).

The statistical significance of the vector strength was evaluated on a single-neuron basis by bootstrapping, in a similar approach to the direction-selectivity case outlined above.

Statistics

As this work principally concerns the first large-scale description of the retinal output of a shark, foundational descriptive statistics are routinely used.

The following inferential statistics were used in a case-by-case basis:

1) Wilcoxon signed-rank test for paired comparisons of control (pre) and pharmacological (post) conditions. Implementation with the scipy.stats package.
2) For comparison of number of spikes for preferred versus null direction of stimulus movement, Wilcoxon signed-rank test for paired comparisons and t-test with Bonferroni correction for multiple comparisons. Implementation with the statsmodels.stats package.
3) Mann–Whitney U rank test, with the *exact* method when the small number of independent samples required it for comparing properties by retinal region (temporal versus nasal). Python implementation with the scipy.stats package .
4) Two-sided confidence intervals (CI) for the mean of population responses – implemented in Python with the statsmodels.stats package.

Unless otherwise specified, alpha was set to 0.05, and error bars represent the standard error of the mean (s.e.m).

Electrical imaging

To evaluate, based on the presence of an axon, whether an identified unit (as a result of the spike sorting and unit clustering) corresponds to an RGC or to a

displaced AC, the electrical footprint of the cell was computed as previously[192]. Briefly, all spikes assigned to the specific unit were reverse correlated with an n= 50 bin (10 frames before and 40 frames after of each spike) MEA voltage signal to compute a spike-triggered average. This algorithm is developed by Dr. Marvin Seifert (see Ref)[192].

Tissue preparation for immunostaining and confocal imaging

Shark hatchlings between the ages of 2 and 5 months were euthanized with MS222 and the pressure-relieved, isolated eyecups were fixed in 4% PFA (Agar Scientific) in phosphate-buffered saline (PBS) or in shark Ringer for 20 mins at room temperature. Tissue was washed three times in PBS, and cornea, lens and pigment epithelium were removed. For permeabilization, tissue was treated with 0.5% Triton X-100 in PBS, followed by the addition of primary antibodies and incubation at 4 degrees Celsius for 3 to 5 days. In between washes with PBS, the tissue was treated with secondary antibodies at 4 degrees Celsius for 1 day. For imaging purposes, the tissue was mounted with Vectashield media (H-1000, Vector Laboratories) between a coverslip and slide microscope glass.

Primary antibodies were Rhodopsin – 1D4 (mouse, 1:500, Santa Cruz Biotechnology), GABA (rabbit, 1:500, Sigma-aldrich), ChAT (goat, 1:100, Sigma-aldrich), RBPMS (rabbit, 1:500, Thermofisher). Image stacks were acquired on a TCS SP8 confocal (Leica).

This protocol was performed in its entirety by Dr. Takeshi Yoshimatsu and Dr. Michael Forsthofer.

Brightness, contrast and pseudo-color were adjusted for presentation in FiJi[201]. Stacks were stitched using the ImageStitching plugin[202], while cells were manually counted using the CellCounter.

Tissue preparation for serial-block face scanning electron microscopy

Shark hatchlings of 3 months age were euthanized with MS222 and the pressure-relieved, isolated eyecups were fixed in 4% glutaraldehyde in 0.1M sodium cacodylate buffer, pH 7.3 for 3 hours at room temperature. Retinal pieces (temporal region) were then shipped to University of Washington (to Dr. Sharm Knecht and Prof. Rachel Wong) for tissue preparation for serial-block face electron microscopy (SBEM) according to previously published protocols[203,204].

The SBEM used was GATAN/Zeiss SIGMA 3View, and the voxel size of the image stacks acquisition was 6x6x60 nm, for a total volume of approximately 123x151x11 µm.

Image Analysis

Following upload of the EM micrographs to WebKnossos[205], they were aligned and stitched by ScalableMinds (https://scalableminds.com/). Cell somata and their processes (dendrites, axons) that stratify in the inner plexiform layer were manually traced as skeletons. In a coordinated manner, bipolar cells were annotated by Prof. David Berson (Brown University), while I evaluated the BC skeletons (and annotated synapses and identity of post-synaptic partners). Furthermore, I focused on skeletonising the retina ganglion and displaced amacrine cells that reside in the ganglion cell layer and in the inner plexiform layer. A cell was categorised as an RGC or AC based on the presence or absence of synaptic vesicles in its dendrites[204,206].

EM Data Analysis

Together with relevant metadata like synapse locations and partners, cell skeletons were exported from Webknossos as .nml files (see supported data formats), and all analysis was performed with custom written scripts in Python.

EM Data Statisticts

As the EM data presented here reflect ongoing, manual and time-intensive work, and many cells types are sparse, perhaps not repeated in the volume, it is currently not feasible to provide statistical support for some of the observations presented.

Chapter 3 – Retina complexity predates the vertebrate eye

Abstract

The complexity of the vertebrate retina, with its more than a hundred molecularly, anatomically and functionally distinct neuronal building blocks, is arguably at least on par with that of the cerebral cortex. However, unlike the cortex, the retina is ancient and common to all vertebrates. The retina's extreme overall conservation across the entire lineage strongly implies that it was already well established in the last common vertebrate ancestor, some 540 million years ago. But what happened before that?

Since the time of Darwin, all influential scenarios put forward widely accept complexity as an emergent property of the vertebrate retina. Here I argue that this is the wrong way round. Complexity appeared first, and in fact enabled the emergence of the lateral eyes.

Specifically, I argue that many of the fundamental building blocks that make up the vertebrate retina, including interneurons such as bipolar cells, predate the lateral eyes. They first emerged in a median eye precursor that uniquely merged ancestral photoreceptor lineages like the ciliary and rhabdomeric. Today, both the pineal and the retina are direct descendants of this ancestral chimeric eye. Of these, the defining novelty for the retina is the intimate connection between ciliary and rhabdomeric circuits, which though present, remain largely independent in the pineal. A retina-like merging of these two ancestral photoreceptive systems is not encountered in eyes outside of vertebrates and might have been facilitated by chimeric cell types that emerged gradually as the result of the rare, close apposition of at least two photosensitive systems.

Introduction

As already outlined, vertebrate vision is highly conserved in its neuronal implementation (see Introduction). Briefly, the blueprint comes neatly organised in alternating layers of cell somata and synaptic wiring, and the five different neuronal cell classes it comprises of do occupy distinct and characteristic positions. Horizontal and bipolar cells are located downstream of photoreceptors, while amacrine and retina ganglion cells occupy the most vitreal position. In terms of information processing, there are two pathways in the vertebrate retina. The

main, glutamatergic pathway is vertical and involves photoreceptors, bipolar and retinal ganglion cells while the laterally spreading one consists of the horizontal and amacrine cells that at separate synapses tweak the vertical by multifaceted codes of feedforward and feed-back connections. Crucially, this layered spatial arrangement, high cellular diversity and the information flow logic are all unequivocally present across the vertebrate lineage and thus ancestrally originating and thereafter inherited. But then, how and from what template did this blueprint arise in the first place?

A possible explanation for the emergence of this high neuronal diversity in the vertebrate eye is by ‘division of labour’ (i.e. duplication of an ancestral precursor and subsequent divergence)[207,208] enabled or accelerated, as is the case with other novelties[209], by two rounds of whole genome duplications occurring basally to all vertebrates[210,211]. As revealed by patterns in expression profiles of transcription factors and effector genes during cell type differentiation, the vertebrate retina is indeed comprising of at least two, ancestrally distinct lineages initially categorised solely on the different origin of their membrane ramifications[212,213], namely ciliary and rhabdomeric. Specifically, horizontal, amacrine and retinal ganglion cells are sister cell types, descending from the same ancestor that has also given rise to the rhabdomeric photoreceptors of invertebrate lateral eyes[207,214], whereas vertebrate retina visual photoreceptors are ciliary in nature and have emerged from a different ancestral cell type. Finally, the bipolar cells, aptly named after their morphology and dealing with the task of synaptically wiring these two ancestrally distinct photoreceptive systems, remain of uncertain origin (but see Ref[116]).

Despite knowledge of the distinct molecular lineage of its components, tracing the origin of the vertebrate retina is still by no means trivial. As soft tissue does not preserve, the fossil record cannot by itself be very informative (but see Ref[215]). And perhaps perplexing things further, vertebrates are unique among extant organisms in possessing in their lateral eyes the high diversity of cell classes outlined above. In fact, in most extant eye-bearing animals the second-order neurons are situated extraocularly, with the eyes exclusively comprising of photoreceptors and supportive cells that are only in some cases pigmented.

Several intriguing hypotheses have been proposed for the evolution of the vertebrate eye. In search for a homologous organ outside of vertebrates, the currently prevalent scenarios nominate the frontal eye (FE) of the cephalochordate amphioxus based on molecular signatures of ciliary cell types and relative position in the body[179,180,216]. Furthermore, it is argued for an evolutionary timeline where the wiring of the ciliary and rhabdomeric lineages, exemplified in the vertebrate retina photoreceptors and ganglion cells respectively, predates the emergence of the eyes themselves. Importantly in this scenario, the proto-retina has only two nuclear layers and resembles the pineal organ in consisting of photoreceptors connecting directly to ganglion cells, while other vertebrate retinal classes such as the bipolar cells, are retina-specific and late additions in the lateral eyes[116,117].

Rooted in the molecular history of its components[129,207], here I propose a novel scenario for the emergence of the vertebrate eye, in which retina-like complexity predates and enables the retina itself. Based on re-evaluation of findings old and new, I posit that the retina originated in the common vertebrate ancestor from a dorsomedially located precursor, an ancestral median eye (AME), that subsequently got lateralised. Crucially, the AME was already complex in its cellular composition and computational power, comprising of ancestrally distinct – as already existing in the common Urbilaterian ancestor – photosensitive clusters, each with their own properties and roles subserved for the organism. Retina-like bipolar cells were already present in the AME as second-order neurons for one photosensitive cluster, but distinctively from the situation in the retina, they did not act locally but were themselves projection neurons, conveying information directly to higher brain regions. Importantly, the close apposition of different photosensitive clusters likely additionally facilitated the emergence of novel, chimeric cell types via co-option[217–219] , and both the ancestrally distinct systems, their modern relatives and the emerged chimaeras can still be found nowadays in an extant version dorsomedially, namely in the pineal organ of early diverging vertebrates. Therefore with regards to the pineal, its sister organ[116,220,221], the defining evolutionary novelty of the retina is not the explosion of cell types but that distinct systems got glued together, wiring it up into existence and expanding its computational prowess.

In the following sections, I summarise relevant findings spanning decades of work in disparate fields and revisit how the currently prevailing scenarios, though influential, need to be revisited in light of recent findings. When possible, I turn the spotlight on individual arguments and gradually build towards the unified hypothesis for the evolution of the vertebrate retina, relying on the extensive and striking similarities it bares with its sister organ, the pineal. For these reasons I include a brief and targeted overview of the pineal organ, before expanding on a case-by-case basis for the construction of my hypothesis. But as the scenario for the evolution of the vertebrate retina is based on the molecular history of its components[129,207], I first present the two photosensitive systems that fundamentally constitute it.

Ciliary and Rhabdomeric Photoreceptors – Ancestrally distinct, serving different tasks

In extant animals, two major photosensitive classes are distinguished, ciliary and rhabdomeric. Coined to describe the distinct origin of their membrane ramifications, these two systems also differ in several other ways. Their development and differentiation depend on distinct gene networks[222]. Functionally, their photopigments belong to ancestrally distinct classes[223,224], and different transduction cascades[225] are utilised to eventually elicit light-driven electric responses of opposite polarity[226]. Ciliary are often unpigmented, compared to their rhabdomeric counterparts. And in terms of roles served for the organism, they seem to differ once again; the ciliary primarily measuring intensity and mediating circadian entrainment, the rhabdomeric body posture, phototaxis and object vision[221,227–229].

Intriguingly, the defining properties of the two systems might even account for the observed order of their wiring in the vertebrate retina. By placing the rhabdomeric system with its topographic projections presynaptically to the slow, endocrine-like ciliary, the properties of the former would have been muted and the latter would become ambiguous. Instead, by having the multifactorial connect on top of the specific, parallel and diverse channels can emerge and convey visual information in a targeted manner to the relevant regions. Of interest, this is the order of wiring not only in the closely apposed case of the vertebrate lateral eye, but also in the

polychaete Platynereis, between the rhabdomeric lateral and ciliary median photosensitive systems[230].

Combining properties to resolve ambiguities

For such fundamentally distinct systems however, they generally do not seem to like each other. Although both were present in the common urbilaterian ancestor[224,231], usually it is the rhabdomeric that builds the eyes of the animal, with the -typical of vertebrates- ciliary lineage either entirely lost or retained, as in the case of polychaetes, as a largely separate photoreceptive system in the brain (Fig. 3.1).

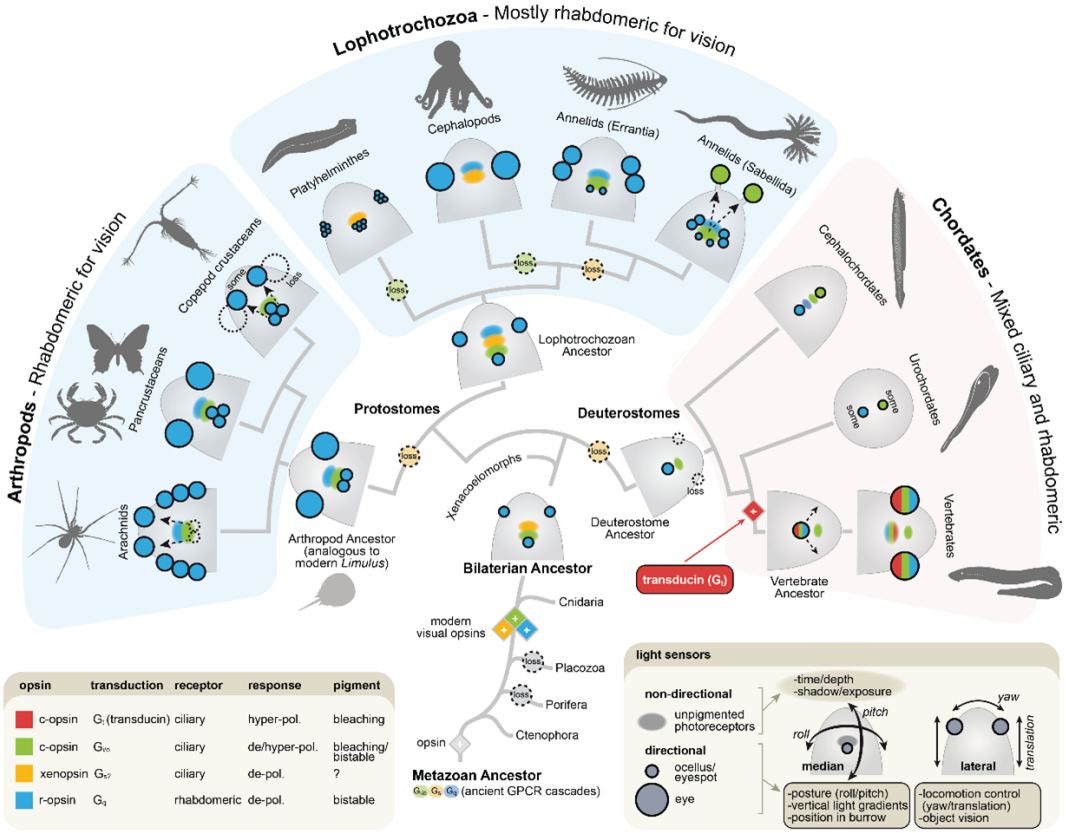

Figure 3.1 – Position and type of photoreceptor cells in the bilaterian head. Schematic (dorsal view) of selected bilaterian heads (based on Refs[180,216,224,231–253]). The position of photoreceptors is indicated as eyes (large circles), simple directional ocelli (small circles) or non-directional clusters (diffuse ellipses). With regards to position, an important distinction exists between photoreceptors in median clusters in the brain or close to it, and paired lateral organs. Colours indicate ciliary versus rhabdomeric photoreceptors, with their specific opsins and properties (*lower left panel*). Typical

functional roles for paired lateral versus median photoreceptors are indicated in the *lower right panel*. The visualised reconstructions overwhelmingly suggest ciliary photoreceptors as unpigmented (non-directional) median clusters in the brain, and rhabdomeric photoreceptors in paired lateral eyes or ocelli (with pigment or not). Vertebrates stand out as exceptions, with both median (pineal/parapineal organ) and lateral eyes containing ciliary photoreceptors located presynaptically to neurons of rhabdomeric origin. Given the general absence in deuterostomes of paired lateral eyes/ocelli with primary rhabdomeric photoreceptors, a loss of the ancestral lateral eyes is likely. Vertebrete eyes are then later derived from the retained median photoreceptors, explaining the unorthodox components and circuits.

Observing the widespread occurrence of such mutually exclusive patterns, one might ponder the functional gains of retaining them both. In keeping them separate, the benefit probably cannot be greater than the sum of its parts. However, novel processing and behavioural traits can likely emerge were they to be closely apposed, inform the same targets, or one feed in or hijack the circuits of the other. We posit that this could be especially handy in assessing the visual environment, a vital task for the organism striving to appropriately adjust its behavioural state. Although the relevant information exists in luminance values, different environmental factors like time of day, weather conditions and – specifically for aquatic environments – water depth or quality all chip in in determining them (see also Introduction).

Therefore, there is strong selection pressure for mechanisms that can de-multiplex and resolve these ambiguities. One solution is to internalise and keep track of time of the day semi-independently of external stimuli; a feat neatly achieved by the circadian clock. Another approach, pertinent to combining photosensitive systems of distinct properties, is using a slow system in integration and output, the ciliary, for measuring the intensity of the vertical light gradient while the other for a different attribute of the same gradient, namely its spectral composition. This can be achieved thanks to the bistable nature of rhabdomeric opsins[112,226,254], with their state being indicative of the wavelengths present in the surrounding world. A third solution can be implemented on the organismal level: by appropriately relocating the photosensitive organs to simultaneously access different regions of the vertical light gradient and in turn gradually subserve

different visual roles[255,256]. For an actively swimming organism, a lateral but not a dorsal eye introduces a dorsoventral gradient of photoreception, which could potentially be gradually fine-tuned to the visual statistics of its subfield of view. Relocating eyes on lateral positions may have lead to gradual increases in fitness, from choice of right depth in the water column, to body posture and visually-guided locomotion (Fig. 3.2).

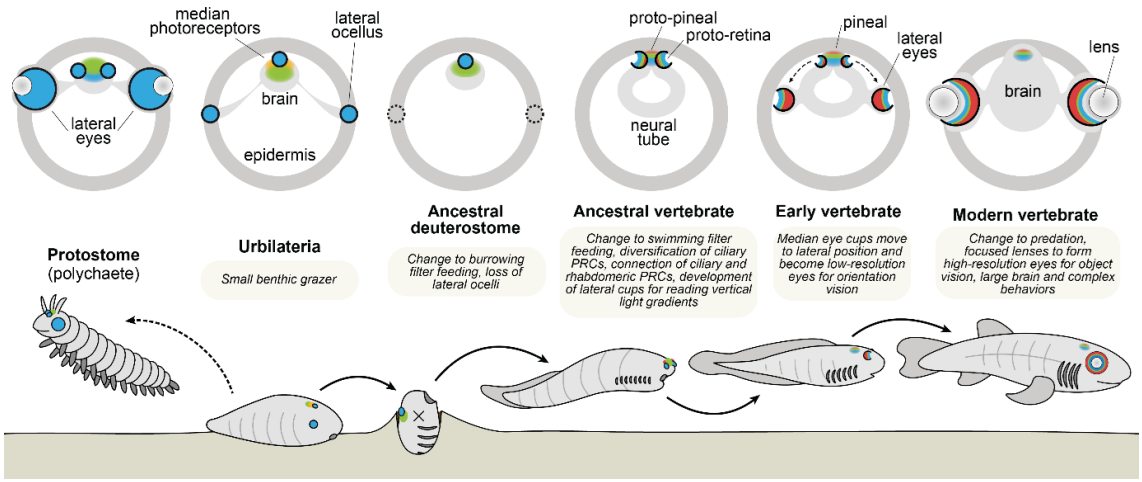

Figure 3.2 – Lifestyle changes align with the unique evolution of vertebrate eyes. Cross-section diagrams of likely photoreceptor and eye structures in the head of ancestral bilaterians (*top panel*), with presumed ancient lifestyles (*bottom panel*). The colours and graphical representations of photoreceptors correspond to Figure 1.

Lateralising a dorsomedial eye

In the few organisms the two photosensitive systems co-exist, their close apposition is extremely rare, observed only dorsomedially in the amphioxus, dorsomedially in the pineal organ and laterally in the eyes of vertebrates. Considering the striking resemblance of the two vertebrate organs that will be hereby covered, I echo past hypotheses in suggesting a median eye ancestry for the vertebrate retina[116,257,258], but I further posit that this close apposition facilitated the emergence of chimeric cell types with fundamental contributions for the emergence of the vertebrate retina.

But first, if the lateral eye has a dorsomedial ancestry as proposed, how can the evident lateralization and resulting location mismatch be mechanistically bridged? In development, both the retina and pineal organ are evaginations of

nearby regions of the neural tube, and their lumen spaces are diverticles of the third ventricle. For the lateral eyes, the processes participating in eye morphogenesis and retina differentiation are largely distinct. In fact, perturbation of the former spares the latter, with seemingly normal retinas forming atypically in direct attachment to the ventral hypothalamus and with the photoreceptor outer segments protruding into the lumen of the third ventricle[259,260]. Eye morphogenesis, which encompasses lateralisation alongside development of accessory ocular structures like the sclera, iris and cornea, is critically dependent on migratory and multipotent neural crest cells[261–263],long considered to be vertebrate lineage innovations[209] (but see[264]). As such, it can be argued that a retina of ancestrally medial origin ends up at a lateral location via largely independent to its differentiation, vertebrate-specific developmental processes.

Previous scenarios paint the proto-vertebrate retina as pineal-like in having ciliary photoreceptors wiring on rhabdomeric projection neurons, with the observed complexity being modern; an emergent, retina-specific property[116] (Fig. 3.3, *top*). In contrast however, I posit that this is the other way round; namely the wiring of the modern versions of the ancestrally distinct photoreceptive systems is a unique, defining novelty of the vertebrate retina that was probably facilitated by the pre-existing, albeit unwired, complexity within the ancestral pineal-like organ (Fig. 3.3, *bottom*).

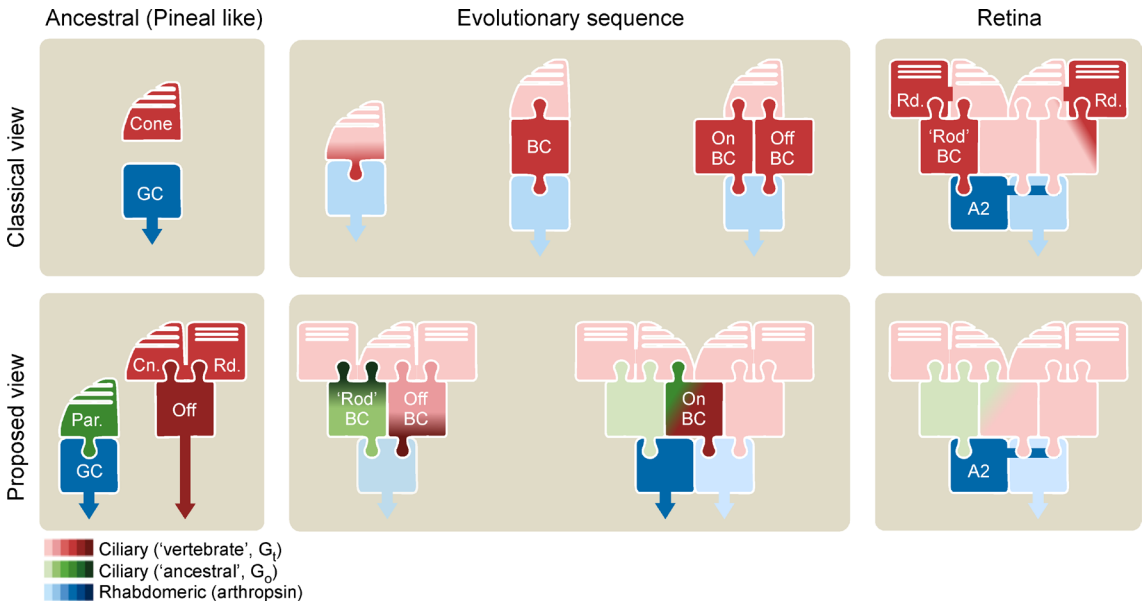

Figure 3.3 - Hypotheses on the evolution of the vertebrate retina. In the classical view (*top panel)*, the ciliary (red) and rhabdomeric lineages (blue) exist in close apposition initially and later get wired, forming a two-layer circuit. Then the emergence of bipolar cells (BCs) create the typical of vertebrates tri-layered motif, with the BC later differentiating in ON and OFF versions. Finally, the modern retina completes with the emergence of the rod photoreceptor together with its signalling system (here the primary pathway is depicted, e.g. rod -> Rod BC -> A2 -> ON and OFF cone-bipolar cells, see also Introduction). In the view (*bottom panel*) I propose in this chapter, bipolar cells are not late additions. Instead, they exist early on, as integral parts of parallel microcircuits (in an ancestral median eye). Notably, they are already present in different versions; OFF retina BC-like that are post-synaptic to pineal rods and cones, and rod BC-like that express parietopsin and feed into projection neurons of presumed rhabdomeric origin. ON BC-like types might not have existed in the ancestral pineal, but instead emerged, possibly more than once, later by co-option of the phototransduction (and later postsynaptic signalling) machinery from RBCs onto ancestrally OFF types.

The Pineal Organ – a median third eye full of gradients

In its evolutionary trajectory, the sensory pineal organ increasingly specialised for a neurosecretory role, exemplified by the increase of pinealocytes at the expense of photoreceptors and the concomitant increase in the production and secretion of melatonin[265]. In emphasising the relevant parallels to the lateral eyes[220], I therefore focus on the pineal organ of early diverging vertebrates that primarily consists of neuronal (photoreceptors and projection neurons) and glial (supportive) cells, with the presence of interneurons being debatable. In lampreys, which arguably possess the most neatly organised pineal organ, the photoreceptors are lining around the pineal lumen with their -typical of ciliary photoreceptors- photosensitive outer segments protruding in it, while the projection neurons display a sharp dorsoventral gradient, almost exclusively detected in the ventral and lateral sides of the lumen[266] (Fig. 3.4c). Interestingly, the response profiles of these neurons differ in a location-dependent, and also species-inspecific, manner, with the majority of rostrolaterally residing ones being chromatic ON and all the ventral luminosity OFF (achromatic)[267–272]. Moreover, the gradients do not seem to be restricted to projection neurons; to the contrary, the photoreceptors are expressing distinct ciliary opsins based on their spatial location too. Specifically, rhodopsin and iodopsin, opsins typically encountered

respectively in the rods and cones photoreceptors of the lateral eyes, are expressed in ventral photoreceptors, while their dorsal and rostrolateral counterparts express non-visual opsins such as parapinopsin and parietopsin[266,272]. And insofar as clear representatives of the rhabdomeric lineage go, melanopsin, namely the vertebrate-expressed opsin phylogenetically more closely related to invertebrate than vertebrate visual opsins, has been detected in the pineal organ of lampreys[273], zebrafish[274] and chicken[275,276]. Although detailed information from the other clades is currently lacking, in zebrafish it is reported in projection neurons, in accordance with its retinal profile in the intrinsically photosensitive ganglion cells[277,278].

Atypical ciliary - a third phototransduction type?

The modern pineal organ thus contains, in close apposition, descendants of the two distinct lineages, namely ciliary and rhabdomeric, whose opsins already existed in the common Urbilaterian ancestor alongside other opsin groups[223,224]. With ON melanopsin-expressing projection neurons belonging to the rhabdomeric and rods and cones to the ciliary, this categorisation seemingly leaves out pineal neurons like the parietopsin-expressing photoreceptors, which I here argue in their properties resemble members of a distinct photoreceptor type.

In being mediated by Go, the phototransduction pathway in parietopsin-expressing photoreceptors is neither characteristic of their rhabdomeric nor modern ciliary counterparts. And although a ciliary opsin itself[279], parietopsin phototransduction thus resembles members of a third, ancient and distinct phylogenetically, Go-utilising class of opsins, that is found in Bilateria except from Ecdysozoa[224] (Fig. 3.1). Further deviating from the robust ciliary and rhabdomeric descriptions, the Go-coupled phototransduction pathway additionally comes with evolutionary plasticity in several ways[219]. Though in mediating its effect through cyclic nucleotide-gated channels it is reminiscent of typical ciliary photoreceptors, physiologically it can lead both to cell depolarization or hyperpolarization in response to light[234,280,281]. Moreover, it can land on either side of extremes, intracellularly co-existing alongside other phototransduction pathways and thus expanding[282] or contributing to a complex, wavelength-dependent cell

response[234,283,284], or with its opsins entirely losing their contribution in phototransduction and instead acquiring an accessory role in enzymatically regenerating the cell's photosensitivity[219,285,286]. In line with the plastic (co-)expression of xenopsins[232,249,287], an originally regarded as typical ciliary but recently identified as distinct opsin clade, phylogenetically close to Go-coupled opsins[224], both these cases do not fit neatly in the ciliary or rhabdomeric phototransduction boundary. Therefore, I collectively group them to a separate phototransduction type, the atypical ciliary, and emphasise its pineal presence, in parietopsin-expressing photoreceptors, alongside the better described rhabdomeric and typical ciliary lineages.

How parietopsin, a ciliary opsin, ended up conveying its signal through Go phototransduction is unclear. Contrary to the lamprey case where expression is distinct[272], in the zebrafish pineal organ[283] as well as in reptilian parietal eyes[234,284], parietopsin and Go are co-expressed with parapinopsin and the -typical for ciliary visual photoreceptors- G protein transducin (Gt). Therefore, parietopsin could have at some point changed signalling from Gt to Go. The latter's broad medial expression without colocalization with a typical ciliary or rhabdomeric opsin has been reported in both protostomes and deuterostomes (Fig. 3.1), thus lending support for its independent presence before the speculated late coupling with parietopsin.

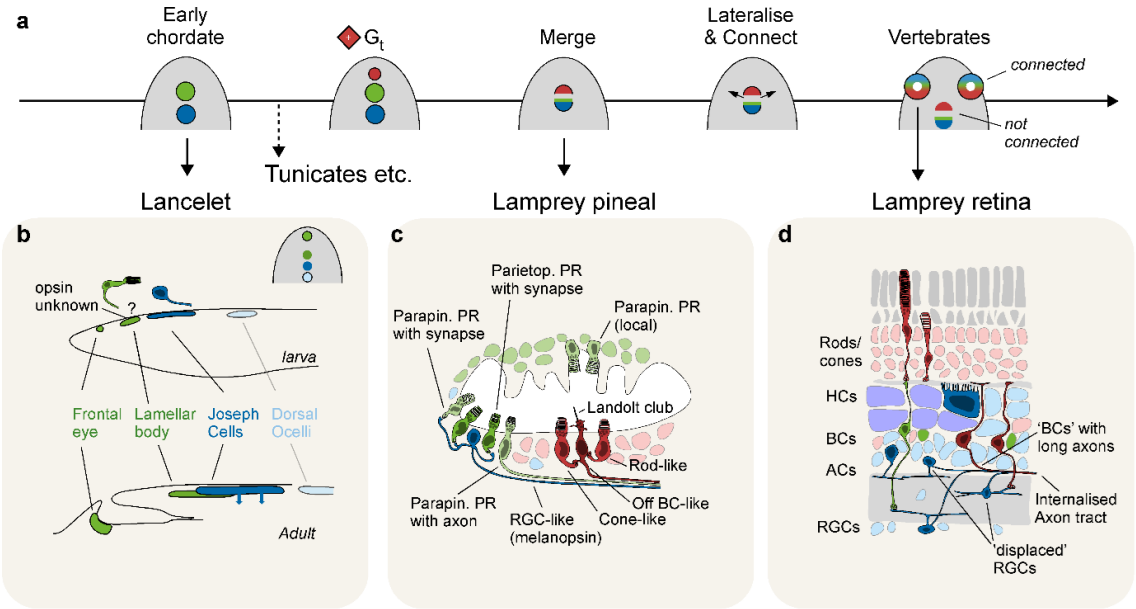

Figure 3.4 – Deuterostome median and lateral eyes. a, Suggested timeline for the emergence of median and lateral eye components leading to modern vertebrate lateral eyes. Resulting from two rounds of whole genome duplication at the root of vertebrates, the novel emergence of the 'fast', modern ciliary G transducing (red, G_t) identity postdates non-vertebrate chordates. b, Lancelets (amphioxus, belonging in cephalochordates) have four median photoreceptors: Two anterior clusters that are ciliary (operating via $G_{i/o}$, green), while the two posterior clusters are rhabdomeric. During development, the two central clusters become superimposed. Schematic adapted from Ref[288]. c, The lamprey pineal organ comprises diverse populations of photoreceptors and projection neurons, forming at least two independent microcircuits: Dorsolaterally, 'ancient ciliary' photoreceptors (green) that express parietopsin and parapinopsin make ribbon synapses onto rhabdomeric projection neurons (blue), whereas ventral, modern ciliary rod- and cone-like photoreceptors (red) make basal ribbon contacts onto Landolt club-like-like bearing ciliary projection neurons (red). Schematic adapted from Refs[265,272]. d, The lamprey retina has a typical of vertebrates tri-layered organization, with modern ciliary rods and cones (red) feeding into rhabdomeric amacrine and ganglion cells (blue). Horizontal cells (rhabdomeric, blue) with notably large somata occupy the space above the bipolar cells. Notably, in lamprey many inner retinal neurons (and their axons) are 'displaced' compared to their positions in jawed vertebrates. Moreover, some bipolar-like neurons project directly to the brain. Schematic adapted from Ref[289].

Retina-like bipolar cells (rlBCs) predate the retina

Noticing the apparent absence of interneurons both in the pineal organ universally and in the eye of jawless vertebrates, Lamb hypothesised that the modern vertebrate retina arises from a two-layered, pineal-like proto-retina that lacks interneurons[116,117]. In light of recent findings however, this highly influential hypothesis should be revisited. Reminiscent of pineal organs, the hagfish retina is indeed organised in two layers. Importantly however, different interneuron markers were recently described in the inner nuclear layer, including PKC-a, a marker of vertebrate rod bipolar cells[141,290,291]. And even in the slowly developing eyes of the larval lamprey, where only the central part of the tissue is differentiated and horizontal and amacrine cells are missing, the retina is nevertheless three-layered, with bipolar cells connecting the photoreceptors to the ganglion cells[143]. Therefore, all vertebrate retinas studied to date possess bipolar cells, seemingly creating a hard boundary with the pineal organs. But are bipolar cells really absent from the pineal?

Retina bipolar cells have certain defining characteristics[95]. They are excitatory, glutamatergic neurons, with their morphology seemingly dictating their function in being the only neurons connecting the inner to the outer retina. Their apical, dendritic pole is postsynaptic to ribbon synapses with rods and cones, while basally they form their own ribbon synapses with ganglion and amacrine cells. In addition to conventional dendrites, some bipolar cells possess a Landolt's club, an ever-narrowing, rich in mitochondria, apical tip of unknown function that terminates freely at the lumen space among photoreceptor inner segments and retinal pigmented epithelium[99,292–294].

Now, these hallmarks of retina bipolar cells are also evident in the ventral subset of pineal projection neurons (Fig. 3.4c). Retrograde tracing has revealed that they too possess not only a structure morphologically like the Landolt's club but also presynaptic ribbon densities of their own, albeit at unconventional cellular locations and potentially with unidentified partners[295]. In both cases in accordance with the vertebrate retina, these projection neurons are postsynaptic partners in ribbon synapses with photoreceptors, and extend their Landolt club in the lumen space, which, like its retinal counterpart, developmentally constitutes a diverticle of the third ventricle[296–298]. Thus, second-order rlBCs exist in the pineal organ, but instead of acting as interneurons, they directly communicate with their long axons to higher brain areas[295,299]. This is key, as in the pineal organ the rlBCs are themselves effector neurons of the ciliary photosensitive system and not responsible for wiring up onto the descendants of the rhabdomeric system, as exemplified by the melanopsin-expressing ganglion cells.

Retina-like bipolar cell diversity – potentially types of distinct lineages?

The similarities described above argue for the retina-like bipolar cell class predating the emergence of the retina. In the retina however, bipolar cells come in all flavours, with over 15 types differing in functional properties like polarity and kinetics[95]. Specifically, some hyperpolarise in response to light (OFF cells) thus conserving the incoming photoreceptor signal while others invert it and depolarise (ON cells). Although both types are encountered in the retina, in the pineal organ the ventrally residing projection neurons are luminosity-OFF units[267], thus arguing for a later emergence of the ON cell type, perhaps from an OFF type.

Alternatively, I here entertain a scenario where the ON bipolar cell type could have emerged from a distinct, photosensitive cell type via the decoupling and repurposing of components of its light-signalling pathway. In ON bipolar cells, the inversion of the incoming photoreceptor-driven signal is mediated by mGluR6, a G-protein coupled receptor (GPCR)[78]. Considering that opsins too are GPCRs, initial hypotheses for the mGluR6-mediated signal inversion suggested a mechanism that recapitulated phototransduction, placing Gt downstream of mGluR6[300]. Multiple lines of evidence however showed that mGluR6 signal transduction is instead mediated by a different family of G proteins, Go[301–303], and thus questioned the relation to phototransduction. Nevertheless and as outlined above, parietopsin-expressing photoreceptors of the pineal organ are similar to retina ON bipolar cells in depolarising in response to light via activation of Go[234]. And in perhaps an interesting example of functional convergence, in some animals these parietopsin-expressing photoreceptors co-express a second opsin and function as colour-opponent units[234,283], paralleling some retina photoreceptors[304] or what some bipolar cells achieve indirectly by comparing synaptic input from spectrally different photoreceptors[305–307]. Now if this hypothesis about the lineage of ON bipolar cells were to be true, not only bipolar cells of different polarity have distinct lineages, but also the template for implementing ON bipolar cell light responses predates the retina itself.

Several evidence point to the RBC, among all ON BCs, as the descendant of the ancestral photosensitive type. First, the RBC is molecularly conserved across lampreys[130], teleosts[206] and mammals[129] and both anatomically and functionally an outlier among BCs (see general Introduction). Second, mGluR6 is consistently expressed at very high levels in RBCs across species, while outside of mammals, mGluR6 expression in cone-ON bipolar cells can be low. Third, and in line with the above, in cone BCs there are alternative systems beyond mGluR6 that can impart ON physiology; one such are the Excitatory Amino Acid Transporters (EAATs) described in teleosts[83,87] but molecularly present also in lampreys[130]. Fourth certain bipolar cells can routinely co-express ‘ON’ and ‘OFF’-acting glutamate receptors or transporters, which renders them functionally ON-OFF[308,309]. And finally fifth, perhaps partially reflecting some of the above, outside

the -probably atypical – mammalian lineage, the molecular separation between ON and OFF cone bipolar cells is not straightforward[130,206] (Fig. 3.5a).

Together, these data suggest that lamprey pineal circuits likely represent two ancient visual modules: the ventrally residing projection neurons giving rise to OFF bipolar cells, and -as we develop below- a chimeric, parietopsin-based photoreceptor system feeding into rhabdomeric ganglion-like neurons -prefiguring rod bipolar cells and the ON pathway. Cone-ON bipolar cells then probably came later, following co-option of the molecular machinery associated with mGluR6 from rod bipolar cells onto an otherwise OFF bipolar cell.

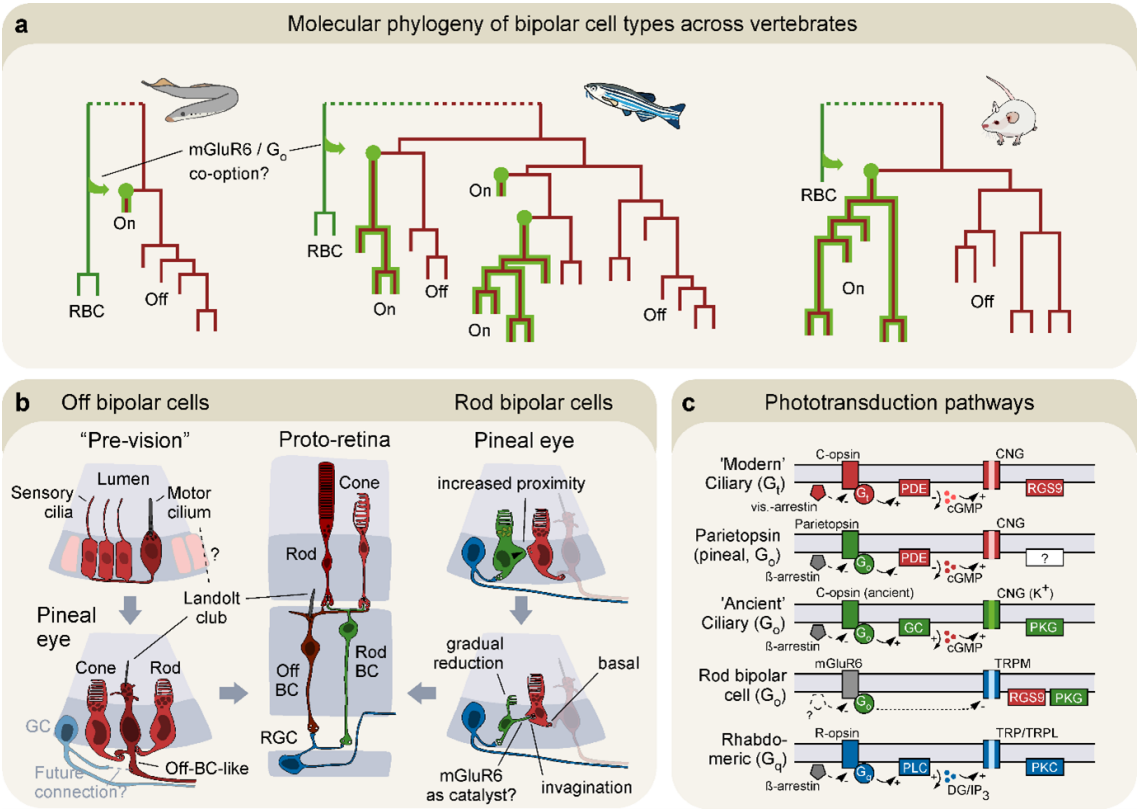

Figure 3.5 – Two evolutionary origins of retina bipolar cells? a, Molecular relationships of bipolar cell types in lamprey, zebrafish and mouse. Datasets are scRNA transcriptomics, and trees are modified from Refs[130,206,310]. Rod bipolar cells (RBCs, green) consistently cluster apart from all other bipolar cell types. In lamprey, cone-bipolar cells are dominated by OFF types(dark red) with a single putative ON (green lining). In zebrafish, members of the two polarities are molecularly intermingled. I suggest that the RBCs and OFF cone-bipolar type have distinct evolutionary origins, and that the ON cone-bipolar types emerged, possibly more than once, by later co-option of mGluR6 (and

its associated molecular machinery) from RBCs onto ancestrally OFF types. b, Suggested sequence of events leading to OFF cone-bipolar cells (left) and rod bipolar cells (right). Retina OFF bipolar cells (middle, dark red) may link with pineal ciliary projection neurons that have a Landolt club-like structure. These cells are already postsynaptic to pineal rods and cones, and a connection onto the nearby rhabdomeric ganglion cells (blue) could explain their position in circuits of the vertebrate retina. Preceding pineal circuits, these neurons may link with a motor-ciliary heritage originally in place to move the small-bodied organism, or to stir cerebro-spinal fluids once ventricles are formed (top left, adapted from Ref[311]). In contrast, retina RBCs (green) may link with pineal photoreceptors expressing parietopsin, which are already presynaptic to putatively rhabdomeric ganglion cells. Connection of parietopsin cells onto pineal rods and cones, possibly facilitated by mGluR6, may explain their circuit position in the retina. c, Phototransduction components across different photoreceptor lineages. Note the molecularly 'chimeric' relationship of RBCs compared to 'modern ciliary' (G_t, red), 'ancient ciliary' ($G_{i/o}$, green) and rhabdomeric lineages (G_q, blue).

Chimeras are instrumental for the evolution of the retina blueprint

As noted above, the AME included three distinct photosensitive systems. Together with the functional benefits in resolving ambiguities, I posit that this close apposition has facilitated the emergence of chimeric cell types via co-option of different ancestral components.

A. Go-coupled signatures of chimeras

Vertebrates present the highly plastic atypical ciliary phototransduction type, albeit in chimeric form. In the ancestral phototransduction cascade, exemplified in the ciliary retina of scallops, Go couples to guanylyl cyclase and mediates light-driven hyperpolarisation[281]. Instead, Go couples to PDE and depolarizes the parietopsin-expressing photoreceptors of the lizard parietal eye, and in such converges antagonistically to the typical ciliary motif of the co-expressed pinopsin[234]. Although information about this pathway is lacking, a similar mode of action is envisioned for pineal parietopsin, where it is either co-expressed[283] or feeds in[272] on the same postsynaptic neurons with the ciliary parapinopsin-expressing photoreceptors.

Despite the lack of expression of representative opsins, the vertebrate retina nevertheless presents signatures of the Go-coupled pathway as well. The signalling cascade of ON bipolar cells is centred around Go, while other of its components are reminiscent of phototransduction in ciliary (RGS) and rhabdomeric (TRP) lineages (Fig. 3.5c). This co-option of phototransduction components is indicative of a chimeric cell type, but comes with a catch, insofar as the ON bipolar cells are not intrinsically photosensitive but instead only indirectly tuned by the light-driven, synaptic output of rods and cones. Here, I advocate that the mGluR6-expressing ON bipolar cells in the retina could be descendants of a pre-existing, chimeric cell type that, specifically at the retina, acquired presynaptic partners feeding in their own light sensitivity and gradually lost their intrinsic (Fig. 3.5b). Without compromising function, the light-dependent presynaptic input could have enabled decoupling the Go-dependent phototransduction pathway from the opsin and repurposing it for mediating the synaptic, mGluR6-mediated signalling instead. Although speculative, such a decoupling might not be unheard of; in nematodes, where Go-coupled opsins have been likely lost[224], a Go phototransduction pathway is now coupled to a taste receptor homologue that is photoreceptive[312–314]. In terms of direct gains, the speculated substitution from a non-visual opsin to mGluR6, a ligand activated GPCR, was probably neutral because their G protein activation efficiency is comparable[315]. But in this theoretical, substituted case, it comes with the added bonus of a new synapse. Supporting a pivotal contribution of the synapse in circuits reorganisation, the mGluR6-mediated postsynaptic signalling cascade is not autonomous, independent of the physical assembly of the synapse between ON bipolar cell and rod and cone photoreceptors. Instead, a growing body of work reveals that these processes are bidirectionally intertwined; you miss components of one and the other fails to form[316–318].

A layout of gradation thus emerges, from a pineal-like to a proto-retina configuration. In the lateralised pineal-like ancestor, the expression of mGluR6 in a chimeric parietopsin-expressing, and thus photosensitive neuron, enabled the trans-synaptic organisation of a novel, and as it turned out pivotal for the retina blueprint, synapse. Now sitting downstream of the typical ciliary photoreceptors, this neuron is tuned both intrinsically and synaptically to the same stimulus, either

redundantly or detrimentally due to temporal misalignment of the one and the same signal. By losing its own opsin and aligning the ‘orphan’ phototransduction cascade to mGluR6, the postsynaptic mediator, the signal processing issues are alleviated., In doing so, the ancestral photoreceptor becomes a second-order neuron that can no longer function independently. Although speculative, this could account for evolutionary constraints on the retina blueprint, which has remained surprisingly unaltered across all modern vertebrates.

B. Parapinopsin signatures in chimeras

The parapinopsin-expressing pineal photoreceptors represent an evolutionarily intermediate state, combining properties of both invertebrate- and vertebrate-type visual opsins[254,319]. At first glance, they present all the defining characteristics of ciliary photoreceptors, namely outer segments that extend as ramifications of a cilium, an opsin in sequence phylogenetically close to ciliary visual opsins and a Gt-coupled phototransduction pathway[320]. At the same time however, several properties are typical of invertebrate photoreceptors and melanopsin-expressing ganglion cells. Contrary to vertebrate visual and thus bleaching opsins, parapinopsin is bistable, with identical amino acid position of its counterion and comparable G protein activation efficiency to rhabdomeric opsins [315,321]. And like melanopsin-expressing ganglion cells, in parapinopsin-expressing photoreceptors the phototransduction pathway is inactivated by beta-arrestin[322] and not visual arrestin, the typical for Gt transduction inactivation in ciliary visual photoreceptors[323]. Overall, this widespread mix and match of phototransduction properties is likely indicative of a transitionary, intermediate photoreceptor, retained and closely apposed to derived ciliary and rhabdomeric photoreceptors in the AME.

Based on their synaptic patterns, parapinopsin-expressing pineal photoreceptors constitute different subtypes. Dorsally to the lumen where there is a rarity of projection neurons, the basal processes of the photoreceptors contact each other and form ‘nerve net’ – like structures[266,324,325] hinting at local and cooperative signalling in functional resemblance to horizontal and amacrine cells of the retina. Rostrolaterally, while most are likely presynaptic to the chromatic ON projection neurons that additionally receive input from the parietopsin-expressing

photoreceptors, still some could have axons of their own[295,299] and thus resemble melanopsin-expressing ganglion cells in combining in a single-cell system intrinsic photosensitivity with long axonal projections.

Starting from the pineal presence of the parapinopsin-expressing neurons, it is tempting to look in the vertebrate retina for chimeras or sister cell candidates. Considered of rhabdomeric origin[207], some horizontal cells nevertheless express, speculatively even alongside melanopsin, the vertebrate ancient (va) opsin[326,327] that is ciliary and phylogenetically close to parapinopsin. In addition to their rhabdomeric phototransduction pathway, certain subtypes of melanopsin-expressing retinal ganglion cells seemingly utilize a ciliary-like phototransduction cascade comprising of adenyl cyclase and cyclic nucleotide-gated channels[328,329] (but see Ref[330]). Such chimeric co-existence of components could be yet another indication of phototransduction cascade co-option between a purely rhabdomeric and a proto-vertebrate ciliary cascade relying on adenyl cyclase[225,331]. Though speculative, the cases above could partially represent extant retinal signatures of parapinopsin-expressing neurons, of this evolutionary intermediate ciliary cell type with a high variability of connectivity patterns.

The vertebrate retina – A tale of chimeras

In aligning this emerging view of retina landscape with the molecular history of its components, likely the only neurons that are credibly pure are rods, cones, and most OFF bipolar cells for the ciliary lineage, and subtypes of melanopsin-expressing horizontal, amacrine and ganglion cells for the rhabdomeric. Together, these capture only but a tiny portion of the astonishing and to a vast extent conserved[129,130] diversity present in the retina, exemplified by about 130 molecularly distinct subtypes in rodents[118]. As a rule therefore, within the vertebrate retina the ‘pure’ label boundaries break in no time, with famous edge cases found in the VGlut3 amacrine cells that functionally echo bipolar cells[332,333] or the GluMi bipolar cell that completely lacks its dendrite[203] (Fig. 3.6). And it was perhaps this ancestral, extraocular jamming of intermediate, derived, and chimeric cell signatures that enabled, within the vertebrate eye, an unprecedented and vast expansion of cell types and processing capacity.

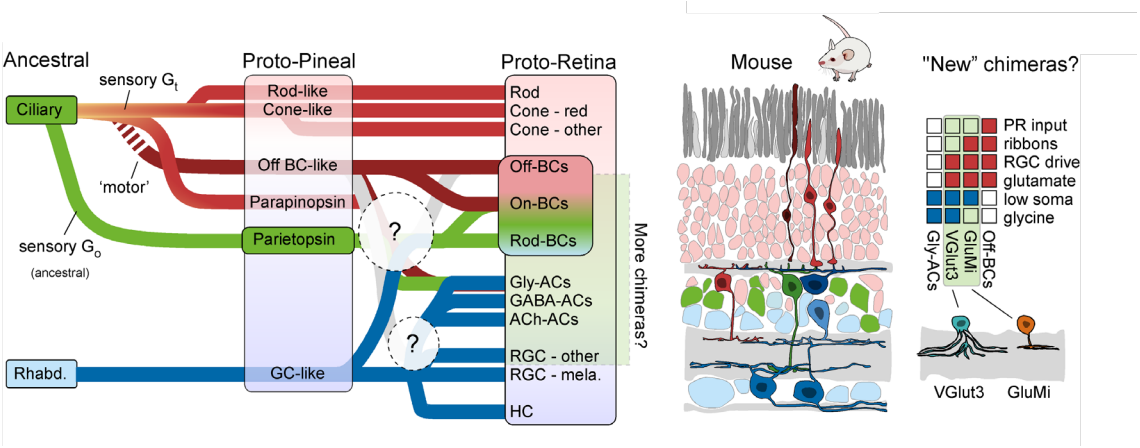

Figure 3.6 – Evolution of retinal neurons. Proposed evolutionary timeline and likely instances of chimerization between the ancestrally distinct photoreceptor lineages (*left panel*). Schematic of mouse retina with colour-coded neurons by their putative ancestral lineage (*middle panel*). Overview of 'modern ciliary' versus 'rhabdomeric' traits found in murine VGlut3 and GluMi cells.

Future tests and open questions

In this chapter, several novel hypotheses have been put forward as structural support to the proposed notion of a common, median eye origin for the modern pineal and retina, where the former has retained an ancestral-like state in remaining unwired compared to the more derived retina. Supported by morphological, functional and only recently emerging transcriptomic data, here I posit that retina-like bipolar cells are found in the pineal organ and thus predate the lateral eye. Building on this observation, a distinct origin of BC types of different polarity is hypothesised. Specifically, ON bipolar cells transduce the light-driven, synaptic input signal with a Go-coupled pathway that combines elements of multiple ancient photoreceptor systems: Ciliary, rhabdomeric, and the Go-pathway (Fig. 3.5c). As such, a chimerization of indicative 'sensory' lineages is suggested. In contrast, OFF bipolar cells together with their presynaptic photoreceptors are highly reminiscent of the cilia-bearing sensorimotor loops found in a plethora of settings and driving a rich diversity of behaviours[334] (Fig. 3.5b). In terminating with a cilium, the Landolt club could represent the effector of this putatively ancient system, nowadays regressed in the environment of the retina but potentially still active in other CSF-contacting neurons[296,335,336]. In both retina and pineal organ, the bipolar cells bearing Landolt

clubs are OFF[99,100], and often found to accumulate serotonin[171,325,337,338], an integral neurotransmitter for cilia beating[230,339,340]. And in the rare cases where the retinal layering is not strictly obeyed, the displaced BC found next to photoreceptors are OFF and always bearing Landolt clubs[73,341], resembling the spatial arrangement of components in sensorimotor systems of smaller organisms[311].

Perhaps unsurprisingly however, not all the hypotheses put forward here are equally supported by the currently available evidence. Based on the presence of Go for example, here I draw parallels between the retina ON bipolar cells and the pineal parietopsin-expressing neurons, whilst additionally likening their transduction pathway to the one employed by the Go-coupled opsins. However, like other G proteins, Go is ubiquitous in diverse cells and mediates GPCR signalling in a plethora of settings. As such, the deployment in the above cases could be entirely coincidental, originating independently from any of numerous cell types. Although definitive evidence will only be acquired when comparing the molecular signatures of the different cells, at present I consider the independent origin plausible but less parsimonious for the retina ON BCs and the pineal parietopsin-expressing photoreceptors. Mounting evidence suggest a 'sister organ' relationship between the retina and pineal[117,220,221,342,343], which concomitantly should translate to molecular similarities or homologies for most cell types. The two aforementioned cell types are the only ones expressing Go in their respective tissue[344], decreasing the likelihood of independent origin.

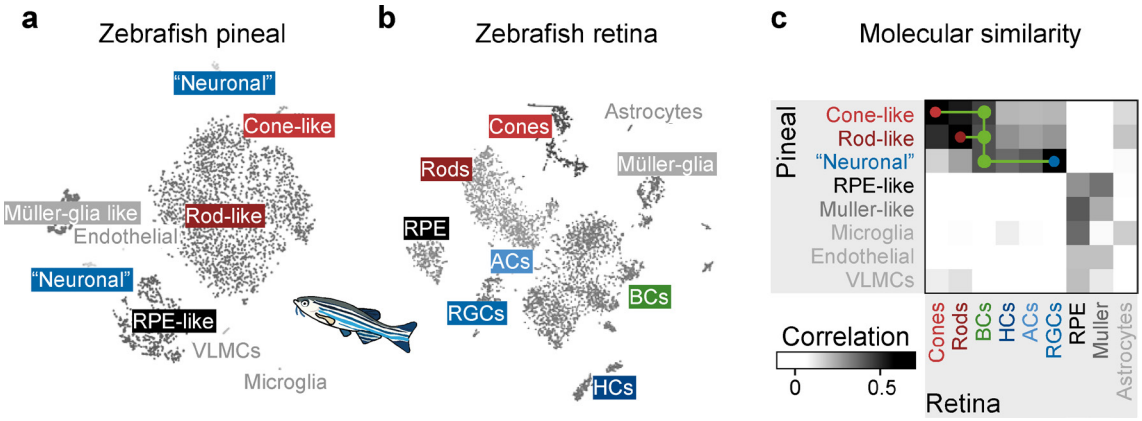

Figure 3.7 – Transcriptomic comparison of zebrafish pineal and retina. a,b, UMAP of single-cell transcriptomic data extracted from pineal (a) and retina (b) of zebrafish,

together with their annotated cell-classes. Modified based on clustering as shown in Ref[345]. c, Correlation matrix of pseudobulk scRNA transcriptomics clusters from (a,b), comparing across the two organs. Note the molecularly intermediate position of retina bipolar cells between pineal rods/cones and pineal 'neurons'. Data replotted from Ref[345].

In general, hypotheses about the evolution of nervous systems naturally attempt to align the past with the present, and as such certain of their aspects can be inherently hard to test. But crucially for the herein proposed scenario, there are different ways to evaluate most of its components. As mentioned above, in accessing the proposed deep molecular homology of retina and pineal neurons, advances in cross-tissue, (spatial) single-cell transcriptomics will prove illuminating. Importantly, such datasets for both tissues and from different species have been recently acquired[129,130,206,273,346–348], and have proved informative for comparative studies within an evolutionary framework. Also instrumental for deciphering the likelihood of such evolutionary scenarios will be cross-tissue comparisons. Recently, a single-cell transcriptomics dataset in zebrafish identified homologs of retinal rod/cones and RGCs in ciliary and rhabdomeric pineal neurons, respectively, in line with the shared ancestry of retina and pineal[220,221]. In this analysis, the ciliary photoreceptors of the pineal organ that co-express parapinopsin and parietopsin were not individually separated from the pineal rods and cones, hindering the comparison that could prove illuminating. Intriguingly however, the retina bipolar cells did not match 1:1 with a pineal counterpart (Fig. 3.7); instead they share molecular signatures with both ciliary and rhabdomeric pineal neurons[345], and therefore increase the likelihood of the chimerization proposed herein.

For future efforts to evaluate the verity or the extent of the retina predating the lateral eye, the understanding of the structure and function of the pineal organ needs to be brought on par with its retinal counterpart. Leveraging electron microscopy can contribute high-resolution, ultrastructural connectivity maps and morphological feature identification, while imaging techniques like 2-photon microscopy or electrophysiology can inform the functional characterisation, perhaps even *in vivo*, of the -conveniently- often superficially located pineal organ. And irrespective of which hypotheses survive the test of experiments, such

efforts will ultimately result in a deeper, and truly general, understanding of vertebrate photoreception.

Chapter 4 - The shark retinal output in function and structure

Abstract

The fundamental structural and cellular blueprint of the vertebrate retina is strikingly conserved. However, its function has yet to be systematically investigated, with currently only limited sampling of the broad, still extant, phylogeny. To identify circuits and computations that are likely to pertain to all vertebrates, here I study elasmobranch fish, the earliest diverging living jawed vertebrates. Using as a model the retina of the small-spotted catshark, *Scyliorhinus canicula*, I describe the response characteristics of its ganglion cells, together with the underlying structural organization of the inner plexiform layer that largely instructs them.

The chromatic profiles of shark RGCs are largely compatible with earlier descriptions of rod-only, single-waveform photoreceptor input, while their encoding of spatial and temporal frequencies are robust but albeit sample a narrow range compared to other vertebrates. Moreover, I describe fundamental asymmetries between the dominant responses, namely ON and OFF, and the existence of direction-selective RGCs in a shark retina.

At the level of structural organization, I characterize the stratification profiles of RGCs together with the properties of their presynaptic partners, and provide the first description of the mammalian primary rod pathway in the earliest diverging, extant jawed vertebrate.

Introduction

The functional diversity of retina ganglion cells, hindered in early work by inherent limitations in the methods used, was first unveiled with single-fiber, optic nerve recordings[69]. About half of the recorded fibers in frogs respond both to initiation and cessation of illumination (ON-OFF) with a transient burst of discharges, while the remaining, in about equal proportion, respond either at the beginning (ON) or at termination (OFF) of illumination, but with a prolonged discharge. Soon identified in other species too[66,68], this response space segregation within elementary coordinates of polarity and kinetics is a fundamental principle[349,350] of vertebrate vision and seemingly indicative of an efficient[57] encoding of different features of the image[351–353].

Overall, such an RGC partition in a polarity-kinetics space is encountered in every vertebrate species studied to date. The representation of each individual combination, however, is not stereotypical across them. In mammalian retinas for example, there are few ON-OFF RGC types[122,124], while the increased representation of OFF visual channels relative to ON is believed to reflect visual space statistics and ethologically relevant stimuli[354–359]. Notably, despite this mammalian imbalance in ON and OFF numbers, the elementary properties of the opposite polarity channels are described as largely symmetric[360–362]. By contrast, teleosts, salamanders and birds all possess retinas whose output is heavily dominated by ONOFF types, and substantially depart from the previously mentioned symmetrical encoding of opposite channels[363–370]. Specifically in birds, the encoding of the same information is highly correlated and multiplexed: OFF circuits are fast and achromatic (wavelength-invariant), while ON slow and wavelength-dependent[370]. And this correlation is additionally reflected in the ON and OFF components of the most populous, ONOFF RGCs respectively, hinting at an extensive, and differing from the classical view, principle of retinal processing.

But how do the functional differences of RGCs arise in the first place? As already outlined for polarity (see General Introduction), but also holding true for kinetics[371], distinct pathways already emerge at the first visual synapse as a result of the neurotransmitter receptors expressed in bipolar cells, and the synaptic circuits are then orderly organized at the IPL in a polarity- and transience-dependent pattern[90,372–376]. At a first glance, this results in RGCs basically ‘inheriting’ the tuning of their presynaptic BCs, and when combined with their own intrinsic properties[377–382], this would determine the heterogenous profiles of RGC responses.

However, ACs can further sculpt the profiles observed. Through inhibition, they can truncate the RGC responses to be more transient[383] or non-linear[384–386] compared to the simpler, and linearly-reflecting the BC input[28,387], RGCs. For example, sustained ON and OFF RGCs in cats are linear and better equipped to function as contrast encoders (X-cells), while Y-cells are non-linear, with often a strong contribution of AC input in their response profile[351,388,389]. As these ON-

OFF neurons are firing irrespectively of the sign of luminance change, they are often employed as motion or edge detectors[68,177,390–392].

Detecting motion is useful, but computing its direction is even more. For successfully navigating the visual world, it is not enough for the organism to detect an approaching predator or fleeing prey but instead it needs to know where they are heading relative to its own position or movement. Neurons capable of encoding direction of motion have been identified around the same time for different levels of the hierarchical visual system; from the retina[68,392–396] and the optic tectum[397–399] of different vertebrates to the dorsal lateral geniculate nucleus[400,401] and the visual cortex[402–405] of mammals. Coined 'direction-selective' (DS), these neurons respond with substantially more impulses when the stimulus is moving in one direction compared to the reverse ("preferred" and "null" directions, respectively), and such units have been described in the visual systems of most animal species studied to date[56,406–418].

Implemented on top of the elementary functional properties outlined above, there are three DS types in the mammalian retina[419–421]: ON[422,423], ONOFF[393,414] and OFF (JAM-B)[424] RGCs. While all OFF DS are selective to upward motion, the ON and ONOFF DS manifest diversity within and can be further split. Specifically, ON DS come in three subtypes separated by 120 degrees in their preferred directions[423,425,426] (but see[427]) while ONOFF in four, sampling preferentially one of the cardinal directions[426,428]. Aside from polarity and number of axes sampled, the DS systems further differ in the roles subserved; ON DS are responsible for gaze stabilization[429–432], while ONOFF for tracking object motion[433]. Notably however, the representation of the DS computation in the different polarity channels seems to depart from the mammalian case for vertebrate branches less thoroughly studied[406–408,410,434,435].

Consequently, although pathway splitting of the visual signal into ON and OFF channels is ancient and conserved across vertebrates[436], distinct strategies across the vertebrate phylogeny are seemingly utilized not only for encoding fundamental properties of the visual image but also for computing ethologically relevant features. With only few species yet systematically studied however, there is limited understanding of how the observed diversity in functional organizational motifs is associated with the underlying retinal composition and structure, and

whether it is rooted in evolutionary constraints, clade-specific adaptations to the visual space statistics or organismal behaviors subserved. Owing to their key phylogenetic position, sharks can therefore inform about the early organization of vertebrate visual circuits.

In this chapter, I systematically describe the functional diversity of the output in the rod-only[13,182,437] retina of the small-spotted catshark *Scyliorhinus canicula*, in what to my knowledge constitutes the first large-scale, high-throughput study of light-driven retinal function in a shark. This description is primarily based on full-field stimuli; chromatic steps of differing wavelengths and 'white' steps of differing duration, as well as "chirp" stimuli that differ either on their temporal frequency or contrast. Completing the stimulus arsenal, a "moving bar" (see Methods) is employed to inform about the existence of direction-selective RGCs. Moreover, I present ongoing analysis of serial block-face scanning electron microscopy data of the shark retina, with the aim to illuminate the underlying structure and connectivity instructing the observed RGC output.

Results

In the present work, I recorded from n=31 pieces (N=23 small-spotted catshark hatchlings) of the shark retina, which yielded n=2966 total detected units passing the minimum quality index criteria (see Methods). Most retina pieces were 2-3 mm in diameter and care was taken to record from a similar eccentricity from the optic nerve head for the different experiments. Regarding the retina regions sampled, most pieces were either from temporal or nasal retina (n=14 and 9, respectively), 1 was from ventral and in the remaining 7 the relative coordinates were not captured.

To gain a first understanding of how shark vision is implemented at the early visual circuits, I mostly presented simple, full-field stimuli, differing in one of the following properties: spectral composition, duration, or spatial and temporal frequency (see Methods). The LEDs (n=6, with peaks at 360, 420, 480, 505, 560, 630 nm) used for the stimulation were calibrated to 55 nW, except for 360 nm (UV) that was already at maximum power (30 nW). During the experiment, stimuli are presented on the photoreceptor side (see also general Discussion), while the shark retinal ganglion cells (RGCs) are in contact with the opaque multielectrode array, facilitating the capture of their responses to light (Fig. 4.1A). Chosen to

depict the general diversity found, responses of eight RGCs to 2s full-field flashes of different wavelength (FFF) are shown in Fig. 4.1B-D. Individual RGCs responded to light increments (ON responses – Fig 4.1B), decrements (OFF responses – Fig. 4.1C) or both (ONOFF responses – Fig. 4.1D). The action potentials fired are referred to as spikes and plotted as individual vertical lines.

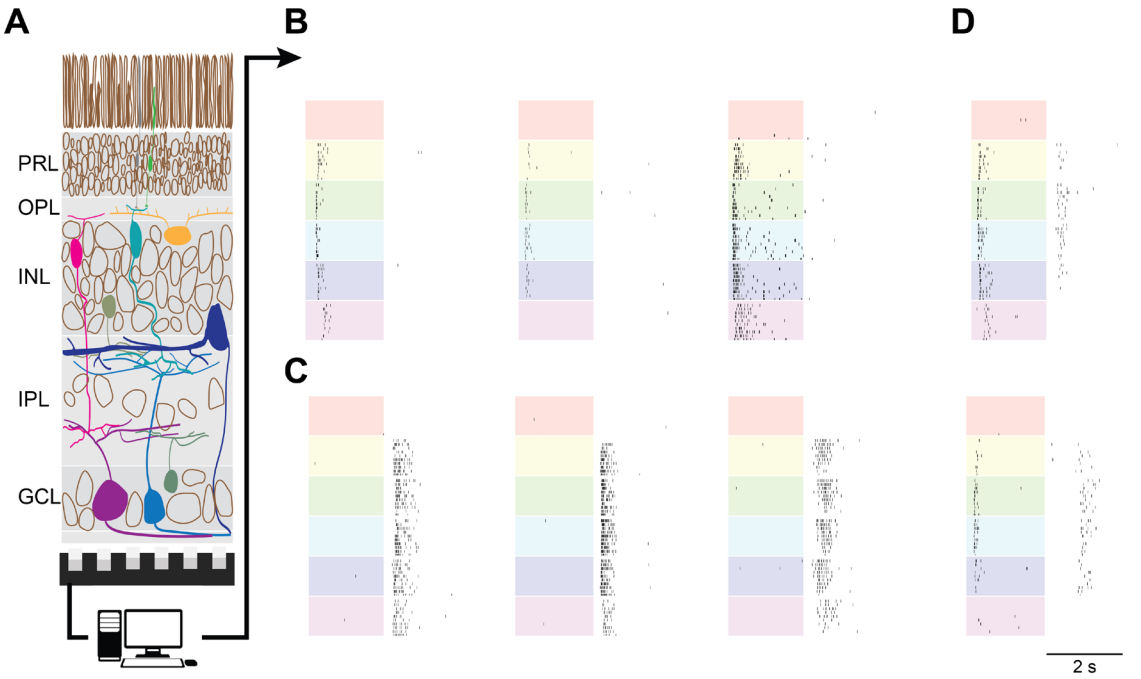

Figure 4.1 – Individual RGC responses to chromatic stimulation. A, Schematic of the shark retina, with photoreceptors up and RGCs in contact to the multi-electrode recording array. B-D, Examples of individual RGCs responses. Colored (according to stimulating LED wavelength) rectangles indicate the 2s 'light-on' stimulus phase. Each row is a single repeat of the stimulus (10 repeats in total for each wavelength, bottom-to-top the temporal sequence). Vertical lines represent single 'spikes', responses of the RGCs. Based on the response polarity (at light onset or offset), RGCs are ON (*B*), OFF (*C*) or ONOFF (*D*). PRL; photoreceptor layer, OPL; outer plexiform layer, INL; inner nuclear layer, IPL: inner plexiform layer, GCL; ganglion cell layer.

To examine the light-driven responses at the population level, the response of each cell across stimulus repeats was averaged before calculating the average peri-stimulus time histogram (PSTH – see Methods) across RGCs (Fig. 4.2). The three general response categories described above for single RGCs pertain to the whole population, with each RGC retaining their response polarity (ON, OFF or ONOFF) irrespective of the light step wavelength. Considering this

consistency, sub-population PSTHs are depicted separately for each polarity, and each cell is assigned to a group based on the computed polarity index that captures the response difference between light increments and decrements (see also Methods).

Spectral Responses of the shark RGCs

Of note, responses to 630 nm (red) are absent both at the single-cell and at the population level. Previous work has detected the presence of a single spectral input channel in the small-spotted catshark retina, namely the rod, with a peak at 502 nm[182]. In general, photoreceptors absorb photons and report signal intensity independent of wavelength; at the absence of a second input channel, the retina response to different wavelengths largely relates to wavelength-dependent probabilities of photon absorption from the photoreceptor. This absence of 'red' responses is therefore not surprising, considering the spectral position of our stimulating LEDs relative to the Govardovskii template[195] for the 502 nm absorption curve (Fig. 4.3A). Overall, both the ON and OFF RGCs response is largely in line with the tuning function of the log-transformed rod opsin (see Methods); more specifically, they are best captured by curves peaking at 499 and 502 nm, respectively (Fig. 4.3B). Interestingly however, although the seemingly poor fit observed for the UV response could be attributed to the less power of this LED relative to the five others, there are still few RGCs across different recordings whose responses do not fit neatly to a single, log-transformed, opsin absorption curve (Fig. S4.1).

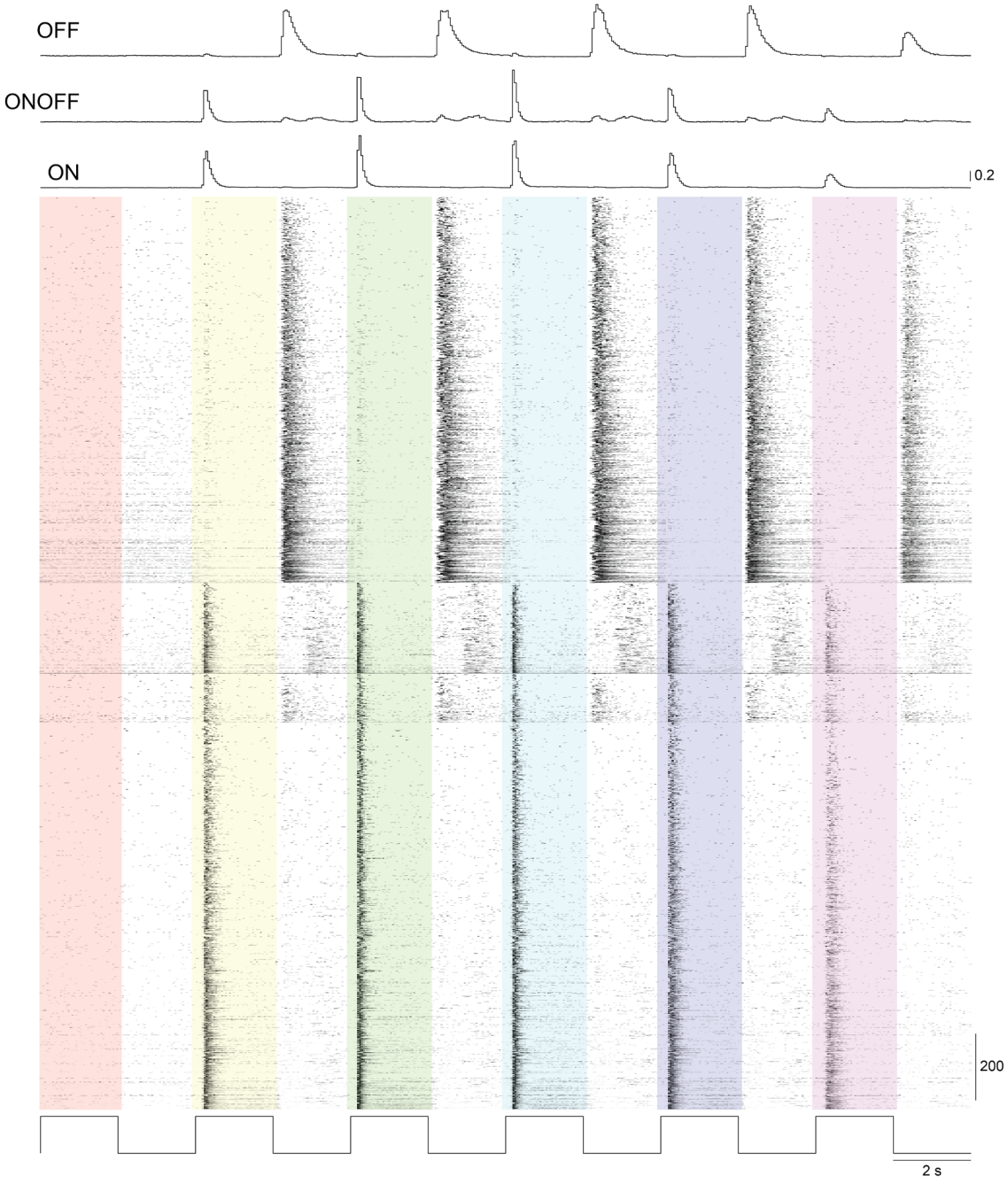

Figure 4.2 – Population responses to chromatic stimulation. Each row corresponds to a single RGC (the spike train is a heatmap of the combined single cell spike trains of the ten repeats (see Fig. 4.1)). At the top of the plot are the normalized PSTHs, separately for each polarity, while the trace at the bottom represents the stimulus intensity (0-1; lights off-on).

Most shark RGCs are ON or OFF, few are ONOFF

With regards to the prevalence of the different response polarities, ON and OFF are more populous than ONOFF RGCs. Specifically, they represent 42.5% ± 24% and 40.3% ± 20.6% of total RGCs respectively, compared to 17.1% ± 13.6% for

the ONOFF (Fig. 4.3C). The two components of ONOFF RGCs are not equally weighted; instead their ON is stronger than the OFF, evident in both the individual cell heatmaps and the ONOFF PSTH of Fig. 4.2, and the polarity index in Fig. 4.4A (with values closer to 0.33 than to -0.33). This relationship is likely inherent to this polarity group because it appears reversed in the general relationship; ON RGCs fire on average less spikes in response to light onset compared to the OFF RGCs for light offset (2-sided Mann-Whitney U, ON median and IQR 2.0 and 1.1-3.9, OFF median and IQR 2.4 and 1.4-5.03, $p= 1.16 \times 10^{-9}$; evaluated for the 480nm (cyan) responses). When grouping the recordings by the retina region they correspond to (n=9 nasal and n=14 temporal retina), null hypotheses (Mann-Whitney U test) can not be rejected for regional specializations neither in representation of response polarities nor for the number of spikes and latency for each polarity (Fig. 4.3D). Notably however, the ON RGCs appear consistently faster than the OFFs relative to the stimulus change eliciting the response (light onset and offset, respectively).

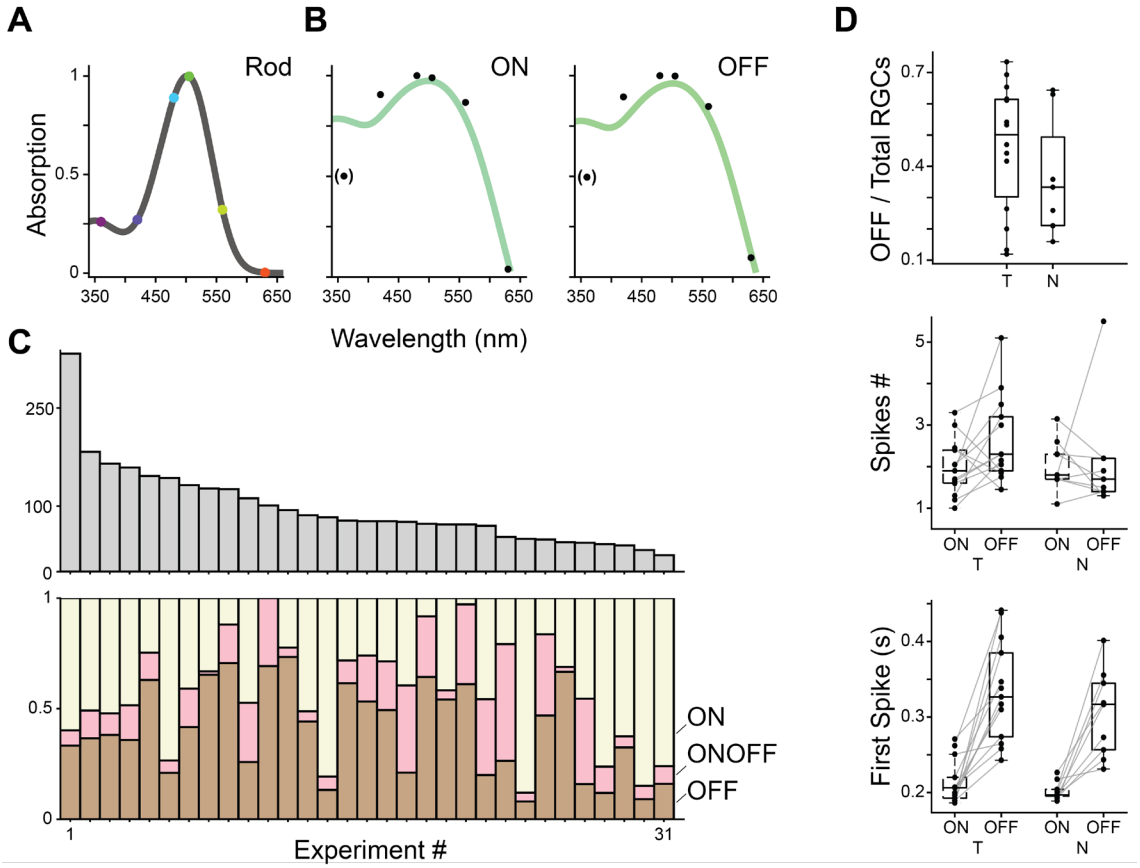

Figure 4.3 – General comparisons of ON and OFF RGCs. A, The photoreceptor absorption curve (Govardovskii template with a 502 nm peak) in relation to the peaks of

LEDs used for visual stimulation. B; The normalized average population responses to the different chromatic light steps (*data points*), together with the best fit of a log-transformed opsin (peaking at 499 and 502 nm respectively). UV response in brackets because LED power is half of the others. C, Total yield of individual experiments (*top*), and representation ratio for the polarity subgroups (*bottom*). D, retina regional relations for subgroup representation (*top*) and RGC elementary response properties (*middle, bottom*).

ON RGCs are fast and transient, OFF are slow and sustained

To further investigate the temporal properties of the RGC responses, I first evaluated how 'compact' they are. Most metrics currently used for quantifying how transient (or reversely, sustained) an RGC response rely on assigning an 'early' and 'late' response window and computing their relationship. This approach however introduces temporal constraints in choosing the width and boundaries of said windows, thus hindering comparisons across different polarities, or species where the same cell type might respond with different latencies. For that reason, I here introduce a time window-free transience index based on the median of absolute deviations from the median of the data (MAD, see also Methods). In relationship to their polarity, ON RGCs are on average more transient than their OFF counterparts (Fig. 4.4A). The population transience value is wavelength-dependent; specifically for the ON RGCs, it positively follows the stimulus intensity that is sensed by the photoreceptor (Fig. 4.4B and 4.3A). In addition, a similar relationship pertains to the response latency: ON RGCs on average respond faster for stronger stimuli, whereas OFF are increasingly delayed. This surprising asymmetry of ON-fast and OFF-slow applies to all response-driving LEDs except for UV (see Discussion) and is likely a fundamental characteristic of the shark retina because it is repeatedly observed in individual experiments (see Fig. 4.3D) and independent of latency metric used (Fig. 4.5A). Notably, the latency distribution of the OFF component of ONOFF cells is bimodal; with a cutoff threshold at 0.7s, the polarity group can be subdivided into 'true' ONOFF, where the two components resemble the ON and OFF RGCs, respectively, and the -here termed- ON-delayed-OFF (ONdOFF) (Fig. 4.5B). The overall prevalence of the four different groups of responses to chromatic full-field flashes is as follows: ON 42.4%, OFF 42.3%, ONOFF 5.4% and ONdOFF 9.9%.

Notably however, different stimuli can unveil weak ‘ON’ responses in some OFF RGCs and vice versa (Fig. S4.2).

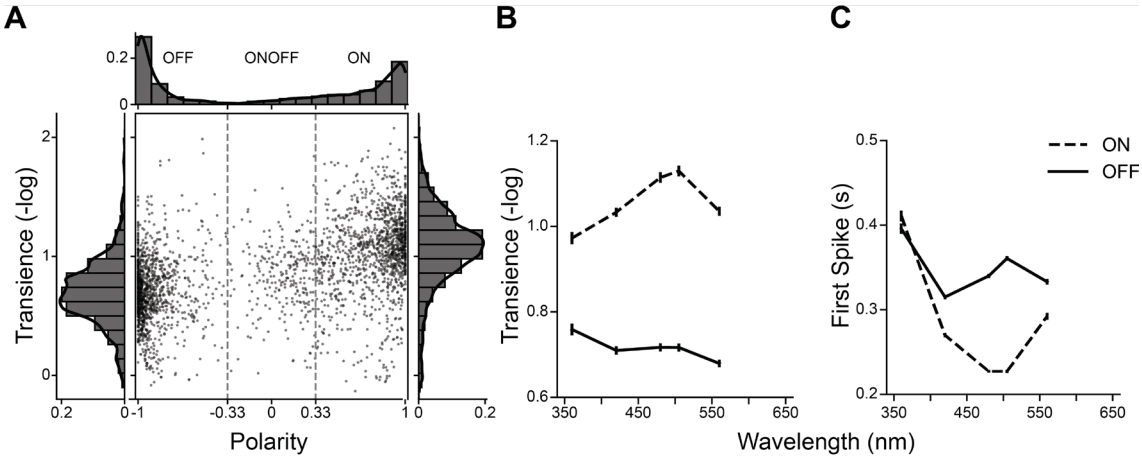

Figure 4.4 – Asymmetries in the ON and OFF properties. A, Polarity-kinetics relationship of the RGC responses. Note the dominance of ON transient and OFF sustained types. See Methods for how the transience and polarity indices are computed. B-C, Response properties vary with stimulus wavelength (mean ± s.e.m). Note the inverse relationship between ON and OFF RGCs. Note the omission of datapoints for 630 nm, instructed by the absence of RGC responses to it (see Fig. 4.1, 4.2).

The ONdOFF RGC type

Although the latencies of all shark RGCs are slow, the OFF component of ONdOFF is characteristically delayed. Moreover, its timing is less aligned at the population level compared to all other response polarities. To confirm that the ONdOFF indeed represent RGCs, I examined their electrical image for evidence of unit mix-up or the lack of an axon, which would indicate the cell could likely be an amacrine. However, axons were easily identifiable, indicating that the sorted units are RGCs (Fig. S4.3).

In the ONdOFF RGCs the ON component is more pronounced than the OFF, in agreement to its less prevalent counterpart, the ‘true’ ONOFF type. The delayed OFF component is however the least sensitive among all response polarities; while strong responses for other polarities were already evident for stimulus durations of 50 ms both at the single-cell and at population levels, the delayed OFF appeared only at stimulus durations of at least 200 ms (Fig. S4.2).

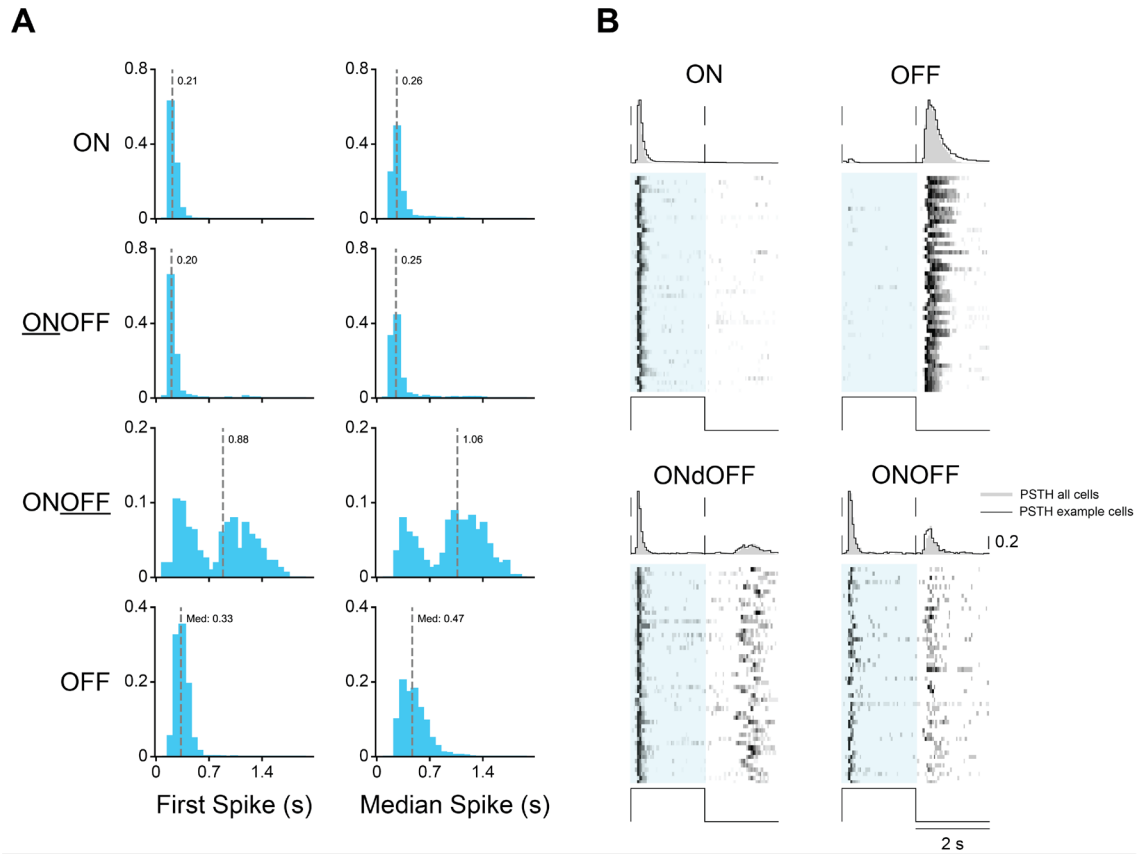

Figure 4.5 – Temporal profiles of RGCs. A, Different metrics of response temporal profiles, with the median value of RGC subgroup populations highlighted (*dashed line*). Note that ON are fast and OFF slow, with a bimodal distribution for the OFF component of ONOFF cells. B, Responses to cyan (480 nm) steps of light of RGC populations classified on polarity and timing of the first spike (cutoff threshold for the ONOFF at 0.7 s). The structure of the plot is similar to Fig. 4.2, but with solid lines of PSTH representing the visualized example cells, and the gray fill PSTH the corresponding whole population. Responses to other LEDs adhere to the same pattern but are omitted for clarity.

Conserved asymmetries of opposite polarity channels

As the pronounced asymmetries in the ON and OFF RGC properties here described for the *Scyliorhinus canicula* are not encountered in the mammalian-centric literature, I next recorded from the retina of the closely related *Scyliorhinus stellaris* (N=3 animals, n=10 pieces, n=1097 cells) to examine the extent of conservation. All three polarities were identified in response to the same chromatic FFF (Fig. S4.4A). On average, ON RGCs are best described by a 505 nm absorption curve while the OFF by 502 nm (Fig. S4.4B). The 'pure' ON and OFF were more populous than the ONOFF, and the ON more transient and fast compared to the OFF (Fig. S4.4C-D). Although a bimodal shape is less

prominent, the OFF component of the ONOFF RGCs is still the most diverse. Overall, all descriptions of elementary response properties of *Scyliorhinus canicula* RGCs seem to pertain to *Scyliorhinus stellaris* as well, highlighting a degree of conservation within Elasmobranch that at least spans catsharks.

Spatiotemporal tuning of RGC responses

To examine the encoding of different contrasts and temporal frequencies at the shark retinal output, I used a white light 'chirp' stimulus that successively altered in the temporal (0.1 – 8 Hz, at 100% contrast) and spatial domain (0-100% contrast for 0.2 Hz). Responses of individual RGCs are chosen to illustrate some of the underlying diversity found (Fig. 4.6).

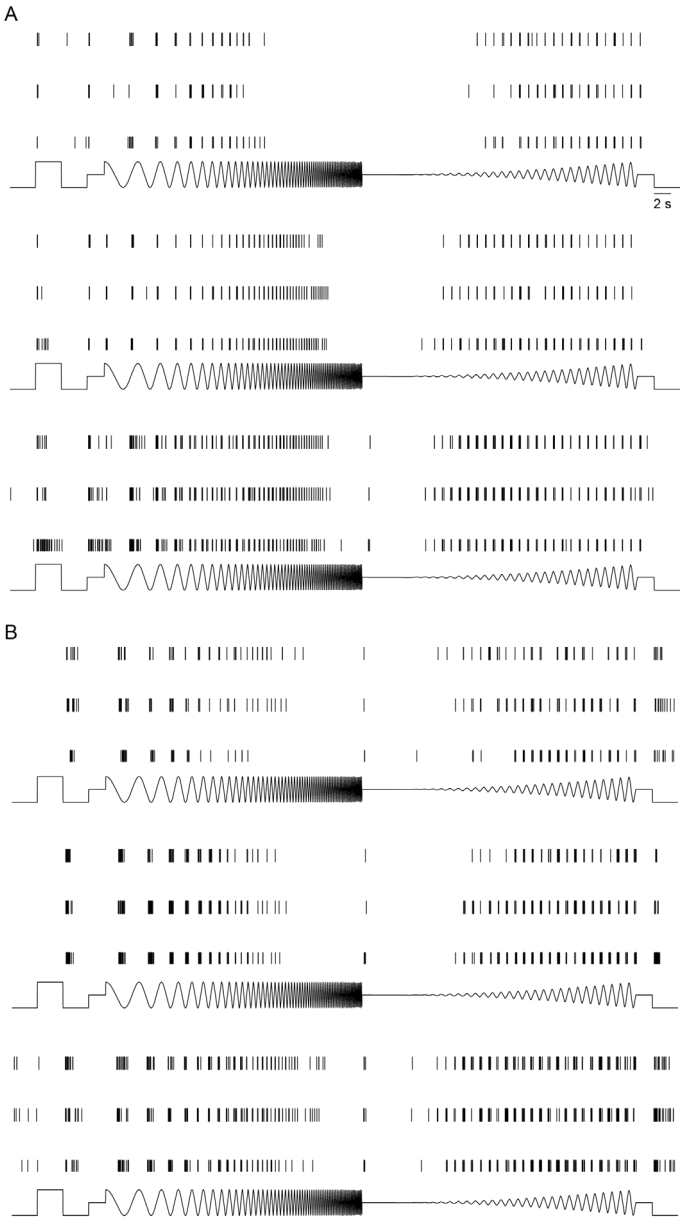

Figure 4.6 – Individual RGC responses to 'chirp' stimulation. Rows represent individual repeats of the same stimulus (bottom trace) for ON (*A*) and OFF (*B*) RGCs. Note that the *bottom* example in each panel is better at encoding higher frequencies and lower contrasts than its counterparts.

Evaluated on the number of spikes, both ON and OFF RGCs preferred low temporal frequencies and high from low spatial contrast (Fig. 4.7 and 4.8). Moreover, the population PSTHs are crisp, with RGCs aligning in the temporal domain and not allocating resources to encoding 'out-of-phase' stimulus intervals.

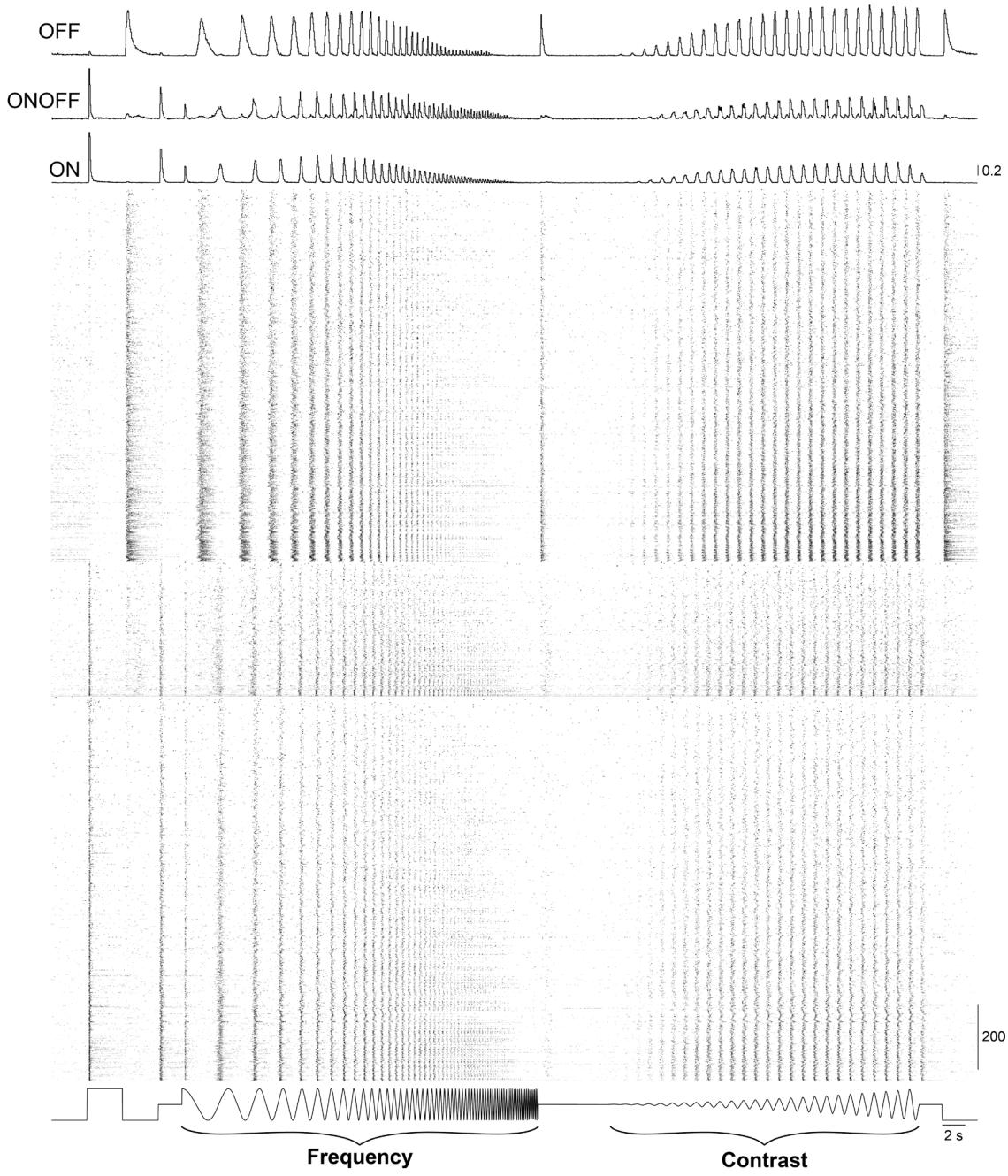

Figure 4.7 – Population responses to 'chirp' stimulation. The structure of the plot is similar to Fig. 4.2, and the two alternating components of the stimulus are highlighted. See Methods for the stimulus parameter space.

To better describe how closely individual RGCs are tuned to the stimulus, I quantified whether their responses were consistently aligned to a particular phase of the stimulus sinusoid (see Methods). This phase-locking index (vector strength) was computed separately for the temporal frequency and contrast domains of the stimulus, and mathematically it can range from 0 (spikes occurring randomly, in different stimulus phases) to 1 (each response spike is perfectly aligned to the same phase of the stimulus). Finally, to evaluate what vector strength values would be expected by chance, for each RGC I generated n=1000 artificial neurons with the same number of spikes but with each spike occurring at random times. The confidence interval of the resulting vector strength distribution represented the upper bound against which I evaluated the statistical significance of the RGCs vector strength.

With regards to the temporal domain, ON and OFF RGCs were similarly phase-locked with an identical population vector strength of 0.82 that is largely above the confidence interval (Fig. 4.8A, see also Fig. S4.6 for percentage of contributing RGCs). Notably however, ON RGCs could follow frequencies up to 6 Hz, while OFF did not respond above 5 Hz. Moreover, they were equally phase-locked to contrasts (0.89 mean phase-lock index), and sensitive to as low as 10% (Fig. 4.8B).

The big-spotted catshark *Schyliorhinus* stellaris displayed similar degree of phase-locking. Specifically, ON RGCs had a mean vector strength of 0.82 and 0.86 for temporal frequency and contrast, respectively, while the OFF RGCs 0.75 and 0.80 (Fig. S4.5). Overall, ON RGCs again could follow frequencies up to 6 Hz, while the OFF were not responding above 5 Hz.

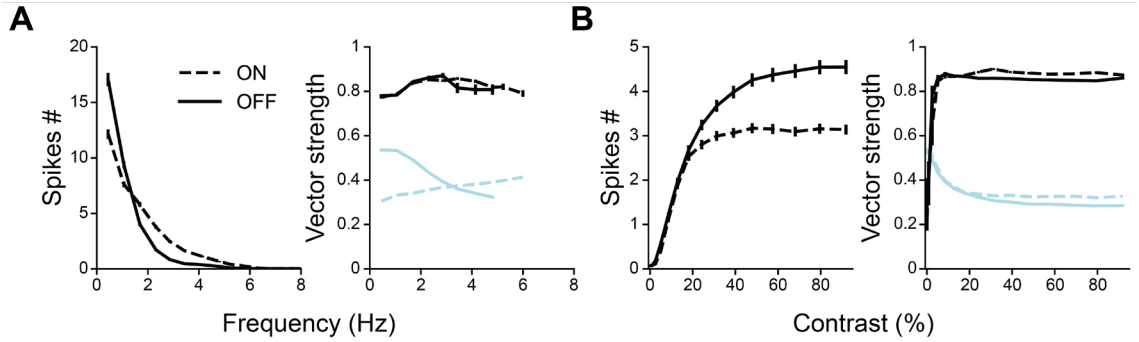

Figure 4.8 – Response characteristics to 'chirp' alternating components. ON and OFF RGCs present similar patterns in the number of spikes (*left*) and degree of phase-locking (*right*) for changes in temporal frequency (*A*) and contrast (*B*). Note that ON RGCs are still following the stimulus at higher frequencies compared to OFF RGCs. Shown is mean ± s.e.m, and cyan lines represent the upper confidence interval for the artificial population of neurons (see Methods).

Next, I examined the existence of direction selective (DS) RGCs in the catshark retina. For that purpose, I used a 'moving bar' stimulus and computed a direction-selective index (DSI) that compares the number of spikes for the dominant (eliciting most spikes) and null (the opposite of the dominant) directions (see also Methods). The statistical significance of the DSI for each RGC was evaluated by a similar bootstrapping to the one employed for the chirp.

The majority of RGCs responded to the moving bar stimulus with indiscernible number of spikes for the different directions. Therefore, they were non-DS (Fig. 4.9A, *top*). However, DS RGCs were also identified (Fig. 4.9A, *bottom*) and constituted 5.11% ± 3.21% (N=20 experiments, n=999 cells) and 5.37% ± 3.76% (N=22, n=1080) of ON and OFF RGCs, respectively (Fig. 4.9C-D). Computed within each experiment, the preferred directions of ON DS RGCs were separated by 120 degrees, whereas the OFF by roughly 90 degrees. In the 360-degree visual space, this means that ON sample directions in 3 axes while OFF in 4. ONOFF DS RGCs were not encountered, except for two cases (Fig. S4.7).

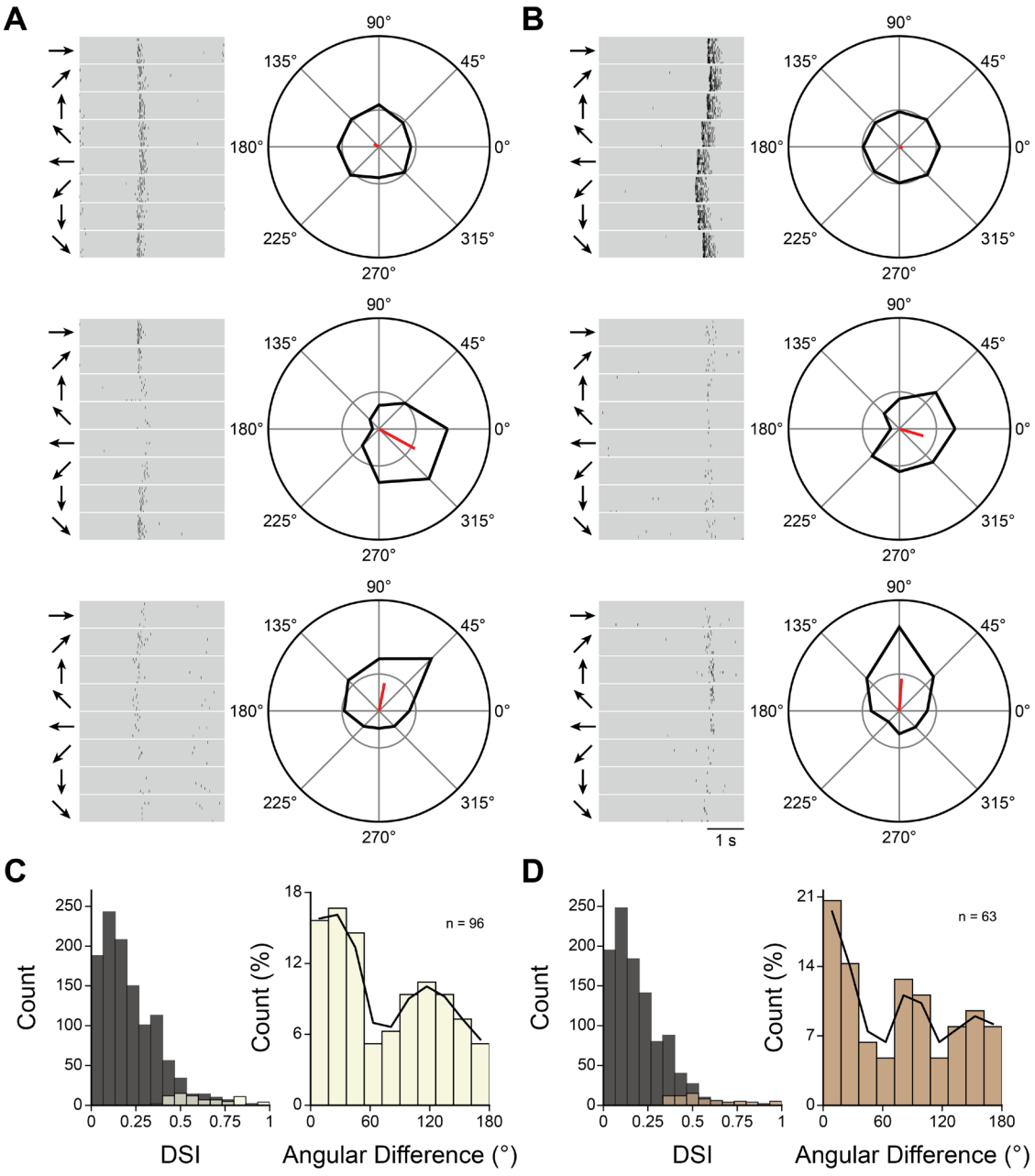

Figure 4.9 – Direction selective RGCs in the shark retina. A,B Individual ON (*left*) and OFF (*right*) RGC responses to 'moving bar' stimulation. Most RGCs were not DS (*A,B top* and black bars in *C,D left*), but some encoded direction of motion (*A,B middle and bottom*, and colored bars in *C,D left*). Angular DS preference pairs were separated by 120 degrees (*C, right*) and 90 degrees (*D, right*) for ON and OFF RGCs, respectively.

Cell somata displaced in IPL and INL-IPL border

As the functional encoding of RGCs is implemented on top of the structural organization of the retina, I examined the morphological patterns within the IPL. Two notable differences to the stereotypical vertebrate blueprint are seen. First, many somata larger than their surrounding INL counterparts are situated more

proximally, at the INL-IPL border (Fig. 4.10). Staining with RBPMS, a selective RGC marker[438], reveals that they are displaced RGCs (Fig. 4.10C). Second, somata are found in the middle (40-60%) of the IPL, and hereby I refer to them as interstitial cells in line with previous literature[439]. Interstitial cells are roughly in equal proportion RGCs and ACs (48.4-52.5%), based on RBPMS staining and evaluated across two different eccentricities along the horizon in the temporal retina. The ratio of interstitial RGCs to their orthotopic counterparts remains relatively stable in these two eccentricities examined (19.3-21.9%). In comparison, the ratio of displaced to orthotopic RGCs is higher than the interstitial and vastly differs with eccentricity (27.1-42.2%).

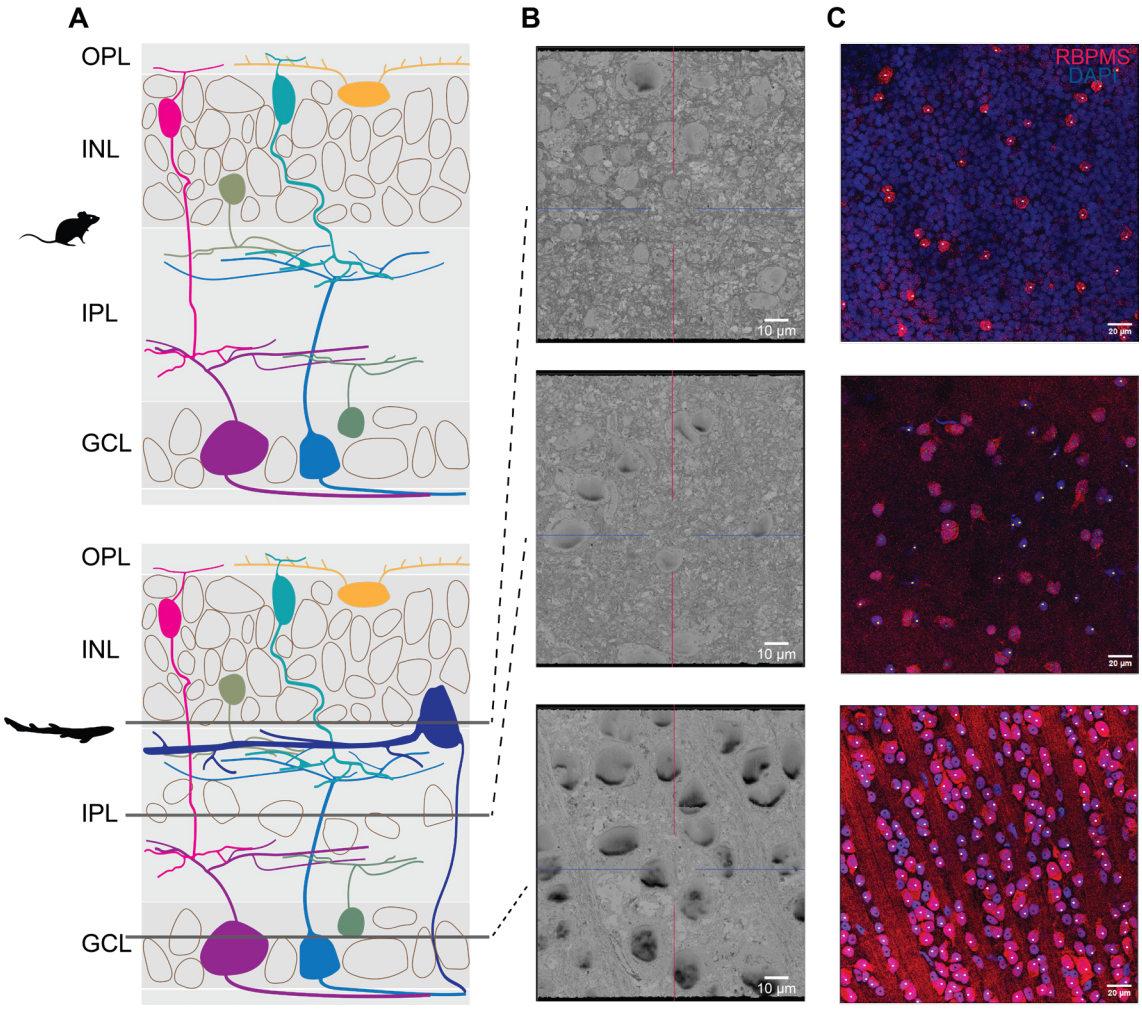

Figure 4.10 – Shark IPL presents distinct characteristics. A, Schematic of mammalian (*top panel*) and elasmobranch (*bottom panel*) retina. The photoreceptor layer is omitted. Note two characteristics of the shark retina, namely the existence of interstitial cells (namely cell somata in the middle of IPL, also visible in B and C *middle*), and the high prevalence of displaced RGCs, situated in the proximal INL (also visible in

B and C *top*). B-C, Electron microscopy and immunostaining data, respectively, from IPL depths corresponding to horizontal lines in A *bottom*. RBPMS is a marker for RGCs. Dot marks in C are the result of CellCounter in Fiji[201], with different colours indicating whether the cell is included in the RGC or non-RGC group count.

Stratification patterns within the IPL

Next, I sought to examine the stratification patterns of RGCs relative to their excitatory, presynaptic partners, the BCs. For this purpose, I used the EM volume we generated (see Methods) and the observations presented here reflect my ongoing efforts in reconstructing all the processes that can be traced back to a soma. Adhering to the division proposed by Cajal and employed for the analysis of mammalian retinas[103], I subdivided the IPL in five strata (sublaminae) of equal thickness, with s1 and s5 at the INL-IPL and IPL-GCL borders respectively. The BC skeleton terminals (identified by the presence of ribbon synapses) terminate uniformly within the IPL, with the exception of a narrow band close to the s2-s3 border (Fig. 4.11). Devoid of BC terminal arborizations, this band contains the soma center of the most distally located interstitial cells.

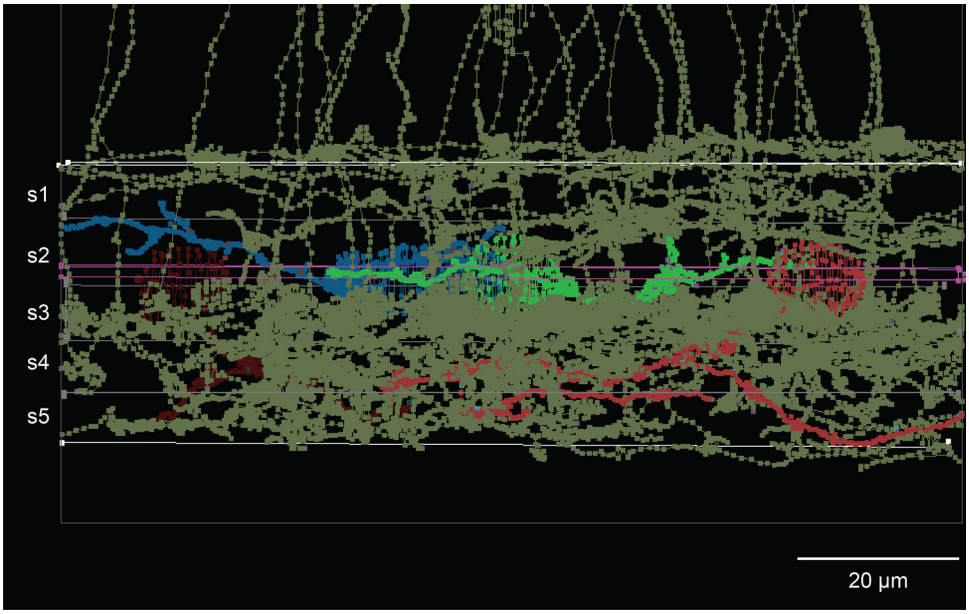

Figure 4.11 – Bipolar Cell terminals in IPL. In line with earlier work, the IPL is divided in five strata of same thickness. Bipolar cell processes (olive green) descend into the IPL and terminate uniformly except from a narrow zone near the s2-s3 border. This zone contains the somata of the most distal interstitial cells (dark red, blue, green, red) – note

their distinct dendritic stratification patterns. Interstitial cells located more proximally are omitted for clarity.

The BC skeletons can be categorized based on the stratification depth, size or complexity of their axon terminals. In my EM dataset, five types can be distinguished (Fig. 4.12 *left*). Type a1, or outer wide, stratifies mostly in s1 and has wide terminals, while type a2 or outer branchy has narrow, multi-stratified terminals in s1 and s2. Types c1 and c2 transverse the IPL to terminate widely in s5 and narrowly s4-s5, respectively, and in such resemble the a1 and a2 types. Finally, type b terminates in the middle (40-60% of the IPL) and have large, bulbous terminals.

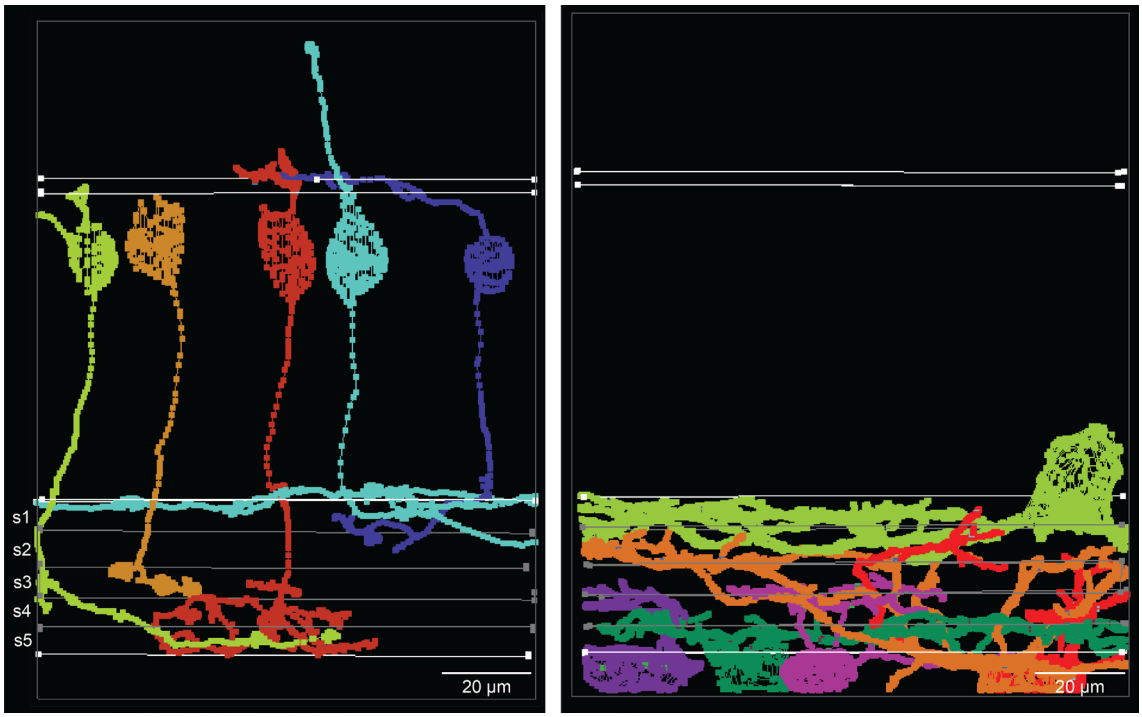

Figure 4.12 – Stratification patterns in the shark IPL. *Left,* Five different types of bipolar cells are identified in the catshark retina; from left to right: inner wide (c1), bulbous (b), inner sparse (c2), outer wide (a1) and outer sparse (a2). Note differences in stratification depth and properties of terminals. Their dendritic processes are currently untraced, but a Landolt club is visualised for the outer wide BC type. *Right*, Example of RGC stratification patterns. Note differences in stratification depth, and location of cell body (orthotopic versus displaced – see also Fig. 4.13).

Amacrine and retinal ganglion cells are postsynaptic to BCs. Compared to RGCs however, ACs possess vesicles in their dendrites and can act as presynaptic partners too. Based on the absence of vesicles, 21 RGCs were therefore

identified in the ganglion cell layer and their dendritic processes traced as skeletons (Fig. 4.12 *right*). Of these, 61.9% (13 out of 21) stratified in s4 and s5, and 2/21 stratified at the border of s4 and s3. One extended dendrites to s2, while the remaining 23.8% (5/21) had terminal arborizations both in s4-s5 and in s2. Two interstitial RGCs were identified, one with dendrites in s2 and the other bi-plexiform, extending both in s4-s5 and in s2. Finally, a single displaced RGC soma is included in my EM volume, with dendrites terminating in s1 and s2. Overall, it appears that both axonal processes of BCs and dendritic processes of RGCs tend to occupy restricted depths of the IPL, likely in a subtype-specific manner, preferentially forming synapses with their co-stratifying partners. Assuming the vertebrate retina correlation of stratification depth to physiological properties pertains in sharks too, then cells stratifying in the outer, distal IPL would be OFF, while the ones terminating proximal to GCL would be ON.

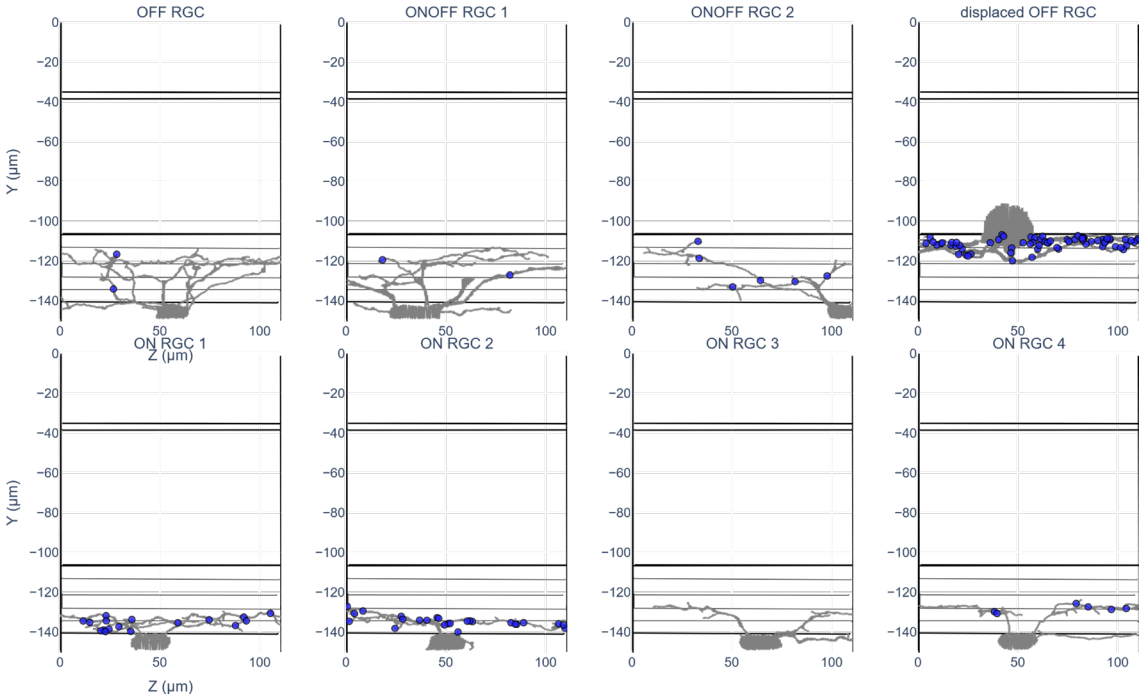

Figure 4.13 – RGCs are postsynaptic to ribbon synapses of BCs. Examples of RGC reconstructions (gray), together with the location of ribbon synapses onto them (blue circles). RGCs stratifying in the distal (*top row*) and proximal (*bottom row*) are depicted. Note the difference in the number of ribbon synapses with relation to stratification depth and cell soma location.

Specifically in numbers of received ribbon synapses, namely the principal mode of BC output, a striking observation becomes apparent: OFF and presumed

ONOFF RGCs of the GCL receive few (0-2) ribbon synapses compared to both their ON-stratifying counterparts (Fig. 4.13 and Fig. S4.8) and the displaced ACs (data not shown). Notably, there is a general scarcity of synapses onto RGCs at the middle of the IPL, where type b BCs terminate (Fig. 4.12 and Fig. S4.8).

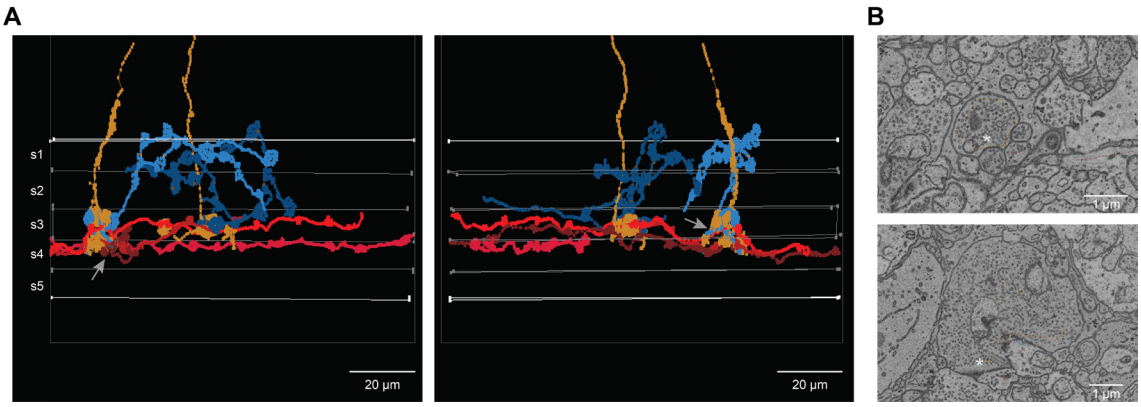

Figure 4.14 – Morphology of type b BC synaptic partners. A, x-y (*left*) and y-z (*right*) view of the shark IPL. Visible are processes of type b BCs (orange), Aii-like ACs (blue) and A17-like ACs (red). Note the different morphologies: narrow, bistratifying for Aii-like and wide, monostratifying for A17-like. B, Electron microscopy data from the shark volume, showing type b BC terminals forming ribbon synapses (asterisk) with three (*top*, Aii-like, A17- and A17-like) and two (*bottom*, Aii-like and A17-like) post-synaptic partners.

As the small-spotted catshark retina is either rod-only or rod-dominated, I next examined which of the identified BCs could correspond to the rod bipolar cell (RBC) of other vertebrates. Based on the morphology of the RBC axon terminal, which in mammals and teleosts is large and bulbous, the most likely shark candidate would be the type b. Therefore, I reconstructed 'dyadic' postsynaptic partners of its ribbon synapses (Fig. 4.14 and Table 4.1). One of them was often a monostratified, sparsely branching, wide-field AC, that had 'beaded' thickenings in regular intervals. The second was a narrow-field, bistratifying AC, with the second stratification in the presumed OFF strata (s1-s2). And in seldom occurrences of type b triadic synapses, the third partner was a duplicate of either. Overall, these reconstructed partners morphologically resemble the typical for mammalian RBCs, namely the A17 and Aii ACs[104,440], and as such increase the likelihood of type b being homologous to the mammalian RBC.

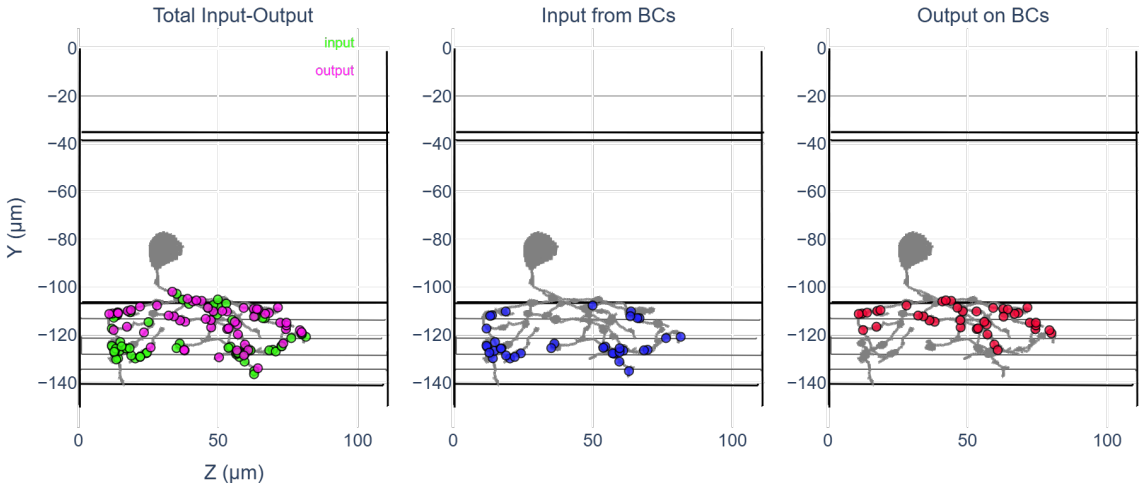

Figure 4.15 – Spatial mapping of input and output of an Aii-like AC. x-y view of the reconstructed skeleton of an Aii-like amacrine cell (for a z-y view see Fig. S4.9). Note the segregation within the IPL for the input (*middle)* – output (*right*) synaptic relationship with BCs.

In mammalian retinas, the structure of these two populous[441] AC types instructs their function. Specifically in their synaptic relationship to BCs, the Aii receives input proximally and forms its own output on BCs distally within the IPL[106,442], while A17 forms reciprocal, feedback synapses at the same terminals it receives its RBC input from[443–445]. For the single Aii-like AC I fully reconstructed and annotated its pre- and post-synaptic partners, a mammalian-like segregation of BC input-output is respected (Fig. 4.15 and Table 4.2). In contrast, the morphologically A17-like ACs come in varieties and seem to deviate from the stereotypical pattern (Fig. 4.16 and Table 4.3).

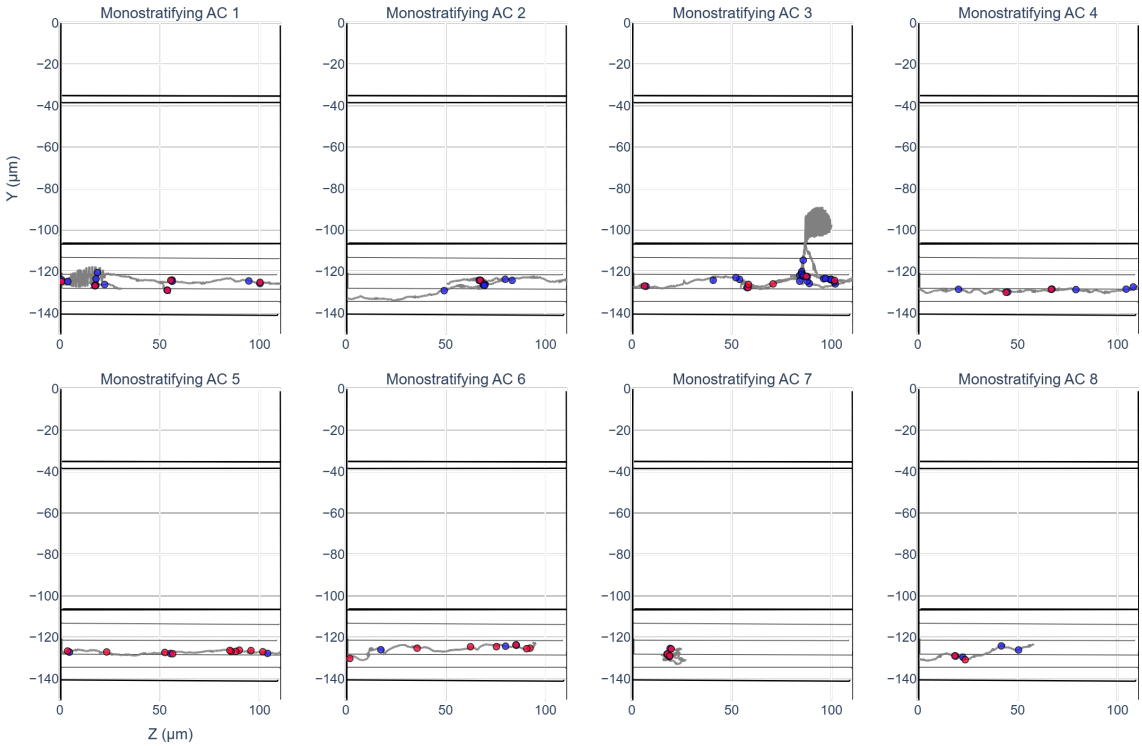

Figure 4.16 – Spatial mapping of A17-like synaptic relationships with BCs. x-y view of the reconstructed skeletons of A17-like amacrine cells. As in Fig. 4.15, blue circles represent BC ribbon synapses on the AC, while red the conventional synapses of AC onto BCs. Note the frequent absence of synapse type pairs; therefore A17-like ACs and BC are likely not governed by reciprocal relationships.

Refocusing on type b BCs however, they too have certain properties that do not neatly fit with their likely mammalian counterparts. First, they terminate in the middle of the IPL (s3), and not at the innermost layer (s1), right on top of RGC somata (Fig. 4.17A and Fig. S4.8). Second and as outlined before, although some of their postsynaptic partners morphologically resemble the A17, some are interstitial cells, a type not encountered in mammals (Fig. 4.17B), and the overall connectivity pattern is atypical. Third, and although such cases are rare, type b BCs do contact RGC dendrites directly (Fig. 4.17C; occurrence of synapses onto RGCs: mean 4.62%, standard deviation 5.30%, n=18 type b BCs, see also Table 4.1). And fourth, most type b (16/18 of currently reconstructed) BCs form *en passant* ribbon synapses as they descend into the IPL, or even within the INL (Fig. 4.17D).

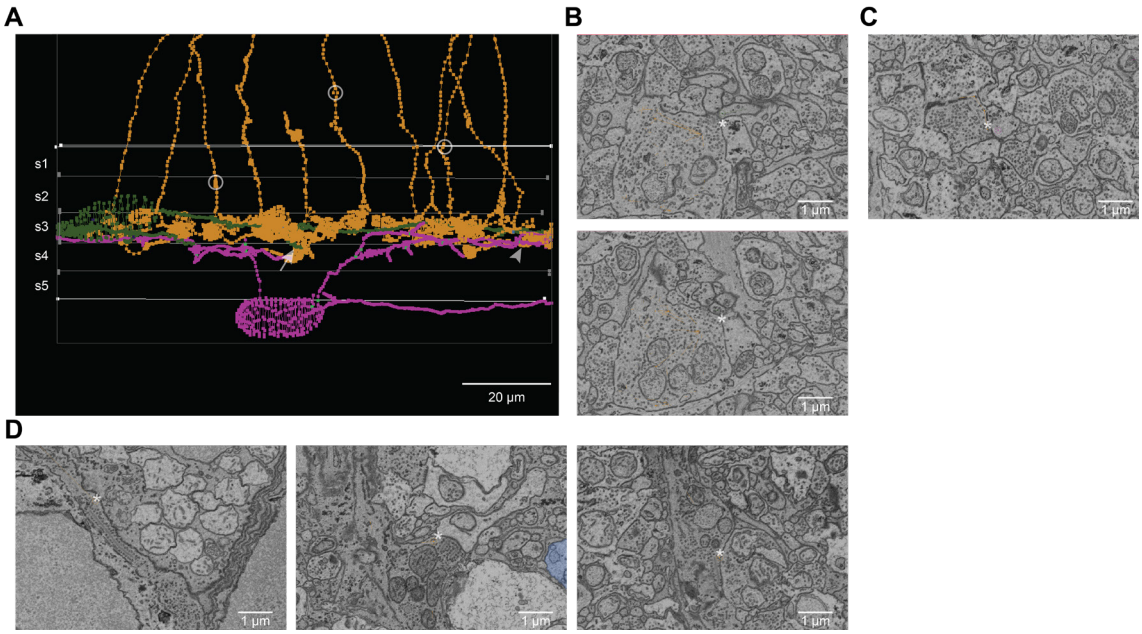

Figure 4.17 – Type b BCs have atypical characteristics for an RBC. A, Skeleton reconstructions of type b BCs (orange), interstitial AC (green) and orthotopic RGC (purple). B, Example of reciprocal synapse between a type b BC and the interstitial AC; *top* indicates a ribbon synapse (asterisk) of the BC onto the AC, while *bottom* is the next slice in the volume and shows a conventional synapse (asterisk) from the AC onto the BC (arrow location in *A*). C, Example of ribbon synapse (asterisk) of the BC onto the RGC (arrowhead location in *A*). D, Example of type b BC *en* passant ribbon synapses (asterisks) of the descending axon (locations circled in *A*).

Discussion

Here I present the first high-throughput description of the elasmobranch retinal output by recording directly from the RGCs of the small-spotted catshark *Scyliorhinus canicula*. The response tuning to different wavelengths is largely in line with previous descriptions of rod-only retinas[13,182]; characteristically the RGC population responses are well described by a log-transformed opsin absorption curve that peaks around 500 nm – the typical for rod photoreceptors. Meanwhile however, I detected a low prevalence of individual RGCs (Fig. S4.1) whose response profiles are offset and therefore poorly described by the aforementioned curve. Different explanations could account for this observation. First, the shark retina possesses a tapetum lucidum (see general Introduction), whose incomplete, patchy removal during dissections could result in filtering or distortion of the presentation wavelengths for some regions. Considering the very low prevalence of such RGCs, this scenario is unlikely. Alternatively, a previously

unreported, sparse cone type could still exist in the retina of the catshark hatchling and contribute with its distinct absorption curve in driving these few 'atypical' RGCs. I therefore relied on immunostaining combinations to inform about occurrences of a second photoreceptor type. Among a sea of rod photoreceptors (labeled by 4D1[446,447] in Fig. S4.10), I was surprised to detect a not too sparse population of PNA-positive cells (that were, importantly, not doubly labeled by 4D1). Although it could label still undifferentiated photoreceptors (see Ref[448] for the retina of skates), PNA is a marker of cone photoreceptors in mammalian retinas[449,450]. Generally however, the putative presence of a cone cell body by itself does not imply a functional photoreceptor. In fact, recent independent transcriptomics studies of the catshark retina did not detect the expression of any cone opsin[451,452], therefore suggesting that a cone absorption curve can not be contributing to the atypical RGC responses I observe here.

The same work, however, has detected the expression of melanopsin, a rhabdomeric opsin[453,454], in horizontal cells. Therefore in a third scenario, its blue-shifted[455,456] absorption profile could explain my observations of a strong UV component but also, if in an antagonistic contribution to the rod opsin curve, a response 'trough' for cyan (Fig. S4.1). Additionally, it could provide support for the surprising relationship of ON and OFF RGC response latencies specifically for UV (Fig. 4.4C); whereas for all other stimulation wavelengths the latencies of the two pathways are mirror images, both are similarly delayed for UV. If intrinsically photosensitive (ip), melanopsin-expressing horizontal cells can account for these atypical observations, it would suggest a radical organization of a vertebrate retina; where most ciliary photoreceptor types are lost, and a rhabdomeric has a prominent role in instructing the same downstream circuits as rods. And strikingly, such a role might even pertain broadly to early vertebrates; in contrast to mammals where melanopsin expression is contained to ipRGCs, teleosts[457,458], elasmobranch[451] and cyclostomes[130,459] (lampreys) all express it in horizontal cells, in close physical and nodal network proximity to the typical vertebrate visual photoreceptors.

The response polarity of a visual neuron is among the earliest and most fundamental descriptions towards characterizing the organization of sensory processing. The shark retina has previously remained largely understudied, likely

because of possessing only a few photoreceptor types[460] and behaviorally being unable to discriminate colours[461] or relying on alternative sensory systems to locate prey[462,463]. Early work on elasmobranch retinas identified ON, ONOFF, and OFF [56,57,57–60]RGCs in species-specific varying ratios[164,169,172–175], but nevertheless came with inherent limitations of low resolution (electroretinograms) or low and perhaps biased sampling (single-electrode recordings). Instead, here I provide the first high-throughput description from two catsharks and different retina regions. Data indicates an overwhelming abundance of 'pure' polarities, namely ON and OFF, relative to the mixed ONOFF (Fig. 4.2, 4.3, S4.4). In this property, sharks more closely resemble mice than other vertebrate clades (see also Introduction). Besides the functional, there are structural similarities too: compared to avian[464] or teleost[465] retinas, the mouse[103] is dominated by monostratifying BCs, and my EM data reveals that so is the shark (Fig. 4.12). Furthermore, both sharks and mice have independently lost some of their photoreceptor input channels, likely accompanied by a decrease in their RGC layer density in comparison to other vertebrates[55]. Together, these likely interconnected structural and functional changes illuminate a path of progression within the vertebrate retina evolution landscape for when the photoreceptor type complement expands or shrinks.

In contrast to mice however, where most descriptions identify largely symmetric ON and OFF pathways in both visual image properties encoding[361,362] and computations performed[466], here I identify dominant asymmetries. Specifically, ON RGCs are fast, transient, and better at encoding temporal frequencies than their OFF counterparts (Fig. 4.4, 4.5, 4.8). This relationship might arise as an inherent property of rod pathway signaling, because fast transient ON versus slow sustained OFF RGCs have been reported for the mammalian retina at light levels where responses are primarily driven by rods[467]. This explanation however does not fully account for the opposite effect of luminance changes; the shark ON pathway accelerates with higher stimulus intensity, as routinely expected from sensory systems[468–470], but the lag in the OFF increases instead (Fig. 4.4c). Future research should examine whether this reverse relationship of response timing to stimulus intensity can be attributed to inhibitory circuits as recently reported for other cases of retina processing[471,472].

Overall among vertebrates, the shark retina is slow in response to the simple, full-field stimuli presented here. This is evident both for full-field flash (Fig. 4.2, 4.5) and the 'chirp' stimulation where the response range presented was maxed at 8 Hz but with responses already absent considerably earlier (Fig. 4.8). These findings could just reflect the lower bound of shark RGC capabilities for a number of reasons. First, full-field stimuli activate uniformly the excitatory center and the -usually extending over greater distances- inhibitory surround of the receptive field of the cell (see also general Discussion). With stimuli of finer spatial scale, the weight of the latter is theoretically expected to be disproportionately smaller and the response times of RGCs faster. Nevertheless, presentations of checkerboard patterns aimed at describing receptive field spatiotemporal properties of shark RGCs kept the retina mostly silent for frequencies above 1Hz (data not shown). Second, the recordings temperature could contribute to the observed timings. Certain species of teleost[473,474] and sharks[475,476] have been found to warm up their brain and eyes relative to the rest of the body to allow for better temporal resolution in their sensory-guided behavior. In contrast to the above animals, however, the catsharks studied here are slow swimming, bottom dwelling species and therefore unlikely to employ such mechanisms. Third, recordings were conducted during daytime, when the animals are mostly resting with their pupil slit only narrowly open. Perhaps an altered neuromodulation state is governing the retina kinetics at nighttime, and future experiments could prove valuable. In general however, long latencies are not necessarily detrimental at the level of behavior. For example, they are likely a great concern for actively hunting, or flying animals, but for stationary predators such delays could even prove advantageous. A characteristic example is the frog, whose extreme long latencies[477] at the sensory level enable longer temporal summation and better predictions of the future position towards which it eventually strikes[478] its tongue, meeting the target prey there.

Besides the dominating ON and OFF types, here I additionally describe two ONOFF RGCs, the most populous of which has a characteristically delayed (>700ms) OFF component (Fig. 4.5). Similar delays have been reported in the mammalian retina in relation to ambient light levels[479], and this explanation likely pertains to sharks considering the latency dependence of the OFF component on

stimulus duration (Fig. S4.2) and intensity (data not shown). Interestingly in connection to their hypothesized role as photoreceptors, this component might arise from horizontal cell contributions[480], but further research is needed.

Here I describe direction-selective RGCs in sharks, which now constitutes the earliest vertebrate case of implementing this neural computation at the level of the retina already. I identify two DS systems, namely an ON DS with their preference axes 120 degrees apart and an OFF DS with 90 degrees of separation (Fig. 4.9). As such, they are in line with the mammalian ON and ONOFF DS, respectively (see Introduction). The shift of DS representation to a different polarity channel (shark OFF DS versus mammalian ONOFF DS) is conceivable if we take into account how DS is implemented in other vertebrates. In salamanders, there are only OFF DS RGCs, but they can be grouped in two distinct subtypes with regards to their properties and preferred directions - resembling the ON and ON-OFF systems of the mammalian retina[407]. Frogs possess DS RGCs of all three polarities (ON, ONOFF and OFF)[434], while in turtles only the latter two have been physiologically reported[410]. Quails have ONOFF and OFF DS RGCs, with the preferred directions within each being separated by 120 degrees[406]. A similar pattern (most ONOFF, few OFF DS) is reported in archerfish, but instead with only the rostral direction strongly encoded[408]. And yet another pattern exists within teleosts: goldfish DS RGCs are in similar proportions either of ON or OFF polarity and both are sampling the visual space with 120 degrees of separation in their preferred directions[435].

One of the key cell types participating in DS retinal computations is the starburst amacrine cell (SAC, see also Chapter 5 Introduction). Other than its characteristic, exploding-star morphology, this cell is quite unusual in utilizing two distinct neurotransmitter (NT) systems, namely GABA and acetylcholine. Transcriptomics work on the small-spotted catshark has identified[451] and I here confirm with immunostainings (Fig. S4.10) the cellular co-localization of the above NTs in what are the prime candidates for a shark SAC. To that front, future characterization of their morphology would be illuminating, for example by utilizing high-resolution electron microscopy datasets. Regardless of morphology however, in Chapter 5 I explore the role inhibition plays in the emergence of DS

to inform about the algorithmic conservation of the mechanism across vertebrates.

To my knowledge, the SBEM volume of the shark retina I generated is the first available dataset with the potential to illuminate the shark retina connectivity from signal input to output (photoreceptors to RGCs). Although it reflects ongoing work, certain key observations are becoming evident. First, some properties appear to generally describe the shark retina. For example, the IPL thickness (39.8 µm) of the small-spotted catshark is identical (40 µm)[99] to the one reported for the adult smooth dogfish, *Mustelus canis*. By using light microscopy in that work, Witkovsky and Stell first identified five bipolar cell types with common morphological properties to the ones described here (Fig. 4.12A); therefore I adhered to their naming convention. And although exceeding the three types recently described with transcriptomics[451] for the small-spotted catshark, a retina with only five BC types generally represents the lowest reported thus far, substituting in for the lamprey with the transcriptomically described eight[130]. Along the course of evolution, a likely explanation for such a reduction may be attributed to the reduced photoreceptor complement in sharks: with BCs relaying, in a switchboard manner[95], photoreceptor signals to RGCs, the evolutionary loss of input channels would conceivably render some BC types useless. Irrespective of the underlying cause, a narrow diversity of photoreceptor and bipolar cell types can heavily influence the limited variability of RGC physiological responses identified here.

Considering that rods are the dominant photoreceptors in the shark retina, what is then the circuit conveying their signals to higher visual areas? In other vertebrate retinas, the rod bipolar cell is the only BC driven predominantly by rod signals, and it comes with a distinct molecular, anatomical and functional profile relative to the mainly cone-driven bipolar cells[95,103,129,130,206,310,440] (see also Introduction). Namely, it possesses large, bulbous terminals, and although it terminates near RGC somata, it does not have a direct communication line to them. Instead, it utilizes the Aii AC and both ON and OFF CBCs to relay its signal to RGCs of both polarities. This primary (or canonical) pathway of rod communication is greatly conserved within mammals, and has additionally recently been identified in zebrafish[206]. In line with previous morphological reports

of shark BCs[99], here I identify the type b BC as the likely RBC candidate in the shark retina. Further strengthened by the ongoing tracing of postsynaptic partners, the whole canonical circuit, with Aii- and A17-like cells (Fig. 4.14, 4.15, 4.16), might be ancient, going back at least to the common ancestor of all jawed vertebrates.

Seemingly at odds with the above statement, type b BCs also display properties uncharacteristic of mammalian RGCs (Fig. 4.17). Here I present this contradicting evidence, together with plausible explanations. First, type b BCs synapse onto A17-like interstitial cells. To my knowledge, there are no reports of interstitial cells in mammalian retinas, therefore this might represent a recently emerged or lost type, or just a misplaced counterpart of the existing orthotopic (in INL) and displaced (in GCL) A17[481,482]. In terms of economising the wiring, the latter scenario seems plausible: compared to the interstitial, both orthotopic and displaced A17 ACs need to spend relatively more resources for their primary dendrite to first transverse the IPL before ramifying at the appropriate stratum. Second, type b BCs form direct synapses to RGCs and *en passant* synapses. The former is also observed developmentally in mammals, before seemingly taken over by t6 CBC during circuit maturation[483,484]. Additionally, it is the t6 in the mammalian retina that forms the most *en passant* synapses, while the RBC lacks them entirely[442] (but also see[485,486]). And finally, it is the t6 that, among the ON CBCs, is predominantly responsible for conveying the rod-RBC-Aii signal to ON RGCs[442]. It thus appears that the roles of t6 and RBC are ontogenetically intertwined, and an altered relationship (or even the absence of t6 altogether) may account for the uncharacteristic traits of the shark type b BC.

Perhaps most importantly, the termination of the type 5 BC in the middle of the IPL (s3, Fig. 4.12, S4.8) is entirely unprecedented for RBCs. If it represents a case of premature termination, it may be associated with a stop signal related to encountering the somata of the interstitial cells. Irrespective of the underlying cause however, I suggest that RBCs conveying signals at the middle of the IPL might not be paradoxical, but just heretofore overlooked. In teleosts for example, there are two types of RBCs that both terminate in s1, but one of which additionally forms synapses at the s3 stratum[206,465]. And although in the exhaustively studied mammalian retina such synapses are often not

encountered[105,440,487,488], similarly ‘paradoxical’ mid-IPL synaptic patterns have nevertheless been reported for the bat[489] and macaque[490] RBCs. Therefore, what has been previously suggested[206] as a teleost-specific emergence or mammalian loss, might actually represent an ancient feature of the jawed vertebrate RBC, still extant in most classes (Fig. 4.18). Even in this case however, the presumed shark RBC represents the first documented case of terminals in s3.

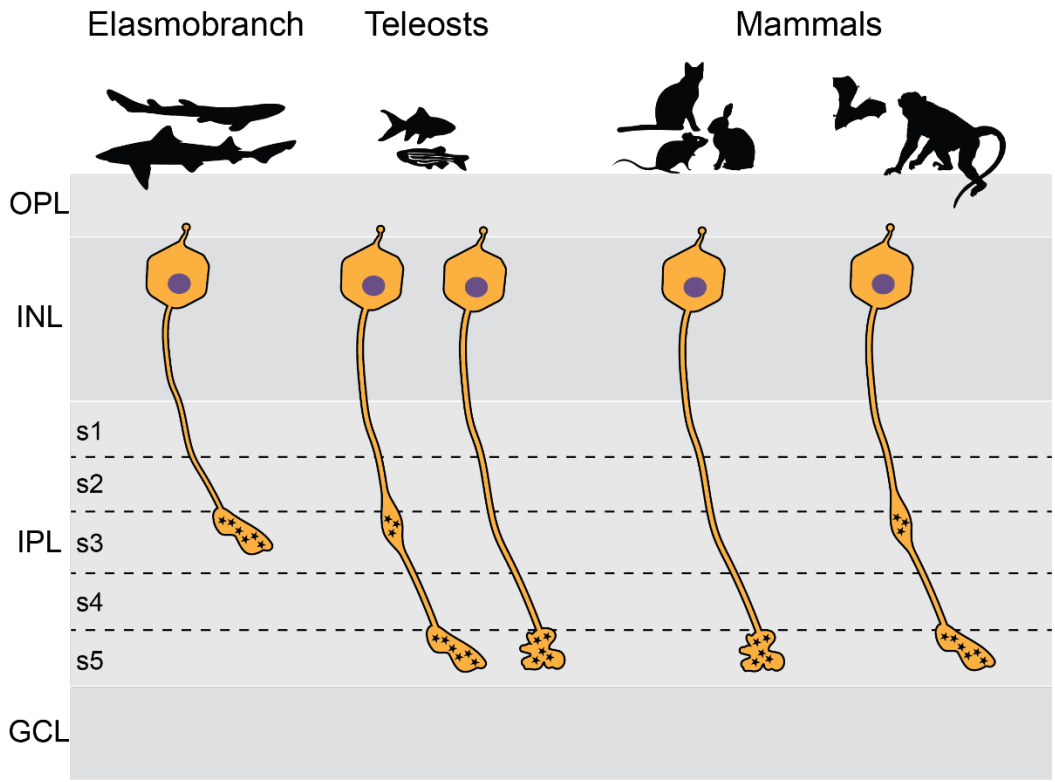

Figure 4.18 – Morphology of Rod Bipolar Cells across vertebrates. Although RBCs in sharks are atypical in terminating in s3 of the IPL, mid-IPL axon thickenings and ribbon synapses (asterisks) have been described both for teleosts and mammals. Shape of terminals is rooted in a recent description of the two RBC types in zebrafish (see Ref[206]) and extended to other vertebrates (present work for shark, see Refs[487],[490] for rabbit and primate RBC respectively). The photoreceptor layer, the RBC dendritic tree and other retina cell types are omitted for clarity.

In terms of type-independent BC projections, the shark IPL appears uniformly covered except for a narrow band close to the s2-s3 border (Fig. 4.11). Such a glutamatergic bouton-free zone has been previously described both in zebrafish[491] and mice[103], and often demarcates IPL sublamina a from b. Although the relationship between IPL stratification depth and polarity of response is currently unknown for shark retina neurons, in species where it has been

investigated directly the pattern is unequivocal; OFF cells stratify in sublamina a while ON in b[93,96,491–497]. If it holds true for sharks, then the IPL volume partitioning is ON-biased (s1-s2 the OFF and s3-s4-s5 the ON), and more closely resembling mice than zebrafish.

Under this assumption for the shark retina, we can then classify the response polarity of cells traced in the EM data based on their dendritic stratification depth. For BCs, type a1 and a2 would be OFF, while type c1 and c2 ON. Stratifying in s3, type b would also be ON, in agreement with its proposed homologous RBCs in other jawed vertebrates. For the RGCs with somata in the ganglion cell layer, 71.4% (15/21) stratified in the ON IPL layers, 4.8% (1/21) in the OFF, while the remaining 5/21 had dendrites ramifying in both sublamina a and b. The disproportionate number of ON versus OFFs is within the range of my physiological data from the temporal region of the retina (Fig. 4.3), but towards the lower bound. Ultimately however, the response polarity of bistratifying cells depends on where they receive excitatory input from BCs, and not solely on their stratification depth. Although here I identify a limited number of ribbon synapses on these RGCs that extend dendrites to s1 and s2 compared to their ‘ON’-stratifying counterparts, bipolar cells can also form conventional synapses, albeit at smaller numbers[204]. Such data has not been systematically assessed in our shark dataset yet. Nevertheless, as in the same bipolar neuron the ribbon-associated synapses can transmit fast, low-threshold signals compared to the delayed, high-threshold of the ribbon-free synapses[498], a potential asymmetrical presence of the two synapse types onto ON and OFF RGC dendrites respectively might account for the difference in delays and transience profiles of the responses I observe (ON fast and transient, OFF delayed and sustained (Fig. 4.4).

Notably, none of the somata residing in GCL extend dendrites deep in s1. This stratum is not void of postsynaptic processes however; rather it is extensively sampled both by the sole displaced RGC in our EM volume and by ACs that reside in its proximity at the INL-IPL border (data not shown). Contrary to the presumed ONOFF and OFF RGCs of the GCL, the displaced RGC receives a large number (>50) of ribbon synapses (Fig. 4.13). However, this cell is likely not captured in my electrophysiology data (see General Discussion), perhaps explaining why I do not observe OFF RGCs matching the latency of the ONs.

Overall, displaced RGCs have been described in most vertebrate species studied to date, including teleosts[499,500] and mammals[501]. Compared however to their low, abundance in mammals (about 2%), displaced RGCs in sharks are often found in comparable numbers to their orthotopic counterparts (27.1-42.2% identified in two regions in the present work, Fig. 4.10). Additionally, the dendritic stratification observed here for the displaced RGC in the s1 and s2 strata is common across vertebrates[500,502,503], and is hypothesised to represent a resource allocation reduction strategy similar to the displaced ON-stratifying ACs of the GCL[504]. Although stratifying in the fundamental OFF IPL sublamina, some of these cells can be physiologically ON due to receiving *en passant* synapses from descending ON BC axons[96,485,486]. Here, we therefore describe the earliest known vertebrate example of such an 'accessory ON layer' in the OFF sublamina, with contributions from type b (14/16) and type c2 (3/8). Type c1 (0/2) *en passant* synapses have not been observed in s1 or s2, although both these neurons form such synapses in s3.

Finally, I have identified many interstitial cells, located at 40-60% of IPL depth (Fig. 4.10). Though less prevalent, interstitial ACs and RGCs have been previously observed in the teleost retina[499,505,506]. These ACs are physiologically ON[507], can form connections with each other[506,508] and may express different neurotransmitters like dopamine[509], GABA[510–512] and, in lampreys, serotonin[513]. Because they are virtually absent from mature mammalian or avian retinas (but see[502]), but have nevertheless been observed transiently during development[514–516], they are hypothesized to represent misplaced cases during histogenesis, that later either migrate to the correct location or undergo apoptosis. Whether homologous to the mammalian or different types altogether, the high prevalence of interstitial cells in sharks and their integration to functional circuits offers an opportunity to understand their role in visual signal processing. If they are to also express a rich repertoire of neurotransmitters as their jawless and teleost relatives, it could hint to an increased representation of these signalling pathways in the visual signal processing of early diverging vertebrates.

Supplementary Figures and Tables

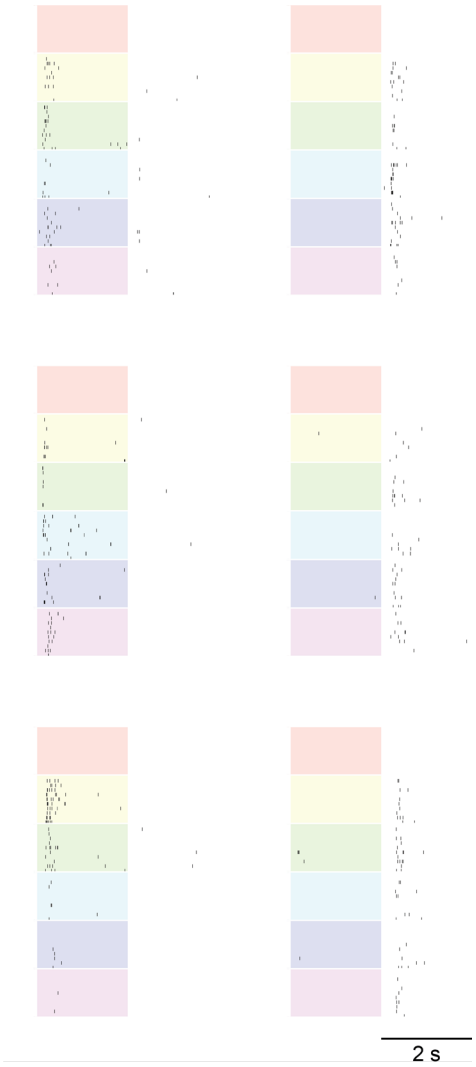

Figure S4.1 – Shark RGCs with atypical chromatic profiles. The figure structure is similar to Fig. 4.1; example ON (*left*) and OFF (*right*) RGCs that are either unresponsive to LEDs that stimulate strongly the rods, or with unexpectedly narrow and offset response profiles.

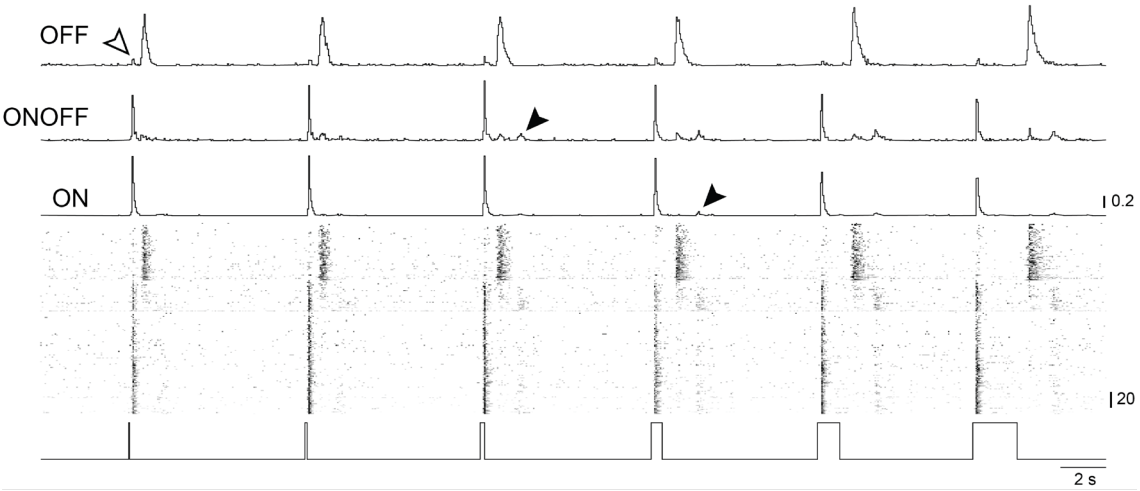

Figure S4.2 – Population responses to 'variable duration flashes' stimulation. The structure of the plot is similar to Fig. 4.2. Note weak ON responses for some classified OFF RGCs (open arrowhead) and the high-threshold emergence of the delayed OFF response component in the ONOFF and some ON RGCs (filled arrowheads).

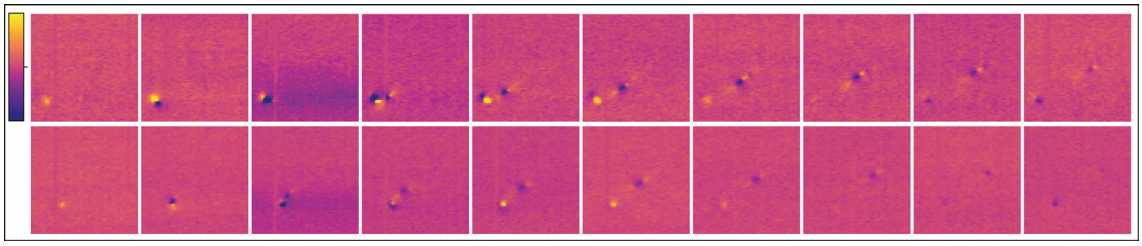

Figure S4.3 – Electrical images (EI) of ONdOFF RGCs. Each shown EI (individual rows) consist of time-series (3 ms apart) of a single spike sorted unit passing the quality index threshold and assigned to the ONdOFF RGC group. The presence of cell soma, axon, and the action potential travelling down the axon towards the optic nerve head confirm that these units are indeed RGCs.

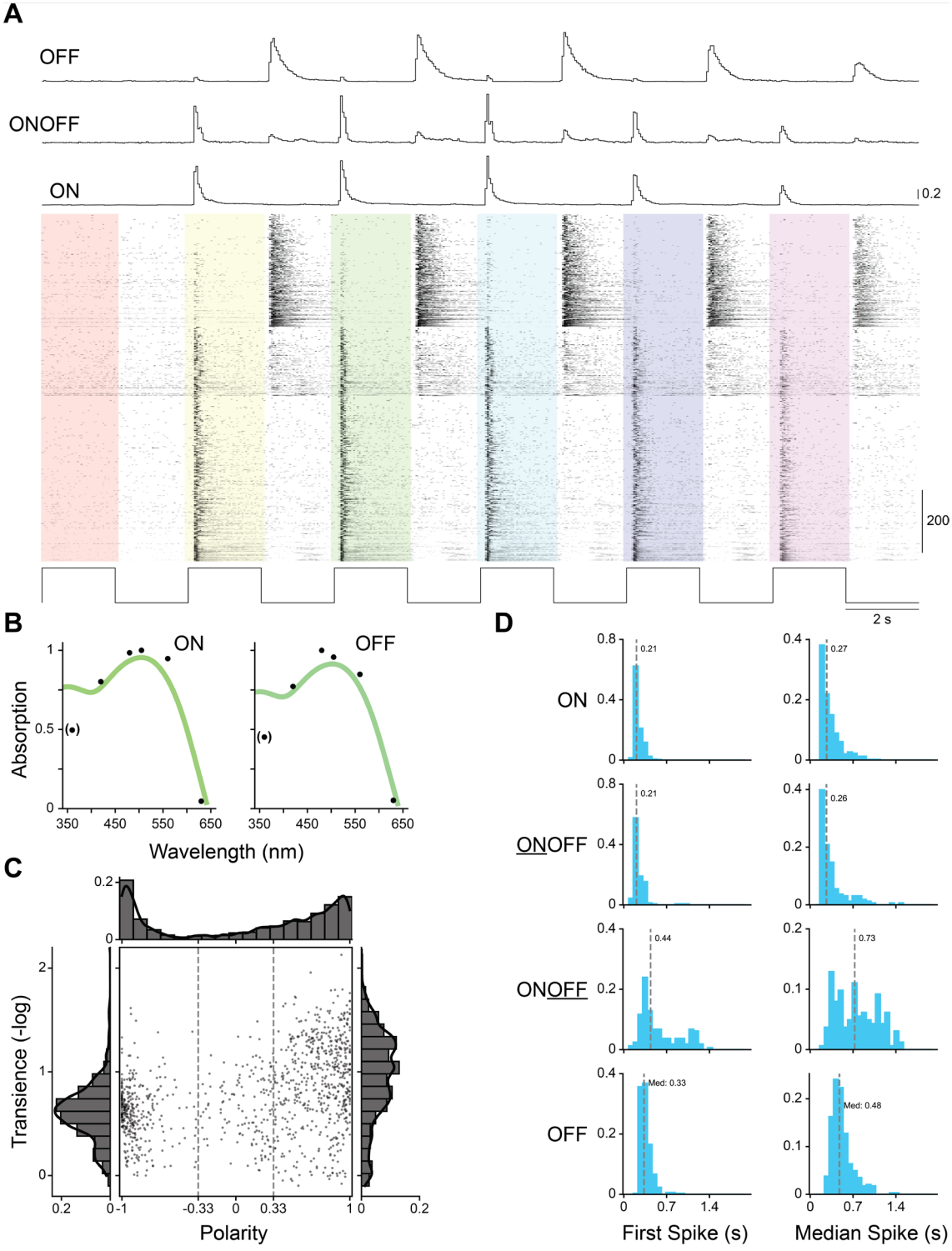

Figure S4.4 – Responses to chromatic stimuli of Scyliorhinus stellaris RGCs. Summary figure, in line with the structure of Figs. 4.2-4.5 for *Scyliorhinus canicula*.

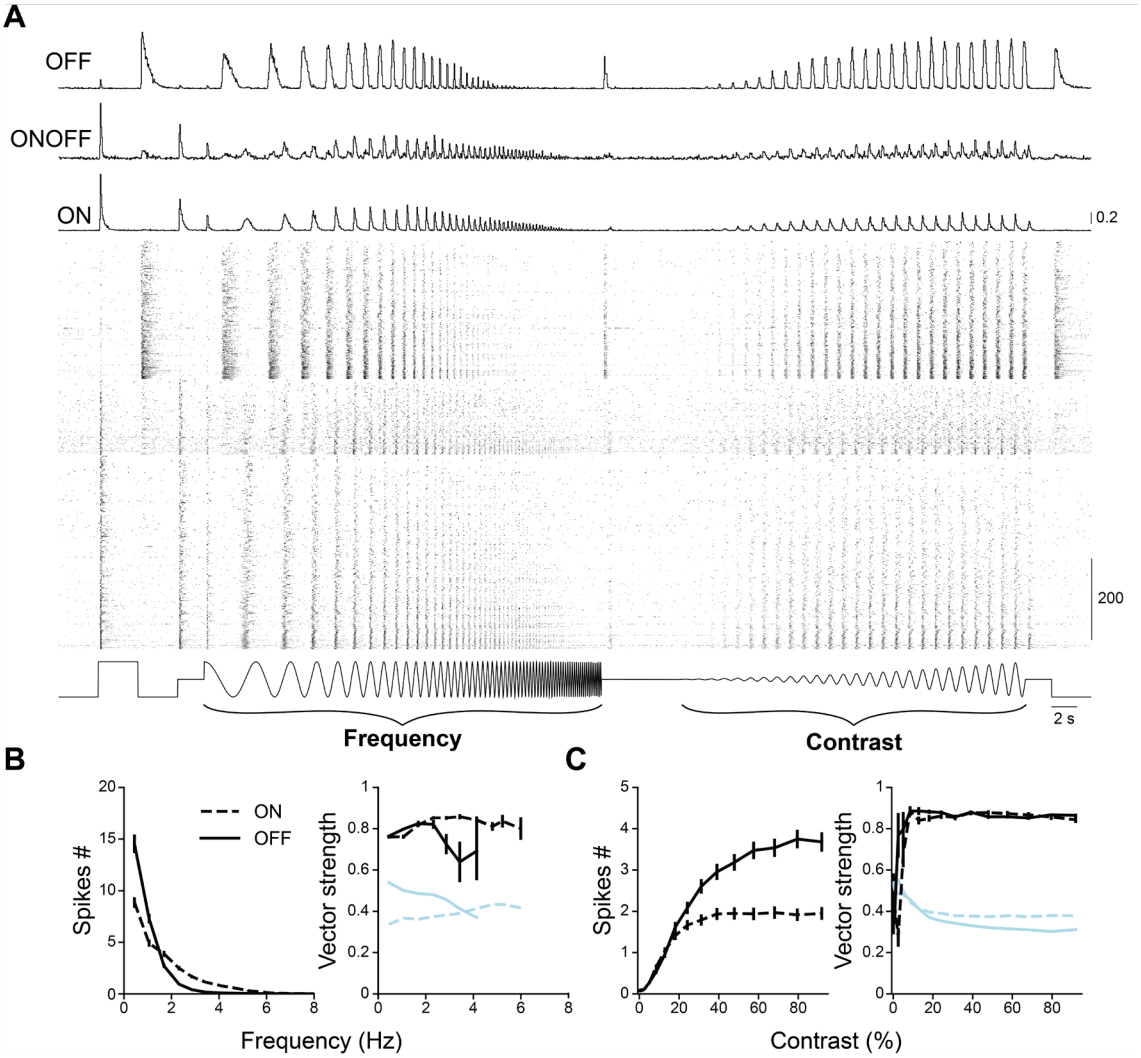

Figure S4.5 – Responses to 'chirp' stimulus of Scyliorhinus stellaris RGCs. Summary figure, in line with the structure of Figs. 4.7-4.8 for *Scyliorhinus canicula*.

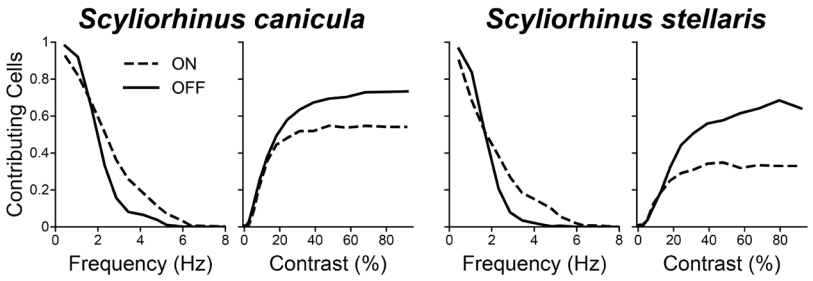

Figure S4.6 – Ratio of contributing cells to the phase-lock index.

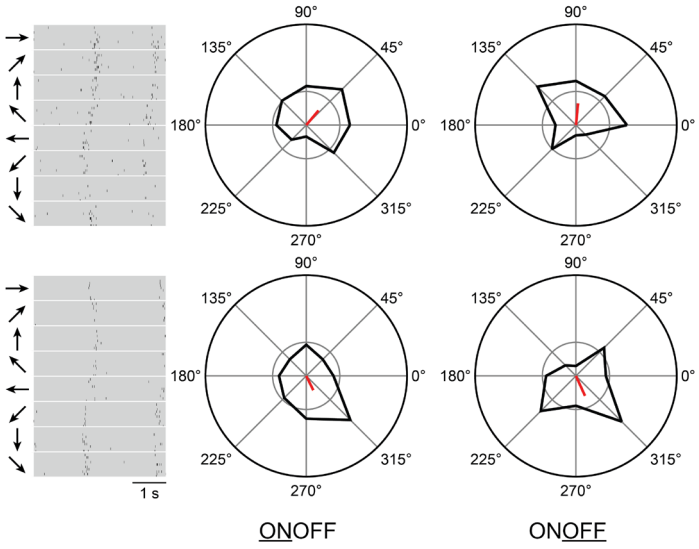

Figure S4.7 – ONOFF direction-selective RGCs are rare. Shown are the two only examples of ONOFF DS RGCs found in the recordings. The two polarity components roughly preferred the same direction of motion, but note how ON spikes are again more numerous.

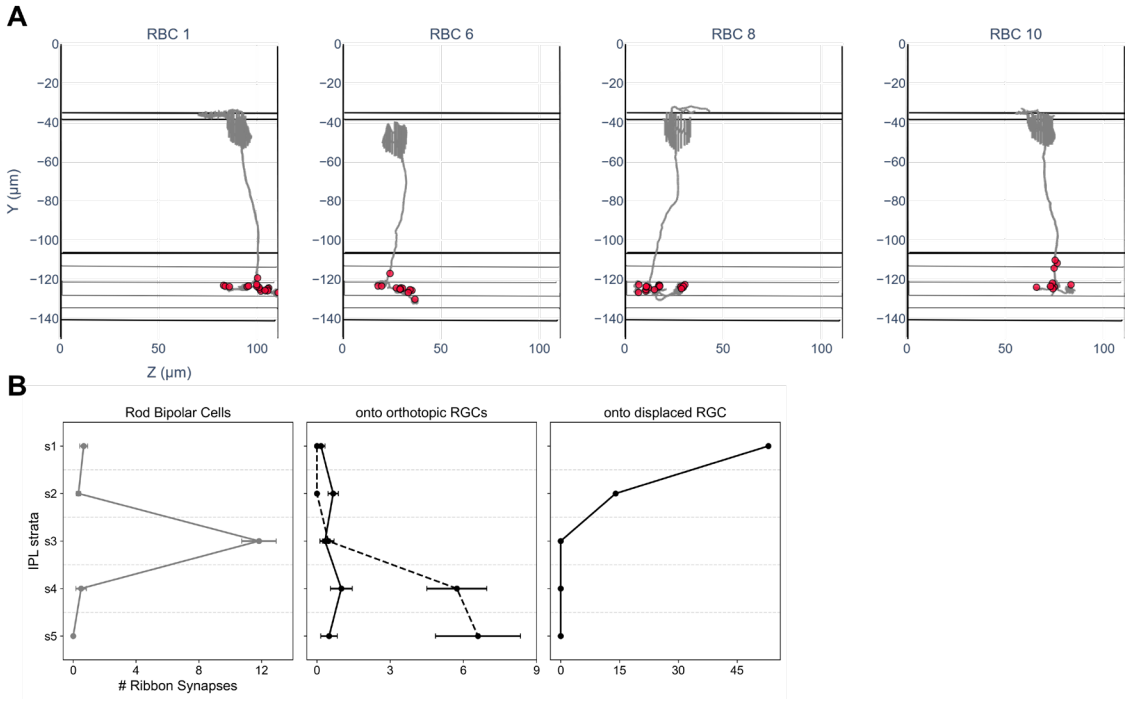

Figure S4.8 – Type b BCs terminals stratify in s3, unlikely to contribute direct input to RGCs. A, Skeleton reconstructions of type b BCs, overlayed with the location (red circles) of their primary synaptic output (ribbon synapses). B, Their overwhelming majority occurs at a stratum (s3) that both displaced and orthotopic, ON and OFF RGCs rarely receive ribbon synapses in.

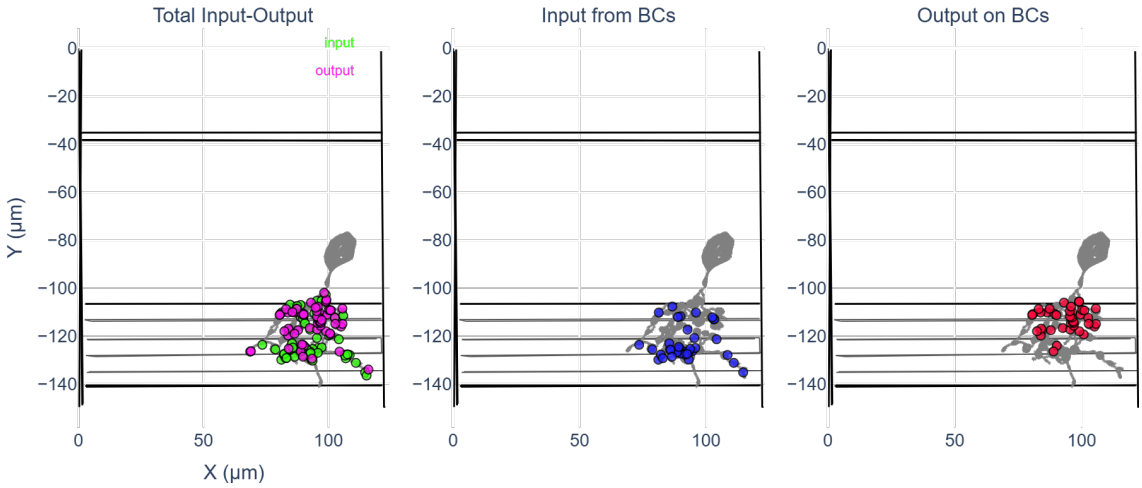

Figure S4.9 – Different (z-y) view of the Aii-like AC. Same cell to Fig. 4.15. Note the disproportionate 'spread' on the x- and z- dimensions in the two figures.

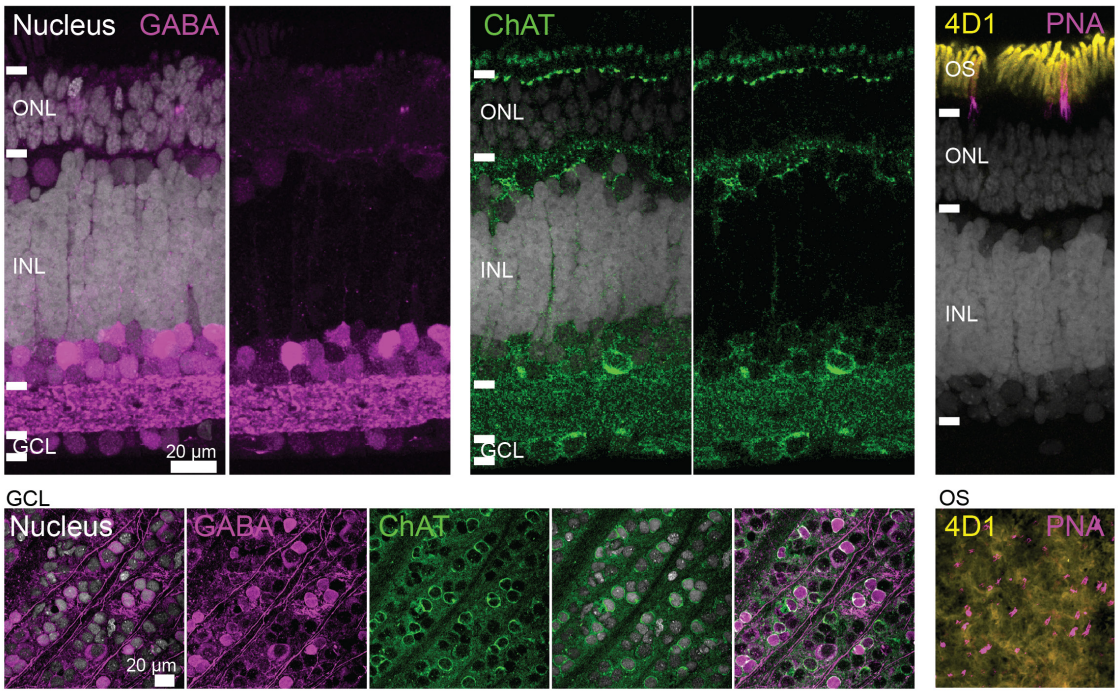

Figure S4.10 – Immunostainings reveal unexpected traits of the shark retina. Different tissues imaged in the sagittal (*top*) and horizontal (*bottom*) plane. Note the broad expression of GABA, the absence of ChAT crisp bands in the IPL but the presence of a clear pattern above the ONL, and the presence of a sparse, but not rare, PNA-positive segment.

Tree	Synapse Type	Combination	Count
RBC 1	Summary-dyad		11
	Summary-triad		3
	dyad	ac ac	11
	triad	ac ac ac	3
RBC 2	Summary-dyad		15
	Summary-triad		2
	dyad	ac ac	14
	dyad	ac rgc	1
	triad	ac ac ac	2
RBC 3	Summary-dyad		11
	dyad	ac ac	8
	dyad	ac ut	2
	dyad	ut ut	1
RBC 4	Summary-dyad		8
	Summary-triad		1
	dyad	ac ac	8
	triad	ac ac ac	1
RBC 5	Summary-dyad		11
	Summary-triad		1
	dyad	ac ac	9
	dyad	ac ut	2
	triad	ac ac rgc	1
RBC 6	Summary-dyad		7
	Summary-triad		4
	dyad	ac ac	6
	dyad	ac ut	1
	triad	ac ac ac	4
RBC 7	Summary-dyad		14
	Summary-triad		1
	dyad	ac ac	14
	triad	ac ac ac	1
RBC 8	Summary-dyad		10
	Summary-monad		2
	Summary-triad		5
	dyad	ac ac	9
	dyad	ac rgc	1
	monad	ac	2
	triad	ac ac ac	5
RBC 9	Summary-dyad		9
	Summary-triad		7
	dyad	ac ac	9
	triad	ac ac ac	7
RBC 10	Summary-dyad		5
	Summary-monad		2
	dyad	ac ac	3
	dyad	ac rgc	1
	dyad	ac ut	1
	monad	ac	1
	monad	ut	1
RBC 11	Summary-dyad		5
	Summary-triad		4
	dyad	ac ac	4
	dyad	ac ut	1
	triad	ac ac ac	2
	triad	ac ac rgc	1
	triad	ac ac ut	1
RBC 12	Summary-dyad		5
	Summary-triad		5
	dyad	ac ac	5
	triad	ac ac ac	4
	triad	ac ac rgc	1

Table S1 – Catalogue of type b BCs in shark (RBC-like). ac; amacrine cell, rgc; retina ganglion cell, ut; unknown type.

Aii-like: Input-Output per Cell & Sublamina

Tree	Sublamina	below ribbon	below psd	psd of my own on BC	psd of my own on AC	psd of my own on RGC
Aii	**OFF (s1+s2)**	**9**	**11**	**35**	**7**	**1**
	ON (s3+s4+s5)	**27**	**20**	**2**	**8**	**3**

Table S2 – Catalogue of the Aii-like AC. Currently includes the only fully skeletonized and synapse-annotated cell of this type. psd; pre/post synaptic density, with '*below*' relating to input and '*of my own*' to output of the AC.

A17-like: Input-Output per Cell & Sublamina

Tree	Sublamina	below ribbon	below psd	psd of my own on BC	psd of my own on AC	psd of my own on RGC
Monostratifying AC 1	OFF (s1+s2)	1	0	0	0	0
	ON (s3+s4+s5)	12	44	5	6	0
Monostratifying AC 2	OFF (s1+s2)	0	0	0	0	0
	ON (s3+s4+s5)	9	14	1	3	0
Monostratifying AC 3	OFF (s1+s2)	2	0	0	0	0
	ON (s3+s4+s5)	20	26	6	6	0
Monostratifying AC 4	OFF (s1+s2)	0	0	0	0	0
	ON (s3+s4+s5)	6	19	2	4	2
Monostratifying AC 5	OFF (s1+s2)	0	0	0	0	0
	ON (s3+s4+s5)	3	4	10	3	0
Monostratifying AC 6	OFF (s1+s2)	0	0	0	0	0
	ON (s3+s4+s5)	3	2	7	1	0
Monostratifying AC 7	OFF (s1+s2)	0	0	0	0	0
	ON (s3+s4+s5)	3	13	3	5	13
Monostratifying AC 8	OFF (s1+s2)	0	0	0	0	0
	ON (s3+s4+s5)	4	2	2	5	0

Table S3 – Catalogue of the A17-like ACs. Terminology in line with Table S2.

Chapter 5 – Pharmacology of the shark retina

Abstract

The retinal output is not shaped solely by the molecular composition and structural wiring of upstream retina cell classes. Rather, it critically depends on the neurotransmitter and nodal network positions of presynaptic partners. Adding to the structural and physiological descriptions of Chapter 4, here I apply different pharmacological agents to inform about the functional organization of visual signals upstream of RGCs.

The effects observed on the shark retina are largely compatible with its mammalian counterpart, including the reliance of the ON pathway on metabotropic glutamate receptors and the implementation of direction-selectivity. Notably however, unexpected crosstalk between ON and OFF pathways is additionally unveiled.

Introduction

Compared to the anatomy levels of structure and circuit wiring of a nervous system, the computation units or their evolution are less straightforward to study, let alone understand. Early studies demonstrated that the retina is not merely transmitting information about light intensity of the visual world but is instead capable of complex processing. Admeasuring on top of that seminal finding, its experimental accessibility, clear input-output functional roles and “tidy” spatial organization of information flow, the retina is arguably among the best candidates for interrogating the implementation and evolution of computations[351,517].

Before the advent of molecular targeting tools in model species, pharmacological perturbations were routinely employed for deciphering computational units, i.e. the wiring diagram and neurotransmitter logic of participating neurons. Use of both agonists and antagonists, which mimic or reverse the natural ligand respectively, has allowed synapse type-specific targeting and isolating effects on the physiological readout either of direct downstream cells or at the tissue level. Though widely used in neuroscience, the following three cases of pharmacological perturbation have advanced our understanding of retina structure and function the most.

Parsing the ON pathway

The visual signal is already divided at the first synapse into two pathways of opposite polarity (see Introduction), with early experiments on the mudpuppy retina demonstrating that the pathways are independent. Specifically, application of 2-amino-4-phosphonobutyric acid (APB), a glutamate agonist, eliminated ON responses from bipolar, amacrine and ganglion cells, while leaving the OFF largely intact[518]. Later confirmed by molecular studies[78,519,520], APB was suggested to mimic the endogenous photoreceptor neurotransmitter effect on the glutamate receptors expressed at the dendrites of the ON, and not the OFF, bipolar cells. Notably, such a selective effect on the ON pathway upon application of APB (or L-AP4, specifically its L-enantiomer) has since been reported for all vertebrate classes studied to date[436,521–526], thus suggesting an ancestral, and maintained, vertebrate implementation of pathway splitting. Finally, this perturbation has been pivotal not only for effectively blocking the ON pathway, but for enabling researchers to study OFF channels in isolation[527,528].

Inhibitory neurotransmitters and the spread of amacrine cell processes

Early receptive-field studies revealed that picrotoxin/bicuculline $GABA_{A/C}$ antagonists) and strychnine (glycine receptor antagonist) had distinct effects on ganglion-cell center–surround organization, implying separable inhibitory streams[529] of action. In general, amacrine cells can exert their effects either as lateral feedback (onto BCs) or feedforward (onto RGCs) inhibition, in both cases influencing the spatial and temporal response profiles of their postsynaptic partners[530–532]. Parallel anatomical and immunocytochemical studies have converged with pharmacology to show that wide-field amacrine cells are predominantly GABAergic whereas narrow-field amacrines glycinergic[533–536]. Because narrow-field amacrines typically extend processes across the ON/OFF boundary of IPL strata, blocking glycine receptors with strychnine in practice attenuates narrow-field, vertical “cross-layer” inhibition[373,537]. Instead, picrotoxin/gabazine preferentially disrupts wide-field, lateral GABAergic inhibition within a layer, matching the cells’ arbor sizes and stratification. Despite conveying their signaling via distinct neurotransmitters, inhibitory interactions occur between different AC types, with often complex, non-linear net effects upon pharmacological perturbation of different neurotransmitter systems or at their

different receptor types[533,538–541]. Overall, this coupling between neurotransmitter employed and amacrine cell anatomy forms the base of many retina circuit motifs in the inner plexiform layer, including for encoding the direction of motion, which is described below.

The building blocks of direction-selectivity (DS)

Although several additional circuits or postsynaptic mechanisms can enhance direction-selectivity or ensure its robustness[542–548], DS in RGCs is primarily driven by asymmetric input from inhibitory neurons[549,550]. Our understanding of the molecular implementation of DS has gradually cumulated. First, pharmacological perturbation of GABA signaling rendered the DS RGCs nonselective[551]. Targeted eliminations then revealed the starburst AC, named after its exploding star morphology, is responsible for conferring DS in ONOFF RGCs[429]. Strikingly, it is specifically the dendrites of starburst amacrine cells (SAC) that are direction-selective, each preferentially tuned in the centrifugal direction of its radial extension[552] and with the tuning strengthened by reciprocal, GABAergic synaptic inhibition from neighboring processes of other SACs[553,554]. Finally, compared to the spatially uniform excitatory synapses from bipolar cells, the asymmetric representation of inhibitory synapses of starburst amacrine dendrites onto DS RGCs[555] results in stronger inhibition that vetoes the BC-driven excitation on the null, but not on the preferred, side. Collectively then for the neurotransmitters involved, glutamate from BCs excite symmetrically, acetylcholine influences the gain, and GABA confers the DS property via null-direction inhibition on RGCs[542,547,552,556,557].

Aiming to gain insights about the physiological wiring upstream of RGCs, I investigate in this chapter the effects of different pharmacological perturbations, alone or in combinations, on the retina output of the catshark retina.

Results

Relying on electrophysiology recordings of RGC responses (see also Chapter 4), I employed the same stimulus arsenal in control (ctr) conditions and in the presence of receptor blockers. Depending on the type of pharmacological perturbation, the experiments I conducted can be grouped in two categories. L-Ap4 was used to inform about the ON pathway in the shark retina as an agonist of group III metabotropic glutamate receptors (mGluR6), while strychnine,

gabazine and TPMPA ((1,2,5,6-Tetrahydropyridin-4-yl)methylphosphinic acid) to block glycine, $GABA_A$ and $GABA_C$ receptors, respectively (see also Methods).

L-AP4 silences ON but reveals OFF inputs to ON and ONOFF RGCs

Administration of L-AP4 (n=6 experiments) had several effects on the retinal output. Primarily, while 74.2% (121 of 163) of OFF RGCs remained OFF (Fig. S5.1B), the ON component was silenced in 207 of 207 RGCs (Fig. 5.1A and Fig. S5.1A, 158 and 49 of ON and ONOFF polarity in control conditions, respectively). Unexpectedly however, 45.6% (72 of 158) of ON and 53.1% (26/49) of ONOFF RGCs did not become completely unresponsive to visual stimulation; they switched polarity responding to light offset (OFF) instead (Fig. 5.1B and Fig. 5.2A).

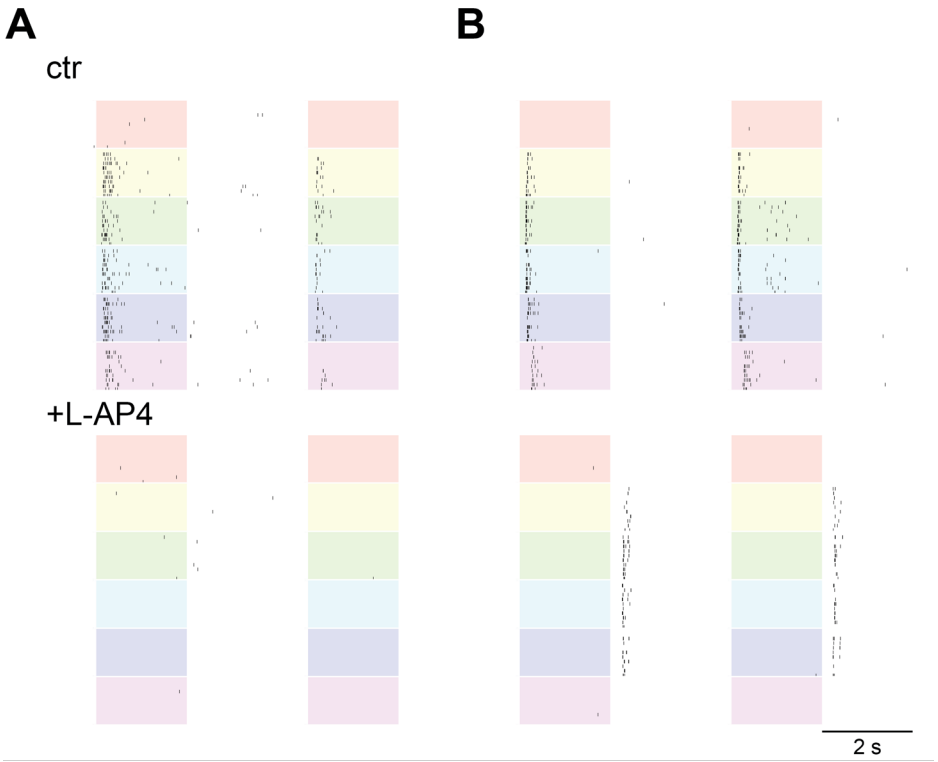

Figure 5.1 – Chromatic profiles of ON RGCs under L-AP4. The figure structure is similar to Fig. 4.1; but with the same ON RGCs in control (*top*) and upon L-AP4 administration (*bottom*) conditions. Note the two groups, some ON RGCs were silenced (*A*) while others switched to OFF polarity (*B*) under L-AP4.

Upstream inhibition plays a minor role in RGC response polarity

To investigate contributions from inhibitory ACs in actively masking this OFF component during normal conditions, I administered strychnine (S, n=3), gabazine (G, n=5 experiments), or both with TPMPA (TSG, n=4). Overall, all three perturbations largely failed to unveil 'switching' crosstalk between the pathways, namely ones that would result only in responses of the opposite polarity (Fig. 5.2B-D). Specifically, strychnine flipped 0% of either ON (0/29) or OFF (0/94) RGCs, while gabazine 0.52% (1/194) and 1.34% (2/224) respectively. Similar effects were observed for TSG, responsible for 0% (0/110) and 1.24% respectively (2/161).

With regards however to unveiling a component of the opposite polarity but without destructing the dominant under normal conditions (i.e. ON or OFF becoming ONOFF), the glycinergic and GABAergic signaling pathways likely exert an asymmetric effect, masking the OFF but not the ON pathway. Strychnine alone unmasked an OFF component in 34.5% (10/29) of ON RGCs but not an ON component (0%, 0/94) in OFF RGCs (Fig. 5.2 D), while gabazine affected 18% (35/194) (Fig. S.5.2) and 0.89% (2/224) respectively. When applied in combination however (TSG), unmasking was rarely observed, only in 1.82% (2/110) and 0% (0/161) of ON and OFF RGCs. This observation suggests either a competing effect when simultaneously perturbing glycinergic and GABAergic signaling, or a vetoing role from the $GABA_C$ receptor (TPMPA effect).

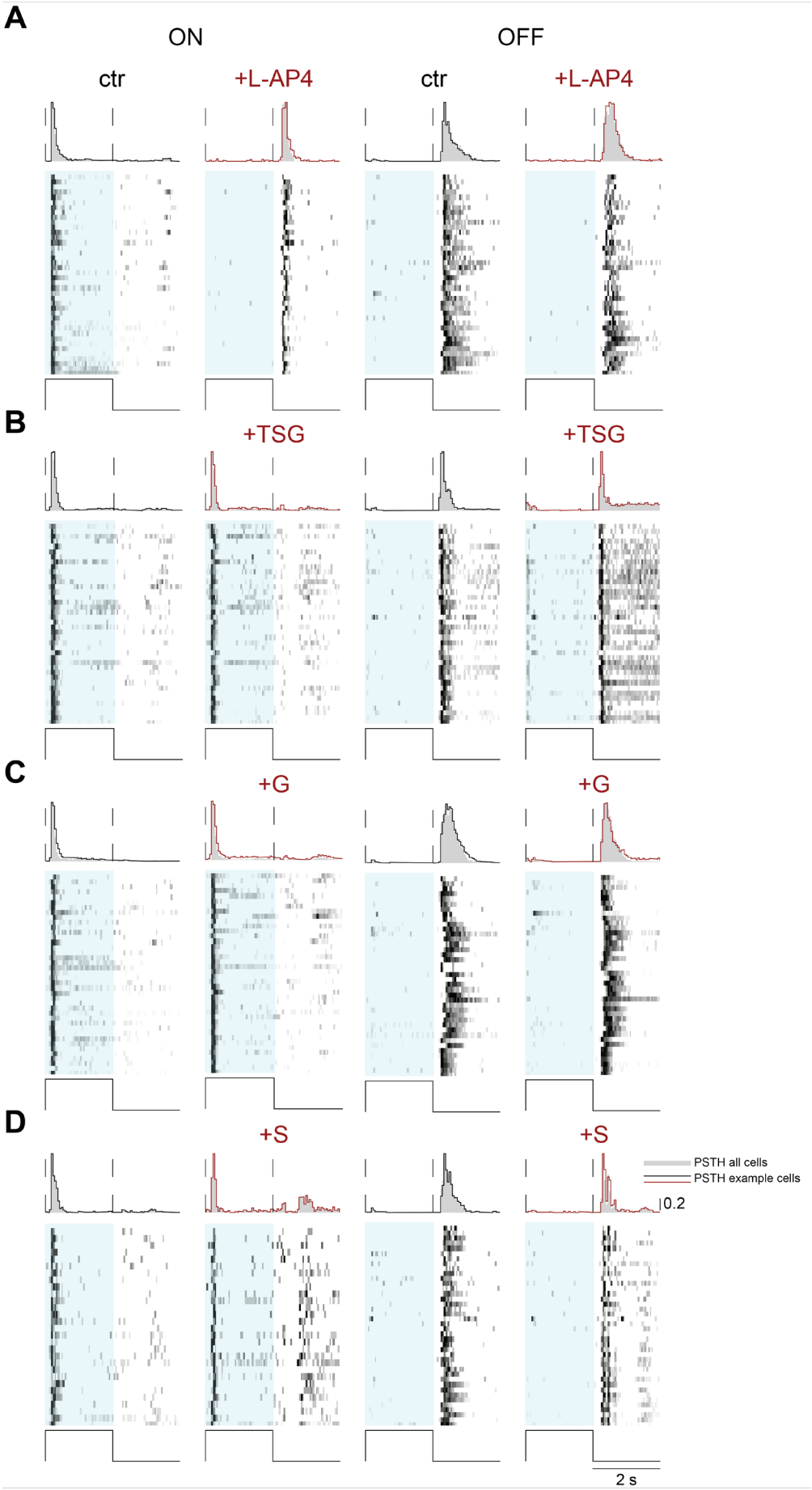
A
ON
OFF
ctr
+L-AP4
ctr
+L-AP4
B
+TSG
+TSG
C
+G
+G
D
+S
+S
PSTH all cells
PSTH example cells
0.2
2 s

Figure 5.2 – Population chromatic profiles upon different perturbations. Visualization of responses to other LEDs is omitted for clarity. For each condition the same cells are shown before and after the drug perturbation. The number of rows plotted was determined by max(len(n), 40), with n the number of responsive cells under the drug. Note distinct effects depending on the pharmacological agent used.

Perturbation effects on other properties of the response

The effects of pharmacological agents on retina output were not limited to the response polarity of RGCs. Blocking the ON pathway did not influence spontaneous activity at the population level (Fig.5.3, p=0.90 for ON RGCs, p=0.99 for OFF, Wilcoxon signed-rank test). In contrast, perturbing the inhibitory signaling caused a significant increase independent of the exact combination of agents tested (p= ($7.108*10^{-4}$, $3.434*10^{-13}$, $5.793*10^{-6}$ for TSG, G, S on the ON pathway) and ($2.393*10^{-22}$, $3.685*10^{-8}$, $3.722*10^{-14}$ on the OFF pathway)). Notably, a sustained disinhibition was additionally observed for light-driven components, but only for the OFF RGCs and upon TSG, but not G or S, administration (Fig. 5.2). Finally, sole administration of strychnine caused a different, distinct effect, namely oscillations on both ON and OFF channels.

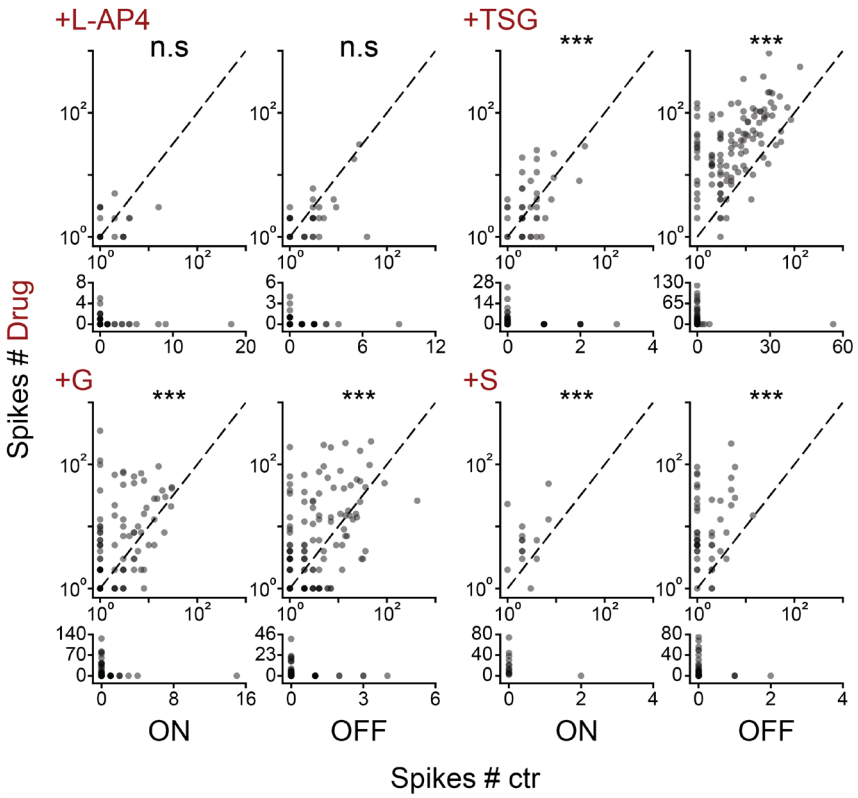

Figure 5.3 – Effect of perturbations on the spontaneous activity of RGCs. Spikes used for computing spontaneous activity are from a window of 10 repeats, 4s each (2s ON, 2s OFF) of a 630nm full-field stimulus that the retina does not respond to (see also Chapter 4). Note how inhibitory signaling blockers have a large effect relative to L-AP4.

With regards to response latency, the contributions were distinct; L-AP4 had a pronounced and perturbations of inhibitory pathways a limited effect (Fig 5.4). To avoid wavelength-dependent, secondary effects for the different pharmacological perturbations, the reported latencies were computed as the median for the two wavelengths maximally absorbed (480 and 505 nm, see also Chapter 4). For the ON RGCs the latency in control conditions was 0.208ms, while upon L-AP4 administration it increased to 0.374ms for the unmasked OFF component. OFF RGCs were also decelerated, with median latencies of 0.332 and 0.394ms, respectively. TSG had minimal, if any, effect (0.202-0.204ms for the ON, 0.265-0.253ms for the OFF, before and after administration), while gabazine preferentially but only slightly accelerated the OFF pathway (0.207-0.202ms for the ON, 0.376-0.345ms for the OFF). Finally, strychnine affected both pathways but in an opposite manner (0.209-0.245ms, 0.342-0.326).

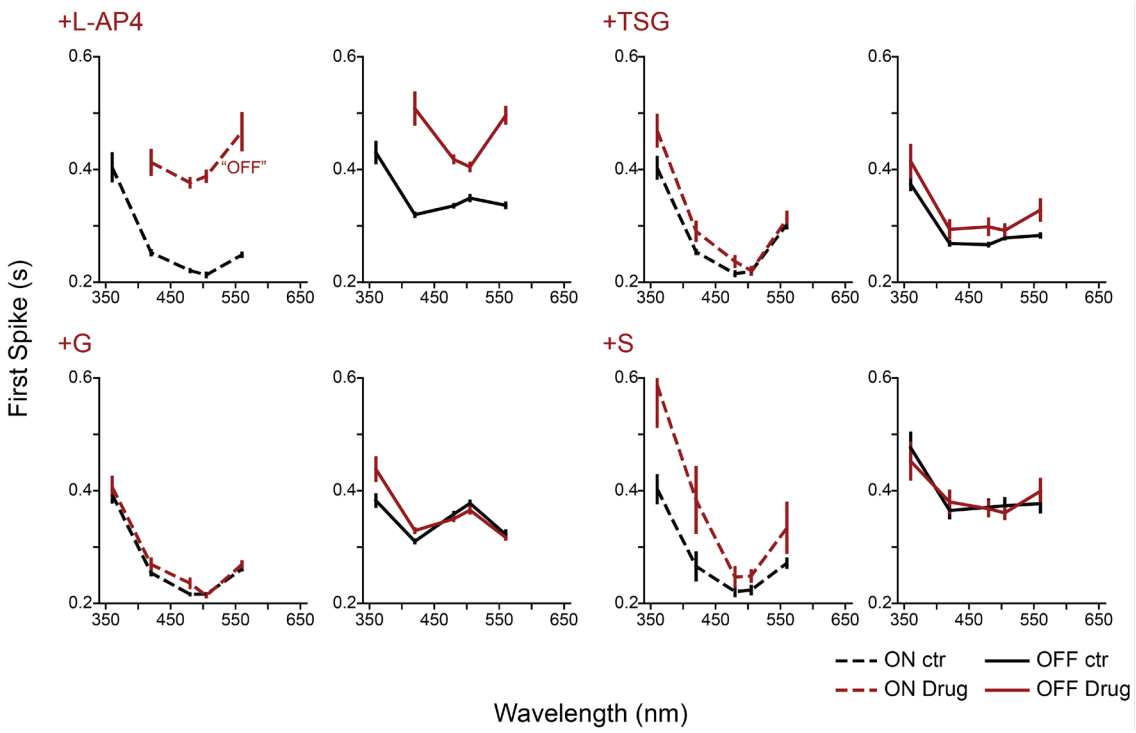

Figure 5.4 – Effect of perturbations on the latency of RGCs. The timing of the first spike (median across 10 stimulus repeats) is computed. Note how L-AP4 has a large effect, and on both pathways, relative to inhibitory signaling blockers.

To further characterize the pharmacological effect on RGC temporal frequency and contrast encoding, I utilized the chirp stimulus (see Chapter 4). L-AP4 had a broad and symmetric effect on both pathways; it dampened the response in the intensity, the percentage of responsive cells, and the vector strength of the phase-lock (Fig. 5.5, Fig. S.5.3). In particular, the stimulus phase was no longer encoded for high temporal frequencies and low spatial contrasts. The different combinations of inhibitory pathway blockers had varying effects in response to chirp stimulation (Fig. S.5.4-9). For the frequency component of the stimulus, TSG extended the range of OFF RGCs towards higher frequencies, without incurring a change on the encoding of ON RGCs (Fig. S.5.7). Conversely, gabazine extended the range of ON without an effect on the OFF (Fig. S.5.8), while strychnine extended both ranges, but only for the OFF pathway the degree of phase-locking remained above 0.85 (Fig. S.5.9). With respect to contrasts encoded, all three extended the response range to include contrasts below 5%, albeit at a lower degree of phase-locking to the stimulus. In contrast however to the other, mostly symmetric perturbations (TSG, S), gabazine primarily affected the ON pathway in the lowest contrasts tested here.

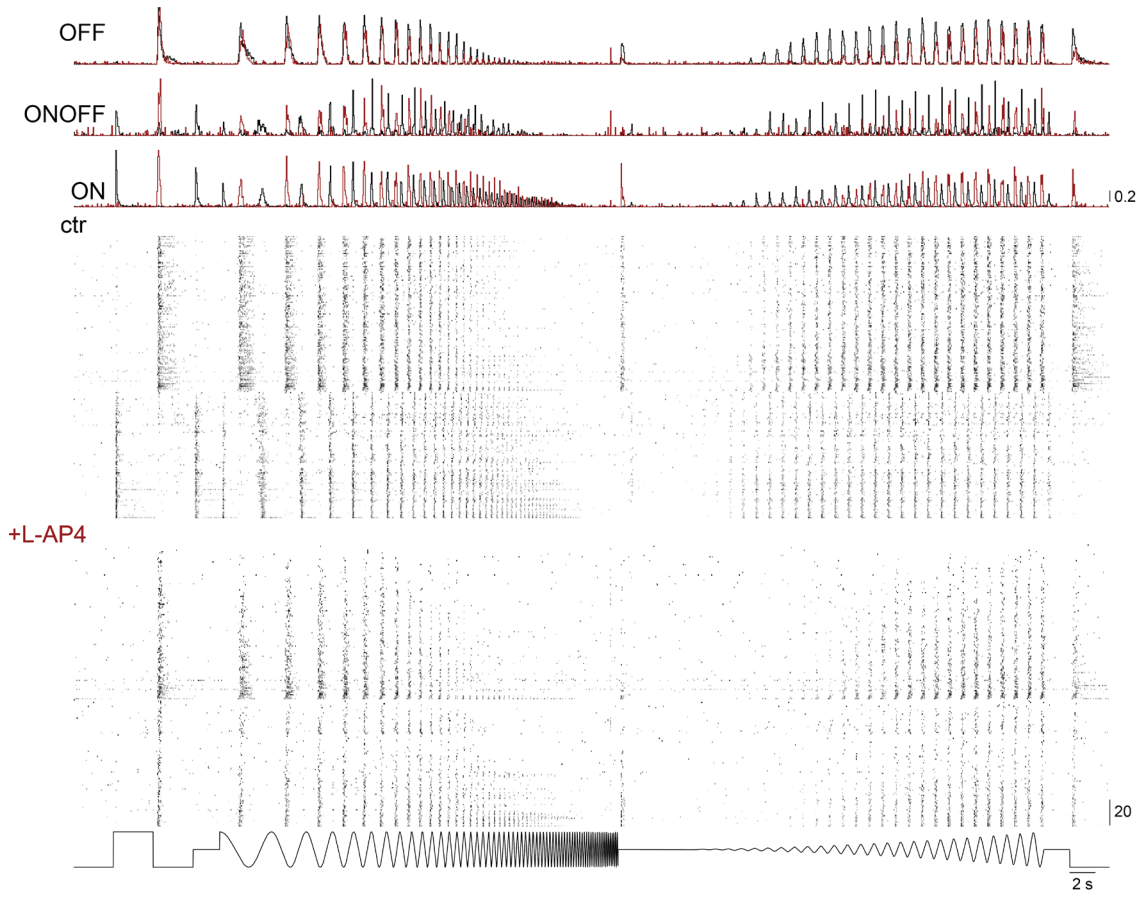

Figure 5.5 – Population responses to chirp stimulation under L-AP4. PSTHs are overlayed for control (*black trace*) and drug (*red trace*) conditions. Rows depict individual RGCs and are matched for control (*top*) and drug (*bottom*) conditions.

Minimal contributions of the primary rod pathway to OFF RGC responses

As already described in Chapter 4, the retina of *Scyliorhinus canicula* is likely rod-only in terms of photoreceptors, and the rod primary pathway conveys signals to both ON and OFF pathways (see also Introduction). The neurotransmitters used in the primary pathway for the signal to reach the OFF RGCs are glutamate (at rod synapse with RBC, glutamate sensed by mGluR6) and strychnine (at Aii AC synapse with OFF BC, glycine sensed by glycinergic receptors). Therefore, OFF RGCs theoretically lose their primary pathway-dependent rod signals in experiments where L-AP4 or strychnine was administered. Few OFF RGCs (89/567 OFF RGCs in total, n=13 experiments) did not pass the quality index threshold for light-driven responses upon either of the three perturbations (21.4% in L-AP4, 19.4% in S, and 10.6% in TSG), and were thus assumed to be exclusively driven by the primary rod pathway (but see Fig. S.5.10). Relative to their counterparts, in control conditions these cells fired on average less spikes and phase-locked to more narrow ranges for both frequency and contrast (Fig. 5.6). However, they had similar vector strength in their overlapping range, with the ones driven only by the primary pathway being marginally better at low frequencies.

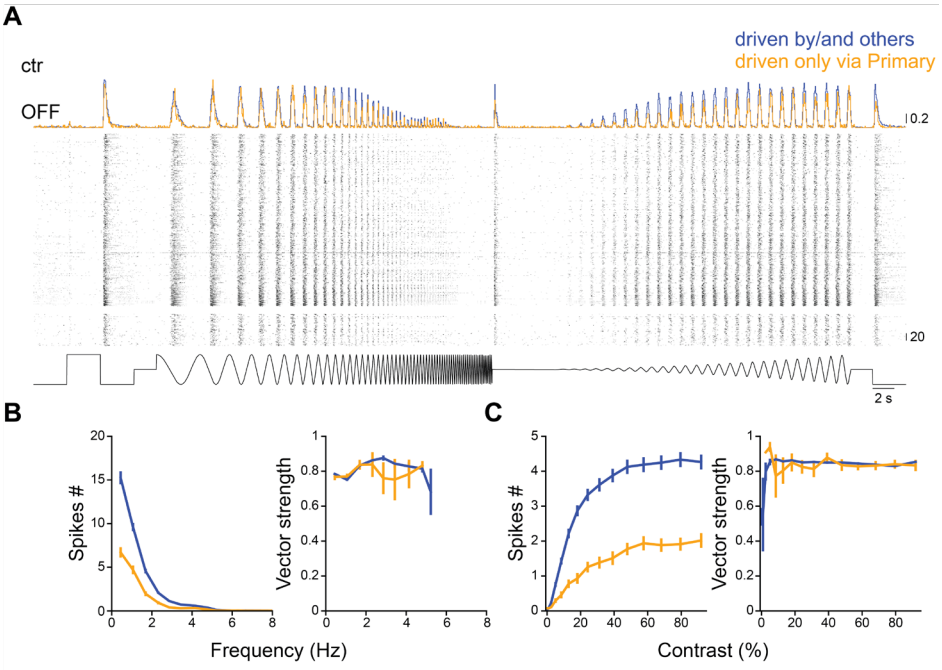

Figure 5.6 – OFF RGC subpopulations responses to chirp stimulation. A, The visualized individual cells and population PSTHs are from experiments of L-AP4, TSG, or S, split based on their post-drug responses (see Fig. S5.9 and main text) into driven exclusively via the primary pathway (*yellow trace*) and not (*blue trace*). B-C, Response characteristics to chirp alternating components. Specifically, number of spikes (*left,* in *B*-C) and degree of phase-locking (*right,* in *B*-C) for stimulus changes in temporal frequency (*B*) and contrast (*C*).

RGC Direction-selectivity depends on asymmetric inhibition

As already outlined, retinal implementation of direction selectivity depends on asymmetric inhibition, specifically on GABAergic signaling (see Introduction). Upon TSG administration (598 RGCs in total, n=4 experiments), which blocks both $GABA_A$ and $GABA_C$ receptors, 59 of 60 previously DS RGCs now responded to all directions of the moving bar (Fig. 5.7), and there was no statistical support at the population level for the encoding of the preferred versus null direction (PD vs ND: p= $2.191*10^{-11}$ for control, p=0.628 for TSG condition). Relative to their counterparts in control conditions, both the distribution of PD and ND differ upon the application of TSG (PD_{pre} vs PD_{post}: p=$7.829*10^{-7}$, ND_{pre} vs ND_{post}: p= $2.455*10^{-4}$).

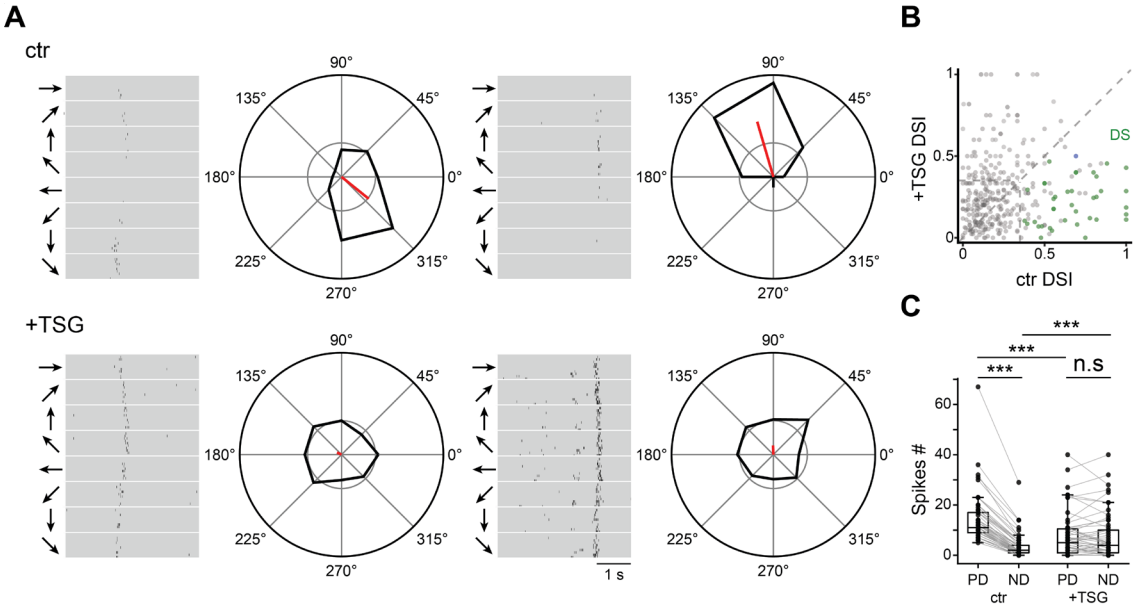

Figure 5.7 – DS emerges in RGCs via asymmetric inhibition. A, Individual ON (*left*) and OFF (*right*) RGC responses to 'moving bar' stimulation in control (*top*) and upon TSG (*bottom*) conditions. Note the absence of direction specificity under TSG. B,

Relation of the direction selectivity index (DSI) in control and upon TSG conditions. C, Relation of spikes in the preferred direction (PD) and null (ND) in control and upon TSG conditions.

Discussion

To complement the functional and anatomical descriptions of retinal output (Chapter 4), here I attempt to illuminate the physiological wiring upstream of RGCs following administration of different pharmacological agents.

L-AP4 effects

In all vertebrate species studied to date, L-AP4 (or APB) have been repeatedly shown to block the retina ON pathway by being functionally selective for mGluR6 at the photoreceptor to ON BC synapse. In this work, I find that this pattern pertains to sharks, with ON responses entirely absent under L-AP4 (Fig 5.1-2, Fig. S.5.1). Unexpectedly however, a previously masked OFF component emerged in about half of the ON and ONOFF RGCs when blocking the ON pathway. Notably, the latencies of both the 'emerging' (in ON and ONOFF RGCs) and 'resistant' (in OFF RGCs) OFF components under L-AP4 were larger than both their control counterparts and the other perturbations (Fig. 5.4).

Several explanations could account for this peculiar polarity switching of the response. First, these neurons might be wired from both ON and OFF BCs, but display at normal conditions a 'dominant' ON response thanks to ON-mediated, active suppression of the OFF inputs by inhibitory circuits[558–560]. Unmasking of OFF components in few ON RGCs was observed in experiments where gabazine and strychnine were separately administered (Fig. S.5.2), suggesting crosstalk inhibition could at least partially account for the polarity switch.

Second, the polarity switch could alternatively be attributed to the distinct wiring of the primary rod pathway. As already mentioned, the Aii AC receives glutamatergic input from the RBC, and forms electrical (sign-conserving) and chemical (glycinergic, sign-inverting) synapses with ON and OFF cone BCs respectively (see general Introduction and Chapter 4). Importantly however, in the shark retina OFF cone BCs not only receive but also form their own, output, ribbon synapses on Aii AC processes in the OFF sublaminae of the IPL (see Table S2). Of note, this finding does not represent a novel description for vertebrates, as it has been previously reported in rodents[442,561], cat[562] and rabbit[106]; however

the physiological contribution of this synapse is either weak or absent in mouse[561,563,564] but likely present in rat[565] and rabbit[566]. If functional in sharks, it could theoretically account for the observed polarity switch in the following manner: in control conditions, Aii receive strong ON input from the RBC and therefore displays an ON response. Under L-AP4 however, RBCs (and ON cone BCs) are silenced while OFF cone BCs are still responsive to light offsets, conveying their OFF signal to Aii AC which now responds as OFF. Given the electrical coupling between Aii AC and ON cone BC, the OFF signal is conveyed to the latter and switches its polarity. In turn, this ON cone BC then conveys this OFF signal to its natural synaptic partners, the ON RGCs, which now respond to light offset. Overall, this means that the OFF responses observed under L-AP4 would first diverge at the level of the OFF cone BC: mediated by a single, chemical synapse with OFF RGCs for the 'resistant' OFF, whereas by an OFF cone BC -> Aii AC --ON cone BC -> ON RGC for the 'emerging' OFF in the ON RGCs. Due to the involvement of additional synapses for the emerging OFF, it would be expected to trail its 'resistant' counterpart; however, the opposite is observed (Fig. 5.4).

A third explanation for this polarity switch centers on the response profiles of bipolar cells. The mammalian-centric, textbook view is that the bipolar cell is responding to light onset (ON BC) or light offset (OFF BC) depending on its dendritic expression of metabotropic (mGluR6) or ionotropic receptors, respectively (see also general Introduction). However, certain mixed rod-cone input bipolar cells in salamanders and teleosts express both metabotropic and ionotropic glutamate receptors, and display ON responses in control and OFF in conditions when the ON pathway is perturbed[308,309]. Strikingly, similar co-expression[567–572] and response-switching[91,492,573] patterns have been reported for mammalian BCs, but still remain -surprisingly- overlooked. Whether certain shark bipolar cells express both glutamate receptor types and switch their response profiles remain to be seen; however direct recordings from type b, ON BCs did not show a depolarization at light offset upon perturbation of the ON pathway[574].

In addition to the changes in polarity, L-AP4 exerted several other effects. In agreement with mammalian descriptions[111], it dampened the response to low contrasts (Fig. 5.5 and Fig. S5.3). Furthermore, it decreased the response-driven

number of spikes (Fig. S5.1 and Fig. S5.3) and further decelerated the latency of both pathways (Fig 5.4). Interestingly, the 'mirror-image' relationship to the ON latencies breaks under L-Ap4; like the ON, OFF RGCs were now responding faster for wavelengths more strongly absorbed by the rod opsin (see also Fig. 4.4C and discussion in Chapter 4). It remains unclear whether these changes in the OFF RGC responses are exerted at the level of photoreceptor -> ON BC, or at metabotropic receptors expressed in the IPL, where glutamate release from BCs can be directly suppressed following the application of L-AP4[575].

Effects of inhibitory signaling receptor blockers

The application of inhibitory signaling receptor blockers, either solely or in combination, produced effects in the shark retina that are largely in line with its mammalian counterpart. This includes an increase in the spontaneous firing of RGCs[576,577] (Fig. 5.3), a sustained disinhibition under blockade of $GABA_C$ receptor[533,541,578] (Fig. 5.2), and oscillatory responses under blockade of glycinergic receptors[579–581] (Fig. 5.2). Also in line with descriptions of the mammalian retina[582,583], different perturbations affected the two polarity pathways asymmetrically, with gabazine subtly but primarily affecting the ON, while strychnine the OFF pathway (Fig. S5.4-5.9).

Vertebrate retina DS: likely a single, shared algorithmic implementation

At the level of information processing, what does a "direction-selective" computation entail? Fundamentally, the system must first be able to distinguish moving from stationary objects, therefore to combinatorically process luminance values that are spatiotemporally separated (by a certain distance and within a temporal delay range)[176,584,585]. As such, the algorithmic design of motion detection is based on the correlation of time-shifted and spatially separated signals[549,586,587].

Then for building directionality on top of motion detection, two 'delay-and-compare' models of opposite polarity have been suggested, inspired by invertebrate and vertebrate motion detectors[176,393,549]. Studying visual behavior of beetles, Hassenstein and Reichardt (HR) proposed a DS model where the computation depends on logical conjunction (a multiplicative process) of two excitatory input signals differing in time course and amplitude. Conceptually, if two adjacent neurons synapse on C, but integration in A is slower than in B, then

their output will overlap at C only for a stimulus moving in the A->B direction but not in the reverse. Working on rabbit RGCs, Barlow and Levick (BL) proposed a similar model, but where instead of multiplicative excitation, it is inhibition from one neuron that suppresses the excitation from the other and thus vetoes in neuron C the encoding of the null but not of the preferred direction. In short, although both models account for DS in the hypothetical neuron C, the algorithm does so with opposite polarity; in the HR detector the preferred direction is emphasized, while in the BL the null is suppressed. While boundaries are increasingly blurred, the BL and HR detector models primarily characterize direction selectivity in vertebrate and invertebrate visual circuits, respectively.

Shark DS RGCs invariably responded to all directions of the moving stimulus following application of TSG (Fig 5.7). In line with evidence from other species[407,529], this finding suggest that the implementation, namely via asymmetric inhibition, of retina direction-selectivity likely arose early in the evolution of vertebrates.

Limitations of Pharmacological Perturbations

Given the absence of genetic tools that would permit targeted perturbations in the shark retina, here I relied on pharmacological perturbations for illuminating the retina wiring upstream of RGCs. However, the interpretation of such results and inference of participating neurons and circuits are not straightforward and must be approached with caution. Irrespective of the drug acting as an agonist or antagonist, it will influence all neurons that express a receptor sensitive to the drug. For example, although L-AP4 has a higher potency for mGluR6, it can nevertheless affect other class III mGluRs (4, 7, 8). Furthermore, the receptor expression is often not confined to a specific type of neuron, and different receptor subunits can give rise to distinct cellular properties. Types of neurotransmitters or receptors can be co-expressed[120,130,588], sometimes at different compartments of the same cell and in a species-specific manner[589,590]. Finally, neurotransmitters can exert different effects depending on the position of the neuron within the network[591,592], or even in relation to ambient light levels; strychnine renders RGC responses more sustained at bright, but completely silences OFF RGCs at dim light levels respectively[593,594].

In my attempts to characterize the pharmacology of the shark retina, I came across a paradoxical observation, probably related to the inherent complexity described above. As already mentioned, application of L-AP4 eliminated the ON but revealed an OFF component, while TSG failed to do either. In combination however (ATSG), I was surprised to observe for the same stimulus the retention of a slow ON together with the unveiling of the OFF component (Fig. S.5.11A). When observed in the teleost retina[595], this inconsistency was attributed to polysynaptic effects of L-Ap4, an explanation likely to extend to the shark retina. Although the retention was short-lived, with the ON component disappearing by the time I presented the chirp stimulus (Fig S.5.11B), this observation might prove informative when studying the participation of neurotransmitters that were not systematically perturbed in this work, like acetylcholine or dopamine, with several contributions already identified in the retina circuits of better studied organisms[596–602].

Supplementary Figures

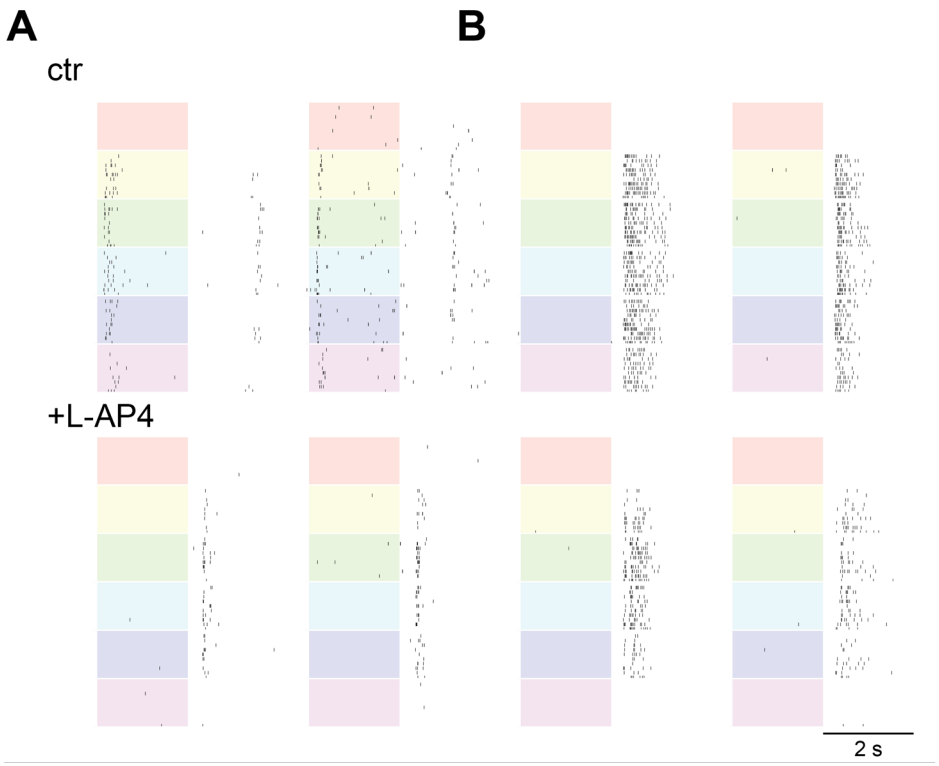

Figure S5.1 – Chromatic profiles of ONOFF and OFF RGCs under L-AP4. The figure structure is similar to Fig. 5.1; example of ONOFF (*A*) and OFF (*B*) RGCs in control (*top*) and upon L-AP4 administration (*bottom*) conditions. Note the ONdOFF RGCs becoming OFF and how OFF RGCs remain largely intact in their response polarity under L-AP4.

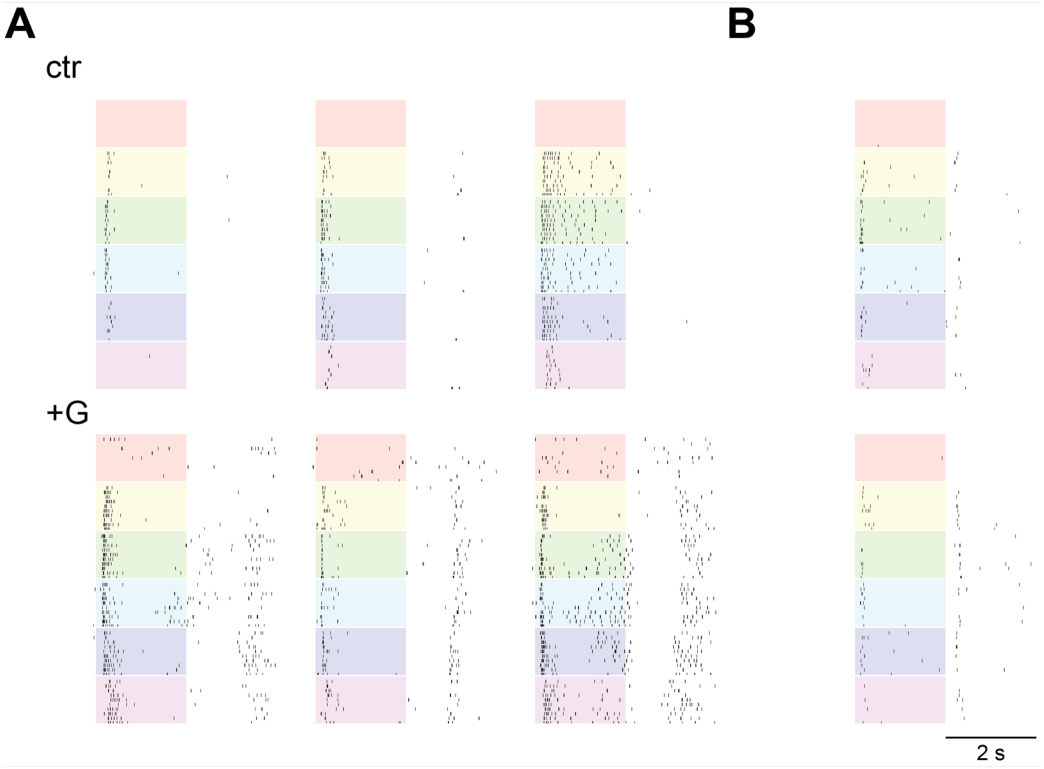

Figure S5.2 – Gabazine unmasks OFF components in ON RGCs. The figure structure is similar to Fig. 5.1; example of ON RGCs converting into ONdOFF (*A*) and ONOFF (*B*) upon gabazine administration. In the majority of cases, the unmasked component was delayed, as in *A*.

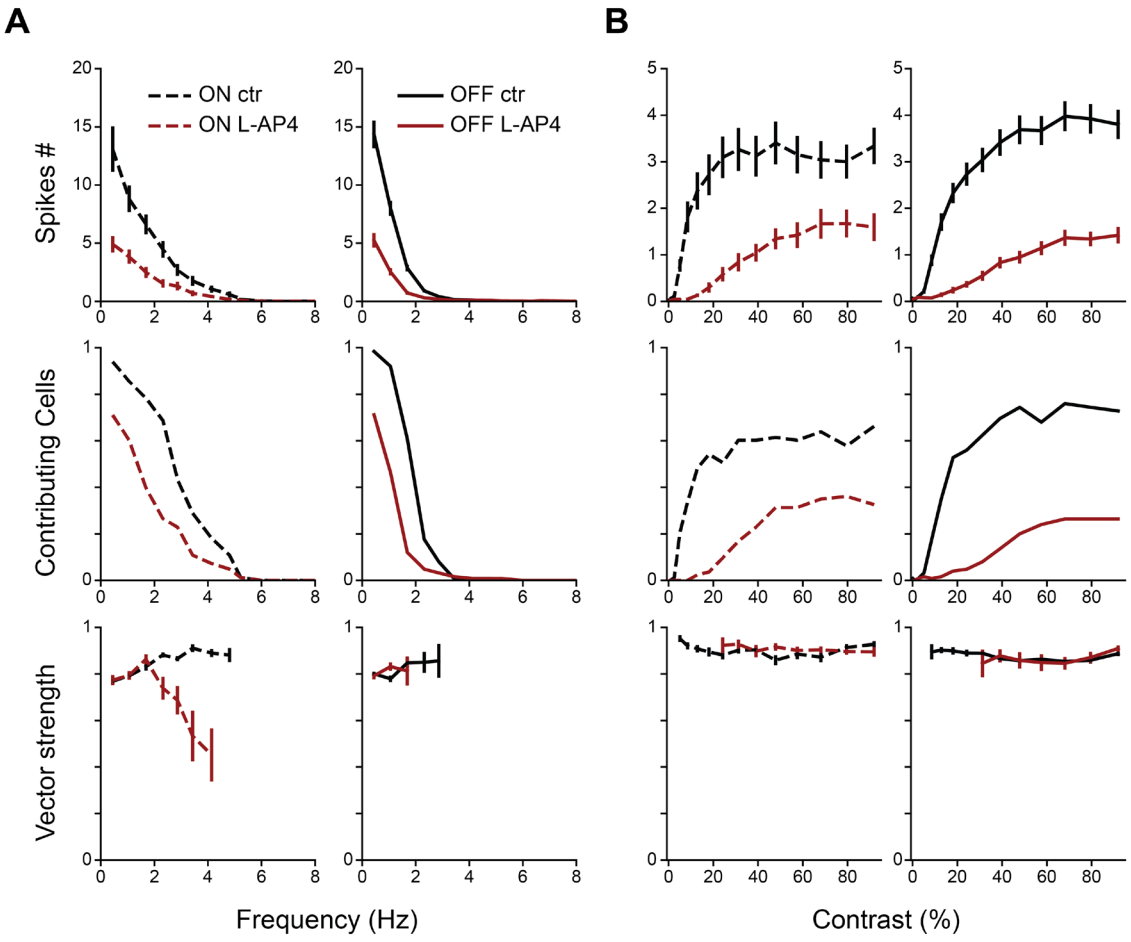

Figure S5.3 – Quantification of chirp responses of ON and OFF RGCs under L-AP4. The figure structure is similar to Fig. 4.8, each row quantifies a different but related property of the population response before (*black trace*) and after (*red trace*) drug.

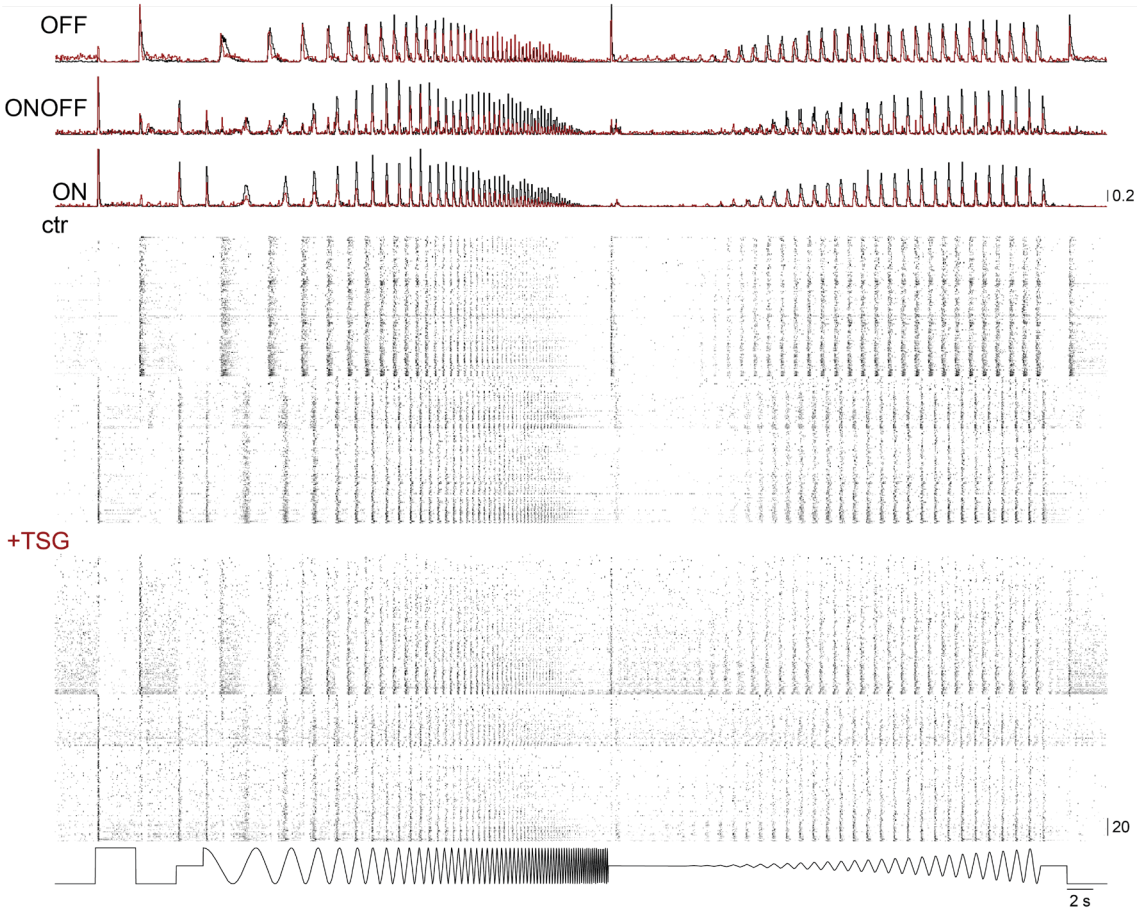

Figure S5.4 – Population responses to chirp stimulation under TSG. The figure structure is similar to Fig. 5.5.

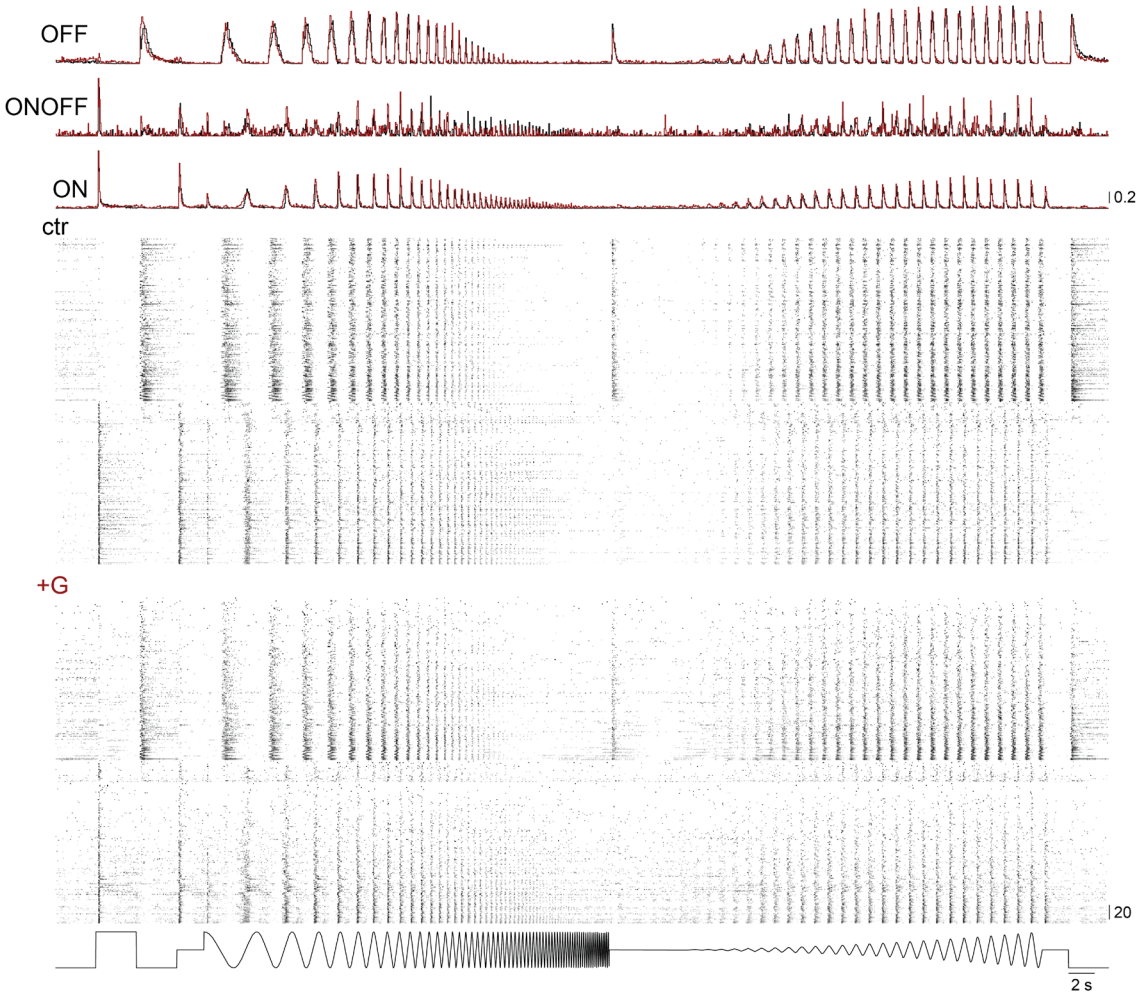

Figure S5.5 – Population responses to chirp stimulation under G. The figure structure is similar to Fig. 5.5.

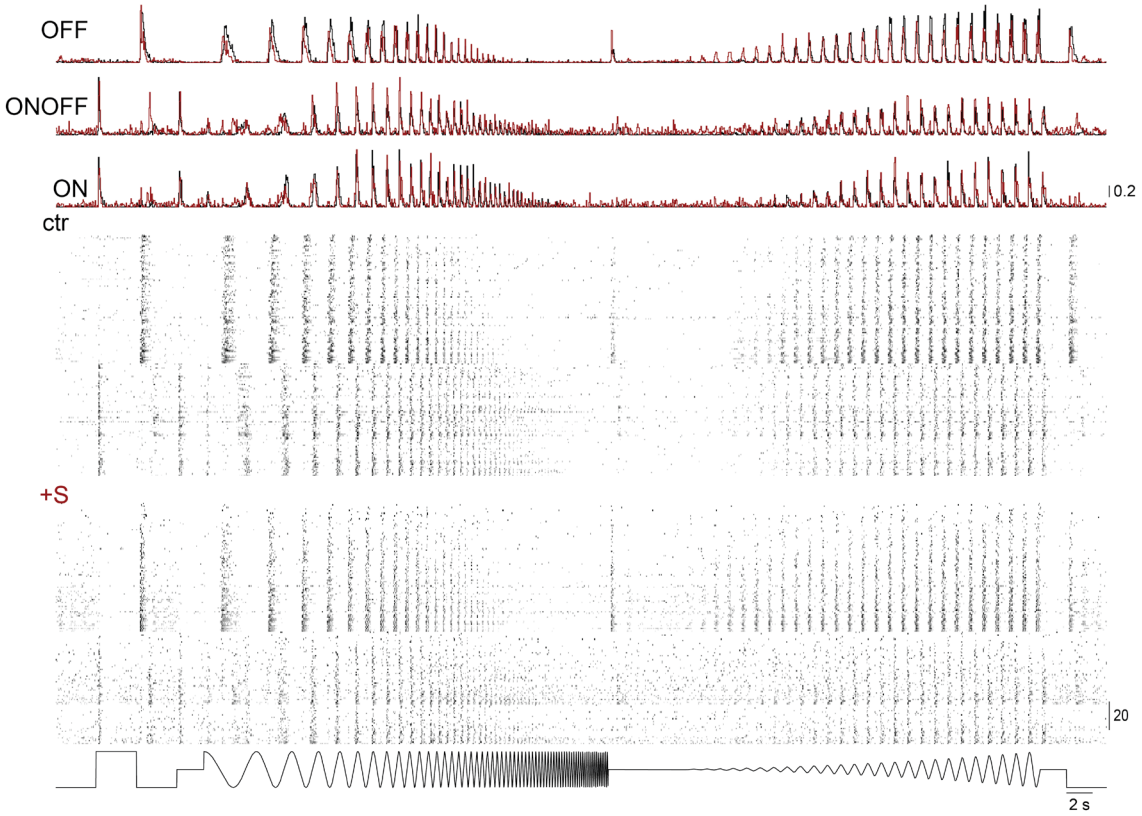

Figure S5.6 – Population responses to chirp stimulation under S. The figure structure is similar to Fig. 5.5.

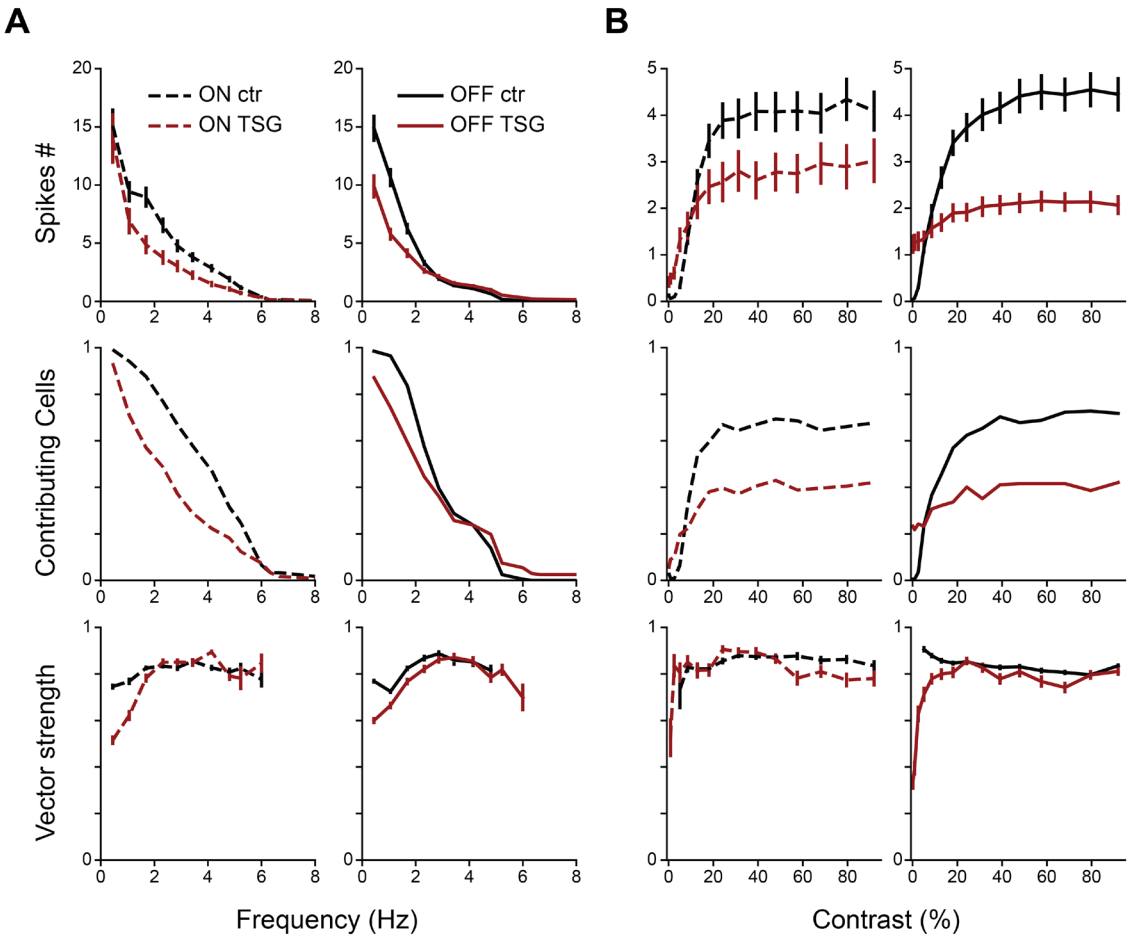

Figure S5.7 – Quantification of chirp responses of ON and OFF RGCs under TSG. The figure structure is similar to Fig. 4.8, each row quantifies a different but related property of the population response before (*black trace*) and after (*red trace*) drug.

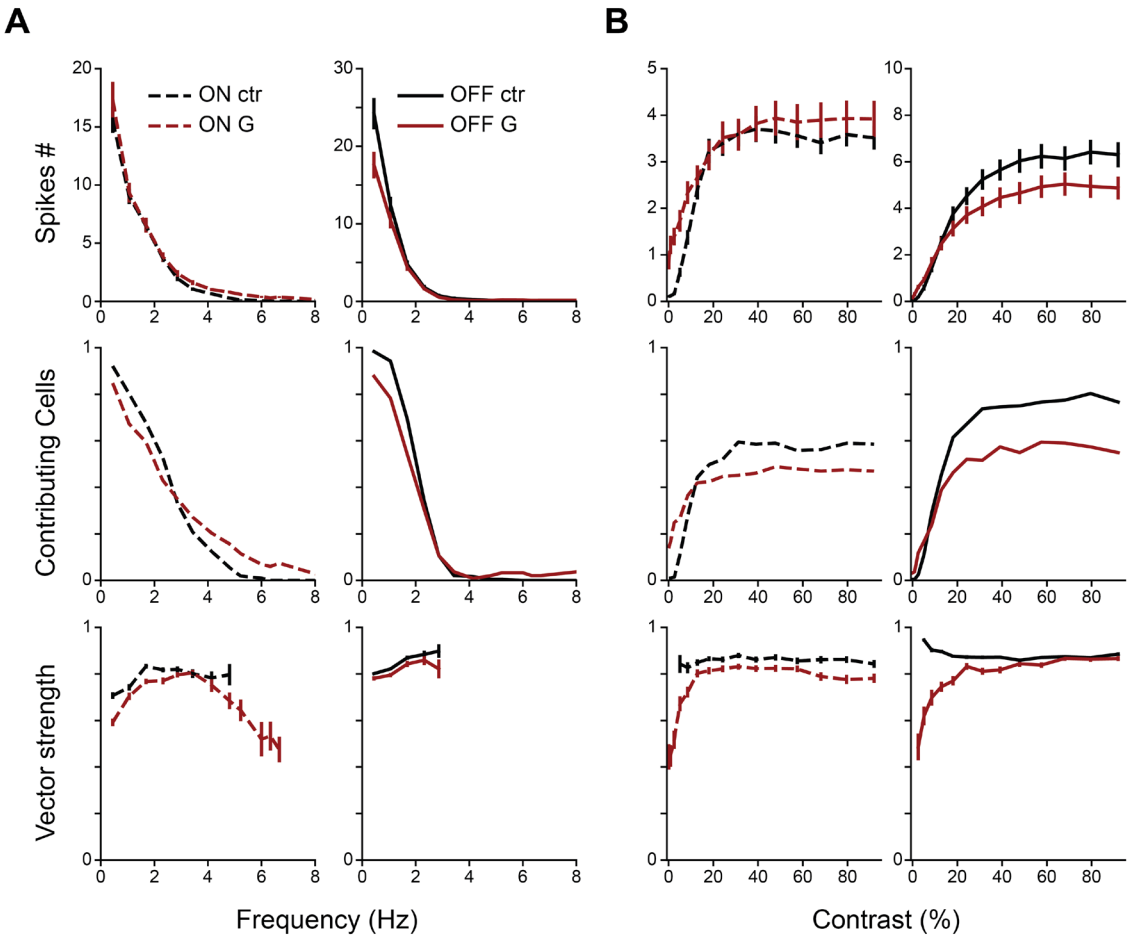

Figure S5.8 – Quantification of chirp responses of ON and OFF RGCs under G. The figure structure is similar to Fig. 4.8, each row quantifies a different but related property of the population response before (*black trace*) and after (*red trace*) drug.

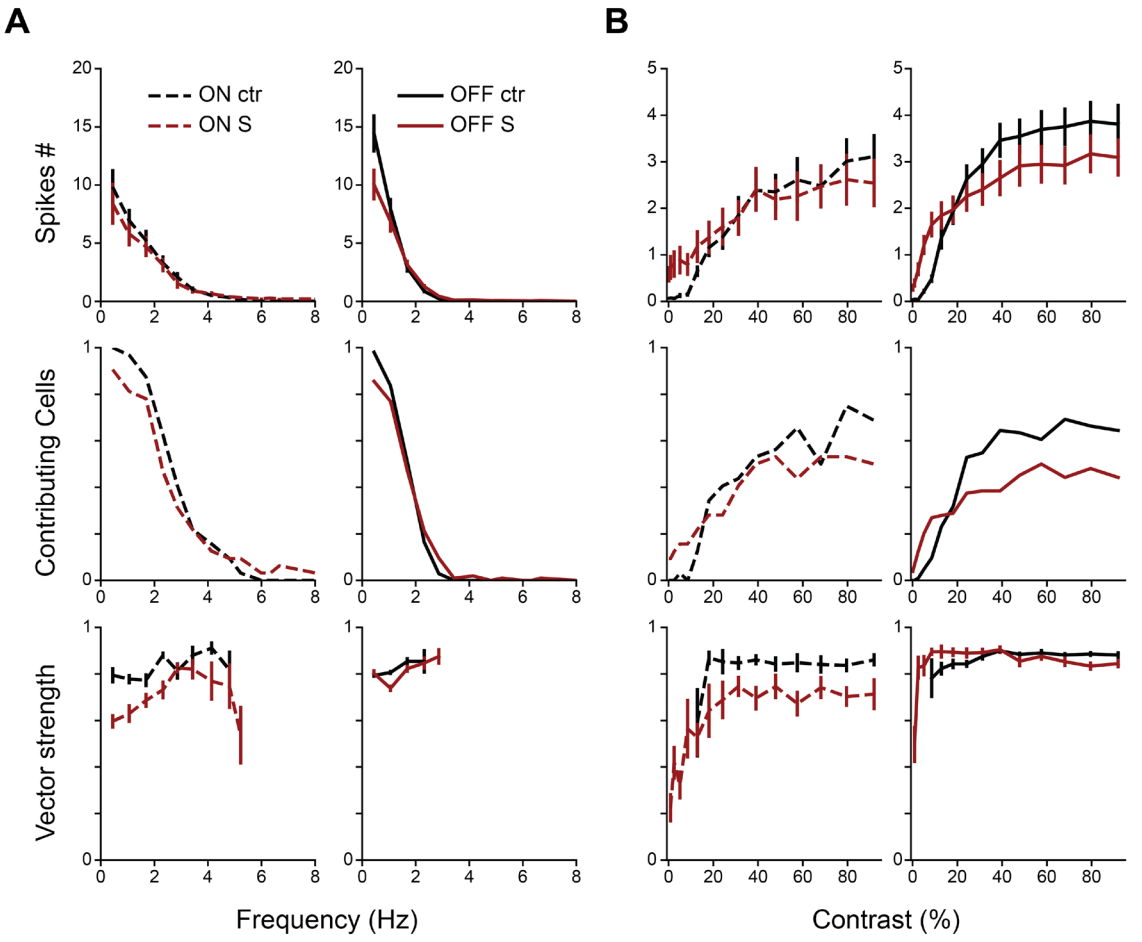

Figure S5.9 – Quantification of chirp responses of ON and OFF RGCs under S. The figure structure is similar to Fig. 4.8, each row quantifies a different but related property of the population response before (*black trace*) and after (*red trace*) drug.

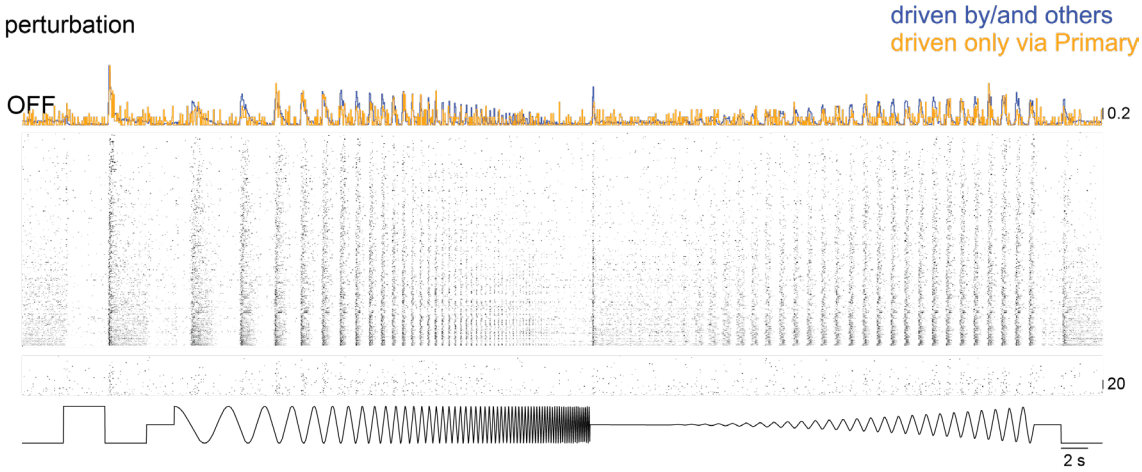

Figure S5.10 – OFF RGC subpopulation responses to chirp stimulation under drug. The figure structure is similar to Fig. 5.6. The visualized individual cells and population PSTHs are from experiments of L-AP4, TSG, or S. Note most cells still demonstrated

light-driven responses (*blue PSTH* and *top rows*), while few were either silenced or only responded weakly (*yellow PSTH* and *bottom rows*) to specific moments of the stimulus.

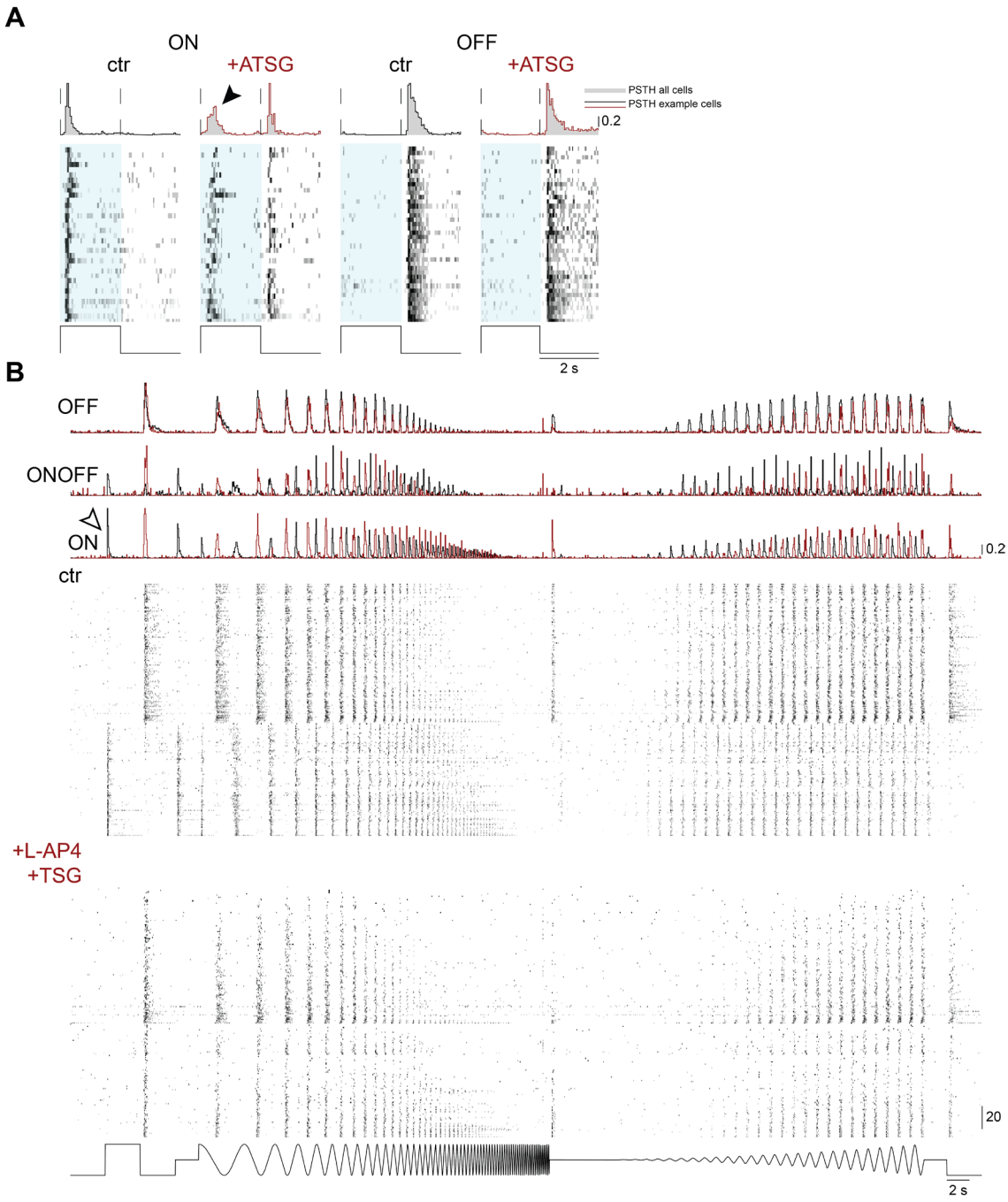

Figure S5.11 – Population responses under L-AP4 and TSG (ATSG). A, Responses to FFF for the ON and OFF RGCs. The panel structure is similar to Fig. 5.2. B, Responses to chirp stimulation for the ON, ONOFF, and OFF RGCs. The panel structure is similar to Fig. 5.5. Note the remaining ON component early upon ATSG application (filled arrowhead) but its disappearance later in the experiment (open arrowhead).

Chapter 6 – Discussion

Ontogenetic Changes and Retinal Processing

As the small-spotted catshark grows, so does its eye[603,604]. Changes are also observed at the layers of the retina: although the photoreceptor density remains stable, perhaps fuelled by a compensating generation of cells across lifetime, both the thickness of the inner nuclear layer and the density of RGCs decrease[605]. How do these structural, ontogenetic alterations affect the organization of retinal circuits and information processing[352]? Given that the input density remains the same whilst the output decreases, a higher degree of signal convergence (photoreceptor pooling) probably occurs. For feature detection specifically, an object moving at constant speed will travel a shorter absolute distance on the ontogenetically bigger surfaces of eye and retina. If such changes are not accordingly accompanied by a reconfiguration of motion detection circuits, for example at the dendritic wiring motifs[553], it will inescapably result in a mismatch of optimally encoded motion velocities between the young hatchling, the juvenile and the adult of the same species.

Together with the unknown degree of reliance on its visual system across the ontogeny of the shark, such considerations will be supported only when retinal processing at different timepoints of lifetime is understood. Although I managed to raise two individuals to the age of three years, the quality of the electrophysiology experiments unfortunately did not allow for any sensible comparisons. To the same end, I tried establishing a contact with public aquaria for the valuable tissue to be utilised when opportunities arise. However, to no avail.

A single elasmobranch species – how representative?

The work presented here is conducted on the visual system of the small-spotted catshark. However, one might ponder the suitability of this model as a window to the past, and more specifically to the retinal circuits and processing template of early vertebrates. There are over 1000 extant elasmobranch species[606], of which the overwhelming majority is, in roughly equal proportion, sharks and batoids. Occupying the depth and breadth of oceans, and sometimes even found in freshwater environments, this anciently diverged vertebrate lineage reflects in its functional diversity and adaptations the various conditions encountered by its

different species. As such, there is likely no single representative of this largely successful subclass.

When determining the appropriate elasmobranch species for studying principles of vertebrate retina evolution, I tried to balance constrains (size, endangerment status) with the scientific relevance for the question in hand, echoing Krogh's principle: "For a large number of problems, there will be some animal of choice or a few such animals on which it can be most conveniently studied". The small-spotted catsharks are good candidates regarding possible constraints: species of least concern[607], small-sized when hatching and easy to maintain in laboratory settings even for previously inexperienced personnel like the author. And in both phylogenetic and aquatic vision terms, they occupy a sweet spot: they belong to the basal group within the most successful, populous order of sharks[608,609] and, though primarily nocturnal, inhabit shallow depths that permit exposure to the full daylight available underwater.

Comparative research within elasmobranch fish

Although here I provided a high-resolution, large-scale description of the output of the *Scyliorhinus canicula* retina and revealed a degree of conservation within catsharks, a lot can be further learned by adopting a comparative framework and applying the present pipeline to other, more distant elasmobranch species. Studying closely related but geographically separated species[610] or ones whose depth distribution or trophic web position only partially overlaps with the small-spotted catsharks will allow for keeping certain parameters "fixed" and isolating contributions of others, like the degree of evolutionary conservation or lifestyle adaptations of the retinal output[611].

In general however, here I not only describe a functional conservation within the *Scyliorhinus* clade for the closely related *Scyliorhinus canicula* and *Scyliorhinus stellaris*, but importantly, identify a morphological conservation at the level of bipolar cell types between *Scyliorhinus canicula* (catsharks, this work) and *Mustelus canis* (houndsharks, see Ref[99]). Within the order *Carchariniformes*, catsharks represent one of the most basal families and houndsharks are more derived, with the separation distance of the two lineages being over 100 million years[612–614]. Whether this character trait is characteristic of all demersal, slow-moving and primarily nocturnal sharks, or instead of the Superorder of

Galeomorphii relative to *Squalomorphii* is currently not possible to claim. Although a richer sampling is required, both superorders are ecologically diverse, containing bottom-dwellers and active pelagic hunters.

With similarly but independently reduced complement of input channels in sharks and mice[517], my study reveals a functional similarity to their retinal output as well. Is this a universal principle of the retina landscape, where the loss of any photoreceptor type from the ancestral vertebrate template results in a stereotypical, functional change at the output level? Information about the retina physiology of marine mammals, whose complement is similarly reduced (elaborated below), might be hard to acquire, but several other batoids with rod-dominated or rod-only retinas have been accessible[164] and can contribute to examining the relationship described here. Reversely, the photoreceptor types are not equally reduced within batoids: certain rays have an atypical for an elasmobranch, rich photoreceptor complement that allows to behaviourally discriminate between different wavelengths[615]. It will be interesting to determine whether, in its elementary properties, their retinal output is closer to teleosts and birds rather than to their close, elasmobranch relatives.

Regardless, the photoreceptor template in sharks and skates is greatly reduced[99,460] from the ancestral state, sometimes to the extreme of retaining only the rods and losing all cones[13,164,182,437,448]. Such a reduction in the number of input channels limits in principle the information available to the sensory system, but the latter's structure and function should be also evaluated relative to the organism's niche space, with sharks being apex or upper predators in dim-light, aquatic environments. Similar light conditions are encountered as well by crepuscular or nocturnal terrestrial organisms, and mammals which evolutionarily transitioned through a twilight bottleneck[616] have also lost some of the ancestral vertebrate photoreceptor types. In marine mammals specifically, a shark-matching, more extreme narrowing of the ancestral palette is observed, where for the independently returning cetaceans and pinnipeds the same photoreceptor type has been convergently lost[617–620]. Like sharks, these marine mammals occupy upper positions, while other mammalian late returnees, exemplified by the manatees, retained the equivalent cone photoreceptor[621], but are instead herbivorous and located at a lower position in the aquatic trophic web. In these

independent cases, it is always the cone complement that undergoes reduction; being responsible for dim-light levels, the rods are always retained. In the electron microscopy data of the shark retina presented here, I identify character traits that collectively resemble the primary rod pathway of mammals, namely the most sensitive pathway that drives scotopic vision down to single-photon detection. This implies that such circuits are truly ancestral, intertwined with rod signal transduction and vertebrate life itself.

Limitations of the study

Choice of visual stimuli

Considering the near complete absence of data heretofore, the primary goal of this work was to fundamentally describe the elasmobranch retinal output. For that reason, the visual stimuli were kept relatively simple and ‘full-field’ in their structure, thus rendering the tuning properties of neurons analytically tractable. Such an approach, though routinely used, comes at the expense of probably stimulating the cells of interest in a suboptimal manner. Most sensory neurons display center-surround receptive fields, i.e. concentric areas in visual space wherein they get excited and inhibited, respectively, and with the surround often spreading considerable distances compared to the center. In such organised fields, in cases where the size of the full-field stimulus far exceeds the diameter of the center, the inhibition weight of the surround can trim or all together silence the excitatory component.

Among vertebrates, shark retinal ganglion cells have strikingly large somas and dendritic tree spread, a parameter typically in agreement with the size of the receptive field center. As such, major compromises can not be foreseen in choosing ‘full-field’ stimuli to study how these cells encode visual information. Nevertheless, in exploring the stimulus parameter space I have determined that big pixel size and low temporal frequencies are efficient to estimate shark receptive field from checkerboard stimulation (data not shown). Future work could build on this and expand the stimulus arsenal to systematically include more complex, naturalistic stimuli for unveiling visual processing properties at a finer spatiotemporal scale.

Recording retina physiology

On the technical front, there are general limitations inherent to the use of multi-electrode arrays (MEAs). First, electrodes can pick up and mix activity from closely apposed, densely packed neurons, complicating analysis steps like spike sorting and single-unit identification. Second, MEAs come with a limited depth accessibility, necessitating direct and unobstructed access to the neurons of interest. To tackle the first issue, in this study I used chips that, owing to the density and number of electrodes employed, currently offer the highest resolution possible amongst the commercially available solutions. Generally however within vertebrates, elasmobranch fish possess retinas with a sparsely populated ganglion cell layer[517], and therefore it is considerably more tractable to identify single-units in these taxon compared to avian or zebrafish retinas[370]. For encouraging the attachment of the tissue on the MEA, 3D-printed weights were used (see Methods), while the unobstructed access was achieved to the extent possible by removing during dissection all potential 'electrical insulators' - vitreous fibres or Mueller glia terminal processes. Despite my optimisation attempts for recording electrophysiology of RGCs however, certain cells of this class are displaced within the INL and IPL, out of the reach of surface electrodes (but see Ref[501]). My EM volume includes only one displaced RGC soma, with its dendritic stratification pattern characteristically distinct from all its orthotopic counterparts. Therefore, it conceivably represents a different shark RGC type, one that is probably not captured in my study.

Finally, MEA chips are not transparent and thus limit the available stimulation light paths, an issue especially pertinent to recordings of visual neurons. As the retina ganglion cell layer is in contact with the opaque MEA, light can not travel its natural light course – through all interneurons before reaching the photoreceptors that lie at the back of our eye. During MEA experiments, visual stimulation is therefore provided with 'photoreceptors first'. Compared to other vertebrate retinas however, where the presence of lipid droplets at the photoreceptor outer segments can filter incoming wavelengths[622,623], the direction of light is not expected to exert a big effect on the neuronal physiology of the shark retina.

Tissue morphology and connectivity with Electron Microscopy

The ultrastructural skeletons presented here are manually carried out and reflect ongoing work. Although all processes that can be traced back to a soma residing in GCL and IPL have been skeletonised, the EM volume still contains many, currently untraced, processes with somata outside the volume. Furthermore, although the ribbon-bearing BC terminals are identified, not all of their postsynaptic partners have been traced yet.

To my knowledge, this EM volume represents the first ultrastructural dataset from a shark retina, and over time will permit identifying connectomics from photoreceptors to RGCs and thus the elementary processing column (tissue input-ouput) of the retina. The data acquired are from the temporal region of a young animal, and future samples of different retina regions or ages could be valuable. The z-thickness of our sections is 60nm and the pixel size is 6x6nm. Although smaller sizes (50 nm and 5x5nm) are typically preferred to better resolve synapses and obliquely-oriented ribbons, acquisition at higher-resolution settings could not be achieved due to artifacts likely caused by electron overdosage.

Inherent to the shark retina biology, cells are sparse, and their dendritic processes extend over considerable distances. As EM data are size-limited, I run into two issues: most processes exit the volume (44/45) before they are full traced, and duplicates of cell types might not be contained, posing challenges for morphologically categorising the traced neurons.

Protein Sequence Divergence

Comparative work between distantly related species is currently not always straightforward. Given that most non-model organisms are either not genetically tractable or their gene annotations confirmed, one often needs to rely on tools developed for targeting other, better studied organisms. For immunostainings for example – and similarly for pharmacological perturbations –, commercially available antibodies usually recognise protein epitopes in mammals. If the specific protein sequence has changed across the large evolutionary distances separating them from sharks, then the antibody binding affinity might be drastically reduced. Absence of signal in immunostainings therefore can be ambiguous, with both lack of protein and lack of antigen recognition as plausible

causes. Such an example in my work is likely reflected in our attempts to stain for PKCα, a mammalian marker for rod bipolar cells[79,80,310]. Although a small-spotted catshark PKCα-like gene annotation exists (LOC119953069 in sScyCan1.1 (RefSeq GCF_902713615.1)) and the transcript is detected in the retina[451], our immunostainings attempts were unsuccessful.

General Outlook

The work presented here is the first, high-throughput, retinal output description of elasmobranch fish, namely the earliest diverging and still extant clade of jawed vertebrates. Relative to their few ONOFF counterparts, I observed an overwhelming presence of ON transient and OFF sustained RGCs. Furthermore, I identified circuit components in the shark retina that in mammals drive vision at dim-light levels, but also the existence of retinal direction-selectivity, a computation that I found to be implemented algorithmically via asymmetric inhibition and thus also like in other vertebrates. Considering the evolutionary distance between sharks and mammals, independent emergence of the same properties is unlikely; these findings therefore inform about circuits and computations that may pertain to vertebrate vision in general.

Finally, pharmacological perturbations unveiled responses of opposite polarity in RGCs that were ‘pure’ in control conditions, suggesting widespread but masked crosstalk between ON and OFF pathways within vertebrates. This intertwined relationship of the two polarities at the level of retinal output increasingly challenges the perspective that distinct retinal pathways encode light increments and decrements; likely this just reflects a converging, ‘reduced input’ solution within the evolution landscape of visual circuits. Across vertebrates, such a clear segregation of RGC response polarities is primarily observed in elasmobranch and mammals, clades that independently have lost some of their photoreceptor input channels and come with monostratifying BCs in the IPL. In stark contrast, extant vertebrates whose photoreceptor type complement resembles the ancestral, proto-vertebrate case, are primarily dominated by multistratifying BCs and mixed, ONOFF RGCs.

References

1. Carlisle, E., Yin, Z., Pisani, D. & Donoghue, P. C. J. Ediacaran origin and Ediacaran-Cambrian diversification of Metazoa. *Sci. Adv.* **10**, eadp7161 (2024).

2. Zhao, F., Bottjer, D. J., Hu, S., Yin, Z. & Zhu, M. Complexity and diversity of eyes in Early Cambrian ecosystems. *Sci. Rep.* **3**, 2751 (2013).

3. Paterson, J. R. *et al.* Acute vision in the giant Cambrian predator Anomalocaris and the origin of compound eyes. *Nature* **480**, 237–240 (2011).

4. Lythgoe, J. N. Light and Vision in the Aquatic Environment. in *Sensory Biology of Aquatic Animals* (eds Atema, J., Fay, R. R., Popper, A. N. & Tavolga, W. N.) 57–82 (Springer New York, New York, NY, 1988). doi:10.1007/978-1-4612-3714-3_3.

5. Douglas, R. H., Partridge, J. C. & Marshall, N. J. The eyes of deep-sea fish I: Lens pigmentation, tapeta and visual pigments. *Prog. Retin. Eye Res.* **17**, 597–636 (1998).

6. Kirk, J. T. O. *Light and Photosynthesis in Aquatic Ecosystems*. (Cambridge University Press, 1994).

7. Marine Optics By N.G. Jerlov Amsterdem: Elsevier Scientific Publishing Company, 1976. xii,231 pp. (Elsevier Oceanography Series, 14.) Price Dfl.77.00 ／$29.75. *J. Mar. Biol. Assoc. U. K.* **58**, 544–544 (1978).

8. Herring, P. J. & Kingdom, M. B. A. of the U. *Light and Life in the Sea*. (Cambridge University Press, 1990).

9. Kampa, E. M. Underwater Daylight and Moonlight Measurements in the Eastern North Atlantic. *J. Mar. Biol. Assoc. U. K.* **50**, 397–420 (1970).

10. The spectral characteristics of luminous marine organisms. *Proc. R. Soc. Lond. B Biol. Sci.* **220**, 183–217 (1983).

11. Widder, E. A., Latz, M. I. & Case, J. F. Marine bioluminescence spectra measured with an optical multichannel detection system. *Biol. Bull.* **165**, 791–810 (1983).

12. Mensinger, A. F. & Case, J. F. Luminescent properties of deep sea fish. *J. Exp. Mar. Biol. Ecol.* **144**, 1–15 (1990).

13. Bozzanao, A., Murgia, R., Vallerga, S., Hirano, J. & Archer, S. The photoreceptor system in the retinae of two dogfishes, Scyliorhinus canicula and Galeus melastomus: possible relationship with depth distribution and predatory lifestyle. *J. Fish Biol.* **59**, 1258–1278 (2001).

14. Rodieck, R. W. *The Vertebrate Retina; Principles of Structure and Function*. (Freeman, San Francisco, 1973).

15. Pugh, E. N. & Lamb, T. D. Chapter 5 Phototransduction in vertebrate rods and cones: Molecular mechanisms of amplification, recovery and light adaptation. in *Handbook of Biological Physics* vol. 3 183–255 (Elsevier, 2000).

16. Musilova, Z. *et al.* Vision using multiple distinct rod opsins in deep-sea fishes. *Science* **364**, 588–592 (2019).

17. Munz, F. W. & McFarland, W. N. Evolutionary Adaptations of Fishes to the Photic Environment. in *The Visual System in Vertebrates* (eds Crescitelli, F. et al.) 193–274 (Springer, Berlin, Heidelberg, 1977). doi:10.1007/978-3-642-66468-7_4.

18. Hagen, J. F. D., Roberts, N. & Johnston, R. J. The evolutionary history and spectral tuning of vertebrate visual opsins. *Dev. Biol.* **493**, 40–66 (2023).

19. Jacobs, G. H. Losses of functional opsin genes, short-wavelength cone photopigments, and color vision--a significant trend in the evolution of mammalian vision. *Vis. Neurosci.* **30**, 39–53 (2013).

20. Nicol, J. A. C. & Somiya, H. *The Eyes of Fishes*. (Clarendon Press, 1989).

21. Nicol, J. a. C. The Tapetum in Scyliorhinus Canicula. *J. Mar. Biol. Assoc. U. K.* **41**, 271–277 (1961).

22. Baylor, D. A., Lamb, T. D. & Yau, K. W. The membrane current of single rod outer segments. *J. Physiol.* **288**, 589–611 (1979).

23. Rieke, F. & Baylor, D. A. Single-photon detection by rod cells of the retina. *Rev. Mod. Phys.* **70**, 1027–1036 (1998).

24. Tinsley, J. N. *et al.* Direct detection of a single photon by humans. *Nat. Commun.* **7**, 12172 (2016).

25. Locket, N. A. Adaptations to the Deep-Sea Environment. in *The Visual System in Vertebrates* (eds Crescitelli, F. et al.) 67–192 (Springer, Berlin, Heidelberg, 1977). doi:10.1007/978-3-642-66468-7_3.

26. Warrant, E. J. Seeing better at night: life style, eye design and the optimum strategy of spatial and temporal summation. *Vision Res.* **39**, 1611–1630 (1999).

27. Copenhagen, D. R., Hemilä, S. & Reuter, T. Signal transmission through the dark-adapted retina of the toad (Bufo marinus): Gain, convergence, and signal/noise. *J. Gen. Physiol.* **95**, 717–732 (1990).

28. McGuire, B. A., Stevens, J. K. & Sterling, P. Microcircuitry of beta ganglion cells in cat retina. *J. Neurosci. Off. J. Soc. Neurosci.* **6**, 907–918 (1986).

29. Field, G. D. & Rieke, F. Nonlinear signal transfer from mouse rods to bipolar cells and implications for visual sensitivity. *Neuron* **34**, 773–785 (2002).

30. Burr, D. C. & Ross, J. Contrast sensitivity at high velocities. *Vision Res.* **22**, 479–484 (1982).

31. van Hateren, J. H. Three modes of spatiotemporal preprocessing by eyes. *J. Comp. Physiol. A* **172**, 583–591 (1993).

32. Pirenne, M. H. & Denton, E. J. Accuracy and Sensitivity of the Human Eye. *Nature* **170**, 1039–1042 (1952).

33. Lythgoe, J. N. *The Ecology of Vision*. (Clarendon Press, 1979).

34. LaVail, M. M. Rod Outer Segment Disk Shedding in Rat Retina: Relationship to Cyclic Lighting. *Science* **194**, 1071–1074 (1976).

35. Goldman, A. I., Teirstein, P. S. & O'Brien, P. J. The role of ambient lighting in circadian disc shedding in the rod outer segment of the rat retina. *Invest. Ophthalmol. Vis. Sci.* **19**, 1257–1267 (1980).

36. Cao, J., Ribelayga, C. P. & Mangel, S. C. A Circadian Clock in the Retina Regulates Rod-Cone Gap Junction Coupling and Neuronal Light Responses via Activation of Adenosine A2A Receptors. *Front. Cell. Neurosci.* **14**, 605067 (2021).

37. Ribelayga, C., Cao, Y. & Mangel, S. C. The Circadian Clock in the Retina Controls Rod-Cone Coupling. *Neuron* **59**, 790–801 (2008).

38. Hornstein, E. P., Verweij, J., Li, P. H. & Schnapf, J. L. Gap-Junctional Coupling and Absolute Sensitivity of Photoreceptors in Macaque Retina. *J. Neurosci.* **25**, 11201–11209 (2005).

39. Bloomfield, S. A. & Völgyi, B. The diverse functional roles and regulation of neuronal gap junctions in the retina. *Nat. Rev. Neurosci.* **10**, 495–506 (2009).

40. Attwell, D. & Wilson, M. Behaviour of the rod network in the tiger salamander retina mediated by membrane properties of individual rods. *J. Physiol.* **309**, 287–315 (1980).

41. Tessier-Lavigne, M., Attwell, D. & Hodgkin, A. L. The effect of photoreceptor coupling and synapse nonlinearity on signal : noise ratio in early visual processing. *Proc. R. Soc. Lond. B Biol. Sci.* **234**, 171–197 (1997).

42. Jin, N. G. & Ribelayga, C. P. Direct Evidence for Daily Plasticity of Electrical Coupling between Rod Photoreceptors in the Mammalian Retina. *J. Neurosci. Off. J. Soc. Neurosci.* **36**, 178–184 (2016).

43. Bloomfield, S. A. & Dacheux, R. F. Rod vision: pathways and processing in the mammalian retina. *Prog. Retin. Eye Res.* **20**, 351–384 (2001).

44. Pyza, E. & Meinertzhagen, I. A. Daily and circadian rhythms of synaptic frequency in the first visual neuropile of the housefly's (Musca domestica L.) optic lobe. *Proc. R. Soc. Lond. B Biol. Sci.* **254**, 97–105 (1997).

45. Dubs, A., Laughlin, S. B. & Srinivasan, M. V. Single photon signals in fly photoreceptors and first order interneurones at behavioral threshold. *J. Physiol.* **317**, 317–334 (1981).

46. Weiler, R., Kohler, K., Kirsch, M. & Wagner, H.-J. Glutamate and dopamine modulate synaptic plasticity in horizontal cell dendrites of fish retina. *Neurosci. Lett.* **87**, 205–209 (1988).

47. Nicol, J. a. C. Migration of chorioidal tapetal pigment in the spur dog Squaluls acanthias. *J. Mar. Biol. Assoc. U. K.* **45**, 405–427 (1965).

48. Fox, D. L. & Kuchnow, K. P. Reversible, Light-Screening Pigment of Elasmobranch Eyes: Chemical Identity with Melanin. *Science* **150**, 612–614 (1965).

49. Kuchnow, K. P. & Martin, R. Pigment migration in the tapetum lucidum of the elasmobranch eye: Evidence for a nervous mechanism. *Vision Res.* **10**, 825-IN4 (1970).

50. Heath, A. R. & Hindman, H. M. The role of cyclic AMP in the control of elasmobranch ocular tapetum lucidum pigment granule migration. *Vision Res.* **28**, 1277–1285 (1988).

51. McFarland, W. N. & Munz, F. W. Part III: The evolution of photopic visual pigments in fishes. *Vision Res.* **15**, 1071–1080 (1975).

52. Wilkins, L., Marshall, N. J., Johnsen, S. & Osorio, D. Modelling colour constancy in fish: implications for vision and signalling in water. *J. Exp. Biol.* **219**, 1884–1892 (2016).

53. Sabbah, S. & Hawryshyn, C. W. What has driven the evolution of multiple cone classes in visual systems: object contrast enhancement or light flicker elimination? *BMC Biol.* **11**, 77 (2013).

54. Maximov, V. V. Environmental factors which may have led to the appearance of colour vision. *Philos. Trans. R. Soc. Lond. B. Biol. Sci.* **355**, 1239–1242 (2000).

55. Baden, T. Ancestral photoreceptor diversity as the basis of visual behaviour. *Nat. Ecol. Evol.* **8**, 374–386 (2024).

56. Fornetto, C., Euler, T. & Baden, T. Vertebrate vision is ancestrally based on competing cone circuits. 2024.11.19.624320 Preprint at https://doi.org/10.1101/2024.11.19.624320 (2024).

57. Gjorgjieva, J., Meister, M. & Sompolinsky, H. Functional diversity among sensory neurons from efficient coding principles. *PLoS Comput. Biol.* **15**, e1007476 (2019).

58. Osorio, D. & Vorobyev, M. A review of the evolution of animal colour vision and visual communication signals. *Vision Res.* **48**, 2042–2051 (2008).

59. Lind, O., Henze, M. J., Kelber, A. & Osorio, D. Coevolution of coloration and colour vision? *Philos. Trans. R. Soc. B Biol. Sci.* **372**, 20160338 (2017).

60. Baden, T. & Osorio, D. The Retinal Basis of Vertebrate Color Vision. *Annu. Rev. Vis. Sci.* **5**, 177–200 (2019).

61. Morshedian, A. & Fain, G. L. Single-Photon Sensitivity of Lamprey Rods with Cone-like Outer Segments. *Curr. Biol.* **25**, 484–487 (2015).

62. Okano, T., Kojima, D., Fukada, Y., Shichida, Y. & Yoshizawa, T. Primary structures of chicken cone visual pigments: vertebrate rhodopsins have evolved out of cone visual pigments. *Proc. Natl. Acad. Sci. U. S. A.* **89**, 5932–5936 (1992).

63. Davies, W. I. L., Collin, S. P. & Hunt, D. M. Molecular ecology and adaptation of visual photopigments in craniates. *Mol. Ecol.* **21**, 3121–3158 (2012).

64. Bowmaker, J. K. Evolution of vertebrate visual pigments. *Vision Res.* **48**, 2022–2041 (2008).

65. Yokoyama, S. Molecular evolution of vertebrate visual pigments. *Prog. Retin. Eye Res.* **19**, 385–419 (2000).

66. Kuffler, S. W. Discharge patterns and functional organization of mammalian retina. *J. Neurophysiol.* **16**, 37–68 (1953).

67. Donner, K. O. & Willmer, E. N. An analysis of the response from single visual-purple-dependent elements, in the retina of the cat. *J. Physiol.* **111**, 160–173 (1950).

68. Lettvin, J. Y., Maturana, H. R., McCulloch, W. S. & Pitts, W. H. What the Frog's Eye Tells the Frog's Brain. *Proc. IRE* **47**, 1940–1951 (1959).

69. Hartline, H. K. The response of single optic nerve fibers of the vertebrate eye to illumination of the retina. *Am. J. Physiol.-Leg. Content* **121**, 400–415 (1938).

70. Gollisch, T. & Meister, M. Eye smarter than scientists believed: neural computations in circuits of the retina. *Neuron* **65**, 150–164 (2010).

71. Dogiel, A. S. Die Retina der Vögel. *Arch. Für Mikrosk. Anat.* **44**, 622–648 (1895).

72. Fritzsch, B. & Collin, S. P. Dendritic distribution of two populations of ganglion cells and the retinopetal fibers in the retina of the silver lamprey (Ichthyomyzon unicuspis). *Vis. Neurosci.* **4**, 533–545 (1990).

73. Maple, B. R., Zhang, J., Pang, J.-J., Gao, F. & Wu, S. M. Characterization of displaced bipolar cells in the tiger salamander retina. *Vision Res.* **45**, 697–705 (2005).

74. Attwell, D., Mobbs, P., Tessier-Lavigne, M. & Wilson, M. Neurotransmitter-induced currents in retinal bipolar cells of the axolotl, Ambystoma mexicanum. *J. Physiol.* **387**, 125–161 (1987).

75. DeVries, S. H. & Schwartz, E. A. Kainate receptors mediate synaptic transmission between cones and 'Off' bipolar cells in a mammalian retina. *Nature* **397**, 157–160 (1999).

76. DeVries, S. H. Bipolar cells use kainate and AMPA receptors to filter visual information into separate channels. *Neuron* **28**, 847–856 (2000).

77. Saito, T. & Kaneko, A. Ionic mechanisms underlying the responses of off-center bipolar cells in the carp retina. I. Studies on responses evoked by light. *J. Gen. Physiol.* **81**, 589–601 (1983).

78. Masu, M. *et al.* Specific deficit of the ON response in visual transmission by targeted disruption of the mGIuR6 gene. *Cell* **80**, 757–765 (1995).

79. Greferath, U., Grünert, U. & Wässle, H. Rod bipolar cells in the mammalian retina show protein kinase C-like immunoreactivity. *J. Comp. Neurol.* **301**, 433–442 (1990).

80. Wässle, H., Yamashita, M., Greferath, U., Grünert, U. & Müller, F. The rod bipolar cell of the mammalian retina. *Vis. Neurosci.* **7**, 99–112 (1991).

81. Nomura, A. *et al.* Developmentally regulated postsynaptic localization of a metabotropic glutamate receptor in rat rod bipolar cells. *Cell* **77**, 361–369 (1994).

82. Grant, G. B. & Dowling, J. E. A glutamate-activated chloride current in cone-driven ON bipolar cells of the white perch retina. *J. Neurosci.* **15**, 3852–3862 (1995).

83. Grant, G. B. & Dowling, J. E. On bipolar cell responses in the teleost retina are generated by two distinct mechanisms. *J. Neurophysiol.* **76**, 3842–3849 (1996).

84. Veruki, M. L., Mørkve, S. H. & Hartveit, E. Activation of a presynaptic glutamate transporter regulates synaptic transmission through electrical signaling. *Nat. Neurosci.* **9**, 1388–1396 (2006).

85. Wersinger, E. *et al.* The glutamate transporter EAAT5 works as a presynaptic receptor in mouse rod bipolar cells. *J. Physiol.* **577**, 221–234 (2006).

86. Rauen, T., Rothstein, J. D. & Wässle, H. Differential expression of three glutamate transporter subtypes in the rat retina. *Cell Tissue Res.* **286**, 325–336 (1996).

87. Niklaus, S. *et al.* Glutamate transporters are involved in direct inhibitory synaptic transmission in the vertebrate retina. *Open Biol.* **14**, 240140 (2024).

88. Nawy, S. & Jahr, C. E. cGMP-gated conductance in retinal bipolar cells is suppressed by the photoreceptor transmitter. *Neuron* **7**, 677–683 (1991).

89. Shiells, R. A. & Falk, G. Glutamate receptors of rod bipolar cells are linked to a cyclic GMP cascade via a G-protein. *Proc. Biol. Sci.* **242**, 91–94 (1990).

90. Famiglietti, E. V. & Kolb, H. Structural Basis for ON-and OFF-Center Responses in Retinal Ganglion Cells. *Science* **194**, 193–195 (1976).

91. Euler, T., Schneider, H. & Wässle, H. Glutamate Responses of Bipolar Cells in a Slice Preparation of the Rat Retina. *J. Neurosci.* **16**, 2934–2944 (1996).

92. Euler, T. & Wässle, H. Immunocytochemical identification of cone bipolar cells in the rat retina. *J. Comp. Neurol.* **361**, 461–478 (1995).

93. Nelson, R., Famiglietti, E. V. & Kolb, H. Intracellular staining reveals different levels of stratification for on- and off-center ganglion cells in cat retina. *J. Neurophysiol.* **41**, 472–483 (1978).

94. Masland, R. H. The Neuronal Organization of the Retina. *Neuron* **76**, 266–280 (2012).

95. Euler, T., Haverkamp, S., Schubert, T. & Baden, T. Retinal bipolar cells: elementary building blocks of vision. *Nat. Rev. Neurosci.* **15**, 507–519 (2014).

96. Hoshi, H., Liu, W.-L., Massey, S. C. & Mills, S. L. ON Inputs to the OFF Layer: Bipolar Cells That Break the Stratification Rules of the Retina. *J. Neurosci.* **29**, 8875–8883 (2009).

97. Wu, S. M., Gao, F. & Maple, B. R. Functional Architecture of Synapses in the Inner Retina: Segregation of Visual Signals by Stratification of Bipolar Cell Axon Terminals. *J. Neurosci.* **20**, 4462–4470 (2000).

98. Pang, J.-J., Gao, F. & Wu, S. M. Stratum-by-stratum projection of light response attributes by retinal bipolar cells of Ambystoma. *J. Physiol.* **558**, 249–262 (2004).

99. Witkovsky, P. & Stell, W. K. Retinal structure in the smooth dogfish, *Mustelus canis* : Light microscopy of bipolar cells. *J. Comp. Neurol.* **148**, 47–59 (1973).

100. Günther, A. *et al.* Double Cones and the Diverse Connectivity of Photoreceptors and Bipolar Cells in an Avian Retina. *J. Neurosci. Off. J. Soc. Neurosci.* **41**, 5015–5028 (2021).

101. Connaughton, V. p., Graham, D. & Nelson, R. Identification and morphological classification of horizontal, bipolar, and amacrine cells within the zebrafish retina. *J. Comp. Neurol.* **477**, 371–385 (2004).

102. Li, Y. N., Tsujimura, T., Kawamura, S. & Dowling, J. E. Bipolar cell–photoreceptor connectivity in the zebrafish (Danio rerio) retina. *J. Comp. Neurol.* **520**, 3786–3802 (2012).

103. Ghosh, K. K., Bujan, S., Haverkamp, S., Feigenspan, A. & Wässle, H. Types of bipolar cells in the mouse retina. *J. Comp. Neurol.* **469**, 70–82 (2004).

104. Kolb, H. & Famiglietti, E. V. Rod and cone pathways in the inner plexiform layer of cat retina. *Science* **186**, 47–49 (1974).

105. Dacheux, R. F. & Raviola, E. The rod pathway in the rabbit retina: a depolarizing bipolar and amacrine cell. *J. Neurosci.* **6**, 331–345 (1986).

106. Strettoi, E., Raviola, E. & Dacheux, R. F. Synaptic connections of the narrow-field, bistratified rod amacrine cell (AII) in the rabbit retina. *J. Comp. Neurol.* **325**, 152–168 (1992).

107. Feigenspan, A., Teubner, B., Willecke, K. & Weiler, R. Expression of Neuronal Connexin36 in AII Amacrine Cells of the Mammalian Retina. *J. Neurosci.* **21**, 230–239 (2001).

108. Deans, M. R., Volgyi, B., Goodenough, D. A., Bloomfield, S. A. & Paul, D. L. Connexin36 Is Essential for Transmission of Rod-Mediated Visual Signals in the Mammalian Retina. *Neuron* **36**, 703–712 (2002).

109. DeVries, S. H. & Baylor, D. A. An alternative pathway for signal flow from rod photoreceptors to ganglion cells in mammalian retina. *Proc. Natl. Acad. Sci.* **92**, 10658–10662 (1995).

110. Hack, I., Peichl, L. & Brandstätter, J. H. An alternative pathway for rod signals in the rodent retina: Rod photoreceptors, cone bipolar cells, and the localization of glutamate receptors. *Proc. Natl. Acad. Sci.* **96**, 14130–14135 (1999).

111. Soucy, E., Wang, Y., Nirenberg, S., Nathans, J. & Meister, M. A novel signaling pathway from rod photoreceptors to ganglion cells in mammalian retina. *Neuron* **21**, 481–493 (1998).

112. Terakita, A. The opsins. *Genome Biol.* **6**, 213 (2005).

113. Shichida, Y. & Matsuyama, T. Evolution of opsins and phototransduction. *Philos. Trans. R. Soc. B Biol. Sci.* **364**, 2881–2895 (2009).

114. Tommasini, D., Yoshimatsu, T., Baden, T. & Shekhar, K. Comparative transcriptomic insights into the evolutionary origin of the tetrapod double cone. *BioRxiv Prepr. Serv. Biol.* 2024.11.04.621990 (2024) doi:10.1101/2024.11.04.621990.

115. Morshedian, A. & Fain, G. L. The evolution of rod photoreceptors. *Philos. Trans. R. Soc. B Biol. Sci.* **372**, 20160074 (2017).

116. Lamb, T. D., Collin, S. P. & Pugh, E. N. Evolution of the vertebrate eye: opsins, photoreceptors, retina and eye cup. *Nat. Rev. Neurosci.* **8**, 960–976 (2007).

117. Lamb, T. D. Evolution of phototransduction, vertebrate photoreceptors and retina. *Prog. Retin. Eye Res.* **36**, 52–119 (2013).

118. Peng, Y.-R. Cell-type specification in the retina: Recent discoveries from transcriptomic approaches. *Curr. Opin. Neurobiol.* **81**, 102752 (2023).

119. Macosko, E. Z. *et al.* Highly Parallel Genome-wide Expression Profiling of Individual Cells Using Nanoliter Droplets. *Cell* **161**, 1202–1214 (2015).

120. Yan, W. *et al.* Mouse Retinal Cell Atlas: Molecular Identification of over Sixty Amacrine Cell Types. *J. Neurosci.* **40**, 5177–5195 (2020).

121. Tran, N. M. *et al.* Single-Cell Profiles of Retinal Ganglion Cells Differing in Resilience to Injury Reveal Neuroprotective Genes. *Neuron* **104**, 1039-1055.e12 (2019).

122. Baden, T. *et al.* The functional diversity of retinal ganglion cells in the mouse. *Nature* **529**, 345–350 (2016).

123. Bae, J. A. *et al.* Digital Museum of Retinal Ganglion Cells with Dense Anatomy and Physiology. *Cell* **173**, 1293-1306.e19 (2018).

124. Goetz, J. *et al.* Unified classification of mouse retinal ganglion cells using function, morphology, and gene expression. *Cell Rep.* **40**, (2022).

125. Farrow, K. & Masland, R. H. Physiological clustering of visual channels in the mouse retina. *J. Neurophysiol.* **105**, 1516–1530 (2011).

126. Koskela, S. The Limits of Visual Sensitivity and its Circadian Control. (2020). doi:10.13140/RG.2.2.35748.19847.

127. Lamb, T. D. Photoreceptor physiology and evolution: cellular and molecular basis of rod and cone phototransduction. *J. Physiol.* **600**, 4585–4601 (2022).

128. Lamb, T. D. Evolution of the genes mediating phototransduction in rod and cone photoreceptors. *Prog. Retin. Eye Res.* **76**, 100823 (2020).

129. Hahn, J. *et al.* Evolution of neuronal cell classes and types in the vertebrate retina. *Nature* **624**, 415–424 (2023).

130. Wang, J. *et al.* Molecular characterization of the sea lamprey retina illuminates the evolutionary origin of retinal cell types. *Nat. Commun.* **15**, 10761 (2024).

131. Baden, T. From water to land: Evolution of photoreceptor circuits for vision in air. *PLOS Biol.* **22**, e3002422 (2024).

132. Davesne, D. *et al.* Fossilized cell structures identify an ancient origin for the teleost whole-genome duplication. *Proc. Natl. Acad. Sci.* **118**, e2101780118 (2021).

133. Amores, A. *et al.* Zebrafish *hox* Clusters and Vertebrate Genome Evolution. *Science* **282**, 1711–1714 (1998).

134. Jaillon, O. *et al.* Genome duplication in the teleost fish Tetraodon nigroviridis reveals the early vertebrate proto-karyotype. *Nature* **431**, 946–957 (2004).

135. Taylor, J. S., Braasch, I., Frickey, T., Meyer, A. & Peer, Y. V. de. Genome Duplication, a Trait Shared by 22,000 Species of Ray-Finned Fish. *Genome Res.* **13**, 382–390 (2003).

136. Glasauer, S. M. K. & Neuhauss, S. C. F. Whole-genome duplication in teleost fishes and its evolutionary consequences. *Mol. Genet. Genomics* **289**, 1045–1060 (2014).

137. Ravi, V. & Venkatesh, B. The Divergent Genomes of Teleosts. *Annu. Rev. Anim. Biosci.* **6**, 47–68 (2018).

138. Anctil, M. & Ali, M. A. Letter: Giant ganglion cells in the retina of the hammerhead shark (Sphyrna lewini). *Vision Res.* **14**, 903–904 (1974).

139. Holmberg, K. The hagfish retina: Electron microscopic study comparing receptor and epithelial cells in the pacific hagfish, Polistotrema stouti, with those in the atlantic hagfish, Myxine glutinosa. *Z. Für Zellforsch. Mikrosk. Anat.* **121**, 249–269 (1971).

140. Fernholm, B. & Holmberg, K. The eyes in three genera of hagfish (Eptatretus, paramyxine andMyxine)—A case of degenerative evolution. *Vision Res.* **15**, 253-IN4 (1975).

141. Dong, E. M. & Allison, W. T. Vertebrate features revealed in the rudimentary eye of the Pacific hagfish (Eptatretus stoutii). *Proc. R. Soc. B Biol. Sci.* **288**, 20202187 (2021).

142. Bradshaw, S. N. & Allison, W. T. Hagfish to Illuminate the Developmental and Evolutionary Origins of the Vertebrate Retina. *Front. Cell Dev. Biol.* **10**, (2022).

143. Suzuki, D. G. & Grillner, S. The stepwise development of the lamprey visual system and its evolutionary implications. *Biol. Rev.* **93**, 1461–1477 (2018).

144. Fain, G. L. Lamprey vision: Photoreceptors and organization of the retina. *Semin. Cell Dev. Biol.* **106**, 5–11 (2020).

145. Fritzsch, B. Ontogenetic Clues to the Phylogeny of the Visual System. in *The Changing Visual System* (eds Bagnoli, P. & Hodos, W.) 33–49 (Springer US, Boston, MA, 1991). doi:10.1007/978-1-4615-3390-0_4.

146. Hara, Y. *et al.* Shark genomes provide insights into elasmobranch evolution and the origin of vertebrates. *Nat. Ecol. Evol.* **2**, 1761–1771 (2018).

147. Tan, M. *et al.* The whale shark genome reveals patterns of vertebrate gene family evolution. *eLife* **10**, e65394 (2021).

148. Sendell-Price, A. T. *et al.* Low mutation rate in epaulette sharks is consistent with a slow rate of evolution in sharks. *Nat. Commun.* **14**, 6628 (2023).

149. Venkatesh, B. *et al.* Elephant shark genome provides unique insights into gnathostome evolution. *Nature* **505**, 174–179 (2014).

150. Freitas, R., Zhang, G. & Cohn, M. J. Biphasic Hoxd Gene Expression in Shark Paired Fins Reveals an Ancient Origin of the Distal Limb Domain. *PLoS ONE* **2**, e754 (2007).

151. Tanaka, M. *et al.* Fin development in a cartilaginous fish and the origin of vertebrate limbs. *Nature* **416**, 527–531 (2002).

152. Carrera, I., Ferreiro-Galve, S., Sueiro, C., Anadón, R. & Rodríguez-Moldes, I. Tangentially migrating GABAergic cells of subpallial origin invade massively the pallium in developing sharks. *Brain Res. Bull.* **75**, 405–409 (2008).

153. Rodríguez-Moldes, I. *et al.* Development of the cerebellar body in sharks: Spatiotemporal relations of Pax6 expression, cell proliferation and differentiation. *Neurosci. Lett.* **432**, 105–110 (2008).

154. Gruber, Samuelh. The Visual System of Sharks: Adaptations and Capability. *Am. Zool.* **17**, 453–469 (1977).

155. Collin, S. P. Scene through the eyes of an apex predator: a comparative analysis of the shark visual system. *Clin. Exp. Optom.* **101**, 624–640 (2018).

156. Walls, G. L. *The Vertebrate Eye and Its Adaptive Radiation*. xiv, 785 (Cranbrook Institute of Science, Oxford, England, 1942). doi:10.5962/bhl.title.7369.

157. Collin, S. P. The Neuroecology of Cartilaginous Fishes: Sensory Strategies for Survival. *Brain. Behav. Evol.* **80**, 80–96 (2012).

158. Gruber, S. H. Duplex Vision in the Elasmobranchs: Histological, Electrophysiological and Psychophysical Evidence. in *Vision in Fishes* (ed. Ali, M. A.) 525–540 (Springer US, Boston, MA, 1975). doi:10.1007/978-1-4757-0241-5_43.

159. Bigelow, H. B. & Schroeder, W. C. *Fishes of the Western North Atlantic: Lancelets, Cyclostomes, Sharks*. (Sears Foundation for Marine Research, Yale University, 1948).

160. Schultze, M. Zur Anatomie und Physiologie der Retina. *Arch. Für Mikrosk. Anat.* **2**, 175–286 (1866).

161. Newman, A. S., Marshall, J. N. & Collin, S. P. Visual eyes: a quantitative analysis of the photoreceptor layer in deep-sea sharks. *Brain. Behav. Evol.* **82**, 237–249 (2013).

162. Kohbara, J., Niwa, H. & Oguri, M. Comparative Light Microscopic Studies on the Retina of Some Elasmobranch Fishes. *Nippon Suisan Gakkaishi* **53**, 2117–2125 (1987).

163. Magaña-Hernández, L. *et al.* Ultrastructural Characteristics and Synaptic Connectivity of Photoreceptors in the Simplex Retina of Little Skate (*Leucoraja erinacea*). *eneuro* **10**, ENEURO.0226-23.2023 (2023).

164. Dowling, J. E. & Ripps, H. Visual Adaptation in the Retina of the Skate. *J. Gen. Physiol.* **56**, 491–520 (1970).

165. Green, D. G. & Siegel, I. M. Double Branched Flicker Fusion Curves from the All-Rod Skate Retina. *Science* **188**, 1120–1122 (1975).

166. Cornwall, M. C., Ripps, H., Chappell, R. L. & Jones, G. J. Membrane current responses of skate photoreceptors. *J. Gen. Physiol.* **94**, 633–647 (1989).

167. Schieber, N. L., Collin, S. P. & Hart, N. S. Comparative retinal anatomy in four species of elasmobranch. *J. Morphol.* **273**, 423–440 (2012).

168. Stell, W. K. & Witkovsky, P. Retinal structure in the smooth dogfish, *Mustelus canis* : General description and light microscopy of giant ganglion cells. *J. Comp. Neurol.* **148**, 1–31 (1973).

169. Stell, W. K., Detwiler, P. B., Wagner, H. G. & Wolbarsht, M. L. Giant Retinal Ganglion Cells in Dogfish (Mustelus): Electrophysiology of Single On-Centre Units. in *Vision in Fishes: New Approaches in Research* (ed. Ali, M. A.) 99–112 (Springer US, Boston, MA, 1975). doi:10.1007/978-1-4757-0241-5_10.

170. Witkovsky, P. & Stell, W. K. Retinal structure in the smooth dogfish *Mustelus canis:* electron microscopy of serially sectioned bipolar cell synaptic terminals. *J. Comp. Neurol.* **150**, 147–167 (1973).

171. Schlemermeyer, E. & Chappell, R. L. Two classes of bipolar cell in the retina of the skateRaja erinacea. *J. Neurocytol.* **25**, 625–635 (1996).

172. Cohen, J. L. Effects of glycine and GABA on the ganglion cells of the retina of the skate Raja erinacea. *Brain Res.* **332**, 169–173 (1985).

173. Cohen, J. L. & Gruber, S. H. Spectral input to lemon shark (Negaprion brevirostris) ganglion cells. *J. Comp. Physiol. A* **156**, 579–586 (1985).

174. Naka, K.-I. & Witkovsky, P. Dogfish ganglion cell discharge resulting from extrinsic polarization of the horizontal cells. *J. Physiol.* **223**, 449–460 (1972).

175. Ashmore, J. F. & Falk, G. Responses of rod-bipolar cells in the dark-adapted retina of the dogfish, *Scyliorhinus canicula*. *J. Physiol.* **300**, 115–150 (1980).

176. Hassenstein, B. & Reichardt, W. Systemtheoretische Analyse der Zeit-, Reihenfolgen- und Vorzeichenauswertung bei der Bewegungsperzeption des Rüsselkäfers Chlorophanus. *Z. Für Naturforschung B* **11**, 513–524 (1956).

177. Barlow, H. B. & Levick, W. R. The mechanism of directionally selective units in rabbit's retina. *J. Physiol.* **178**, 477–504 (1965).

178. Borst, A. & Euler, T. Seeing Things in Motion: Models, Circuits, and Mechanisms. *Neuron* **71**, 974–994 (2011).

179. Lacalli, T. C., Holland, N. D. & West, J. E. Landmarks in the anterior central nervous system of amphioxus larvae. *Philos. Trans. R. Soc. Lond. B. Biol. Sci.* **344**, 165–185 (1997).

180. Vopalensky, P. *et al.* Molecular analysis of the amphioxus frontal eye unravels the evolutionary origin of the retina and pigment cells of the vertebrate eye. *Proc. Natl. Acad. Sci.* **109**, 15383–15388 (2012).

181. Pergner, J., Vavrova, A., Kozmikova, I. & Kozmik, Z. Molecular Fingerprint of Amphioxus Frontal Eye Illuminates the Evolution of Homologous Cell Types in the Chordate Retina. *Front. Cell Dev. Biol.* **8**, 705 (2020).

182. Gačić, Z., Damjanović, I., Mićković, B., Hegediš, A. & Nikčević, M. Spectral sensitivity of the dogfish shark (Scyliorhinus canicula). *Fish Physiol. Biochem.* **33**, 21–27 (2007).

183. Bellono, N. W., Leitch, D. B. & Julius, D. Molecular tuning of electroreception in sharks and skates. *Nature* **558**, 122–126 (2018).

184. Malchow, R. P. & Ripps, H. Effects of γ-Aminobutyric Acid on Skate Retinal Horizontal Cells: Evidence for an Electrogenic Uptake Mechanism. *Proc. Natl. Acad. Sci. U. S. A.* **87**, 8945–8949 (1990).

185. BABKIN, B. P., BOWIE, D. J. & NICHOLLS, J. V. V. Structure and reactions to stimuli of arteries (and conus) in the elasmobranch genus raja. *Contrib. Can. Biol. Fish.* **8**, 207–225 (1933).

186. Brin, K. P. & Ripps, H. Rhodopsin photoproducts and rod sensitivity in the skate retina. *J. Gen. Physiol.* **69**, 97–120 (1977).

187. Marine Biological Laboratory (Woods Hole, Mass.), Marine Biological Laboratory (Woods Hole, M.) & Cavanaugh, G. M. *Formulae and Methods IV [i.e., 4th Ed.] of the Marine Biological Laboratory Chemical Room*. (Woods Hole, Mass, 1956). doi:10.5962/bhl.title.5845.

188. Hartman, F. A., Lewis, L. A., Brownell, K. A., Shelden, F. F. & Walther, R. F. Some Blood Constituents of the Normal Skate. *Physiol. Zool.* **14**, 476–486 (1941).

189. Kriebel, M. E., Dowdall, M. J., Pappas, G. D. & Downie, D. L. Detached, Purified Nerve Terminals From Skate Electric Organ for Biochemical and Physiological Studies. *Biol. Bull.* **190**, 88–97 (1996).

190. Anderson, W. G., Good, J. P., Pillans, R. D., Hazon, N. & Franklin, C. E. Hepatic urea biosynthesis in the euryhaline elasmobranch Carcharhinus leucas. *J. Exp. Zoolog. A Comp. Exp. Biol.* **303A**, 917–921 (2005).

191. Shiells, R. & Falk, G. Retinal on-bipolar cells contain a nitric oxide-sensitive guanylate cyclase. *NeuroReport* **3**, 845 (1992).

192. Seifert, M., Roberts, P. A., Kafetzis, G., Osorio, D. & Baden, T. Birds multiplex spectral and temporal visual information via retinal On- and Off-channels. *bioRxiv* 2022.10.20.513047 (2022).

193. Franke, K. *et al.* An arbitrary-spectrum spatial visual stimulator for vision research. *eLife* **8**, e48779 (2019).

194. Muthmann, J.-O. *et al.* Spike Detection for Large Neural Populations Using High Density Multielectrode Arrays. *Front. Neuroinformatics* **9**, (2015).

195. Govardovskii, V. I., Fyhrquist, N., Reuter, T., Kuzmin, D. G. & Donner, K. In search of the visual pigment template. *Vis. Neurosci.* **17**, 509–528 (2000).

196. Yoshimatsu, T. *et al.* Ancestral circuits for vertebrate color vision emerge at the first retinal synapse. *Sci. Adv.* **7**, eabj6815 (2021).

197. Mulansky, M. & Kreuz, T. PySpike—A Python library for analyzing spike train synchrony. *SoftwareX* **5**, 183–189 (2016).

198. Baden, T., Esposti, F., Nikolaev, A. & Lagnado, L. Spikes in Retinal Bipolar Cells Phase-Lock to Visual Stimuli with Millisecond Precision. *Curr. Biol.* **21**, 1859–1869 (2011).

199. Goldberg, J. M. & Brown, P. B. Response of binaural neurons of dog superior olivary complex to dichotic tonal stimuli: some physiological mechanisms of sound localization. *J. Neurophysiol.* **32**, 613–636 (1969).

200. Köppl, C. Phase Locking to High Frequencies in the Auditory Nerve and Cochlear Nucleus Magnocellularis of the Barn Owl, *Tyto alba*. *J. Neurosci.* **17**, 3312–3321 (1997).

201. Schindelin, J. *et al.* Fiji: an open-source platform for biological-image analysis. *Nat. Methods* **9**, 676–682 (2012).

202. Preibisch, S., Saalfeld, S. & Tomancak, P. Globally optimal stitching of tiled 3D microscopic image acquisitions. *Bioinformatics* **25**, 1463–1465 (2009).

203. Della Santina, L. *et al.* Glutamatergic Monopolar Interneurons Provide a Novel Pathway of Excitation in the Mouse Retina. *Curr. Biol.* **26**, 2070–2077 (2016).

204. Yu, W.-Q. *et al.* Distinctive synaptic structural motifs link excitatory retinal interneurons to diverse postsynaptic partner types. *Cell Rep.* **42**, 112006 (2023).

205. Boergens, K. M. *et al.* webKnossos: efficient online 3D data annotation for connectomics. *Nat. Methods* **14**, 691–694 (2017).

206. Hellevik, A. M. *et al.* Ancient origin of the rod bipolar cell pathway in the vertebrate retina. *Nat. Ecol. Evol.* **8**, 1165–1179 (2024).

207. Arendt, D. Evolution of eyes and photoreceptor cell types. *Int. J. Dev. Biol.* **47**, 563–571 (2003).

208. Arendt, D., Hausen, H. & Purschke, G. The ‘division of labour’ model of eye evolution. *Philos. Trans. R. Soc. B Biol. Sci.* **364**, 2809–2817 (2009).

209. Shimeld, S. M. & Holland, P. W. H. Vertebrate innovations. *Proc. Natl. Acad. Sci.* **97**, 4449–4452 (2000).

210. Holland, L. Z. & Ocampo Daza, D. A new look at an old question: when did the second whole genome duplication occur in vertebrate evolution? *Genome Biol.* **19**, 209 (2018).

211. Smith, J. J. *et al.* The sea lamprey germline genome provides insights into programmed genome rearrangement and vertebrate evolution. *Nat. Genet.* **50**, 270–277 (2018).

212. Eakin, R. M. Evolution of photoreceptors. *Cold Spring Harb. Symp. Quant. Biol.* **30**, 363–370 (1965).

213. Eakin, R. M. Evolutionary Significance of Photoreceptors: In Retrospect. *Am. Zool.* **19**, 647–653 (1979).

214. Arendt, D. The evolution of cell types in animals: emerging principles from molecular studies. *Nat. Rev. Genet.* **9**, 868–882 (2008).

215. Young, G. C. Early Evolution of the Vertebrate Eye—Fossil Evidence. *Evol. Educ. Outreach* **1**, 427–438 (2008).

216. Pergner, J. & Kozmik, Z. Amphioxus photoreceptors - insights into the evolution of vertebrate opsins, vision and circadian rhythmicity. *Int. J. Dev. Biol.* **61**, 665–681 (2017).

217. Holland, L. Z. & Short, S. Gene duplication, co-option and recruitment during the origin of the vertebrate brain from the invertebrate chordate brain. *Brain. Behav. Evol.* **72**, 91–105 (2008).

218. Oakley, T. H. Furcation and fusion: The phylogenetics of evolutionary novelty. *Dev. Biol.* **431**, 69–76 (2017).

219. Plachetzki, D. C. & Oakley, T. H. Key transitions during the evolution of animal phototransduction: novelty, ‘tree-thinking,’ co-option, and co-duplication. *Integr. Comp. Biol.* **47**, 759–769 (2007).

220. Mano, H. & Fukada, Y. A Median Third Eye: Pineal Gland Retraces Evolution of Vertebrate Photoreceptive Organs†. *Photochem. Photobiol.* **83**, 11–18 (2007).

221. Tosches, M. A. & Arendt, D. The bilaterian forebrain: an evolutionary chimaera. *Curr. Opin. Neurobiol.* **23**, 1080–1089 (2013).

222. Fritzsch, B. & Martin, P. R. Vision and retina evolution: How to develop a retina. *IBRO Neurosci. Rep.* **12**, 240–248 (2022).

223. Feuda, R., Hamilton, S. C., McInerney, J. O. & Pisani, D. Metazoan opsin evolution reveals a simple route to animal vision. *Proc. Natl. Acad. Sci.* **109**, 18868–18872 (2012).

224. Ramirez, M. *et al.* The last common ancestor of most bilaterian animals possessed at least 9 opsins. *Genome Biol. Evol.* evw248 (2016) doi:10.1093/gbe/evw248.

225. Yau, K.-W. & Hardie, R. C. Phototransduction Motifs and Variations. *Cell* **139**, 246–264 (2009).

226. Fain, G. L., Hardie, R. & Laughlin, S. B. Phototransduction and the Evolution of Photoreceptors. *Curr. Biol.* **20**, R114–R124 (2010).

227. Brodrick, E. & Jékely, G. Photobehaviours guided by simple photoreceptor systems. *Anim. Cogn.* **26**, 1817–1835 (2023).

228. Nilsson, D.-E. Eye evolution and its functional basis. *Vis. Neurosci.* **30**, 5–20 (2013).

229. Nilsson, D.-E. The evolution of eyes and visually guided behaviour. *Philos. Trans. R. Soc. B Biol. Sci.* **364**, 2833–2847 (2009).

230. Verasztó, C. *et al.* Ciliary and rhabdomeric photoreceptor-cell circuits form a spectral depth gauge in marine zooplankton. *eLife* **7**, e36440 (2018).

231. Arendt, D., Tessmar-Raible, K., Snyman, H., Dorresteijn, A. W. & Wittbrodt, J. Ciliary Photoreceptors with a Vertebrate-Type Opsin in an Invertebrate Brain. *Science* **306**, 869–871 (2004).

232. Döring, C. C., Kumar, S., Tumu, S. C., Kourtesis, I. & Hausen, H. The visual pigment xenopsin is widespread in protostome eyes and impacts the view on eye evolution. *eLife* **9**, e55193 (2020).

233. Bok, M. J., Porter, M. L. & Nilsson, D.-E. Phototransduction in fan worm radiolar eyes. *Curr. Biol. CB* **27**, R698–R699 (2017).

234. Su, C.-Y. *et al.* Parietal-Eye Phototransduction Components and Their Potential Evolutionary Implications. *Science* **311**, 1617–1621 (2006).

235. Krishnan, A. *et al.* Evolutionary hierarchy of vertebrate-like heterotrimeric G protein families. *Mol. Phylogenet. Evol.* **91**, 27–40 (2015).

236. Oakley, T. H. & Speiser, D. I. How Complexity Originates: The Evolution of Animal Eyes. *Annu. Rev. Ecol. Evol. Syst.* **46**, 237–260 (2015).

237. Vöcking, O., Macias-Muñoz, A., Jaeger, S. J. & Oakley, T. H. Deep Diversity: Extensive Variation in the Components of Complex Visual Systems across Animals. *Cells* **11**, 3966 (2022).

238. Backfisch, B. *et al.* Stable transgenesis in the marine annelid Platynereis dumerilii sheds new light on photoreceptor evolution. *Proc. Natl. Acad. Sci.* **110**, 193–198 (2013).

239. Battelle, B.-A. *et al.* Opsin Repertoire and Expression Patterns in Horseshoe Crabs: Evidence from the Genome of Limulus polyphemus (Arthropoda: Chelicerata). *Genome Biol. Evol.* **8**, 1571–1589 (2016).

240. Bonadè, M., Ogura, A., Corre, E., Bassaglia, Y. & Bonnaud-Ponticelli, L. Diversity of Light Sensing Molecules and Their Expression During the Embryogenesis of the Cuttlefish (Sepia officinalis). *Front. Physiol.* **11**, 521989 (2020).

241. Braun, K. & Stach, T. Structure and ultrastructure of eyes and brains of Thalia democratica (Thaliacea, Tunicata, Chordata): BRAUN and STACH. *J. Morphol.* **278**, 1421–1437 (2017).

242. De Vivo, G., Crocetta, F., Ferretti, M., Feuda, R. & D'Aniello, S. Duplication and Losses of Opsin Genes in Lophotrochozoan Evolution. *Mol. Biol. Evol.* **40**, msad066 (2023).

243. Eakin, R. M. & Brandenburger, J. L. Fine structure of the eyes of Pseudoceros canadensis (Turbellaria, Polycladida). *Zoomorphology* **98**, 1–16 (1981).

244. Esposito, R. *et al.* The ascidian pigmented sensory organs: structures and developmental programs. *genesis* **53**, 15–33 (2015).

245. Friedrich, M. Newly discovered harvestmen relict eyes eyeing for their functions. *BioEssays* **47**, 2400194 (2025).

246. Fukuzawa, S., Kawaguchi, T., Shimomura, T., Kubo, Y. & Tsukamoto, H. Characterization and Engineering of a Blue-Sensitive, Gi/o-Biased, and Bistable Ciliary Opsin from a Fan Worm. *Biochemistry* **64**, 1020–1031 (2025).

247. Maselli, V. *et al.* Extraocular Photoreception in Optic Lobes, Suckers, and Skin of Octopus vulgaris. *Integr. Zool.* **n/a**,.

248. McElroy, K. E., Audino, J. A. & Serb, J. M. Molluscan Genomes Reveal Extensive Differences in Photopigment Evolution Across the Phylum. *Mol. Biol. Evol.* **40**, msad263 (2023).

249. Rawlinson, K. A. *et al.* Extraocular, rod-like photoreceptors in a flatworm express xenopsin photopigment. *eLife* **8**, e45465 (2019).

250. Shettigar, N. *et al.* Hierarchies in light sensing and dynamic interactions between ocular and extraocular sensory networks in a flatworm. *Sci. Adv.* **3**, e1603025 (2017).

251. Sumner-Rooney, L. 'Distributed' vision and the architecture of animal visual systems. *J. Exp. Biol.* **226**, jeb245392 (2023).

252. Velarde, R. A., Sauer, C. D., O. Walden, K. K., Fahrbach, S. E. & Robertson, H. M. Pteropsin: A vertebrate-like non-visual opsin expressed in the honey bee brain. *Insect Biochem. Mol. Biol.* **35**, 1367–1377 (2005).

253. Yamashita, T., Fujii, K., Fujiyabu, C., Sakai, K. & Shiga, Y. Molecular diversity of protostome non-visual opsin arthropsin. *iScience* **28**, (2025).

254. Terakita, A., Kawano-Yamashita, E. & Koyanagi, M. Evolution and diversity of opsins. *Wiley Interdiscip. Rev. Membr. Transp. Signal.* **1**, 104–111 (2012).

255. Nilsson, D.-E. The Evolution of Visual Roles – Ancient Vision Versus Object Vision. *Front. Neuroanat.* **16**, 789375 (2022).

256. Nilsson, D.-E., Smolka, J. & Bok, M. The vertical light-gradient and its potential impact on animal distribution and behavior. *Front. Ecol. Evol.* **10**, 951328 (2022).

257. Satir, P. A Comment On the Origin of the Vertebrate Eye. *Anat. Rec.* **261**, 224–227 (2000).

258. Walls, G. L. & Walls, G. L. *The Vertebrate Eye and Its Adaptive Radiation*. 1–814 (Cranbrook Institute of Science, Bloomfield Hills, Mich, 1942). doi:10.5962/bhl.title.7369.

259. Evans, A. L. & Gage, P. J. Expression of the homeobox gene Pitx2 in neural crest is required for optic stalk and ocular anterior segment development. *Hum. Mol. Genet.* **14**, 3347–3359 (2005).

260. Manns, M. & Fritzsch, B. The eye in the brain: retinoic acid effects morphogenesis of the eye and pathway selection of axons but not the differentiation of the retina in Xenopus laevis. *Neurosci. Lett.* **127**, 150–154 (1991).

261. Matt, N., Ghyselinck, N. B., Pellerin, I. & Dupé, V. Impairing retinoic acid signalling in the neural crest cells is sufficient to alter entire eye morphogenesis. *Dev. Biol.* **320**, 140–148 (2008).

262. Matt, N. *et al.* Retinoic acid-dependent eye morphogenesis is orchestrated by neural crest cells. *Development* **132**, 4789–4800 (2005).

263. Williams, A. L. & Bohnsack, B. L. Neural crest derivatives in ocular development: Discerning the eye of the storm. *Birth Defects Res. Part C Embryo Today Rev.* **105**, 87–95 (2015).

264. Todorov, L. G., Oonuma, K., Kusakabe, T. G., Levine, M. S. & Lemaire, L. A. Neural crest lineage in the protovertebrate model Ciona. *Nature* **635**, 912–916 (2024).

265. Ekström, P. & Meissl, H. Evolution of photosensory pineal organs in new light: the fate of neuroendocrine photoreceptors. *Philos. Trans. R. Soc. Lond. B. Biol. Sci.* **358**, 1679–1700 (2003).

266. Kawano-Yamashita, E. *et al.* Immunohistochemical characterization of a parapinopsin-containing photoreceptor cell involved in the ultraviolet/green discrimination in the pineal organ of the river lamprey Lethenteron japonicum. *J. Exp. Biol.* **210**, 3821–3829 (2007).

267. Berlucchi, G. *et al. Visual Centers in the Brain*. vol. 7 / 3 / 3 B (Springer Berlin Heidelberg, Berlin, Heidelberg, 1973).

268. Dodt, E. & Heerd, E. Mode of action of pineal nerve fibers in frogs. *J. Neurophysiol.* **25**, 405–429 (1962).

269. Korf, H.-W., Liesner, R., Meissl, H. & Kirk, A. Pineal complex of the clawed toad, Xenopus laevis Daud.: Structure and function. *Cell Tissue Res.* **216**, 113–130 (1981).

270. Morita, Y. Entladungsmuster pinealer Neurone der Regenbogenforelle (Salmo irideus) bei Belichtung des Zwischenhirns. *Pflüg. Arch. Für Gesamte Physiol. Menschen Tiere* **289**, 155–167 (1966).

271. Uchida, K. & Morita, Y. Spectral sensitivity and mechanism of interaction between inhibitory and excitatory responses of photosensory pineal neurons. *Pflüg. Arch.* **427**, 373–377 (1994).

272. Wada, S. *et al.* Insights into the evolutionary origin of the pineal color discrimination mechanism from the river lamprey. *BMC Biol.* **19**, 188 (2021).

273. Lamanna, F. *et al.* A lamprey neural cell type atlas illuminates the origins of the vertebrate brain. *Nat. Ecol. Evol.* **7**, 1714–1728 (2023).

274. Sapède, D., Chaigne, C., Blader, P. & Cau, E. Functional heterogeneity in the pineal projection neurons of zebrafish. *Mol. Cell. Neurosci.* **103**, 103468 (2020).

275. Bailey, M. J. & Cassone, V. M. Melanopsin expression in the chick retina and pineal gland. *Mol. Brain Res.* **134**, 345–348 (2005).

276. Torii, M. *et al.* Two isoforms of chicken melanopsins show blue light sensitivity. *FEBS Lett.* **581**, 5327–5331 (2007).

277. Berson, D. M., Dunn, F. A. & Takao, M. Phototransduction by Retinal Ganglion Cells That Set the Circadian Clock. *Science* **295**, 1070–1073 (2002).

278. Provencio, I., Rollag, M. D. & Castrucci, A. M. Photoreceptive net in the mammalian retina. *Nature* **415**, 493–493 (2002).

279. Gühmann, M., Porter, M. L. & Bok, M. J. The Gluopsins: Opsins without the Retinal Binding Lysine. *Cells* **11**, 2441 (2022).

280. Kojima, D. *et al.* A Novel Go-mediated Phototransduction Cascade in Scallop Visual Cells. *J. Biol. Chem.* **272**, 22979–22982 (1997).

281. McReynolds, J. S. & Gorman, A. L. F. Photoreceptor Potentials of Opposite Polarity in the Eye of the Scallop, Pecten irradians. *J. Gen. Physiol.* **56**, 376–391 (1970).

282. Gühmann, M. *et al.* Spectral Tuning of Phototaxis by a Go-Opsin in the Rhabdomeric Eyes of Platynereis. *Curr. Biol.* **25**, 2265–2271 (2015).

283. Wada, S. *et al.* Color opponency with a single kind of bistable opsin in the zebrafish pineal organ. *Proc. Natl. Acad. Sci.* **115**, 11310–11315 (2018).

284. Wada, S., Kawano-Yamashita, E., Koyanagi, M. & Terakita, A. Expression of UV-Sensitive Parapinopsin in the Iguana Parietal Eyes and Its Implication in UV-Sensitivity in Vertebrate Pineal-Related Organs. *PLOS ONE* **7**, e39003 (2012).

285. Shen, D. *et al.* A Human Opsin-Related Gene That Encodes a Retinaldehyde-Binding Protein. *Biochemistry* **33**, 13117–13125 (1994).

286. Chen, P. *et al.* A photic visual cycle of rhodopsin regeneration is dependent on Rgr. *Nat. Genet.* **28**, 256–260 (2001).

287. Vöcking, O., Kourtesis, I., Tumu, S. C. & Hausen, H. Co-expression of xenopsin and rhabdomeric opsin in photoreceptors bearing microvilli and cilia. *eLife* **6**, e23435 (2017).

288. Lacalli, T. C. Sensory systems in amphioxus: a window on the ancestral chordate condition. *Brain. Behav. Evol.* **64**, 148–162 (2004).

289. Baden, T. Vertebrate vision: Lessons from non-model species. *Semin. Cell Dev. Biol.* **106**, 1–4 (2020).

290. Haverkamp, S. & Wassle, H. Immunocytochemical analysis of the mouse retina. *J. Comp. Neurol.* **424**, 1–23 (2000).

291. Koistinaho, J. & Sagar, S. M. Localization of protein kinase C subspecies in the rabbit retina. *Neurosci. Lett.* **177**, 15–18 (1994).

292. Hazlett, L. D., Hazlett, J. C. & Meyer, D. B. Landolt's club in the Japanese quail retina: a fine structural study. *Exp. Eye Res.* **20**, 407–416 (1975).

293. Locket, N. A. Landolt's club in the retina of the african lungfish, Protopterus aethiopicus, heckel. *Vision Res.* **10**, 299–VI (1970).

294. Quesada, A. & Génis-Gálvez, J. M. Morphological and structural study of Landolt's club in the chick retina. *J. Morphol.* **184**, 205–214 (1985).

295. Ekstrom, P. Photoreceptors and CSF-contacting neurons in the pineal organ of a teleost fish have direct axonal connections with the brain: an HRP-electron-microscopic study. *J. Neurosci.* **7**, 987–995 (1987).

296. Vigh, B. & Vigh-Teichmann, I. Actual problems of the cerebrospinal fluid-contacting neurons. *Microsc. Res. Tech.* **41**, 57–83 (1998).

297. Vigh-Teichmann, I., Vigh, B., Olsson, R. & van Veen, Th. Opsin-immunoreactive outer segments of photoreceptors in the eye and in the lumen of the optic nerve of the hagfish, Myxine glutinosa. *Cell Tissue Res.* **238**, 515–522 (1984).

298. Vigh-Teichmann, I. *et al.* Opsin-immunoreactive outer segments in the pineal and parapineal organs of the lamprey (Lampetra fluviatilis), the eel (Anguilla anguilla), and the rainbow trout (Salmo gairdneri). *Cell Tissue Res.* **230**, 289–307 (1983).

299. Samejima, M., Tamotsu, S., Watanabe, K. & Morita, Y. Photoreceptor cells and neural elements with long axonal processes in the pineal organ of the lamprey, Lampetra japonica, identified by use of the horseradish peroxidase method. *Cell Tissue Res.* **258**, 219–224 (1989).

300. Snellman, J., Kaur, T., Shen, Y. & Nawy, S. Regulation of ON bipolar cell activity. *Prog. Retin. Eye Res.* **27**, 450–463 (2008).

301. Dhingra, A. *et al.* Light Response of Retinal ON Bipolar Cells Requires a Specific Splice Variant of $G\alpha_o$. *J. Neurosci.* **22**, 4878–4884 (2002).

302. Nawy, S. The Metabotropic Receptor mGluR6 May Signal Through G_o , But Not Phosphodiesterase, in Retinal Bipolar Cells. *J. Neurosci.* **19**, 2938–2944 (1999).

303. Vardi, N. Alpha subunit of Go localizes in the dendritic tips of ON bipolar cells. *J. Comp. Neurol.* **395**, 43–52 (1998).

304. Chang, L., Breuninger, T. & Euler, T. Chromatic Coding from Cone-type Unselective Circuits in the Mouse Retina. *Neuron* **77**, 559–571 (2013).

305. Bartel, P., Yoshimatsu, T., Janiak, F. K. & Baden, T. Spectral inference reveals principal cone-integration rules of the zebrafish inner retina. *Curr. Biol.* **31**, 5214-5226.e4 (2021).

306. Kaneko, A. & Tachibana, M. Retinal bipolar cells with double colour-opponent receptive fields. *Nature* **293**, 220–222 (1981).

307. Shimbo, K., Toyoda, J.-I., Kondo, H. & Kujiraoka, T. Color-opponent responses of small and giant bipolar cells in the carp retina. *Vis. Neurosci.* **17**, 609–621 (2000).

308. Wong, K. Y. & Dowling, J. E. Retinal Bipolar Cell Input Mechanisms in Giant Danio. III. ON-OFF Bipolar Cells and Their Color-Opponent Mechanisms. *J. Neurophysiol.* **94**, 265–272 (2005).

309. Pang, J.-J., Gao, F. & Wu, S. M. Ionotropic glutamate receptors mediate OFF responses in light-adapted ON bipolar cells. *Vision Res.* **68**, 48–58 (2012).

310. Shekhar, K. *et al.* Comprehensive Classification of Retinal Bipolar Neurons by Single-Cell Transcriptomics. *Cell* **166**, 1308-1323.e30 (2016).

311. Jékely, G. Origin and early evolution of neural circuits for the control of ciliary locomotion. *Proc. Biol. Sci.* **278**, 914–922 (2011).

312. Gong, J. *et al.* The C. elegans Taste Receptor Homolog LITE-1 Is a Photoreceptor. *Cell* **167**, 1252-1263.e10 (2016).

313. Liu, J. *et al.* C. elegans phototransduction requires a G protein–dependent cGMP pathway and a taste receptor homolog. *Nat. Neurosci.* **13**, 715–722 (2010).

314. Ward, A., Liu, J., Feng, Z. & Xu, X. Z. S. Light-sensitive neurons and channels mediate phototaxis in C. elegans. *Nat. Neurosci.* **11**, 916–922 (2008).

315. Tsukamoto, H. & Terakita, A. Diversity and functional properties of bistable pigments. *Photochem. Photobiol. Sci.* **9**, 1435–1443 (2010).

316. Neuillé, M. *et al.* LRIT3 is essential to localize TRPM1 to the dendritic tips of depolarizing bipolar cells and may play a role in cone synapse formation. *Eur. J. Neurosci.* **42**, 1966–1975 (2015).

317. Tummala, S. R. *et al.* Lack of mGluR6-related cascade elements leads to retrograde trans-synaptic effects on rod photoreceptor synapses via matrix-associated proteins. *Eur. J. Neurosci.* **43**, 1509–1522 (2016).

318. Tummala, S. R., Neinstein, A., Fina, M. E., Dhingra, A. & Vardi, N. Localization of Cacna1s to ON Bipolar Dendritic Tips Requires mGluR6-Related Cascade Elements. *Investig. Opthalmology Vis. Sci.* **55**, 1483 (2014).

319. Koyanagi, M. & Terakita, A. Diversity of animal opsin-based pigments and their optogenetic potential. *Biochim. Biophys. Acta BBA - Bioenerg.* **1837**, 710–716 (2014).

320. Kawano-Yamashita, E. *et al.* Activation of Transducin by Bistable Pigment Parapinopsin in the Pineal Organ of Lower Vertebrates. *PLOS ONE* **10**, e0141280 (2015).

321. Terakita, A. *et al.* Counterion displacement in the molecular evolution of the rhodopsin family. *Nat. Struct. Mol. Biol.* **11**, 284–289 (2004).

322. Kawano-Yamashita, E. *et al.* Beta-Arrestin Functionally Regulates the Non-Bleaching Pigment Parapinopsin in Lamprey Pineal. *PLOS ONE* **6**, e16402 (2011).

323. Nikonov, S. S. *et al.* Mouse Cones Require an Arrestin for Normal Inactivation of Phototransduction. *Neuron* **59**, 462–474 (2008).

324. Koyanagi, M. *et al.* Bistable UV pigment in the lamprey pineal. *Proc. Natl. Acad. Sci. U. S. A.* **101**, 6687–6691 (2004).

325. Tamotsu, S., Korf, H.-W., Morita, Y. & Oksche, A. Immunocytochemical localization of serotonin and photoreceptor-specific proteins (rod-opsin, S-antigen) in the pineal complex of the river lamprey, Lampetra japonica, with special reference to photoneuroendocrine cells. *Cell Tissue Res.* **262**, 205–216 (1990).

326. Sato, K., Yamashita, T., Ohuchi, H. & Shichida, Y. Vertebrate Ancient-Long Opsin Has Molecular Properties Intermediate between Those of Vertebrate and Invertebrate Visual Pigments. *Biochemistry* **50**, 10484–10490 (2011).

327. Soni, B. G. & Foster, R. G. A novel and ancient vertebrate opsin. *FEBS Lett.* **406**, 279–283 (1997).

328. Chen, L., Li, G., Jiang, Z. & Yau, K.-W. Unusual phototransduction via cross-motif signaling from Gq to adenylyl cyclase in intrinsically photosensitive retinalganglion cells. *Proc. Natl. Acad. Sci.* **120**, e2216599120 (2023).

329. Jiang, Z., Yue, W. W. S., Chen, L., Sheng, Y. & Yau, K.-W. Cyclic-Nucleotide- and HCN-Channel-Mediated Phototransduction in Intrinsically Photosensitive Retinal Ganglion Cells. *Cell* **175**, 652-664.e12 (2018).

330. Contreras, E., Bhoi, J. D., Sonoda, T., Birnbaumer, L. & Schmidt, T. M. Melanopsin activates divergent phototransduction pathways in intrinsically photosensitive retinal ganglion cell subtypes. *eLife* **12**, e80749 (2023).

331. Lamb, T. D. & Hunt, D. M. Evolution of the vertebrate phototransduction cascade activation steps. *Dev. Biol.* **431**, 77–92 (2017).

332. Haverkamp, S. & Wässle, H. Characterization of an amacrine cell type of the mammalian retina immunoreactive for vesicular glutamate transporter 3. *J. Comp. Neurol.* **468**, 251–263 (2004).

333. Lee, S. *et al.* An Unconventional Glutamatergic Circuit in the Retina Formed by vGluT3 Amacrine Cells. *Neuron* **84**, 708–715 (2014).

334. Bezares-Calderón, L. A., Berger, J. & Jékely, G. Diversity of cilia-based mechanosensory systems and their functions in marine animal behaviour. *Philos. Trans. R. Soc. B Biol. Sci.* **375**, 20190376 (2019).

335. Vigh, B., Vigh-Teichmann, I., R□hlich, P. & Oksche, A. Cerebrospinal fluid-contacting neurons, sensory pinealocytes and Landolt's clubs of the retina as revealed by means of an electron-microscopic immunoreaction against opsin. *Cell Tissue Res.* **233**, (1983).

336. D'Gama, P. P. *et al.* Cilia-mediated cerebrospinal fluid flow modulates neuronal and astroglial activity in the zebrafish larval brain. 2024.02.01.578354 Preprint at https://doi.org/10.1101/2024.02.01.578354 (2024).

337. Brunken, W. J., Jin, X. T. & Pis-Lopez, A. M. The properties of the serotoninergic system in the retina. *Prog. Retin. Res.* **12**, 75–99 (1993).

338. Schütte, M. Serotonergic and serotonin-synthesizing cells of the Xenopus retina. *Int. J. Neurosci.* **78**, 67–73 (1994).

339. Audesirk, G., McCaman, R. E. & Willows, A. O. D. The role of serotonin in the control of pedal ciliary activity by identified neurons in *Tritonia diomedea*. *Comp. Biochem. Physiol. Part C Comp. Pharmacol.* **62**, 87–91 (1979).

340. Christopher, K., Chang, J. & Goldberg, J. Stimulation of cilia beat frequency by serotonin is mediated by a Ca2+ influx in ciliated cells of Helisoma trivolvis embryos. *J. Exp. Biol.* **199**, 1105–1113 (1996).

341. Kouyama, N. & Ohtsuka, T. Quantitative morphological study of the outer nuclear layer in the turtle retina. *Brain Res.* **345**, 200–203 (1985).

342. Kalluraya, C. A., Weitzel, A. J., Tsu, B. V. & Daugherty, M. D. Bacterial origin of a key innovation in the evolution of the vertebrate eye. *Proc. Natl. Acad. Sci.* **120**, e2214815120 (2023).

343. Rodrigues, M. M. *et al.* Interphotoreceptor retinoid-binding protein in retinal rod cells and pineal gland. *Invest. Ophthalmol. Vis. Sci.* **27**, 844–850 (1986).

344. Vardi, N., Matesic, D. F., Manning, D. R., Liebman, P. A. & Sterling, P. Identification of a G-protein in depolarizing rod bipolar cells. *Vis. Neurosci.* **10**, 473–478 (1993).

345. Zheng, J. *et al.* Cross-species single-cell landscape of vertebrate pineal gland. *J. Pineal Res.* **76**, e12927 (2024).

346. Han, L. *et al.* Cell transcriptomic atlas of the non-human primate Macaca fascicularis. *Nature* **604**, 723–731 (2022).

347. Mays, J. C. *et al.* Single-cell RNA sequencing of the mammalian pineal gland identifies two pinealocyte subtypes and cell type-specific daily patterns of gene expression. *PLOS ONE* **13**, e0205883 (2018).

348. Shainer, I. *et al.* Agouti-Related Protein 2 Is a New Player in the Teleost Stress Response System. *Curr. Biol.* **29**, 2009-2019.e7 (2019).

349. Westheimer, G. The ON-OFF dichotomy in visual processing: from receptors to perception. *Prog. Retin. Eye Res.* **26**, 636–648 (2007).

350. Masland, R. H. The fundamental plan of the retina. *Nat. Neurosci.* **4**, 877–886 (2001).

351. Dowling, J. E. *The Retina: An Approachable Part of the Brain*. (Harvard University Press, 2012). doi:10.2307/j.ctv31zqj2d.

352. Baden, T., Euler, T. & Berens, P. Understanding the retinal basis of vision across species. *Nat. Rev. Neurosci.* **21**, 5–20 (2020).

353. Kerschensteiner, D. Feature Detection by Retinal Ganglion Cells. *Annu. Rev. Vis. Sci.* **8**, 135–169 (2022).

354. Ratliff, C. P., Borghuis, B. G., Kao, Y.-H., Sterling, P. & Balasubramanian, V. Retina is structured to process an excess of darkness in natural scenes. *Proc. Natl. Acad. Sci. U. S. A.* **107**, 17368–17373 (2010).

355. Qiu, Y. *et al.* Natural environment statistics in the upper and lower visual field are reflected in mouse retinal specializations. *Curr. Biol. CB* **31**, 3233-3247.e6 (2021).

356. Baden, T. *et al.* A Tale of Two Retinal Domains: Near-Optimal Sampling of Achromatic Contrasts in Natural Scenes through Asymmetric Photoreceptor Distribution. *Neuron* **80**, 1206–1217 (2013).

357. Xing, D., Yeh, C.-I. & Shapley, R. M. Generation of Black-Dominant Responses in V1 Cortex. *J. Neurosci.* **30**, 13504–13512 (2010).

358. Yeh, C.-I., Xing, D. & Shapley, R. M. “Black” Responses Dominate Macaque Primary Visual Cortex V1. *J. Neurosci.* **29**, 11753–11760 (2009).

359. Kremkow, J., Jin, J., Wang, Y. & Alonso, J. M. Principles underlying sensory map topography in primary visual cortex. *Nature* **533**, 52–57 (2016).

360. Wässle, H., Peichl, L. & Boycott, B. B. Morphology and topography of on- and off-alpha cells in the cat retina. *Proc. R. Soc. Lond. B Biol. Sci.* **212**, 157–175 (1981).

361. Roy, S., Jun, N. Y., Davis, E. L., Pearson, J. & Field, G. D. Inter-mosaic coordination of retinal receptive fields. *Nature* **592**, 409–413 (2021).

362. Lee, K.-S., Huang, X. & Fitzpatrick, D. Topology of ON and OFF inputs in visual cortex enables an invariant columnar architecture. *Nature* **533**, 90–94 (2016).

363. Rocha, F. a. F., Saito, C. A., Silveira, L. C. L., Souza, J. M. D. & Ventura, D. F. Twelve chromatically opponent ganglion cell types in turtle retina. *Vis. Neurosci.* **25**, 307–315 (2008).

364. Guggiana Nilo, D. A., Riegler, C., Hübener, M. & Engert, F. Distributed chromatic processing at the interface between retina and brain in the larval zebrafish. *Curr. Biol. CB* **31**, 1945-1953.e5 (2021).

365. Wang, X., Roberts, P. A., Yoshimatsu, T., Lagnado, L. & Baden, T. Amacrine cells differentially balance zebrafish color circuits in the central and peripheral retina. *Cell Rep.* **42**, 112055 (2023).

366. Fornetto, C., Tiso, N., Pavone, F. S. & Vanzi, F. Colored visual stimuli evoke spectrally tuned neuronal responses across the central nervous system of zebrafish larvae. *BMC Biol.* **18**, 172 (2020).

367. Zhou, M. *et al.* Zebrafish Retinal Ganglion Cells Asymmetrically Encode Spectral and Temporal Information across Visual Space. *Curr. Biol. CB* **30**, 2927-2942.e7 (2020).

368. Rosa, J. M., Ruehle, S., Ding, H. & Lagnado, L. Crossover Inhibition Generates Sustained Visual Responses in the Inner Retina. *Neuron* **90**, 308–319 (2016).

369. Wang, J., Jacoby, R. & Wu, S. M. Physiological and morphological characterization of ganglion cells in the salamander retina. *Vision Res.* **119**, 60–72 (2016).

370. Seifert, M., Roberts, P. A., Kafetzis, G., Osorio, D. & Baden, T. Birds multiplex spectral and temporal visual information via retinal On- and Off-channels. *Nat. Commun.* **14**, 5308 (2023).

371. Awatramani, G. B. & Slaughter, M. M. Origin of transient and sustained responses in ganglion cells of the retina. *J. Neurosci. Off. J. Soc. Neurosci.* **20**, 7087–7095 (2000).

372. Wässle, H. Parallel processing in the mammalian retina. *Nat. Rev. Neurosci.* **5**, 747–757 (2004).

373. Roska, B. & Werblin, F. Vertical interactions across ten parallel, stacked representations in the mammalian retina. *Nature* **410**, 583–587 (2001).

374. Baden, T., Berens, P., Bethge, M. & Euler, T. Spikes in mammalian bipolar cells support temporal layering of the inner retina. *Curr. Biol. CB* **23**, 48–52 (2013).

375. Zhao, Z. *et al.* The temporal structure of the inner retina at a single glance. *Sci. Rep.* **10**, 4399 (2020).

376. Kuo, S. P. *et al.* Cone bipolar cell synapses generate transient versus sustained signals in parallel ON pathways of the mouse retina. *eLife* **13**, (2024).

377. O'Brien, B. J., Isayama, T., Richardson, R. & Berson, D. M. Intrinsic physiological properties of cat retinal ganglion cells. *J. Physiol.* **538**, 787–802 (2002).

378. Tabata, T. & Ishida, A. T. Transient and sustained depolarization of retinal ganglion cells by Ih. *J. Neurophysiol.* **75**, 1932–1943 (1996).

379. Ishida, A. T. Ion channel components of retinal ganglion cells. *Prog. Retin. Eye Res.* **15**, 261–280 (1995).

380. Skaliora, I., Scobey, R. P. & Chalupa, L. M. Prenatal development of excitability in cat retinal ganglion cells: action potentials and sodium currents. *J. Neurosci. Off. J. Soc. Neurosci.* **13**, 313–323 (1993).

381. Kaneda, M. & Kaneko, A. Voltage-gated sodium currents in isolated retinal ganglion cells of the cat: relation between the inactivation kinetics and the cell type. *Neurosci. Res.* **11**, 261–275 (1991).

382. Lipton, S. A. & Tauck, D. L. Voltage-dependent conductances of solitary ganglion cells dissociated from the rat retina. *J. Physiol.* **385**, 361–391 (1987).

383. Nirenberg, S. & Meister, M. The light response of retinal ganglion cells is truncated by a displaced amacrine circuit. *Neuron* **18**, 637–650 (1997).

384. Watanabe, M., Fukuda, Y., Hsiao, C. F. & Ito, H. Electron microscopic analysis of amacrine and bipolar cell inputs on Y-, X-, and W-cells in the cat retina. *Brain Res.* **358**, 229–240 (1985).

385. Freed, M. A. & Sterling, P. The ON-alpha ganglion cell of the cat retina and its presynaptic cell types. *J. Neurosci. Off. J. Soc. Neurosci.* **8**, 2303–2320 (1988).

386. West, R. W. & Dowling, J. E. Synapses onto different morphological types of retinal ganglion cells. *Science* **178**, 510–512 (1972).

387. Weber, A. J., McCall, M. A. & Stanford, L. R. Synaptic inputs to physiologically identified retinal X-cells in the cat. *J. Comp. Neurol.* **314**, 350–366 (1991).

388. Enroth-Cugell, C. & Robson, J. G. The contrast sensitivity of retinal ganglion cells of the cat. *J. Physiol.* **187**, 517–552 (1966).

389. Troy, J. B., Einstein, G., Schuurmans, R. P., Robson, J. G. & Enroth-Cugell, C. Responses to sinusoidal gratings of two types of very nonlinear retinal ganglion cells of cat. *Vis. Neurosci.* **3**, 213–223 (1989).

390. Cleland, B. G. & Levick, W. R. Properties of rarely encountered types of ganglion cells in the cat's retina and an overall classification. *J. Physiol.* **240**, 457–492 (1974).

391. Jacoby, J. & Schwartz, G. W. Three Small-Receptive-Field Ganglion Cells in the Mouse Retina Are Distinctly Tuned to Size, Speed, and Object Motion. *J. Neurosci. Off. J. Soc. Neurosci.* **37**, 610–625 (2017).

392. Levick, W. R. Receptive fields and trigger features of ganglion cells in the visual streak of the rabbit's retina. *J. Physiol.* **188**, 285–307 (1967).

393. Barlow, H. B. & Hill, R. M. Selective sensitivity to direction of movement in ganglion cells of the rabbit retina. *Science* **139**, 412–414 (1963).

394. Barlow, H. B., Hill, R. M. & Levick, W. R. Retinal ganglion cells responding selectively to direction and speed of image motion in the rabbit. *J. Physiol.* **173**, 377–407 (1964).

395. Maturana, H. R. & Frenk, S. Directional Movement and Horizontal Edge Detectors in the Pigeon Retina. *Science* **142**, 977–979 (1963).

396. Michael, C. R. Receptive fields of single optic nerve fibers in a mammal with an all-cone retina. II: directionally selective units. *J. Neurophysiol.* **31**, 257–267 (1968).

397. Jassik-Gerschenfeld, D., Minois, F. & Conde´-Courtine, F. Receptive field properties of directionally selective units in the pigeon's optic tectum. *Brain Res.* **24**, 407–421 (1970).

398. Jacobson, M. & Gaze, R. M. Types of Visual Response from Single Units in the Optic Tectum and Optic Nerve of the Goldfish. *Q. J. Exp. Physiol. Cogn. Med. Sci.* **49**, 199–209 (1964).

399. Cronly-Dillon, J. R. Units Sensitive to Direction of Movement in Goldfish Optic Tectum. *Nature* **203**, 214–215 (1964).

400. Levick, W. R., Oyster, C. W. & Takahashi, E. Rabbit Lateral Geniculate Nucleus: Sharpener of Directional Information. *Science* **165**, 712–714 (1969).

401. Montero, V. M. & Brugge, J. F. Direction of movement as the significant stimulus parameter for some lateral geniculate cells in the rat. *Vision Res.* **9**, 71–88 (1969).

402. Hubel, D. H. Single unit activity in striate cortex of unrestrained cats. *J. Physiol.* **147**, 226–238 (1959).

403. Hubel, D. H. & Wiesel, T. N. Receptive fields, binocular interaction and functional architecture in the cat's visual cortex. *J. Physiol.* **160**, 106-154.2 (1962).

404. Hubel, D. H. & Wiesel, T. N. Receptive fields of single neurones in the cat's striate cortex. *J. Physiol.* **148**, 574–591 (1959).

405. Baumgartner, G., Brown, J. L. & Schulz, A. Visual Motion Detection in the Cat. *Science* **146**, 1070–1071 (1964).

406. Uchiyama, H., Kanaya, T. & Sonohata, S. Computation of motion direction by quail retinal ganglion cells that have a nonconcentric receptive field. *Vis. Neurosci.* **17**, 263–271 (2000).

407. Kühn, N. K. & Gollisch, T. Joint Encoding of Object Motion and Motion Direction in the Salamander Retina. *J. Neurosci.* **36**, 12203–12216 (2016).

408. Tsvilling, V., Donchin, O., Shamir, M. & Segev, R. Archer fish fast hunting maneuver may be guided by directionally selective retinal ganglion cells. *Eur. J. Neurosci.* **35**, 436–444 (2012).

409. Jensen, R. J. & DeVoe, R. D. Comparisons of directionally selective with other ganglion cells of the turtle retina: intracellular recording and staining. *J. Comp. Neurol.* **217**, 271–287 (1983).

410. Bowling, D. B. Light responses of ganglion cells in the retina of the turtle. *J. Physiol.* **299**, 173–196 (1980).

411. Rasmussen, R. & Yonehara, K. Contributions of Retinal Direction Selectivity to Central Visual Processing. *Curr. Biol.* **30**, R897–R903 (2020).

412. Wang, A. Y. M. *et al.* An ON-type direction-selective ganglion cell in primate retina. *Nature* **623**, 381–386 (2023).

413. Kim, Y. J. *et al.* Origins of direction selectivity in the primate retina. *Nat. Commun.* **13**, 2862 (2022).

414. Weng, S., Sun, W. & He, S. Identification of ON–OFF direction-selective ganglion cells in the mouse retina. *J. Physiol.* **562**, 915–923 (2005).

415. Lien, A. D. & Scanziani, M. Cortical direction selectivity emerges at convergence of thalamic synapses. *Nature* **558**, 80–86 (2018).

416. Stanley, G. B. *et al.* Visual Orientation and Directional Selectivity through Thalamic Synchrony. *J. Neurosci.* **32**, 9073–9088 (2012).

417. Hillier, D. *et al.* Causal evidence for retina-dependent and -independent visual motion computations in mouse cortex. *Nat. Neurosci.* **20**, 960–968 (2017).

418. Shi, X. *et al.* Retinal origin of direction selectivity in the superior colliculus. *Nat. Neurosci.* **20**, 550–558 (2017).

419. Kay, J. N. *et al.* Retinal ganglion cells with distinct directional preferences differ in molecular identity, structure, and central projections. *J. Neurosci. Off. J. Soc. Neurosci.* **31**, 7753–7762 (2011).

420. Sanes, J. R. & Masland, R. H. The types of retinal ganglion cells: current status and implications for neuronal classification. *Annu. Rev. Neurosci.* **38**, 221–246 (2015).

421. Kerschensteiner, D. Feature Detection by Retinal Ganglion Cells. *Annu. Rev. Vis. Sci.* **8**, 135–169 (2022).

422. Hoshi, H., Tian, L.-M., Massey, S. C. & Mills, S. L. Two distinct types of ON directionally selective ganglion cells in the rabbit retina. *J. Comp. Neurol.* **519**, 2509–2521 (2011).

423. Sun, W., Deng, Q., Levick, W. R. & He, S. ON direction-selective ganglion cells in the mouse retina. *J. Physiol.* **576**, 197–202 (2006).

424. Kim, I.-J., Zhang, Y., Yamagata, M., Meister, M. & Sanes, J. R. Molecular identification of a retinal cell type that responds to upward motion. *Nature* **452**, 478–482 (2008).

425. Dhande, O. S. *et al.* Genetic Dissection of Retinal Inputs to Brainstem Nuclei Controlling Image Stabilization. *J. Neurosci.* **33**, 17797–17813 (2013).

426. Oyster, C. W. & Barlow, H. B. Direction-Selective Units in Rabbit Retina: Distribution of Preferred Directions. *Science* **155**, 841–842 (1967).

427. Sabbah, S. *et al.* A retinal code for motion along the gravitational and body axes. *Nature* **546**, 492–497 (2017).

428. Fiscella, M. *et al.* Visual coding with a population of direction-selective neurons. *J. Neurophysiol.* **114**, 2485–2499 (2015).

429. Yoshida, K. *et al.* A key role of starburst amacrine cells in originating retinal directional selectivity and optokinetic eye movement. *Neuron* **30**, 771–780 (2001).

430. Tarpey, P. *et al.* Mutations in FRMD7, a newly identified member of the FERM family, cause X-linked idiopathic congenital nystagmus. *Nat. Genet.* **38**, 1242–1244 (2006).

431. Yonehara, K. *et al.* Identification of Retinal Ganglion Cells and Their Projections Involved in Central Transmission of Information about Upward and Downward Image Motion. *PLOS ONE* **4**, e4320 (2009).

432. Yonehara, K. *et al.* Congenital Nystagmus Gene FRMD7 Is Necessary for Establishing a Neuronal Circuit Asymmetry for Direction Selectivity. *Neuron* **89**, 177–193 (2016).

433. Rivlin-Etzion, M. *et al.* Transgenic Mice Reveal Unexpected Diversity of On-Off Direction-Selective Retinal Ganglion Cell Subtypes and Brain Structures Involved in Motion Processing. *J. Neurosci.* **31**, 8760–8769 (2011).

434. Watanabe, S. & Murakami, M. Synaptic Mechanisms of Directional Selectivity in Ganglion Cells of Frog Retina as Revealed by Intracellular Recordings. *Jpn. J. Physiol.* **34**, 497–511 (1984).

435. Maximov, V., Maximova, E. & Maximov, P. Direction Selectivity in the Goldfish Tectum Revisited. *Ann. N. Y. Acad. Sci.* **1048**, 198–205 (2005).

436. Ellis, E. M., Frederiksen, R., Morshedian, A., Fain, G. L. & Sampath, A. P. Separate ON and OFF pathways in vertebrate vision first arose during the Cambrian. *Curr. Biol. CB* **30**, R633–R634 (2020).

437. Ali, M.-A. & Anctil, M. *Retinas of Fishes*. (Springer Berlin Heidelberg, Berlin, Heidelberg, 1976). doi:10.1007/978-3-642-66435-9.

438. Rodriguez, A. R., de Sevilla Müller, L. P. & Brecha, N. C. The RNA binding protein RBPMS is a selective marker of ganglion cells in the mammalian retina. *J. Comp. Neurol.* **522**, 1411–1443 (2014).

439. R, C. S. La retine des vertebres. *Cellule* **9**, 119–255 (1893).

440. Tsukamoto, Y., Morigiwa, K., Ueda, M. & Sterling, P. Microcircuits for night vision in mouse retina. *J. Neurosci. Off. J. Soc. Neurosci.* **21**, 8616–8623 (2001).

441. Helmstaedter, M. *et al.* Connectomic reconstruction of the inner plexiform layer in the mouse retina. *Nature* **500**, 168–174 (2013).

442. Tsukamoto, Y. & Omi, N. Classification of Mouse Retinal Bipolar Cells: Type-Specific Connectivity with Special Reference to Rod-Driven AII Amacrine Pathways. *Front. Neuroanat.* **11**, (2017).

443. Nelson, R. & Kolb, H. A17: a broad-field amacrine cell in the rod system of the cat retina. *J. Neurophysiol.* **54**, 592–614 (1985).

444. Hartveit, E. Reciprocal synaptic interactions between rod bipolar cells and amacrine cells in the rat retina. *J. Neurophysiol.* **81**, 2923–2936 (1999).

445. Zhang, C., Hellevik, A., Takeuchi, S. & Wong, R. O. Hierarchical partner selection shapes rod-cone pathway specificity in the inner retina. *iScience* **25**, 105032 (2022).

446. Molday, R. S. & MacKenzie, D. Monoclonal antibodies to rhodopsin: characterization, cross-reactivity, and application as structural probes. *Biochemistry* **22**, 653–660 (1983).

447. Sato, H. *et al.* A monogenic dominant mutation in Rom1 generated by N-ethyl-N-nitrosourea mutagenesis causes retinal degeneration in mice. *Mol. Vis.* **16**, 378–391 (2010).

448. Szamier, R. B. & Ripps, H. The visual cells of the skate retina: structure, histochemistry, and disc-shedding properties. *J. Comp. Neurol.* **215**, 51–62 (1983).

449. Pang, J.-J., Yang, Z., Jacoby, R. A. & Wu, S. M. Cone synapses in mammalian retinal rod bipolar cells. *J. Comp. Neurol.* **526**, 1896–1909 (2018).

450. Blanks, J. C. & Johnson, L. V. Specific binding of peanut lectin to a class of retinal photoreceptor cells. A species comparison. *Invest. Ophthalmol. Vis. Sci.* **25**, 546–557 (1984).

451. Vidal-Vázquez, N. *et al.* A single-nucleus RNA sequencing atlas of the postnatal retina of the shark Scyliorhinus canicula. *Sci. Data* **12**, 228 (2025).

452. Mayeur, H. *et al.* The Sensory Shark: High-quality Morphological, Genomic and Transcriptomic Data for the Small-spotted Catshark Scyliorhinus Canicula Reveal the Molecular Bases of Sensory Organ Evolution in Jawed Vertebrates. *Mol. Biol. Evol.* **41**, msae246 (2024).

453. Shichida, Y. & Matsuyama, T. Evolution of opsins and phototransduction. *Philos. Trans. R. Soc. B Biol. Sci.* **364**, 2881–2895 (2009).

454. Bellingham, J. & Foster, R. G. Opsins and mammalian photoentrainment. *Cell Tissue Res.* **309**, 57–71 (2002).

455. Bailes, H. J. & Lucas, R. J. Human melanopsin forms a pigment maximally sensitive to blue light (λmax ≈ 479 nm) supporting activation of G(q/11) and G(i/o) signalling cascades. *Proc. Biol. Sci.* **280**, 20122987 (2013).

456. Panda, S. *et al.* Illumination of the melanopsin signaling pathway. *Science* **307**, 600–604 (2005).

457. Jenkins, A. *et al.* VA Opsin, Melanopsin, and an Inherent Light Response within Retinal Interneurons. *Curr. Biol.* **13**, 1269–1278 (2003).

458. Bellingham, J., Whitmore, D., Philp, A. R., Wells, D. J. & Foster, R. G. Zebrafish melanopsin: isolation, tissue localisation and phylogenetic position. *Brain Res. Mol. Brain Res.* **107**, 128–136 (2002).

459. Sun, L. *et al.* Distribution of Mammalian-Like Melanopsin in Cyclostome Retinas Exhibiting a Different Extent of Visual Functions. *PLoS ONE* **9**, e108209 (2014).

460. Hart, N. S. Vision in sharks and rays: Opsin diversity and colour vision. *Semin. Cell Dev. Biol.* **106**, 12–19 (2020).

461. Schluessel, V., Rick, I. P. & Plischke, K. No rainbow for grey bamboo sharks: evidence for the absence of colour vision in sharks from behavioural discrimination experiments. *J. Comp. Physiol. A Neuroethol. Sens. Neural. Behav. Physiol.* **200**, 939–947 (2014).

462. Kalmijn, A. J. The Electric Sense of Sharks and Rays. *J. Exp. Biol.* **55**, 371–383 (1971).

463. Dijkgraaf, S. & Kalmijn, A. J. Untersuchungen über die Funktion der Lorenzinischen Ampullen an Haifischen. *Z. Für Vgl. Physiol.* **47**, 438–456 (1963).

464. Günther, A. *et al.* Double Cones and the Diverse Connectivity of Photoreceptors and Bipolar Cells in an Avian Retina. *J. Neurosci.* **41**, 5015–5028 (2021).

465. Sherry, D. M. & Yazulla, S. Goldfish bipolar cells and axon terminal patterns: A Golgi study. *J. Comp. Neurol.* **329**, 188–200 (1993).

466. Greene, M. J., Kim, J. S., Seung, H. S., & EyeWirers. Analogous Convergence of Sustained and Transient Inputs in Parallel On and Off Pathways for Retinal Motion Computation. *Cell Rep.* **14**, 1892–1900 (2016).

467. Field, G. D., Sampath, A. P. & Rieke, F. Retinal processing near absolute threshold: from behavior to mechanism. *Annu. Rev. Physiol.* **67**, 491–514 (2005).

468. Ganczer, A. *et al.* Transience of the Retinal Output Is Determined by a Great Variety of Circuit Elements. *Cells* **11**, 810 (2022).

469. Donner, K. Visual latency and brightness: An interpretation based on the responses of rods and ganglion cells in the frog retina. *Vis. Neurosci.* **3**, 39–51 (1989).

470. Gollisch, T. & Meister, M. Rapid neural coding in the retina with relative spike latencies. *Science* **319**, 1108–1111 (2008).

471. Mani, A. & Schwartz, G. W. Circuit mechanisms of a retinal ganglion cell with stimulus dependent response latency and activation beyond its dendrites. *Curr. Biol. CB* **27**, 471–482 (2017).

472. Ebert, S., Buffet, T., Sermet, B. S., Marre, O. & Cessac, B. Temporal pattern recognition in retinal ganglion cells is mediated by dynamical inhibitory synapses. *Nat. Commun.* **15**, 6118 (2024).

473. Linthicum, D. S. & Carey, F. G. Regulation of brain and eye temperatures by the bluefin tuna. *Comp. Biochem. Physiol. A* **43**, 425–433 (1972).

474. Carey, F. G. A brain heater in the swordfish. *Science* **216**, 1327–1329 (1982).

475. Block, B. A. & Carey, F. G. Warm brain and eye temperatures in sharks. *J. Comp. Physiol. B* **156**, 229–236 (1985).

476. Tubbesing, V. A. & Block, B. A. Orbital rete and red muscle vein anatomy indicate a high degree of endothermy in the brain and eye of the salmon shark. *Acta Zool.* **81**, 49–56 (2000).

477. Pickering, S. G. The extremely long latency response from on-off retinal ganglion cells: Relationship to dark adaptation. *Vision Res.* **8**, 383–387 (1968).

478. Aho, A.-C., Donner, K., Helenius, S., Larsen, L. O. & Reuter, T. Visual performance of the toad (Bufo bufo) at low light levels: retinal ganglion cell responses and prey-catching accuracy. *J. Comp. Physiol. A* **172**, 671–682 (1993).

479. Tikidji-Hamburyan, A. *et al.* Retinal output changes qualitatively with every change in ambient illuminance. *Nat. Neurosci.* **18**, 66–74 (2015).

480. Drinnenberg, A. *et al.* How Diverse Retinal Functions Arise from Feedback at the First Visual Synapse. *Neuron* **99**, 117-134.e11 (2018).

481. Sandell, J. & Masland, R. A system of indoleamine-accumulating neurons in the rabbit retina. *J. Neurosci.* **6**, 3331–3347 (1986).

482. Menger, N. & Wässle, H. Morphological and physiological properties of the A17 amacrine cell of the rat retina. *Vis. Neurosci.* **17**, 769–780 (2000).

483. Morgan, J. L., Soto, F., Wong, R. O. L. & Kerschensteiner, D. Development of cell type-specific connectivity patterns of converging excitatory axons in the retina. *Neuron* **71**, 1014–1021 (2011).

484. Tien, N.-W., Soto, F. & Kerschensteiner, D. Homeostatic plasticity shapes cell-type-specific wiring in the retina. *Neuron* **94**, 656-665.e4 (2017).

485. Lauritzen, J. S. *et al.* ON Cone Bipolar Cell Axonal Synapses in the OFF Inner Plexiform Layer of the Rabbit Retina. *J. Comp. Neurol.* **521**, 977–1000 (2013).

486. Dumitrescu, O. N., Pucci, F. G., Wong, K. Y. & Berson, D. M. Ectopic retinal ON bipolar cell synapses in the OFF inner plexiform layer: Contacts with dopaminergic amacrine cells and melanopsin ganglion cells. *J. Comp. Neurol.* **517**, 226–244 (2009).

487. Strettoi, E., Dacheux, R. F. & Raviola, E. Synaptic connections of rod bipolar cells in the inner plexiform layer of the rabbit retina. *J. Comp. Neurol.* **295**, 449–466 (1990).

488. Kolb, H. The inner plexiform layer in the retina of the cat: electron microscopic observations. *J. Neurocytol.* **8**, 295–329 (1979).

489. Müller, B., Butz, E., Peichl, L. & Haverkamp, S. The Rod Pathway of the Microbat Retina Has Bistratified Rod Bipolar Cells and Tristratified AII Amacrine Cells. *J. Neurosci.* **33**, 1014–1023 (2013).

490. Grunert, U. & Martin, P. R. Rod bipolar cells in the macaque monkey retina: immunoreactivity and connectivity. *J. Neurosci.* **11**, 2742–2758 (1991).

491. Connaughton, V. P., Behar, T. N., Liu, W.-L. S. & Massey, S. C. Immunocytochemical localization of excitatory and inhibitory neurotransmitters in the zebrafish retina. *Vis. Neurosci.* **16**, 483–490 (1999).

492. Hartveit, E. Functional Organization of Cone Bipolar Cells in the Rat Retina. *J. Neurophysiol.* **77**, 1716–1730 (1997).

493. Ammermüller, J. & Kolb, H. The organization of the turtle inner retina. I. ON- and OFF-center pathways. *J. Comp. Neurol.* **358**, 1–34 (1995).

494. Puller, C., Ondreka, K. & Haverkamp, S. Bipolar cells of the ground squirrel retina. *J. Comp. Neurol.* **519**, 759–774 (2011).

495. Ichinose, T. & Habib, S. On and off signaling pathways in the retina and the visual system. *Front. Ophthalmol.* **2**, (2022).

496. Boycott, B. B. & Wässle, H. Morphological Classification of Bipolar Cells of the Primate Retina. *Eur. J. Neurosci.* **3**, 1069–1088 (1991).

497. Pang, J.-J., Gao, F. & Wu, S. M. Segregation and Integration of Visual Channels: Layer-by-Layer Computation of ON–OFF Signals by Amacrine Cell Dendrites. *J. Neurosci.* **22**, 4693–4701 (2002).

498. Midorikawa, M., Tsukamoto, Y., Berglund, K., Ishii, M. & Tachibana, M. Different roles of ribbon-associated and ribbon-free active zones in retinal bipolar cells. *Nat. Neurosci.* **10**, 1268–1276 (2007).

499. Tachibana, M. Displaced ganglion cells in carp retina revealed by the horseradish peroxidase technique. *Neurosci. Lett.* **9**, 153–157 (1978).

500. Cook, J. E. & Becker, D. L. Regular mosaics of large displaced and non-displaced ganglion cells in the retina of a cichlid fish. *J. Comp. Neurol.* **306**, 668–684 (1991).

501. Duda, S. *et al.* Spatial distribution and functional integration of displaced retinal ganglion cells. *Sci. Rep.* **15**, 7123 (2025).

502. Kolb, H., Nelson, R. & Mariani, A. Amacrine cells, bipolar cells and ganglion cells of the cat retina: A Golgi study. *Vision Res.* **21**, 1081–1114 (1981).

503. Cook, J. & Noden, A. Somatic and Dendritic Mosaics Formed by Large Ganglion Cells in the Retina of the Common House Gecko *(Hemidactylus frenatus)*. *Brain. Behav. Evol.* **51**, 263–283 (1998).

504. Vaney, D. I., Peichl, L. & Boycott, B. B. Matching populations of amacrine cells in the inner nuclear and ganglion cell layers of the rabbit retina. *J. Comp. Neurol.* **199**, 373–391 (1981).

505. Teranishi, T. & Negishi, K. Dendritic morphology of a class of interstitial and normally placed amacrine cells revealed by intracellular Lucifer yellow injection in carp retina. *Vision Res.* **31**, 463–475 (1991).

506. Zimmerman, R. P. Bar synapses and gap junctions in the inner plexiform layer: synaptic relationships of the interstitial amacrine cell of the retina of the cichlid fish, Astronotus ocellatus. *J. Comp. Neurol.* **218**, 471–479 (1983).

507. Teranishi, T., Negishi, K. & Kato, S. Correlations between photoresponse and morphology of amacrine cells in the carp retina. *Neurosci. Res. Suppl.* **2**, S211–S226 (1985).

508. Negishi, K. & Teranishi, T. Close tip-to-tip contacts between dendrites of transient amacrine cells in carp retina. *Neurosci. Lett.* **115**, 1–6 (1990).

509. Ehinger, B. Biogenic Monoamines and Amino Acids as Retinal Neurotransmitters. in *Frontiers in Visual Science* (eds Cool, S. J. & Smith, E. L.) 42–53 (Springer, Berlin, Heidelberg, 1978). doi:10.1007/978-3-540-35397-3_7.

510. Ball, A. K. Immunocytochemical and autoradiographic localization of GABAergic neurons in the goldfish retina. *J. Comp. Neurol.* **255**, 317–325 (1987).

511. Ball, A. K. & Brandon, C. Localization of 3H-GABA, -muscimol, and -glycine in goldfish retinas stained for glutamate decarboxylase. *J. Neurosci.* **6**, 1621–1627 (1986).

512. Wagner, H.-J., Wulle, I., Meerfeld, N. & Wewetzer, K. Characterization of a GABAergic population of interstitial amacrine cells in the teleost retina. *Vision Res.* **31**, 1489–1500 (1991).

513. Versaux-Botteri, C. *et al.* Immunohistochemical localization of retinal serotonin cells in the lamprey (Lampetra fluviatilis). *Vis. Neurosci.* **7**, 171–177 (1991).

514. Nishimura, Y. Determination of the developmental pattern of retinal ganglion cells in chick embryos by golgi impregnation and other methods. *Anat. Embryol. (Berl.)* **158**, 329–347 (1980).

515. Hinds, J. W. & Hinds, P. L. Development of retinal amacrine cells in the mouse embryo: Evidence for two modes of formation. *J. Comp. Neurol.* **213**, 1–23 (1983).

516. Génis Gálvez, J., Puelles, L. & Prada, C. Inverted (displaced) retinal amacrine cells and their embryonic development in the chick. *Exp. Neurol.* **56**, 151–157 (1977).

517. Baden, T. The vertebrate retina: a window into the evolution of computation in the brain. *Curr. Opin. Behav. Sci.* **57**, 101391 (2024).

518. Slaughter, M. M. & Miller, R. F. 2-Amino-4-Phosphonobutyric Acid: A New Pharmacological Tool for Retina Research. *Science* **211**, 182–185 (1981).

519. Morgans, C. W. *et al.* TRPM1 is required for the depolarizing light response in retinal ON-bipolar cells. *Proc. Natl. Acad. Sci. U. S. A.* **106**, 19174–19178 (2009).

520. Koike, C. *et al.* TRPM1 is a component of the retinal ON bipolar cell transduction channel in the mGluR6 cascade. *Proc. Natl. Acad. Sci. U. S. A.* **107**, 332–337 (2010).

521. Chappell, R. L. & Rosenstein, F. J. Pharmacology of the skate electroretinogram indicates independent ON and OFF bipolar cell pathways. *J. Gen. Physiol.* **107**, 535–544 (1996).

522. Petersen-Jones, S. M., Shaw, G. C. & Montiani-Ferreira, F. Drug Dissection of the RGE Chicken Electroretinogram Suggests That GNB3 Plays a Role in Inner Retinal Function. *Invest. Ophthalmol. Vis. Sci.* **48**, 1939 (2007).

523. Nawy, S. Desensitization of the mGluR6 transduction current in tiger salamander On bipolar cells. *J. Physiol.* **558**, 137–146 (2004).

524. Connaughton, V. P. & Nelson, R. Axonal stratification patterns and glutamate-gated conductance mechanisms in zebrafish retinal bipolar cells. *J. Physiol.* **524**, 135–146 (2000).

525. Massey, S. C., Redburn, D. A. & Crawford, M. L. J. The effects of 2-amino-4-phosphonobutyric acid (APB) on the ERG and ganglion cell discharge of rabbit retina. *Vision Res.* **23**, 1607–1613 (1983).

526. Knapp, A. G. & Schiller, P. H. The contribution of on-bipolar cells to the electroretinogram of rabbits and monkeys. A study using 2-amino-4-phosphonobutyrate (APB). *Vision Res.* **24**, 1841–1846 (1984).

527. Popova, E., Mitova, L., Vitanova, L. & Kupenova, P. Effect of 2-amino-4-phosphonobutyrate on the OFF responses of frog retinal ganglion cells and local ERG after glycinergic blockade. *Comp. Biochem. Physiol. C Pharmacol. Toxicol. Endocrinol.* **126**, 139–151 (2000).

528. Völgyi, B., Deans, M. R., Paul, D. L. & Bloomfield, S. A. Convergence and Segregation of the Multiple Rod Pathways in Mammalian Retina. *J. Neurosci.* **24**, 11182–11192 (2004).

529. Caldwell, J. H., Daw, N. W. & Wyatt, H. J. Effects of picrotoxin and strychnine on rabbit retinal ganglion cells: lateral interactions for cells with more complex receptive fields. *J. Physiol.* **276**, 277–298 (1978).

530. Werblin, F. S. & Copenhagen, D. R. Control of retinal sensitivity. 3. Lateral interactions at the inner plexiform layer. *J. Gen. Physiol.* **63**, 88–110 (1974).

531. Dong, C.-J. & Hare, W. A. Temporal Modulation of Scotopic Visual Signals by A17 Amacrine Cells in Mammalian Retina In Vivo. *J. Neurophysiol.* **89**, 2159–2166 (2003).

532. Grimes, W. N. *et al.* Complex inhibitory microcircuitry regulates retinal signaling near visual threshold. *J. Neurophysiol.* **114**, 341–353 (2015).

533. Eggers, E. D. & Lukasiewicz, P. D. Multiple pathways of inhibition shape bipolar cell responses in the retina. *Vis. Neurosci.* **28**, 95–108 (2011).

534. MacNeil, M. A. & Masland, R. H. Extreme diversity among amacrine cells: implications for function. *Neuron* **20**, 971–982 (1998).

535. Wässle, H. *et al.* Glycinergic transmission in the mammalian retina. *Front. Mol. Neurosci.* **2**, 702 (2009).

536. Zhang, C. & McCall, M. A. Receptor targets of amacrine cells. *Vis. Neurosci.* **29**, 11–29 (2012).

537. Molnar, A., Hsueh, H.-A., Roska, B. & Werblin, F. S. Crossover inhibition in the retina: circuitry that compensates for nonlinear rectifying synaptic transmission. *J. Comput. Neurosci.* **27**, 569–590 (2009).

538. Zhang, J., Jung, C. S. & Slaughter, M. M. Serial inhibitory synapses in retina. *Vis. Neurosci.* **14**, 553–563 (1997).

539. Roska, B., Nemeth, E. & Werblin, F. S. Response to change is facilitated by a three-neuron disinhibitory pathway in the tiger salamander retina. *J. Neurosci. Off. J. Soc. Neurosci.* **18**, 3451–3459 (1998).

540. Eggers, E. D., McCall, M. A. & Lukasiewicz, P. D. Presynaptic inhibition differentially shapes transmission in distinct circuits in the mouse retina. *J. Physiol.* **582**, 569–582 (2007).

541. Eggers, E. D. & Lukasiewicz, P. D. GABA(A), GABA(C) and glycine receptor-mediated inhibition differentially affects light-evoked signalling from mouse retinal rod bipolar cells. *J. Physiol.* **572**, 215–225 (2006).

542. Vaney, D. I., Sivyer, B. & Taylor, W. R. Direction selectivity in the retina: symmetry and asymmetry in structure and function. *Nat. Rev. Neurosci.* **13**, 194–208 (2012).

543. Hanson, L., Sethuramanujam, S., deRosenroll, G., Jain, V. & Awatramani, G. B. Retinal direction selectivity in the absence of asymmetric starburst amacrine cell responses. *eLife* **8**, e42392.

544. Chen, Q. & Wei, W. Stimulus-dependent engagement of neural mechanisms for reliable motion detection in the mouse retina. *J. Neurophysiol.* **120**, 1153–1161 (2018).

545. Chander, P. R., Hanson, L., Chundekkad, P. & Awatramani, G. B. Neural Circuits Underlying Multifeature Extraction in the Retina. *J. Neurosci.* **44**, (2024).

546. Strauss, S. *et al.* Center-surround interactions underlie bipolar cell motion sensitivity in the mouse retina. *Nat. Commun.* **13**, 5574 (2022).

547. Trenholm, S., Johnson, K., Li, X., Smith, R. G. & Awatramani, G. B. Parallel mechanisms encode direction in the retina. *Neuron* **71**, 683–694 (2011).

548. Hoggarth, A. *et al.* Specific Wiring of Distinct Amacrine Cells in the Directionally Selective Retinal Circuit Permits Independent Coding of Direction and Size. *Neuron* **86**, 276–291 (2015).

549. Barlow, H. B. & Levick, W. R. The mechanism of directionally selective units in rabbit's retina. *J. Physiol.* **178**, 477–504 (1965).

550. Vaney, D. I. & Young, H. M. GABA-like immunoreactivity in cholinergic amacrine cells of the rabbit retina. *Brain Res.* **438**, 369–373 (1988).

551. Wyatt, H. J. & Day, N. W. Specific effects of neurotransmitter antagonists on ganglion cells in rabbit retina. *Science* **191**, 204–205 (1976).

552. Euler, T., Detwiler, P. B. & Denk, W. Directionally selective calcium signals in dendrites of starburst amacrine cells. *Nature* **418**, 845–852 (2002).

553. Ding, H., Smith, R. G., Poleg-Polsky, A., Diamond, J. S. & Briggman, K. L. Species-specific wiring for direction selectivity in the mammalian retina. *Nature* **535**, 105–110 (2016).

554. Lee, S. & Zhou, Z. J. The synaptic mechanism of direction selectivity in distal processes of starburst amacrine cells. *Neuron* **51**, 787–799 (2006).

555. Briggman, K. L., Helmstaedter, M. & Denk, W. Wiring specificity in the direction-selectivity circuit of the retina. *Nature* **471**, 183–188 (2011).

556. Kittila, C. A. & Massey, S. C. Pharmacology of Directionally Selective Ganglion Cells in the Rabbit Retina. *J. Neurophysiol.* **77**, 675–689 (1997).

557. Sethuramanujam, S., Awatramani, G. B. & Slaughter, M. M. Cholinergic excitation complements glutamate in coding visual information in retinal ganglion cells. *J. Physiol.* **596**, 3709–3724 (2018).

558. Rentería, R. C. *et al.* Intrinsic ON responses of the retinal OFF pathway are suppressed by the ON pathway. *J. Neurosci. Off. J. Soc. Neurosci.* **26**, 11857–11869 (2006).

559. Farajian, R., Pan, F., Akopian, A., Völgyi, B. & Bloomfield, S. A. Masked excitatory crosstalk between the ON and OFF visual pathways in the mammalian retina. *J. Physiol.* **589**, 4473–4489 (2011).

560. Ackert, J. M., Farajian, R., Völgyi, B. & Bloomfield, S. A. GABA blockade unmasks an OFF response in ON direction selective ganglion cells in the mammalian retina. *J. Physiol.* **587**, 4481–4495 (2009).

561. Graydon, C. W. *et al.* Synaptic Transfer between Rod and Cone Pathways Mediated by AII Amacrine Cells in the Mouse Retina. *Curr. Biol.* **28**, 2739-2751.e3 (2018).

562. Sterling, P. Microcircuitry of the cat retina. *Annu. Rev. Neurosci.* **6**, 149–185 (1983).

563. Pang, J.-J. *et al.* Relative contributions of rod and cone bipolar cell inputs to AII amacrine cell light responses in the mouse retina. *J. Physiol.* **580**, 397–410 (2007).

564. Nath, A., Grimes, W. N. & Diamond, J. S. Layers of inhibitory networks shape receptive field properties of AII amacrine cells. *Cell Rep.* **42**, (2023).

565. Veruki, M. L., Mørkve, S. H. & Hartveit, E. Functional Properties of Spontaneous EPSCs and non-NMDA Receptors in Rod Amacrine (AII) Cells in the Rat Retina. *J. Physiol.* **549**, 759–774 (2003).

566. Xin, D. & Bloomfield, S. A. Comparison of the responses of AII amacrine cells in the dark- and light-adapted rabbit retina. *Vis. Neurosci.* **16**, 653–665 (1999).

567. Kamphuis, W., Klooster, J. & Dijk, F. Expression of AMPA-type glutamate receptor subunit (GluR2) in ON-bipolar neurons in the rat retina. *J. Comp. Neurol.* **455**, 172–186 (2003).

568. Kamphuis, W., Dijk, F. & O'Brien, B. J. Gene expression of AMPA-type glutamate receptor subunits in rod-type ON bipolar cells of rat retina. *Eur. J. Neurosci.* **18**, 1085–1092 (2003).

569. Hughes, T. E. Are there ionotropic glutamate receptors on the rod bipolar cell of the mouse retina? *Vis. Neurosci.* **14**, 103–109 (1997).

570. Calkins, D. J. Localization of ionotropic glutamate receptors to invaginating dendrites at the cone synapse in primate retina. *Vis. Neurosci.* **22**, 469–477 (2005).

571. Hanna, M. C. & Calkins, D. J. Expression of genes encoding glutamate receptors and transporters in rod and cone bipolar cells of the primate retina determined by single-cell polymerase chain reaction. *Mol. Vis.* **13**, 2194–2208 (2007).

572. Haverkamp, S., Grünert, U. & Wässle, H. Localization of kainate receptors at the cone pedicles of the primate retina. *J. Comp. Neurol.* **436**, 471–486 (2001).

573. Soto, F. *et al.* Molecular mechanism establishing the OFF pathway in vision. *Nat. Commun.* **16**, 1–14 (2025).

574. Shiells, R. A., Falk, G. & Naghshineh, S. Action of glutamate and aspartate analogues on rod horizontal and bipolar cells. *Nature* **294**, 592–594 (1981).

575. Awatramani, G. B. & Slaughter, M. M. Intensity-dependent, rapid activation of presynaptic metabotropic glutamate receptors at a central synapse. *J. Neurosci. Off. J. Soc. Neurosci.* **21**, 741–749 (2001).

576. Yu, J. *et al.* Hyperactivity of ON-Type Retinal Ganglion Cells in Streptozotocin-Induced Diabetic Mice. *PLOS ONE* **8**, e76049 (2013).

577. Roy, S., Yao, X., Rathinavelu, J. & Field, G. D. GABAergic Inhibition Controls Receptive Field Size, Sensitivity, and Contrast Preference of Direction Selective Retinal Ganglion Cells Near the Threshold of Vision. *J. Neurosci.* **44**, (2024).

578. Pan, Z. H. & Lipton, S. A. Multiple GABA receptor subtypes mediate inhibition of calcium influx at rat retinal bipolar cell terminals. *J. Neurosci. Off. J. Soc. Neurosci.* **15**, 2668–2679 (1995).

579. Zhou, Z. J. A critical role of the strychnine-sensitive glycinergic system in spontaneous retinal waves of the developing rabbit. *J. Neurosci. Off. J. Soc. Neurosci.* **21**, 5158–5168 (2001).

580. Toychiev, A. H., Yee, C. W. & Sagdullaev, B. T. Correlated Spontaneous Activity Persists in Adult Retina and Is Suppressed by Inhibitory Inputs. *PLoS ONE* **8**, e77658 (2013).

581. Manookin, M. B., Beaudoin, D. L., Ernst, Z. R., Flagel, L. J. & Demb, J. B. Disinhibition Combines with Excitation to Extend the Operating Range of the OFF Visual Pathway in Daylight. *J. Neurosci.* **28**, 4136–4150 (2008).

582. Murphy, G. J. & Rieke, F. Network variability limits stimulus-evoked spike timing precision in retinal ganglion cells. *Neuron* **52**, 511–524 (2006).

583. Sagdullaev, B. T., McCall, M. A. & Lukasiewicz, P. D. Presynaptic Inhibition Modulates Spillover, Creating Distinct Dynamic Response Ranges of Sensory Output. *Neuron* **50**, 923–935 (2006).

584. Reichardt, W. Evaluation of optical motion information by movement detectors. *J. Comp. Physiol. A* **161**, 533–547 (1987).

585. Borst, A. & Helmstaedter, M. Common circuit design in fly and mammalian motion vision. *Nat. Neurosci.* **18**, 1067–1076 (2015).

586. Egelhaaf, M., Borst, A. & Reichardt, W. Computational structure of a biological motion-detection system as revealed by local detector analysis in the fly's nervous system. *J. Opt. Soc. Am. A* **6**, 1070–1087 (1989).

587. Borst, A. Correlation versus gradient type motion detectors: the pros and cons. *Philos. Trans. R. Soc. B Biol. Sci.* **362**, 369–374 (2007).

588. Sawant, A. *et al.* Organization and emergence of a mixed GABA-glycine retinal circuit that provides inhibition to mouse ON-sustained alpha retinal ganglion cells. *Cell Rep.* **34**, 108858 (2021).

589. Qian, H., Li, L., Chappell, R. L. & Ripps, H. GABA Receptors of Bipolar Cells From the Skate Retina: Actions of Zinc on GABA-Mediated Membrane Currents. *J. Neurophysiol.* **78**, 2402–2412 (1997).

590. Shields, C. R., Tran, M. N., Wong, R. O. L. & Lukasiewicz, P. D. Distinct Ionotropic GABA Receptors Mediate Presynaptic and Postsynaptic Inhibition in Retinal Bipolar Cells. *J. Neurosci.* **20**, 2673–2682 (2000).

591. Diamond, J. S. Inhibitory Interneurons in the Retina: Types, Circuitry, and Function. *Annu. Rev. Vis. Sci.* **3**, 1–24 (2017).

592. Popova, E. ON-OFF Interactions in the Retina: Role of Glycine and GABA. *Curr. Neuropharmacol.* **12**, 509–526 (2014).

593. Bolz, J., Thier, P., Voigt, T. & Wässle, H. Action and localization of glycine and taurine in the cat retina. *J. Physiol.* **362**, 395–413 (1985).

594. Muller, F., Wassle, H. & Voigt, T. Pharmacological modulation of the rod pathway in the cat retina. *J. Neurophysiol.* **59**, 1657–1672 (1988).

595. Wong, K. Y., Adolph, A. R. & Dowling, J. E. Retinal Bipolar Cell Input Mechanisms in Giant Danio. I. Electroretinographic Analysis. *J. Neurophysiol.* **93**, 84–93 (2005).

596. Contini, M. *et al.* Synaptic input of ON-bipolar cells onto the dopaminergic neurons of the mouse retina. *J. Comp. Neurol.* **518**, 2035–2050 (2010).

597. Jardon, B., Bonaventure, N. & Scherrer, E. Possible involvement of cholinergic and glycinergic amacrine cells in the inhibition exerted by the ON retinal channel on the OFF retinal channel. *Eur. J. Pharmacol.* **210**, 201–207 (1992).

598. Maguire, G. & Hamasaki, D. I. The retinal dopamine network alters the adaptational properties of retinal ganglion cells in the cat. *J. Neurophysiol.* **72**, 730–741 (1994).

599. Strang, C. E., Long, Y., Gavrikov, K. E., Amthor, F. R. & Keyser, K. T. Nicotinic and muscarinic acetylcholine receptors shape ganglion cell response properties. *J. Neurophysiol.* **113**, 203–217 (2015).

600. Neal, M. J., Cunningham, J. R., James, T. A., Joseph, M. & Collins, J. F. The effect of 2-amino-4-phosphonobutyrate (APB) on acetylcholine release from the rabbit retina: evidence for on-channel input to cholinergic amacrine cells. *Neurosci. Lett.* **26**, 301–305 (1981).

601. Masland, R. H. & Ames, A. Responses to acetylcholine of ganglion cells in an isolated mammalian retina. *J. Neurophysiol.* **39**, 1220–1235 (1976).

602. Hellmer, C. B. *et al.* Cholinergic feedback to bipolar cells contributes to motion detection in the mouse retina. *Cell Rep.* **37**, 110106 (2021).

603. Litherland, L., Collin, S. P. & Fritsches, K. A. Eye growth in sharks: Ecological implications for changes in retinal topography and visual resolution. *Vis. Neurosci.* **26**, 397–409 (2009).

604. Litherland, L., Collin, S. P. & Fritsches, K. A. Visual optics and ecomorphology of the growing shark eye: a comparison between deep and shallow water species. *J. Exp. Biol.* **212**, 3583–3594 (2009).

605. Hernández-Núñez, I. *et al.* Loss of Active Neurogenesis in the Adult Shark Retina. *Front. Cell Dev. Biol.* **9**, 628721 (2021).

606. Pimiento, C. *et al.* Functional diversity of sharks and rays is highly vulnerable and supported by unique species and locations worldwide. *Nat. Commun.* **14**, 7691 (2023).

607. Finucci, B. *et al.* The IUCN Red List of Threatened Species. *IUCN Red List of Threatened Species* https://www.iucnredlist.org/species/161307554/124478351 (2021).

608. Coolen, M. *et al.* The Dogfish *Scyliorhinus canicula:* A Reference in Jawed Vertebrates. *Cold Spring Harb. Protoc.* **2008**, pdb.emo111 (2008).

609. Pavan-Kumar, A. *et al.* Molecular Phylogeny of Elasmobranchs. in *DNA Barcoding and Molecular Phylogeny* (eds Trivedi, S., Rehman, H., Saggu, S., Panneerselvam, C. & Ghosh, S. K.) 137–151 (Springer International Publishing, Cham, 2020). doi:10.1007/978-3-030-50075-7_9.

610. Muguruma, K., Stell, W. K. & Yamamoto, N. A Morphological Classification of Retinal Ganglion Cells in the Japanese Catshark Scyliorhinus torazame. *Brain. Behav. Evol.* **83**, 199–215 (2014).

611. Allen, A. E. *et al.* Reconfiguration of the visual code and retinal cell type complement in closely related diurnal and nocturnal mice. 2024.06.14.598659 Preprint at https://doi.org/10.1101/2024.06.14.598659 (2024).

612. Winn, J. C., Maduna, S. N. & Bester-van der Merwe, A. E. A comprehensive phylogenomic study unveils evolutionary patterns and challenges in the mitochondrial genomes of Carcharhiniformes: A focus on Triakidae. *Genomics* **116**, 110771 (2024).

613. Iglésias, S. P., Lecointre, G. & Sellos, D. Y. Extensive paraphylies within sharks of the order Carcharhiniformes inferred from nuclear and mitochondrial genes. *Mol. Phylogenet. Evol.* **34**, 569–583 (2005).

614. Brée, B., Condamine, F. L. & Guinot, G. Combining palaeontological and neontological data shows a delayed diversification burst of carcharhiniform sharks likely mediated by environmental change. *Sci. Rep.* **12**, 21906 (2022).

615. Van-Eyk, S. M., Siebeck, U. E., Champ, C. M., Marshall, J. & Hart, N. S. Behavioural evidence for colour vision in an elasmobranch. *J. Exp. Biol.* **214**, 4186–4192 (2011).

616. Davies, W. I. L., Collin, S. P. & Hunt, D. M. Molecular ecology and adaptation of visual photopigments in craniates. *Mol. Ecol.* **21**, 3121–3158 (2012).

617. Levenson, D. H. & Dizon, A. Genetic evidence for the ancestral loss of short-wavelength-sensitive cone pigments in mysticete and odontocete cetaceans. *Proc. Biol. Sci.* **270**, 673–679 (2003).

618. Levenson, D. H. *et al.* Visual pigments of marine carnivores: pinnipeds, polar bear, and sea otter. *J. Comp. Physiol. A Neuroethol. Sens. Neural. Behav. Physiol.* **192**, 833–843 (2006).

619. Newman, L. A. & Robinson, P. R. Cone visual pigments of aquatic mammals. *Vis. Neurosci.* **22**, 873–879 (2005).

620. Peichl, L. & Moutairou, K. Absence of short-wavelength sensitive cones in the retinae of seals (Carnivora) and African giant rats (Rodentia). *Eur. J. Neurosci.* **10**, 2586–2594 (1998).

621. Newman, L. A. & Robinson, P. R. The visual pigments of the West Indian manatee (Trichechus manatus). *Vision Res.* **46**, 3326–3330 (2006).

622. Goldsmith, T. H., Collins, J. S. & Licht, S. The cone oil droplets of avian retinas. *Vision Res.* **24**, 1661–1671 (1984).

623. Toomey, M. B. & Corbo, J. C. Evolution, Development and Function of Vertebrate Cone Oil Droplets. *Front. Neural Circuits* **11**, 97 (2017).